

Decoherence due to Unconventional Environments: Nonlinear Versus Linear Baths

INAUGURALDISSERTATION

ZUR

Erlangung der Würde eines Doktors der Philosophie

vorgelegt der

Philosophisch-Naturwissenschaftlichen Fakultät

der Universität Basel

VON

Hanno Gassmann

aus Oberglatt (ZH)

Basel, 2004

Genehmigt von der Philosophisch-Naturwissenschaftlichen Fakultät auf Antrag von

Prof. Dr. Christoph Bruder

Prof. Dr. Milena Grifoni

Basel, den 6. Juli 2004

Prof. Dr. Marcel Tanner
Dekan

Contents

1	Introduction	5
1.1	Decoherence example, Markoffian, and non-Markoffian behavior	7
1.2	Linear and Nonlinear Environments	10
1.3	Flow equation method	11
1.4	Single-spin quantum measurement	14
1.5	Leakage	15
1.6	Outline	15
2	Non-Markoffian Effects of a Nonlinear Bath	17
2.1	Introduction	17
2.2	The linear oscillator bath	19
2.3	The Feynman-Vernon influence functional	20
2.4	Non-linear environments	24
2.5	Non-linear baths in the weak-coupling limit	25
2.6	The nonlinear-bath model	28
2.7	Infinite temperature results	28
2.8	The exact solution: “Approach 1”	31
2.9	The bath-correlation function	36
2.10	The master equation: “Approach 2”	39
2.11	The nonlinear bath replaced by a linear bath: “Approach 3”	42
2.12	Numerical generation of the random field	44
2.13	The weak-coupling approximation: “Approach 4”	47
2.14	Conclusions	48
3	Flow Equation Results for Low Temperatures	51
3.1	Introduction	51
3.2	The general framework for a dissipative system	52
3.2.1	The model Hamiltonian	53
3.2.2	Flow equations for the Hamiltonian	54
3.2.3	Flow equations for the observables	56
3.3	Flow equations for the dissipative four-state system	56

3.4	Flow equations for the nonlinear bath	58
3.5	The linear-bath approximation	61
3.6	Details of the numerical calculation	68
3.7	Comparison of nonlinear with linear bath	70
3.8	Conclusions	75
4	Quantum Dissipative Dynamics of the Magnetic Resonance Force Microscope in the Single-Spin Detection Limit	83
4.1	Introduction	83
4.2	Model of the MRFM	85
4.3	Estimation of the spin-flip rate	90
4.4	Coherent solution without bath	91
4.5	Dynamics of the spin	93
4.6	Dynamics of the cantilever	95
4.7	Master equation	101
4.8	The correlation function	110
4.9	Classical limit of the cantilever	111
4.10	MRFM as a quantum measurement device	113
4.11	Conclusions	115
5	Leakage of Josephson qubits	117
5.1	Leakage of Josephson qubits during a NMR-like microwave pulse op- eration	117
5.2	The model in a restricted Hilbert space	118
5.3	A perturbative approach	121
5.4	Conclusions	126
6	Summary and Open Questions	127
A	Appendices	131
A.1	Spin in a fluctuating field	131
A.2	Selection rules	133
A.3	Equilibrium correlator for Approach 4	133
A.4	The flow equations for the Hamiltonian	134
A.5	The generator coefficients	136
A.6	The flow equations for the observables	137
A.7	Formulas for the Pauli matrix tensor products	138
A.8	Flow equations for the biased case	139
A.9	The master-equation solution for the nonlinear bath	142
A.10	The weak-coupling solution of the nonlinear bath	144
A.11	Path-integral formulas	149
A.12	Relaxation of a non-thermal initial state	154
	Bibliography	155

Chapter 1

Introduction

Sometimes friends, which work in unrelated, different fields from physics ask me about our work and want to know what we are actually doing and what my thesis is about. An answer to this question might be a good and understandable addition to my thesis. The conversation might go as follows: You know how classical computers work. The basic unit is a bit, which is a system that can be in two states, for instance a transistor that behaves like a switch turned on or turned off. By manipulating these bits, calculations can be done in a binary number system. Physicists had the idea to use quantum bits or qubits as the basic building block for a quantum computer. Qubits are, as usual bits, two-state systems but they are modeled with quantum theory. The quantum world, obeying the laws of quantum mechanics, is distinct from the classical world, evolving according to Newton's laws. The two basis states are orthogonal elements of a vector space. The idea is to use special quantum behavior as engineers to build a quantum computer. Qubit implementations have been realized in diverse experiments. For example, in Japan a team [Nakamura99] has performed experiments with a qubit. They used a small superconducting island separated by a Josephson tunnel junction from a superconducting reservoir. The two states correspond to the situation when an excess Cooper pair has either tunneled onto the island or has stayed in the reservoir.

The two-state system (qubit) is the simplest non-trivial quantum mechanical system, because in contrast to a one-state system transitions are possible from one to the other state. In classical mechanics these would be in accordance with the situation where a particle could be at two positions at the same time. We could draw a graph like shown in Fig. 1.1 to see the time evolution of the particle. As soon as the particle has left one position or state it is in the other, it is never at both positions simultaneously. In contrast, quantum mechanics works differently and contradicts everyday life experience such that the particle can be at the two distinct positions at the same time. The two-state system is then said to be in a coherent superposition of the two states. This peculiar property of the superposition can be used for quantum computing and is necessary in order to perform some powerful quantum algorithms. With the help of these algorithms one can perform certain task much faster than with

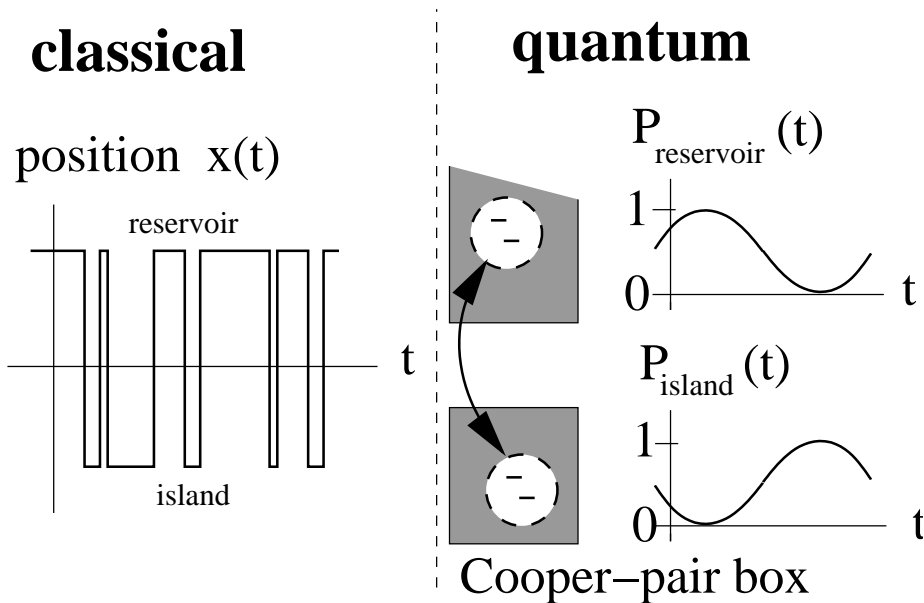


Figure 1.1: Classical and quantum two-state systems. In the classical case the particle is always at a definite position at a time t , as opposed to the quantum behavior, where the two states can be in a coherent superposition and probabilities to find the Cooper-pair in the reservoir or on the island have to be introduced.

a usual computer [Nielsen00], which has made quantum information popular and led to a tremendous growth of the field during the past decade.

And now we come to our work. You can imagine that it is very hard to isolate two states from the rest of the world, which can be considered as a huge system with infinitely many degrees of freedom. The surrounding environment (bath) interacts with the two-state system, i.e., exchanges energy and perturbs it. What is now the effect of the environment? The result is that the superposition or the interference property of the qubit state, which distinguishes it from a classical bit, is destroyed over a certain timescale. The destruction is described by a decay as shown in Fig. 1.3. It has the qualitative shape of a radioactive decay: some quantity gets smaller and disappears after a certain time. This decay is called decoherence. In Fig. 1.3 the off-diagonal element of the density matrix, which quantifies decoherence, is used to show the decoherent dynamics of a qubit.

Since superpositions of the two qubit states, which are necessary for quantum computing, are destroyed due to the interaction with the environment, scientists try to understand the mechanism of decoherence and try to find ways to suppress it. Over the past years, several models for the environment have been proposed, which are basically a large quantum system with many degrees of freedom. The total systems (qubit and environment together) are referred to as quantum dissipative systems [Weiss00]. One important recent development in physics is the experimental test of the macroscopic quantum coherence [Nakamura99, Cottet02, Vion02, Chiorescu03]. The decay of the coherent oscillations turned out to be sufficiently weak, such that

coherent oscillations could be observed. Still, decoherence represents a serious limitation for these experiments.

Quantum information processing and further issues of decoherence, namely the measurement problem, the appearance of a classical mechanics out of the quantum world are fields connected to all these experiments. In this thesis we will focus on the decoherence of two-state systems, being a key feature in the design of qubits.

1.1 Decoherence example, Markoffian, and non-Markoffian behavior

The effect of decoherence on a two-state system is that a coherent superposition of the two states is destroyed within a certain time scale, which is known as the decoherence time. The dynamics of a completely isolated the two-state system is coherent. Such a situation is never realized in practice, because in a physical setup there is always some coupling to the surrounding environment. Therefore, if one would like to create a model for decoherence, one can couple the two-state system to a much larger system or environment, which produces the described effect. To set an example of such an environment, we can consider a classical fluctuating external force, acting on the two-state system. A case in point is the loss of coherence in the Cooper-pair box experiment, where the simplest description of decoherence is achieved using a fluctuating gate voltage [Nakamura99]. If the environment acts like a classically fluctuating potential, then the system does not react back on the environment. Such an environment is called a non-dynamical environment because there is no significant effect on it.

The degree of coherence can be quantified with the density matrix: The system is in a coherent superposition of the basis states $|+\rangle$ and $|-\rangle$, if the density matrix is not diagonal in the $|+\rangle$, $|-\rangle$ representation. If the system is in a pure state, it is called completely coherent. In contrast, if the density matrix is diagonal it is referred to as an incoherent superposition of the basis states $|+\rangle$, $|-\rangle$ [Blum96]. The density matrix becomes diagonal over the time scale of the decoherence time

$$\begin{bmatrix} \rho_{++}(0) & \rho_{+-}(0) \\ \rho_{-+}(0) & \rho_{--}(0) \end{bmatrix} \rightarrow \begin{bmatrix} \rho_{++}(t) & 0 \\ 0 & \rho_{--}(t) \end{bmatrix}, \quad (1.1)$$

which quantifies decoherence.

The decay varies depending on the surrounding environment. To illustrate this concept, let us exemplify the specific results of such a decay due to a fluctuating classical Gaussian noise force $B(t)$. We take a look at the Hamiltonian of a two-state system with energy splitting 2ϵ and fluctuations $B(t)$

$$\mathcal{H}(t) = [\epsilon + B(t)]\hat{\sigma}_z. \quad (1.2)$$

Such a system could be a spin in a static and fluctuating magnetic field applied in the z -direction, see Fig. 1.2. A Gaussian process is a random process where, at every

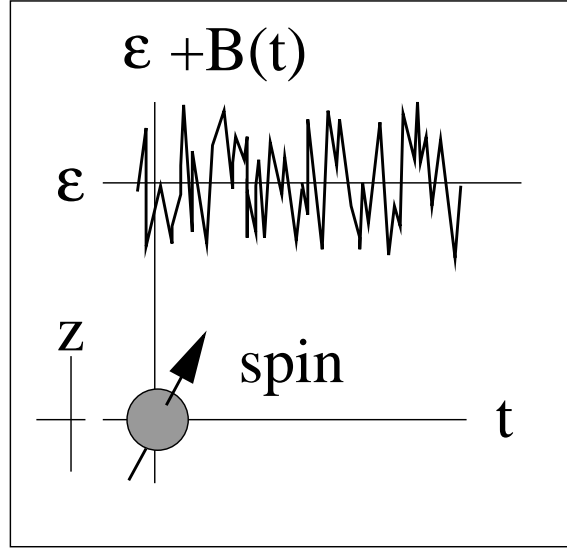


Figure 1.2: Spin in “magnetic field” applied in the z -direction fluctuating around its mean ϵ with strength $B(t)$.

point in time $B(\cdot)$ has a Gaussian probability distribution. A Gaussian process is characterized by the first two moments $\langle B(t) \rangle$ and $\langle B(t)B(0) \rangle$, i.e., all the higher moments can be expressed by the first two. The correlation function $\langle B(t)B(0) \rangle$ or its Fourier transform¹

$$\langle BB \rangle_{\omega} \equiv \frac{1}{2\pi} \int_{-\infty}^{+\infty} dt e^{i\omega t} \langle B(t)B(0) \rangle, \quad (1.3)$$

describe the correlations of the random process $B(\cdot)$ at various points in time. To be more precise, let us choose the following correlation function

$$\langle BB \rangle_{\omega} = \frac{\omega_0^2 \gamma}{\pi} \frac{1}{(\omega^2 - 4\omega_0^2)^2 + 4\omega^2 \gamma^2} \quad (1.4)$$

and a vanishing mean $\langle B(t) \rangle = 0$. Our choice of the correlation function describes so-called colored noise, where the memory and the history of the process plays a role. The solution for the off-diagonal element of the density matrix, with respect to the $\hat{\sigma}_z$ eigenbasis $\{|+\rangle, |-\rangle\}$, for one specific sample $B(t)$ of the Gaussian random process

$$\rho_{+-}(t) = \exp[-2i\epsilon t - i\Phi(t)] \rho_{+-}(0), \quad (1.5)$$

where $\Phi(t) \equiv 2 \int_0^t d\tau B(\tau)$ is a phase depending on the time integral over the sample. $B(t)$ has to be averaged over many different Gaussian noise fields, i.e., we form a superposition of many samples, each of them having a slightly different time evolution. In the beginning, at $t = 0$ the solutions all look the same with the same phase.

¹This convention for the Fourier transform will be used throughout the whole thesis.

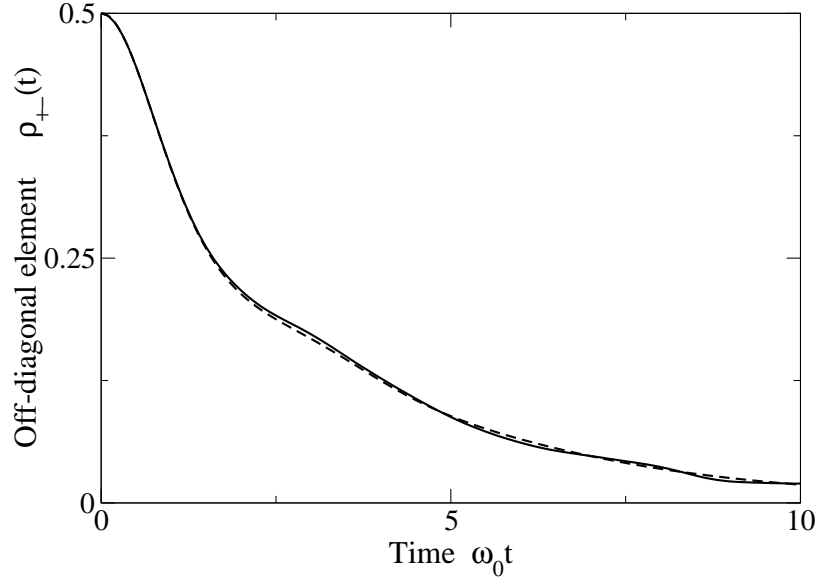


Figure 1.3: Decay under the action of a colored-noise field with the correlation function $\langle BB \rangle_\omega$ given by Eq. (1.4) starting from the $\hat{\sigma}_x$ eigenstate $(|+\rangle + |-\rangle)/\sqrt{2}$ as initial condition. Dashed line: analytical result, see Appendix A.1. Solid line: numerical simulation, averaged over many samples of numerically generated Gaussian processes. The parameters are: $\omega_0 = 1$ and $\gamma = 0.1/(2\pi)$.

However, as time evolves, they become more and more out of phase [Marquardt03]. They become randomized, such that on the average, a decay of the off-diagonal element shown in Fig. 1.3 occurs. The off-diagonal element of the density matrix is shown in the interaction picture with respect to $\mathcal{H}_0 = \epsilon \hat{\sigma}_z$ in order to emphasize the special features of the decay. For small times $\omega_0 t \ll 1$ the decay is of Gaussian shape and in the long-time limit $\omega_0 t \gg 1$, we find an exponential decay. Furthermore, the decay is pure dephasing because, in the chosen model, only the off-diagonal elements are affected, i.e., no thermalization of the diagonal elements takes place. Moreover, the dynamics is non-Markoffian. To illustrate this, let us look at the special case of white noise correlations, where the correlation function would be given by $\langle B(t)B(0) \rangle = \delta(t)$ or $\langle BB \rangle_\omega = 1/(2\pi)$. Further, the time evolution in the interaction picture is determined by

$$\rho_{+-}(t) = e^{-2t} \rho_{+-}(0). \quad (1.6)$$

Here, we have obtained an exponential decay. The environment has no memory or history. There is no connection between different time points of the external noisy field due to the environment. They are uncorrelated. This is what is referred to as a Markoffian process, unlike the colored noise case, where correlations of the noise field with times in the past are important. The same result could be obtained using a Markoff approximation, see, e.g., Chapter 2, which becomes exact in the limit of white-noise correlations, i.e., the bath-correlation time is zero.

1.2 Linear and Nonlinear Environments

In the last section we saw that quantum coherence can be destroyed by an external fluctuating force. This was an example of a non-dynamical environment. More generally, one can introduce dynamical environments. This is achieved by defining a second quantum system with many more degrees of freedom than the two-state system. A common choice is an environment which consists of many mutually non-interacting harmonic oscillators, with mass m_k , momentum \hat{p}_k , and coordinate \hat{x}_k :

$$\mathcal{H} = \Delta \hat{\sigma}_x - \hat{\sigma}_z \sum_k c_k \hat{x}_k + \sum_k \left[\frac{\hat{p}_k^2}{2m_k} + \frac{m_k \omega_k^2}{2} \hat{x}_k^2 \right]. \quad (1.7)$$

Each of these oscillators has a different frequency ω_k and a different coupling strength c_k to the two-state system. Moreover, the coupling $-\hat{\sigma}_z \sum_k c_k \hat{x}_k$ is assumed to be linear. Such an environment is called a linear oscillator bath. Linear baths can have different spectral distributions of the couplings c_k , which determines the bath spectral densities $J(\omega) = \sum_k \pi c_k^2 \delta(\omega - \omega_k) / (2m_k \omega_k)$. Ohmic bath-spectral densities, where $J(\omega) = \alpha \omega$, are common choices, although many studies assume a power law form. One other possibility is to choose an oscillator bath with a peaked bath spectral density. Here, there are well-defined peaks present at characteristic frequencies, i.e., the system couples to an environment, featuring rather strong resonances. Prominent examples are discussed in [Garg85, Thorwart00, Thorwart03, Wilhelm03a, Kleff03a]. In our work the same peaked non-ohmic bath spectral density shows up, e.g., due to the special choice of the measurement device, see Chapter 4. One group of popular environments is linear oscillator baths characterized by an appropriate bath spectral density. Photon and phonon baths, for example, are linear environments. However, the environment has a much more complicated structure in most cases.

When we talk about nonlinear environments, we think of environments which deviate from the linear oscillator bath. Therefore, one deals usually with nonlinear environments. Nonlinear environments, e.g., spin baths [Stamp00, Khaetskii02, Coish04] have received recent interest in the field of spin-based quantum computing [Loss98]. A spin bath is fundamentally different from an oscillator bath. It is a bath consisting of spins, each of which has only a few accessible states. Complementary to a linear oscillator bath the energy of a spin bath saturates at temperatures above the excitation energy. Every nonlinear bath is between these two extreme cases [Weiss00]. Another case-in-point was recently discussed in the context of the Nakamura experiment, where it is not clear which mechanism is responsible for the loss of coherence due to $1/f$ noise. In [Paladino02], a microscopic model of bistable fluctuators, each of them characterized by a switching rate and an effective bias voltage acting on a qubit was considered. It is not clear how many of such fluctuators are really involved in the decohering process, maybe only a few. The limit of a similar nonlinear bath corresponding to one such fluctuating charge is treated in our work, see Chapters 2 and 3.

Often, the general environments are approximated phenomenologically by linear

baths with an appropriate bath spectral density. One can show that this replacement becomes exact for small system-bath coupling, see Chapter 2, but in the general case, the two types of environments behave differently. For quantum computing one seeks the ideal of a completely controllable qubit system, weakly interacting with its environment. This constitutes the essential starting point for a qubit operation. Now one might ask why one needs to investigate nonlinear baths, because they can be mimicked by linear ones in the low-coupling limit of interest. For quantum computation, it is necessary to examine nonlinear environments for couplings which are small, but still high enough, such that the linear bath approximation might fail. This is exactly the regime of our interest, where we would like to reveal the differences between linear and nonlinear baths. A further reason is the following. Even if the induced decay rate is small, one can see non-Markoffian processes. This is the case if the bath has a peaked bath spectral density. Such non-Markoffian processes can depend on the linear or nonlinear nature of the bath.

1.3 Flow equation method

The flow-equation approach is a nice tool to treat quantum dissipative systems. The entire framework has been developed recently [Wegner94, Kehrein96b]. The flow equations are ordinary differential equations derived from a continuous basis transformation. Usually, a Hamiltonian is diagonalized using a set of discrete unitary transformations. The basic idea of the flow equations is to replace this discrete transformation by a continuous one. Thus, in principle, the flow equation formalism deals with infinitely many infinitesimal transformation steps. To carry out the transformation, the Hamiltonian \mathcal{H} is understood to be a function of a real flow parameter l

$$\mathcal{H}(0) \rightarrow \mathcal{H}(l). \quad (1.8)$$

$\mathcal{H}(0)$ is the initial operator and $\mathcal{H}(l \rightarrow \infty)$ is the simplified effective Hamiltonian. The continuous transformation is effected by $\mathcal{U}(l)$

$$\mathcal{H}(l) = \mathcal{U}(l)\mathcal{H}(0)\mathcal{U}^\dagger(l). \quad (1.9)$$

By introducing an infinitesimal generator $\hat{\eta}$ one can write the continuous transformation in analogy with the time evolution of the usual Schrödinger equation as

$$\frac{d}{dl}\mathcal{H}(l) = [\hat{\eta}(l), \mathcal{H}(l)], \quad (1.10)$$

with the initial condition $\mathcal{H}(0) = \mathcal{H}$ for the differential equation.

If one is interested in a certain observable \mathcal{O} , one has to transform it with the same transformation $\mathcal{U}(l)$. We are especially interested in correlation functions which depend on the Hamiltonian \mathcal{H} of the total system $\langle \mathcal{O}(t)\mathcal{O}(0) \rangle_{\mathcal{H}}$:

$$\langle \mathcal{O}_{l=0}(t)\mathcal{O}_{l=0}(0) \rangle_{\mathcal{H}(l=0)} \rightarrow \langle \mathcal{O}_{l \rightarrow \infty}(t)\mathcal{O}_{l \rightarrow \infty}(0) \rangle_{\mathcal{H}(l \rightarrow \infty)}. \quad (1.11)$$

Note that the trace appearing in the definition of the correlation function is basis independent. For each l of the flow, we have a different possible basis. It is, of course, most convenient to evaluate the correlation function for $l \rightarrow \infty$, where the Hamiltonian is supposed to have a simplified form. That is why the success of the flow equation method depends crucially on the choice of generator. Wegner proposed the following choice

$$\hat{\eta}(l) = [\mathcal{H}_0(l), \mathcal{H}(l)], \quad (1.12)$$

where $\mathcal{H}_0(l)$ is the diagonal part of $\mathcal{H}(l)$. At least for finite dimensional systems one can show that

$$\lim_{l \rightarrow \infty} \hat{\eta}(l) = 0, \quad (1.13)$$

which means that the initial Hamiltonian is always transformed to a block diagonal form, but a complete diagonalization is not guaranteed. Wegner's choice is certainly a good starting point, but generally the generator has to be adapted to the concrete problem under investigation. In Chapter 3 we use a modified generator which is appropriate for linear oscillator bath environments.

To illustrate and motivate the method, let us discuss a concrete introductory example. Let us assume, we wish to diagonalize the two-state Hamilton operator given with respect to a certain basis:

$$H = \begin{bmatrix} \epsilon & \Delta \\ \Delta & -\epsilon \end{bmatrix}. \quad (1.14)$$

The eigenvalues are given by $E_{\pm} = \pm\sqrt{\epsilon^2 + \Delta^2}$. Now we would like to do the same using the flow equation formalism. It is clear that generally this does not make sense in such a situation, but it is instructive to apply the method first in a well-understood, analytically solvable case. To start with, we understand the Hamiltonian as function of the flow parameter

$$H(l) = \begin{bmatrix} \epsilon(l) & \Delta(l) \\ \Delta(l) & -\epsilon(l) \end{bmatrix}, \quad (1.15)$$

where $H(0) = H$, i.e. $\epsilon(0) = \epsilon$ and $\Delta(0) = \Delta$. We choose now for $H_0(l)$ the canonical choice of Wegner, i.e., the diagonal part of the Hamiltonian

$$H_0(l) = \begin{bmatrix} \epsilon(l) & 0 \\ 0 & -\epsilon(l) \end{bmatrix}. \quad (1.16)$$

This leads to the following anti-hermitian generator $\eta(l)$

$$\eta(l) = [H_0(l), H(l)] = 2\epsilon(l)\Delta(l) \begin{bmatrix} 0 & 1 \\ -1 & 0 \end{bmatrix}. \quad (1.17)$$

Finally, we can write down the flow equations

$$\frac{d}{dl} H(l) = \frac{d}{dl} \begin{bmatrix} \epsilon(l) & \Delta(l) \\ \Delta(l) & -\epsilon(l) \end{bmatrix} = [\eta(l), H(l)] = \begin{bmatrix} 4\epsilon(l)\Delta(l)^2 & -4\epsilon(l)^2\Delta(l) \\ -4\epsilon(l)^2\Delta(l) & -4\epsilon(l)\Delta(l)^2 \end{bmatrix}. \quad (1.18)$$

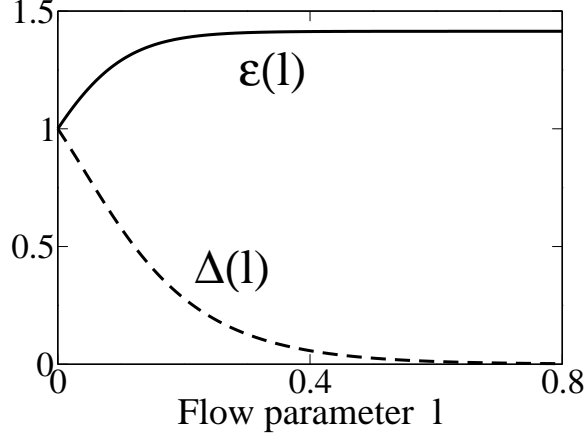


Figure 1.4: Solution of the flow equations starting from an initial Hamiltonian $H(0) = \sigma_x + 1$ specified by $\epsilon(0) = \Delta(0) = 1$. The flow equations lead to the result exponentially quickly.

Note that the Hamiltonian is a linear combination of the two basis operators σ_x and σ_z with coefficients $\epsilon(l)$ and $\Delta(l)$. The l -derivative leads to a derivative of the coefficients, therefore the right-hand side $dH(l)/dl$ remains a superposition of the same basis operators. The left-hand side $[\eta(l), H(l)]$ turns out to be a linear combination of the same basis. There are no new basis operators generated compared to the ones contained in $dH(l)/dl$. Therefore the flow equations are closed in this elementary example.

The whole procedure leads to two distinct ordinary differential equations

$$\begin{aligned} \frac{d}{dl}\epsilon(l) &= 4\epsilon(l)\Delta(l)^2 \\ \frac{d}{dl}\Delta(l) &= -4\epsilon(l)^2\Delta(l). \end{aligned} \quad (1.19)$$

These two equations can be solved analytically,

$$\begin{aligned} \epsilon(l) &= \left[\frac{(\Delta^2 + \epsilon^2)\epsilon^2 e^{8(\Delta^2 + \epsilon^2)l}}{\Delta^2 + \epsilon^2 e^{8(\Delta^2 + \epsilon^2)l}} \right]^{\frac{1}{2}} \\ \Delta(l) &= \left[\frac{(\Delta^2 + \epsilon^2)\Delta^2 e^{-8(\Delta^2 + \epsilon^2)l}}{\epsilon^2 + \Delta^2 e^{-8(\Delta^2 + \epsilon^2)l}} \right]^{\frac{1}{2}}, \end{aligned} \quad (1.20)$$

which is in general not possible for more complicated systems, where one has to integrate the differential equations numerically. The behavior of the solution is shown in Fig. 1.4. In the limit $l \rightarrow \infty$ the Hamiltonian is of diagonal form because we get $\epsilon(l \rightarrow \infty) = \sqrt{\epsilon^2 + \Delta^2}$ and $\Delta(l \rightarrow \infty) = 0$

$$\mathcal{H}(l \rightarrow \infty) = \begin{bmatrix} \epsilon(l \rightarrow \infty) & \Delta(l \rightarrow \infty) \\ \Delta(l \rightarrow \infty) & -\epsilon(l \rightarrow \infty) \end{bmatrix} = \begin{bmatrix} \sqrt{\epsilon^2 + \Delta^2} & 0 \\ 0 & -\sqrt{\epsilon^2 + \Delta^2} \end{bmatrix}. \quad (1.21)$$

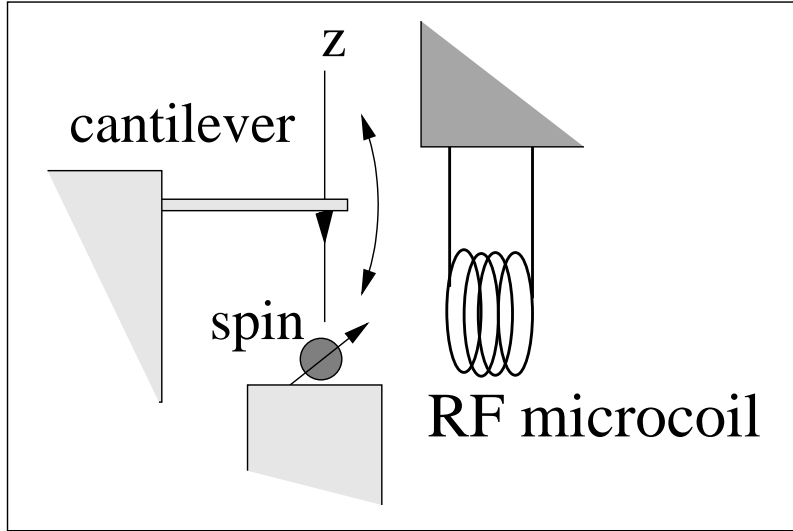


Figure 1.5: MRFM setup

We have seen that this example is solvable with flow equations without using any approximation. The reason for this is that the flow can be closed. However, this is not possible in the general case. We will use the flow-equation formalism to treat the dissipative four-state system, see Chapter 3. There we will see that we have to neglect certain terms in order to close the flow. Naturally, we must justify the approximation scheme later on.

1.4 Single-spin quantum measurement

So far we have only mentioned that the phase coherence of the qubit is lost due to unwished and uncontrollable decohering effects. The laws of quantum mechanics lead to additional peculiar behavior completely unrelated to macroscopic everyday-life experience. A quantum superposition is destroyed by the measurement, in contrast to classical physics, where perturbations due to a measurement can in principle be made negligibly small. Because the final stage of the read-out is governed by the laws of classical physics, a transition from the “quantum world” to the “classical world” is inevitable. The classical stage of the experiment is necessary and leads to controversies. We will not focus on these problems, but discuss a concrete model of a measurement of a spin one-half using magnetic resonance force microscopy (MRFM) [Sidles95], which might one day accomplish single-spin detection, one of its ultimate goals.

The idea of an MRFM measurement is to combine the principles of magnetic resonance imaging with the atomic precision of a scanning probe microscope. Fig. 1.5 shows a typical experimental setup. The key components are a sensitive cantilever probe with a high-coercivity ferromagnetic tip, a radio-frequency coil to manipulate

the spin at its Larmor frequency, and finally a fiber-optic interferometer to detect the tip motion. The applied magnetic fields are chosen such that adiabatic spin flips occur at a rate which equals the cantilever resonance frequency. The interaction between the magnetic tip and the magnetic moment of the spin leads to a spin-state dependent motion of the cantilever, which can be detected using optical methods.

Treating the system in an open way, interacting with a large surrounding environment, can be used to model certain types of quantum measurements. In contrast to a projective measurement, in a more realistic measurement model the measurement is done by a quantum device with a read-out variable which can be probed macroscopically. The MRFM-measurement setup can be modeled as an indirect measurement. This means that the quantum system, the spin, is measured via the cantilever which is also assumed to be a quantum object. To read out the result, the cantilever position is measured macroscopically by a classical laser interferometer. The decoherent dynamics of the system occurs in a controlled way, in the sense that we can decide when it should start. Contrary to a projective measurement, such a weak measurement does not occur instantaneously. Distinct time scales turn out to be important. A further discussion of these issues will be presented in detail in Chapter 4.

1.5 Leakage

So far the disturbance of quantum information processing due to decoherence has been reviewed. In contrast, in Chapter 5 we briefly discuss another perturbing effect, namely leakage. What is leakage? In the Cooper-pair box system the lowest two energy levels were used to implement the qubit, i.e., they constitute the computational basis. These two states are well-separated from the other levels. But still, a population transfer to higher levels may take place while controlling the qubit. This effect is denoted as leakage [Fazio99]. We investigate these effects in the context of a recent experiment in Saclay with a Josephson qubit [Cottet02, Vion02].

1.6 Outline

This thesis consists largely of a discussion of unconventional environments. It is organized in the following way. The first topic which is addressed in our work constitutes a new model for an environment, motivated by recent experiments. It is an example of a nonlinear bath having a variety of manifestations in miscellaneous realms of physics. To learn about the special behavior of a nonlinear environment we compare it with the results of a linear bath with an appropriate bath spectral density. The nonlinear bath is discussed in Chapter 2, where we focus on high temperatures, and in Chapter 3, where we treat the low-temperature limit. At low temperatures we are largely concerned with using flow equations.

The second major topic we investigate is addressed in Chapter 4, where we outline the in-depth analysis of the measurement of a spin one-half using magnetic resonance

force microscopy. Finally, we provide a brief summary and give an outlook, reporting some open questions.

Chapter 2

Non-Markoffian Effects of a Nonlinear Bath

We analyze a model of a nonlinear bath consisting of a single two-level system coupled to a linear bath. This allows us to study the effects of a nonlinear, non-Markoffian bath in a particularly simple situation. First, we analyze the effects of this bath on the dynamics of a spin by calculating the decay of the equilibrium correlator of the spin's z -component. The purpose of this work is to compare the exact results with those obtained by substituting a linear bath for the original nonlinear bath. On the whole, we show results for two limits, namely, low and high temperatures. In this chapter we concentrate on high temperatures.

2.1 Introduction

The linear bath of oscillators plays a prominent role in discussions of dissipation and decoherence [Caldeira83b, Caldeira83c, Weiss00]. Moreover, in the classical limit, the force fluctuations derived from a linear bath correspond to a Gaussian random process. Although this is a generic case (due to the central limit theorem), there are physical situations when non-Gaussian random processes are important. Here, we examine the simplest possible quantum-mechanical bath whose fluctuations correspond to classical telegraph noise: a single two-level system subject to a white noise force. The effects of this nonlinear bath are analyzed by coupling it, in turn, to a spin, whose relaxational dynamics under the action of the bath is calculated.

In the literature, another type of physically relevant nonlinear bath is often discussed: the spin bath [Stamp00, Khaetskii02], consisting of a large number of spins which are coupled to the system under consideration. Our model system is simpler since it contains only a single “nonlinear element”, the two-level system. In our system, irreversibility is generated, not from a larger number of spins, but by the coupling to the linear bath. Although designed as a drastically simplified model system, it may be physically relevant, e.g., for charged tunneling systems [Paladino02] in the vicinity of a mesoscopic quantum-coherent device (e.g. a Cooper-pair box [Nakamura99]),

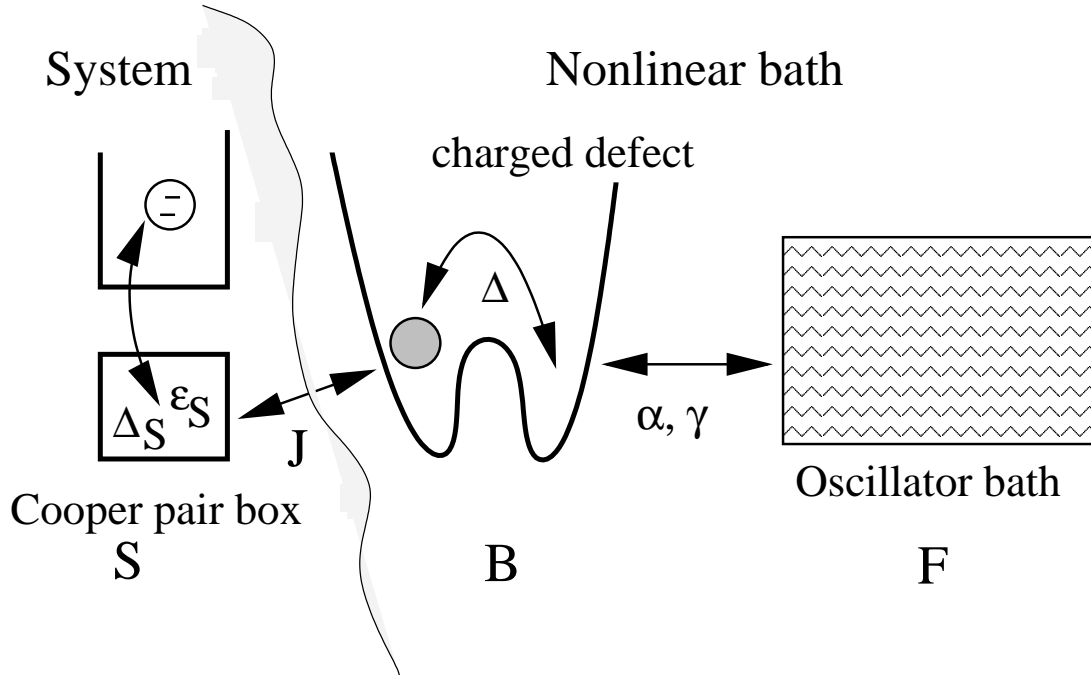


Figure 2.1: Possible application of the nonlinear-bath model: A Cooper pair box under the influence of fluctuating gate charges.

which lead to electrostatic potential fluctuations and which are, themselves, also subject to dissipation and decoherence by their environment, see Fig. 2.1. Viewed as a whole, our model consists of two coupled two-level systems, one of which is coupled to a linear bath. Of course, such systems have been studied before, both in the context of the quantum measurement problem [Zurek81] and decoherence of coupled qubit systems. The model of two spins (qubits) coupled to an environment has been analyzed in detail in [Loss98], [Dube01], [Governale01], and [Thorwart02]. However, our perspective and the questions addressed in this work are different from these approaches, since we are interested primarily in the differences arising from substituting the nonlinear bath (in the form of the dissipative two-level system) by a linear bath (see Fig. 2.3). This question is relevant, since, in many physical situations where the precise nature of the bath decohering a given system is unknown, it is treated as a linear bath, with some given correlation function. It is, therefore, desirable to understand in more detail the type and magnitude of possible errors introduced by such an approximation, in cases where the coupling cannot be assumed to be weak.

The basic strategy is to calculate the equilibrium correlator of the two-level system exactly (which can be done without any further approximation in the limit of infinite temperature) and to compare the results to three common approximations. One approximation involves replacing the nonlinear bath by a linear bath, whose correlation function is chosen to be the same as that of the nonlinear bath. Other approximations involve a Markoffian master equation and a weak-coupling, applied

to the dynamics of the spin under the influence of the bath.

Let us now sketch the general structure of the chapter, which is organized as follows: Before we give the model Hamiltonian in Sec. 2.6, we recall in Secs. 2.2–2.5 some general features of linear and nonlinear environments. Secs. 2.8, 2.10, 2.11 and 2.13, describe the four different approaches, which are defined by specifying the evolution equation for the density matrix in each case. For each approach, we explain how the equilibrium correlator of the z -component of the spin may be obtained by solving these equations. Finally, we present plots showing numerical results for the spin correlator, along with a comparison of the different approaches.

2.2 The linear oscillator bath

Before we discuss our model of a nonlinear environment, we introduce the common model for an environment or bath known as the linear oscillator bath [Caldeira83b, Caldeira83c, Weiss00]. The Heisenberg equations of motion are linear for the operators of the oscillator bath problem and this is the origin of the name. The bath consists of a large number of non-interacting oscillators, each with a distinct frequency and a different coupling strength to the system under consideration. The spectral distribution of all these couplings is described by the bath-spectral density. The Hamiltonian for system, bath, and interaction is given by

$$\mathcal{H} = \mathcal{H}_S + \sum_k \left[\frac{\hat{p}_k^2}{2m_k} + \frac{m_k \omega_k^2}{2} \left(\hat{x}_k - \frac{c_k}{m_k \omega_k^2} \hat{q} \right)^2 \right]. \quad (2.1)$$

The operators \hat{p}_k and \hat{x}_k are the momentum and coordinate of the k -th oscillator and m_k, ω_k are the associated mass and frequency respectively. Note that the interaction part of the Hamiltonian is also linear in the oscillator coordinates. \mathcal{H}_S is the system Hamiltonian and \hat{q} is an operator which acts only on the system part of the Hilbert space. These operators are left unspecified. The coupling strength of the k -th oscillator to the system is c_k and the bath-spectral density is defined by

$$J(\omega) \equiv \frac{\pi}{2} \sum_k \frac{c_k^2}{m_k \omega_k} \delta(\omega - \omega_k). \quad (2.2)$$

A common choice for $J(\omega)$ would be a linear frequency dependence

$$J(\omega) = \alpha \omega f\left(\frac{\omega}{\omega_C}\right). \quad (2.3)$$

A bath with such a spectral density is called an ohmic bath. $f(x)$ is the cutoff function which is defined such that $J(\omega)$ is negligible for $\omega \gg \omega_C$. In the rest of this thesis we assume a sharp cutoff, i.e. $f(x) \equiv \Theta(1 - x)$. Note that the Hamiltonian \mathcal{H} also contains a counter-term which does not depend on the dynamical variable \hat{x}_k of the environment. This additional potential term compensates the renormalization of the system potential.

We rewrite the linear oscillator bath Hamiltonian in terms of creation and annihilation operators with Bose commutation relations. We use $\hat{x}_k = (1/\sqrt{2m_k\omega_k})(\hat{b}_k^\dagger + \hat{b}_k)$ and $\hat{p}_k = i\sqrt{m_k\omega_k/2}(\hat{b}_k^\dagger - \hat{b}_k)$ and obtain

$$\mathcal{H} = \mathcal{H}_S + \sum_k \left[\omega_k \hat{b}_k^\dagger \hat{b}_k - \frac{c_k}{\sqrt{2m_k\omega_k}} \hat{q}(\hat{b}_k^\dagger + \hat{b}_k) + \frac{c_k^2}{2m_k\omega_k^2} \hat{q}^2 \right]. \quad (2.4)$$

If $\hat{q}^2 = \hat{1}$, which is true for our systems, where $\hat{q} = \hat{\sigma}_z$ and $\hat{q} = \hat{1} \otimes \hat{\sigma}_z$ respectively, we find

$$\mathcal{H} = \mathcal{H}_S + \sum_k \left[\omega_k \hat{b}_k^\dagger \hat{b}_k - \lambda_k \hat{q}(\hat{b}_k^\dagger + \hat{b}_k) \right] + E. \quad (2.5)$$

The constant energy shift E leads to a global phase and does not play a role when we calculate correlation functions. This shift is therefore omitted in further considerations in this chapter and Chapter 3. The λ_k are found to be

$$\lambda_k = \frac{c_k}{\sqrt{2m_k\omega_k}} \quad (2.6)$$

and the bath spectral density in terms of the λ_k is given by

$$J(\omega) = \pi \sum_k \lambda_k^2 \delta(\omega - \omega_k). \quad (2.7)$$

One way of studying the decoherence of a two-state system or a spin is to couple it to a linear oscillator bath. Here we introduce the relevant popular spin-boson model. This is a well-studied model which has yielded considerable insight into the decoherence of two-state systems. The spin-boson model is governed by the Hamiltonian

$$\mathcal{H} = \Delta \hat{\sigma}_x + \epsilon \hat{\sigma}_z - \hat{\sigma}_z \sum_k \lambda_k (\hat{b}_k^\dagger + \hat{b}_k) + \sum_k \omega_k \hat{b}_k^\dagger \hat{b}_k. \quad (2.8)$$

The special case of $\epsilon = 0$ is called the symmetric spin-boson system. In this chapter and in Chapter 3 we will present numerical solutions of the spin-boson problem. The model will appear in two places: First when we calculate the bath-spectral density of the nonlinear bath and second, when we perform the linear bath approximation on the nonlinear bath, see Sec. 2.11.

The case $\Delta = 0$ describes a pure dephasing situation without relaxation to thermal equilibrium. This case can be solved in closed form. We will use this solution in Chapter 4, where a time-dependent coupling occurs.

2.3 The Feynman-Vernon influence functional

Feynman's path integral is a very clear approach to the physics of quantum mechanics, although lacking in mathematical rigor. This formalism can be applied to open

quantum systems to give a very ostensive description of the reduced dynamics. In this section we recall the main ideas and results for the Feynman-Vernon influence functional applied to the linear oscillator environment first obtained in [Feynman63].

The state of the whole system can be written as a path integral

$$\psi(q_t, X_t, t) = \int \mathcal{D}q \mathcal{D}X e^{iS_S[q] + iS_I[q, X] + iS_B[X]} \psi(q_0, X_0, 0), \quad (2.9)$$

where the actions $S_S[q]$, $S_I[q, X]$ and $S_B[X]$ belong to the system, interaction and environment. We make the assumption of factorized initial conditions

$$\psi(q_0, X_0, 0) = \psi_0(q_0) \chi_0(X_0), \quad (2.10)$$

which means that the system and the reservoir are independent at $t = 0$. The state of the whole system can be written as a path integral over the free non-interacting system combined with a path integral over the interaction part

$$\begin{aligned} \psi(q_t, X_t, t) &= \int \mathcal{D}q e^{iS_S[q]} \psi_0(q_0) \int \mathcal{D}X e^{iS_I[q, X] + iS_B[X]} \chi_0(X_0) \\ &= \int \mathcal{D}q e^{iS_0[q]} \psi_0(q_0) \chi(X_t | q(\cdot)), \end{aligned} \quad (2.11)$$

where

$$\chi(X_t | q(\cdot)) = \int \mathcal{D}X e^{iS_I[q, X] + iS_B[X]} \chi_0(X_0). \quad (2.12)$$

$\chi(X_t | q(\cdot))$ is the bath state evolved from $\chi_0(X_0)$ under the action of the c-number path $q(\cdot)$. The system drives the reservoir via the c-number $q(\cdot)$. The density matrix of the whole system can be found to be

$$\rho(q_t^>, q_t^<, X_t^>, X_t^<, t) = \psi(q_t^>, X_t^>, t) \psi(q_t^<, X_t^<, t)^*. \quad (2.13)$$

The reduced density matrix is obtained by taking a trace over the reservoir degrees of freedom (integral over X_t)

$$\rho(q_t^>, q_t^<, t) = \int dX_t \psi(q_t^>, X_t, t) \psi(q_t^<, X_t, t)^*. \quad (2.14)$$

$$\begin{aligned} \rho(q_t^>, q_t^<, t) &= \int dX_t \left[\int \mathcal{D}q^> e^{iS_S[q^>]} \psi_0(q_0^>) \chi(X_t | q^>(\cdot)) \right] \\ &\quad \times \left[\int \mathcal{D}q^< e^{iS_S[q^<]} \psi_0(q_0^<) \chi(X_t | q^<(\cdot)) \right]^*, \end{aligned} \quad (2.15)$$

which defines the Feynman-Vernon influence functional $\mathcal{F}[q^>, q^<]$ and leads to

$$\rho(q_t^>, q_t^<, t) = \int \mathcal{D}q^> \mathcal{D}q^< e^{iS_S[q^>] - iS_S[q^<]} \mathcal{F}[q^>, q^<] \rho_0(q_0^>, q_0^<, 0). \quad (2.16)$$

The density matrix $\rho_0(q_0^>, q_0^<, 0) = \psi_0(q_0^>)\psi_0(q_0^<)^*$ is the initial density matrix of the system and $\mathcal{F}[q^>, q^<]$ is the influence functional given by

$$\mathcal{F}[q^>, q^<] = \int dX_t \chi(X_t|q^>(\cdot))\chi(X_t|q^<(\cdot))^* = \langle \mathcal{U}(t, 0|q^<) \chi_0 | \mathcal{U}(t, 0|q^>) \chi_0 \rangle_{\chi_0}. \quad (2.17)$$

For the case of finite temperatures a thermal average over χ_0 is necessary

$$\mathcal{F}[q^>, q^<] = Z_B^{-1} \text{tr}_B \left\{ e^{-\beta \mathcal{H}_B} \hat{T}_A e^{i \int_0^t ds \mathcal{H}_I(q^<(s))} \hat{T} e^{-i \int_0^t ds \mathcal{H}_I(q^>(s))} \right\}, \quad (2.18)$$

where $Z_B = \text{tr}_B \left\{ e^{-\beta \mathcal{H}_B} \right\}$ is the partition function and \hat{T}_A is the anti-time ordering. A shorter notation is possible using a Keldysh time-ordering along a contour C in the complex plane

$$\mathcal{F}[q] = Z_B^{-1} \text{tr}_B \left\{ e^{-\beta \mathcal{H}_B} \hat{T}_C e^{-i \oint_C d\tau \mathcal{H}_I(q(\tau))} \right\} = \left\langle \hat{T}_C e^{-i \oint_C d\tau \mathcal{H}_I(q(\tau))} \right\rangle_{\beta}, \quad (2.19)$$

where $q(\tau) = q^>(\tau)$ on the forward path $0 \rightarrow t$ and $q(\tau) = q^<(\tau)$ on the backward path $t \rightarrow 0$. The reduced dynamics can then be written as

$$\rho(q_t^>, q_t^<, t) = \int \mathcal{D}q e^{i S_S[q]} \mathcal{F}[q] \rho_0(q_0^>, q_0^<, 0). \quad (2.20)$$

The action is integrated along the contour C

$$S_S[q] = \oint_C d\tau L_S(q, \dot{q}), \quad (2.21)$$

where $\dot{q} = \frac{dq}{d\tau}$.

Our aim is now to apply these results to the oscillator environment. Specializing to the linear oscillator bath environment, we use the interaction given in Eq. (2.1)

$$\mathcal{H}_I = -\hat{q} \sum_k c_k x_k \equiv -\hat{q} \hat{X}. \quad (2.22)$$

We can introduce the bath-correlation function for the linear bath

$$\langle \hat{X}(t) \hat{X}(t') \rangle \equiv K_R(t - t') + i K_I(t - t'), \quad (2.23)$$

where $K_R(t)$ and $K_I(t)$ are its real and imaginary part

$$K_R(t) \equiv \frac{1}{\pi} \int_0^\infty d\omega J(\omega) \cos(\omega t) \coth\left(\frac{\beta\omega}{2}\right) \quad (2.24)$$

and

$$K_I(t) \equiv -\frac{1}{\pi} \int_0^\infty d\omega J(\omega) \sin(\omega t). \quad (2.25)$$

After a cumulant expansion we get for the Feynman-Vernon influence functional

$$\mathcal{F}[q] = e^{-\frac{1}{2} \oint_C d\tau \oint_C d\tau' \langle \hat{T}_C \hat{X}(\tau) \hat{X}(\tau') \rangle_\beta q(\tau) q(\tau')}, \quad (2.26)$$

where $\langle \cdot \rangle_\beta = Z_B^{-1} \text{tr}_B \{ \cdot \}$ is the thermal average. The cumulant expansion cannot be done for a general nonlinear environment. This is a special feature of the linear bath with linear coupling. For nonlinear environments higher-order correlation functions do play a role, e.g., four-time correlation functions being averages of four operators.

Using the expressions for the bath-correlation function, the influence functional can then be put into the form

$$\begin{aligned} \mathcal{F}[q^>, q^<] &= \exp \left(- \int_0^t d\tau \int_0^\tau d\tau' \left\{ i[q^>(\tau) - q^<(\tau)] K_I(\tau - \tau') [q^>(\tau') + q^<(\tau')] \right. \right. \\ &\quad \left. \left. + [q^>(\tau) - q^<(\tau)] K_R(\tau - \tau') [q^>(\tau) - q^<(\tau')] \right\} \right), \end{aligned} \quad (2.27)$$

and finally introducing relative coordinates $R = (q^> + q^<)/2$ and $r = (q^> - q^<)/2$ we find

$$\begin{aligned} \mathcal{F}[R, r] &= \exp \left(\frac{1}{\pi} \int_0^\infty d\omega J(\omega) \int_0^t d\tau \int_0^\tau d\tau' \left\{ 2ir(\tau) \sin(\omega(\tau - \tau')) R(\tau') \right. \right. \\ &\quad \left. \left. - r(\tau) \cos(\omega(\tau - \tau')) \coth \left(\frac{\beta\omega}{2} \right) r(\tau') \right\} \right), \end{aligned} \quad (2.28)$$

or in terms of the bath-correlation function:

$$\begin{aligned} \mathcal{F}[R, r] &= \exp \left(- \int_0^t d\tau \int_0^\tau d\tau' \left\{ 2ir(\tau) K_I(\tau - \tau') R(\tau') \right. \right. \\ &\quad \left. \left. + r(\tau) K_R(\tau - \tau') r(\tau') \right\} \right). \end{aligned} \quad (2.29)$$

Note that we have made no assumption about the bath-spectral density of the linear oscillator bath. For later use in Chapter 4, we simplify Eq. (2.29) further for the special choice of an ohmic bath-spectral density, as in Eq. (2.3), according to [Caldeira83b]. In the limit $\omega_C \rightarrow \infty$ the imaginary part of the correlation function becomes

$$K_I(t) = \alpha \frac{d}{dt} \delta(t). \quad (2.30)$$

Integrating the first term in the exponent of $\mathcal{F}[R, r]$ by parts, we obtain

$$\begin{aligned} &2i \int_0^t d\tau \int_0^\tau d\tau' r(\tau) K_I(\tau - \tau') R(\tau') \\ &= 2i\alpha \int_0^t d\tau \int_0^\tau d\tau' r(\tau) \frac{d}{d(\tau - \tau')} \delta(\tau - \tau') R(\tau') \end{aligned} \quad (2.31)$$

$$= -2i\alpha \int_0^t d\tau R(\tau) r(\tau) \delta(0) + i\alpha \int_0^t d\tau \dot{R}(\tau) r(\tau), \quad (2.32)$$

where

$$\delta(0) = \lim_{\omega_C \rightarrow \infty} \frac{\omega_C}{\pi}, \quad (2.33)$$

which exactly cancels the counter-term introduced in Eq. (2.1), because

$$\frac{\alpha\omega_C}{\pi} = \frac{1}{\pi} \int_0^{\omega_C} d\omega \frac{J(\omega)}{\omega} = \sum_k \frac{c_k^2}{2m_k\omega_k^2}. \quad (2.34)$$

We obtain the final result for the Ohmic bath-spectral density:

$$\mathcal{F}[R, r] = \exp \left(-i\alpha \int_0^t d\tau \dot{R}(\tau)r(\tau) - \int_0^t d\tau \int_0^\tau d\tau' r(\tau)K_R(\tau - \tau')r(\tau') \right). \quad (2.35)$$

Now, together with this ohmic influence functional one must use a system action which no longer includes the counter-term. We will see later in Chapter 4, where this result for the Ohmic bath spectral density is used further, that this action leads to decoupled equations of motion (see Eq. (4.50) and Eq. (4.51)). Decoupling the equations of motion makes their solution simpler.

2.4 Non-linear environments

Every environment which is not a linear oscillator bath with linear coupling, we call a nonlinear bath. In contrast to the linear oscillator bath, the physics of nonlinear environments is surveyed to a lesser extent. Many problems in this field remain unsolved.

To quote an example, let us look at the spin bath [Caldeira93, Stamp00, Khaetskii02]. The total Hamiltonian consists of three parts

$$\mathcal{H} = \mathcal{H}_S + \mathcal{H}_I + \mathcal{H}_B. \quad (2.36)$$

The interaction and the bath Hamiltonian are defined by

$$\mathcal{H}_I = - \sum_k J_k \hat{q} \otimes \hat{\sigma}_x^k \quad (2.37)$$

and

$$\mathcal{H}_B = \sum_k \frac{\omega_k}{2} \hat{\sigma}_z^k. \quad (2.38)$$

We can regard the spins of this bath as the projection onto the first two levels of each oscillator in the oscillator bath.

Nonlinear couplings also lead to nonlinear baths. One recent example [Makhlin03a, Makhlin03b] is a Josephson qubit controlled at an optimal point where quadratic low-frequency noise plays a role

$$\mathcal{H} = -\frac{1}{2}[\Delta E \hat{\sigma}_z + \lambda X^2 \hat{\sigma}_z + \zeta Y \hat{\sigma}_x]. \quad (2.39)$$

The Hamiltonian describes a quadratic longitudinal and a linear transverse coupling. X and Y are assumed to be Gaussian noise sources.

2.5 Non-linear baths in the weak-coupling limit

If we wish to learn about the special behavior of our nonlinear bath, we have to compare it with a linear one, i.e., the quantum system is analyzed twice, once by coupling it to a nonlinear bath and then to a linear one. To quantify the deviations we need a limit, where the two completely different environments lead to the same behavior of the system, and moreover, we also need to know how to choose the linear bath by defining an appropriate bath spectral density. In this section we will see that every non-linear bath behaves like a linear oscillator bath, if the coupling between bath and system is sufficiently small [Caldeira93, Weiss00]. The oscillator bath which shows a similar behavior as the nonlinear one is characterized by a bath-spectral density, which depends on the nonlinear environment. Additionally, one has to choose, for each temperature, a different bath spectral density, in order to approximate the nonlinear bath in an optimal way. The derivation of this optimal choice is given in this section.

To begin, we assume to have a general system, interaction, and bath

$$\mathcal{H} = \mathcal{H}_S + \mathcal{H}_I + \mathcal{H}_B, \quad (2.40)$$

where \mathcal{H}_S represents the system Hamiltonian. \mathcal{H}_I is a separable interaction

$$\mathcal{H}_I = \hat{x} \otimes \hat{B}, \quad (2.41)$$

where \hat{x} acts on the system and \hat{B} acts on the environment part of the Hilbert space. Further, we use the convention that the operator \hat{B} also contains the coupling strength between system and bath, i.e., \hat{B} is equal to the coupling strength times some operator which acts on the bath part of the Hilbert space. Finally, \mathcal{H}_B describes the environment.

The Feynman-Vernon influence functional [Caldeira93] is given by

$$\mathcal{F}[x, y] = Z_B^{-1} \text{tr}_B \left\{ e^{-\beta \mathcal{H}_B} A_{y'y}(0, t) A_{xx'}(t, 0) \right\}, \quad (2.42)$$

where

$$A_{y'y}(0, t) = \hat{T}_A \exp \left[i \int_0^t d\tau \tilde{\mathcal{H}}_I(y(\tau)) \right] e^{i \mathcal{H}_B t}, \quad (2.43)$$

$$A_{xx'}(t, 0) = e^{-i \mathcal{H}_B t} \hat{T} \exp \left[-i \int_0^t d\tau \tilde{\mathcal{H}}_I(x(\tau)) \right], \quad (2.44)$$

and

$$\tilde{\mathcal{H}}_I(x(\tau)) = e^{i \mathcal{H}_B \tau} \mathcal{H}_I(x(\tau)) e^{-i \mathcal{H}_B \tau} \quad (2.45)$$

is the interaction Hamiltonian, written in the interaction representation. This result can be obtained from Eq. (2.18) using the relation

$$\hat{T} e^{-i \int_0^t d\tau \mathcal{H}_I(x(\tau))} = e^{-i \mathcal{H}_B t} \hat{T} e^{-i \int_0^t d\tau \tilde{\mathcal{H}}_I(x(\tau))}, \quad (2.46)$$

where $x(\tau)$ is the forward path $q^>(\tau)$ and $y(\tau)$ is the backward path $q^<(\tau)$, respectively. We are interested in the weak-coupling expansion of the influence functional and calculate the expressions up to second order in the interaction strength. We get

$$A_{y'y}(0, t) \approx \left[1 + i \int_0^t d\tau \tilde{\mathcal{H}}_I(y(\tau)) - \int_0^t d\tau \int_0^\tau d\tau' \tilde{\mathcal{H}}_I(y(\tau)) \tilde{\mathcal{H}}_I(y(\tau')) \right] e^{i\mathcal{H}_B t} \quad (2.47)$$

and

$$A_{xx'}(t, 0) \approx e^{-i\mathcal{H}_B t} \left[1 + i \int_0^t d\tau \tilde{\mathcal{H}}_I(x(\tau)) - \int_0^t d\tau \int_0^\tau d\tau' \tilde{\mathcal{H}}_I(x(\tau)) \tilde{\mathcal{H}}_I(x(\tau')) \right]. \quad (2.48)$$

The second order approximation of the influence functional is found to be

$$\mathcal{F}[x, y] \approx 1 - \int_0^t d\tau \int_0^\tau d\tau' \left[\langle \tilde{\mathcal{H}}_I(y(\tau')) \tilde{\mathcal{H}}_I(y(\tau)) \rangle + \langle \tilde{\mathcal{H}}_I(y(\tau)) \tilde{\mathcal{H}}_I(x(\tau')) \rangle - \langle \tilde{\mathcal{H}}_I(y(\tau)) \tilde{\mathcal{H}}_I(x(\sigma)) \rangle - \langle \tilde{\mathcal{H}}_I(y(\sigma)) \tilde{\mathcal{H}}_I(x(\tau)) \rangle \right], \quad (2.49)$$

where $\langle \cdot \rangle$ denotes the thermal average over the bath. $\langle \tilde{\mathcal{H}}_I(x(\tau)) \rangle$ is assumed to be zero, so all linear terms vanish. In the next step we express the influence functional in terms of the bath correlation function $\langle B(\tau)B(\sigma) \rangle$

$$\mathcal{F}[x, y] \approx 1 - \int_0^t d\tau \int_0^\tau d\tau' \left[y(\tau')y(\tau) \langle B(\tau')B(\tau) \rangle + x(\tau)x(\tau') \langle B(\tau)B(\tau') \rangle - y(\tau)x(\tau') \langle B(\tau)B(\tau') \rangle - y(\tau')x(\tau) \langle B(\tau')B(\tau) \rangle \right]. \quad (2.50)$$

Using the operator identity

$$\hat{A}\hat{B} = \frac{1}{2}[\hat{A}, \hat{B}] + \frac{1}{2}\{\hat{A}, \hat{B}\} \quad (2.51)$$

this can be rearranged to give

$$\mathcal{F}[x, y] \approx 1 - \int_0^t d\tau \int_0^\tau d\tau' \left[\frac{1}{2} \left(y(\tau') + x(\tau') \right) \left(y(\tau) - x(\tau) \right) \langle [B(\tau'), B(\tau)] \rangle + \frac{1}{2} \left(y(\tau') - x(\tau') \right) \left(y(\tau) - x(\tau) \right) \langle \{B(\tau'), B(\tau)\} \rangle \right]. \quad (2.52)$$

We introduce relative coordinates $R = (x + y)/2$ and $r = x - y$, respectively, in order to find

$$\mathcal{F}[R, r] \approx 1 - \int_0^t d\tau \int_0^\tau d\tau' \left[-r(\tau)R(\tau') \langle [B(\tau'), B(\tau)] \rangle + \frac{1}{2}r(\tau)r(\tau') \langle \{B(\tau'), B(\tau)\} \rangle \right]. \quad (2.53)$$

To proceed, we introduce the Fourier transform of the bath-correlation function

$$\langle BB \rangle_{\omega}^T = \frac{1}{2\pi} \int_{-\infty}^{\infty} dt e^{i\omega t} \langle B(t)B(0) \rangle. \quad (2.54)$$

We have

$$\langle BB \rangle_{\omega}^T = \frac{1}{2}(\langle BB \rangle_{\omega}^T + \langle BB \rangle_{-\omega}^T) + \frac{1}{2}(\langle BB \rangle_{\omega}^T - \langle BB \rangle_{-\omega}^T). \quad (2.55)$$

For the symmetric part:

$$\frac{1}{2}(\langle BB \rangle_{\omega}^T + \langle BB \rangle_{-\omega}^T) = \frac{1}{2\pi} \int_{-\infty}^{\infty} dt e^{i\omega t} \frac{1}{2} \langle \{B(t), B(0)\} \rangle, \quad (2.56)$$

and for the anti-symmetric part:

$$\frac{1}{2}(\langle BB \rangle_{\omega}^T - \langle BB \rangle_{-\omega}^T) = \frac{1}{2\pi} \int_{-\infty}^{\infty} dt e^{i\omega t} \frac{1}{2} \langle [B(t), B(0)] \rangle. \quad (2.57)$$

In terms of the symmetric and antisymmetric parts, we find

$$\begin{aligned} \mathcal{F}[R, r] \approx & 1 - \int_0^t d\tau \int_0^{\tau} d\tau' \int_{-\infty}^{\infty} d\omega \left[-2r(\tau)R(\tau') \left[\frac{1}{2}(\langle BB \rangle_{\omega}^T - \langle BB \rangle_{-\omega}^T) \right] e^{-i\omega(\tau'-\tau)} \right. \\ & \left. + r(\tau)r(\tau') \left[\frac{1}{2}(\langle BB \rangle_{\omega}^T + \langle BB \rangle_{-\omega}^T) \right] e^{-i\omega(\tau'-\tau)} \right]. \end{aligned} \quad (2.58)$$

Using the fluctuation dissipation theorem,

$$\langle BB \rangle_{-\omega}^T = e^{-\beta\omega} \langle BB \rangle_{\omega}^T, \quad (2.59)$$

so we find

$$\begin{aligned} \mathcal{F}[R, r] \approx & 1 - \int_0^t d\tau \int_0^{\tau} d\tau' \int_0^{\infty} d\omega \langle BB \rangle_{\omega}^T (1 + e^{-\beta\omega}) \left[r(\tau)r(\tau') \cos(\omega(\tau - \tau')) \right. \\ & \left. - 2ir(\tau)R(\tau') \tanh\left(\frac{\beta\omega}{2}\right) \sin(\omega(\tau - \tau')) \right]. \end{aligned} \quad (2.60)$$

Since we consider only terms up to second order in J , we can use $1 - x^2 \approx e^{-x^2}$, valid for small $x \ll 1$, leading to

$$\begin{aligned} \mathcal{F}[R, r] \approx & \exp \left\{ - \int_0^t d\tau \int_0^{\tau} d\tau' \int_0^{\infty} d\omega \langle BB \rangle_{\omega}^T (1 + e^{-\beta\omega}) \left[r(\tau)r(\tau') \cos(\omega(\tau - \tau')) \right. \right. \\ & \left. \left. - 2ir(\tau)R(\tau') \tanh\left(\frac{\beta\omega}{2}\right) \sin(\omega(\tau - \tau')) \right] \right\}. \end{aligned} \quad (2.61)$$

Comparing this result with the influence functional for the linear bath environment, Eq. (2.29), we see that the nonlinear bath is similar to the linear one for low coupling J , if one chooses the bath spectral density of the linear bath to be

$$J_{\text{nonlinear}}^T(\omega) = \pi \langle BB \rangle_{\omega}^T (1 - e^{-\beta\omega}). \quad (2.62)$$

This is the main result of this section. To summarize, the effects of a nonlinear environment are described up to second order in the coupling by a linear bath with a temperature-dependent bath-spectral density.

For later purposes we note two special cases. First, the zero temperature case used in Chapter 3

$$J_{\text{nonlinear}}^0(\omega) = \pi \langle BB \rangle_{\omega}^0, \quad (2.63)$$

and second, the infinite temperature result used in this chapter

$$\mathcal{F}[R, r] \approx \exp\left\{-\int_0^t d\tau \int_0^{\tau} d\tau' \int_{-\infty}^{\infty} d\omega \langle BB \rangle_{\omega} r(\tau) r(\tau') \cos(\omega(\tau - \tau'))\right\}, \quad (2.64)$$

where the influence functional is the one for a classical fluctuating Gaussian noise force $B(t)$, with the correlation function $\langle BB \rangle_{\omega} \equiv \langle BB \rangle_{\omega}^{T \rightarrow \infty}$.

2.6 The nonlinear-bath model

We consider a two-level system S coupled to another two-level system B , which represents an example of a nonlinear dissipative bath, since it is coupled to an oscillator bath via $\hat{X} = -\sum_k c_k \hat{x}_k$ (see Fig. 2.2). The total Hamiltonian is given by

$$\mathcal{H} = \epsilon_S \hat{\sigma}_z^S + \Delta_S \hat{\sigma}_x^S + J \hat{\sigma}_z^S \hat{\sigma}_z^B + \Delta \hat{\sigma}_x^B + \hat{\sigma}_z^B \hat{X} + \mathcal{H}_F, \quad (2.65)$$

where

$$\mathcal{H}_F = \sum_k \left[\frac{\hat{p}_k^2}{2m_k} + \frac{m_k \omega_k^2}{2} \hat{x}_k^2 \right]. \quad (2.66)$$

Here, the parameters ϵ_S and Δ_S serve to define any desired two-level system S . The system S is coupled to B via $\hat{\sigma}_z^B$, with the coupling strength between S and B being given by J , which is therefore the system-bath coupling strength to the nonlinear bath. Furthermore, the coupling strength of the two state system B to the oscillator bath F determines, as we will see below, the structure of the nonlinear bath. The bath-spectral density is assumed to be Ohmic, see Eq. (2.3). Still, we have not made any restriction to a certain temperature range. In the sections below we will specialize to the limiting case of infinite temperature, where \hat{X} becomes a purely classical noise force. Results valid in the low-temperature limit are then presented in Chapter 3.

The dissipative dynamics of S can be characterized in terms of several different quantities. Here we will analyze the decay of the equilibrium correlator $\langle \hat{\sigma}_z^S(t) \hat{\sigma}_z^S(0) \rangle$.

2.7 Infinite temperature results

There are two ways to define the border between system and bath in our system described by Eq. (2.65). The first is to consider one spin to be the system and the

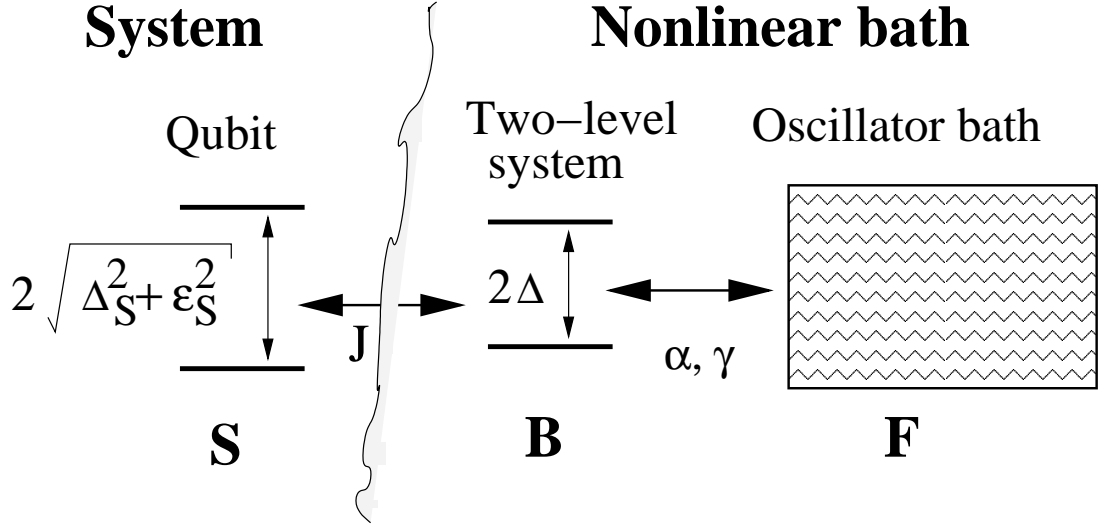


Figure 2.2: System qubit S , denoted by its two energy levels, coupled to the nonlinear bath. The nonlinear bath consists of another two-level system B and a linear oscillator bath F . J constitutes the system-bath coupling. α parametrizes the coupling strength between B and F at finite temperatures and γ determines the coupling strength at infinite temperature. α (γ) is an internal parameter of the bath defining different structured nonlinear environments.

other spin to belong to the bath, as we do here (see Fig. 2.3b). The bath then consists of the spin B and the oscillators F together. This makes it nonlinear. The second way to define system and bath is shown in Fig. 2.3c. There we have a system of two interacting spins, coupled to a linear bath. This is how we perform the calculations, but we interpret the system-bath borders of the model as shown in Fig. 2.3b. Note that the nonlinear bath is therefore determined by defining the system-bath borders. Solving the full model of a system of two interacting spins coupled to a linear bath at arbitrary temperatures and coupling strengths represents a formidable problem in itself. It has been analyzed in the past using the Feynman-Vernon influence functional [Feynman63], both analytically [Dube01] (in certain limiting cases), and numerically [Thorwart02]. For our purposes, we will be content with first analyzing a technically simpler special case: high temperatures $T \rightarrow \infty$.

In this limit the linear bath behaves like a classical Gaussian noise force. This can be seen by evaluating the expressions for the oscillator bath correlation function given in Eq. (2.24) for $T \rightarrow \infty$. One obtains $K_R(t) = \frac{2}{\pi}\alpha T \sin(\omega_C t)/t$, which becomes a delta distribution for an infinite bath cutoff: $K_R(t) \rightarrow 2\alpha T \delta(t)$, for $\omega_C \rightarrow \infty$. The limit of infinite temperature T of the bath is taken such that the overall noise strength $\gamma \equiv 2\alpha T$ remains constant: $\alpha \rightarrow 0$ while $T \rightarrow \infty$ and $K_I(t)$ vanishes, see Eq. (2.25). It follows that $\langle \hat{X}(t)\hat{X}(t') \rangle$ is a real and symmetric function. This is why the Ohmic bath corresponds to a classical white noise fluctuating force $F(t)$ in the high-temperature limit [Lesovik02]. This leads to the following Hamiltonian

$$\mathcal{H} = \epsilon_S \hat{\sigma}_z^S + \Delta_S \hat{\sigma}_x^S + J \hat{\sigma}_z^S \hat{\sigma}_z^B + \Delta \hat{\sigma}_x^B + \hat{\sigma}_z^B F(t). \quad (2.67)$$

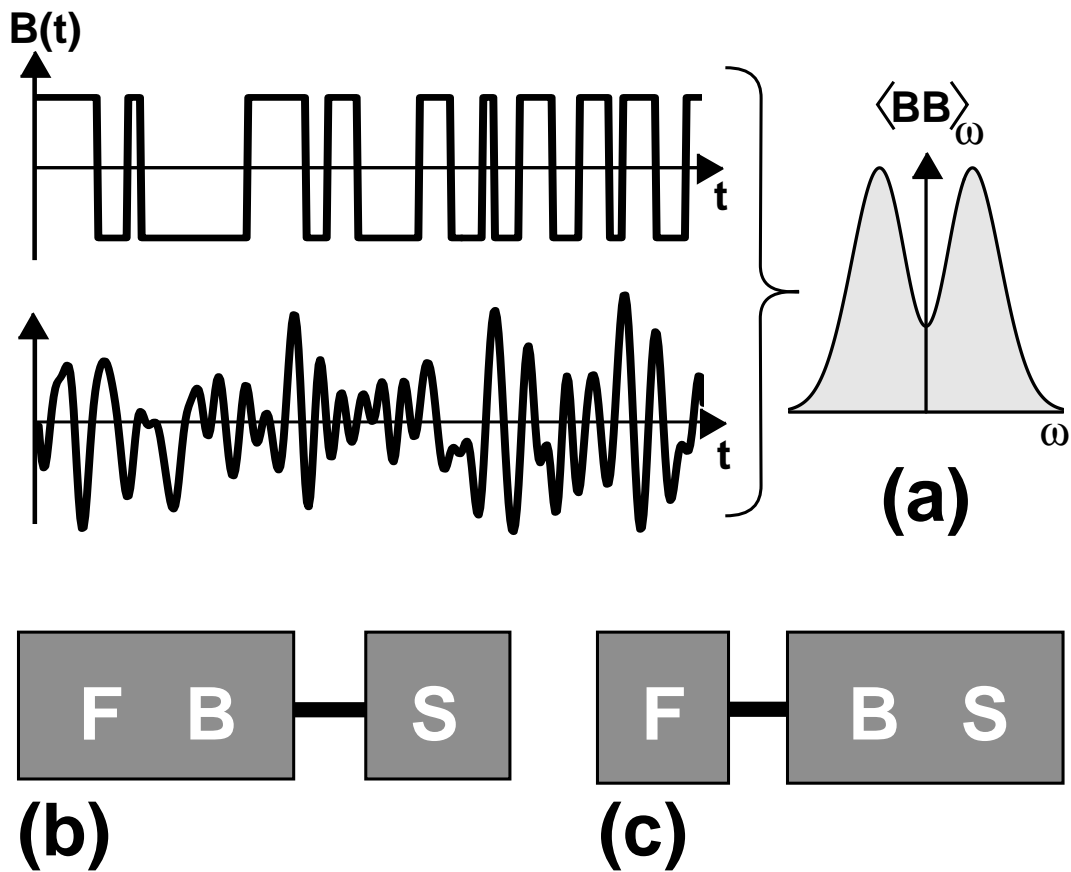


Figure 2.3: (a) Schematic representation of two stochastic processes corresponding to a classical two-level fluctuator, or “telegraph noise” (top), and a Gaussian process (bottom), yielding the same power spectrum (right). (b) In our model, the two-level fluctuator B is coupled to a noise force F and therefore represents a (nonlinear and non-Markoffian) bath that acts on a system S . (c) The exact master equation description (Approach 1 in main text) treats S and B as a composite system, subject to F .

The oscillations of $\hat{\sigma}_z^B(t)$ at the frequency 2Δ are noisy, due to the action of the fluctuating force $F(t)$ with the correlation function

$$\langle F(t)F(0) \rangle \equiv \langle \hat{X}(t)\hat{X}(t') \rangle = \gamma\delta(t). \quad (2.68)$$

Miscellaneous structured nonlinear baths $B+F$ are defined by varying the parameter γ .

Under these circumstances, the dissipative dynamics of $S+B$ under the action of F can be described exactly by using a Markoffian master equation. Note that this is, of course, unrelated to the validity of a master equation description for the action of B on S alone, which we will discuss below. The limit of infinite temperature is dictated mostly by the desire to have a comparatively strong decay of the correlator of $\hat{\sigma}_z^B(t)$ (with a decay rate on the order of B 's transition frequency 2Δ), while still retaining the validity of a Markoffian master equation description (for the full system $S+B$). The concept of generating colored noise by coupling to a degree of freedom subject to white noise is also employed in classical stochastic mechanics, see [Kampen92] and [Risken89].

In the following considerations, we obtain exact results which are compared with those obtained using three commonly used approximations: a Markoffian master equation for the spin dynamics, a weak-coupling approximation, and the substitution of a linear bath for the original nonlinear bath. In the following, we will call the exact solution “Approach 1”, while “Approach 2” refers to a master equation applied to S alone, “Approach 3” replaces the nonlinear by a linear bath, and “Approach 4” is the weak-coupling approximation.

2.8 The exact solution: “Approach 1”

Derivation of the master equation - First we derive the exact master equation description, which is used for the action of F on the combined system $B+S$

$$\frac{d}{dt}\hat{\rho}_{SB}(t) = -i[\mathcal{H}_{SB}, \hat{\rho}_{SB}(t)] - \gamma\hat{\rho}_{SB}(t) + \gamma\hat{\sigma}_z^B\hat{\rho}_{SB}(t)\hat{\sigma}_z^B. \quad (2.69)$$

\mathcal{H}_{SB} is the Hamiltonian for the system $B+S$ alone. We start with the von Neumann equation

$$i\frac{d}{dt}\hat{\rho}_{SB}^{(F)}(t) = [\mathcal{H}(t), \hat{\rho}_{SB}^{(F)}(t)] = [\mathcal{H}_{SB} + \hat{\sigma}_z^B F(t), \hat{\rho}_{SB}^{(F)}(t)], \quad (2.70)$$

where $\hat{\rho}_{SB}^{(F)}(t)$ is the density matrix for one realization of the force $F(t)$. $\mathcal{H}(t)$ is the Hamiltonian for the system $B+S$ under the action of the force $F(t)$. Rewriting Eq. (2.70) in integral form, we obtain

$$\hat{\rho}_{SB}^{(F)}(t) - \hat{\rho}_{SB}^{(F)}(0) = (-i) \int_0^t d\tau [\mathcal{H}_{SB} + \hat{\sigma}_z^B F(\tau), \hat{\rho}_{SB}^{(F)}(\tau)]. \quad (2.71)$$

Now we iterate Eq. (2.71) once

$$\begin{aligned} \frac{d}{dt} \hat{\rho}_{SB}^{(F)}(t) &= (-i)[\mathcal{H}_{SB}, \hat{\rho}_{SB}^{(F)}(t)] + (-i) \left[\hat{\sigma}_z^B F(t), \right. \\ &\quad \left. \hat{\rho}_{SB}^{(F)}(0) + (-i) \int_0^t d\tau [\mathcal{H}_{SB} + \hat{\sigma}_z^B F(\tau), \hat{\rho}_{SB}^{(F)}(\tau)] \right]. \end{aligned} \quad (2.72)$$

In the next step we average over $F(\cdot)$ and use $\langle F(t) \rangle = 0$ and $\langle \hat{\rho}_{SB}^{(F)}(t) \rangle = \hat{\rho}_{SB}(t)$. Note that, for a white noise force, $F(t)$ averages factorize like

$$\langle F(t) F(\tau) \hat{\rho}_{SB}^{(F)}(\tau) \rangle = \langle F(t) F(\tau) \rangle \langle \hat{\rho}_{SB}^{(F)}(\tau) \rangle, \quad (2.73)$$

since $\hat{\rho}_{SB}^{(F)}(\tau)$ depends only on the previous history of $F(\cdot)$. Therefore we find

$$\begin{aligned} \frac{d}{dt} \hat{\rho}_{SB}(t) &= (-i)[\mathcal{H}_{SB}, \hat{\rho}_{SB}(t)] \\ &+ (-i)^2 \int_0^t d\tau \left[\hat{\sigma}_z^B, [\hat{\sigma}_z^B, \hat{\rho}_{SB}(\tau)] \right] \langle F(t) F(\tau) \rangle. \end{aligned} \quad (2.74)$$

This leads to Eq. (2.69) by using Eq. (2.68). Note that, unlike the usual master equation, *no* secular approximation [Blum96] has been used in deriving this equation, which means the resulting decay rate does not have to be small when compared to the transition frequencies of the system $S + B$. This is possible because the bath correlation function is a delta function, which also makes the equation exact. We remark further that Eq. (2.69) is solved directly in the basis where $\hat{\sigma}_z^B$ and $\hat{\sigma}_z^S$ are diagonal. A transformation to the interaction picture (as is commonly performed for the usual master equation description) would lead to explicitly time-dependent terms in this equation.

Decay of the equilibrium correlator - We want to obtain the equilibrium correlator of $\hat{\sigma}_z^S(t)$,

$$\langle \hat{\sigma}_z^S(t) \hat{\sigma}_z^S(0) \rangle \equiv \text{tr} \left\{ \hat{\rho}_{SB}^{(eq)} \hat{\sigma}_z^S(t) \hat{\sigma}_z^S(0) \right\}. \quad (2.75)$$

It is convenient to rewrite Eq. (2.75) in terms of the projector onto the spin-up state of S , $\hat{P} \equiv |\uparrow\rangle_S \langle \uparrow|_S = \frac{1}{2}(1 + \hat{\sigma}_z^S)$

$$\langle \hat{\sigma}_z^S(t) \hat{\sigma}_z^S(0) \rangle = 4 \langle \hat{P}(t) \hat{P}(0) \rangle - 1. \quad (2.76)$$

Here, we have used $\hat{\rho}_{SB}^{(eq)} = \frac{1}{4}$. The correlator of $\hat{P}(t)$ can be found by calculating the probability to find the system S in the state “up” at the time t , if it had been “up” at the time 0. This has to be averaged over all realizations of the random process $F(\cdot)$

$$\langle \hat{P}(t) \hat{P}(0) \rangle = \frac{1}{2} \text{tr}_B \left\langle \langle \uparrow|_S \mathcal{U}_F(t) \hat{P} \otimes \hat{\rho}_B^{(eq)} \mathcal{U}_F^\dagger(t) |\uparrow\rangle_S \right\rangle_F. \quad (2.77)$$

Here $\hat{U}_F(t)$ is the time-evolution operator for $S + B$ under the action of a given realization of $F(\cdot)$. This equation is valid only because, in the limit of infinite temperature considered here, the probability of finding “spin up” at a certain instant of time is independent of the history of $F(\cdot)$. The expression (2.77) is nothing but the population $\rho_{S11}(t)$ of the state $|\uparrow\rangle_S$ for a time-evolution starting from the initial condition of “spin up”, $\hat{\rho}_{SB}(0) = \hat{P} \otimes \hat{\rho}_B^{(eq)}$

$$\langle \hat{P}(t)\hat{P}(0) \rangle = \frac{1}{2}\rho_{S11}(|t|). \quad (2.78)$$

Note that ρ_{S11} decays towards $1/2$, such that $\langle \hat{\sigma}_z^S(t)\hat{\sigma}_z^S(0) \rangle$ vanishes for $t \rightarrow \infty$ (as it should be). We have used the fact that the correlator is symmetric in time, since the potentially antisymmetric imaginary part vanishes (again, due to the limit of infinite temperature). $\hat{\rho}_S(t)$ can be calculated by applying the master equation that describes the action of F onto $S + B$. Put differently, Eq. (2.78) constitutes an example of the quantum regression theorem. Using $\hat{\rho}_S$, we calculate the Fourier transform of the equilibrium correlator of $\hat{\sigma}_z^S(t)$

$$\begin{aligned} K_{zz}^S(\omega) &\equiv \frac{1}{2\pi} \int_{-\infty}^{+\infty} dt e^{i\omega t} \langle \hat{\sigma}_z^S(t)\hat{\sigma}_z^S(0) \rangle \\ &= \frac{1}{\pi} \int_{-\infty}^{+\infty} dt e^{i\omega t} (\rho_{S11}(|t|) - 1/2). \end{aligned} \quad (2.79)$$

$K_{zz}^S(\omega)$ is a real-valued and symmetric function and the integral over all frequencies gives 1.

Time-evolution of the density matrix - The master equation (2.69) for the density matrix $\hat{\rho}$ ($\equiv \hat{\rho}_{SB}$) in the four-dimensional Hilbert space of $S + B$ represents a system of linear differential equations with constant coefficients. The latter are given by a complex-valued 16×16 matrix C that corresponds to the “superoperator”¹ on the right-hand side of the master equation. The solution is the complex vector ρ , which consists of the 16 components of the density matrix $\hat{\rho}$

$$\frac{d\rho}{dt} = -C\rho. \quad (2.80)$$

The entries of C can be read-off directly from Eq. (2.69). The formal solution of Eq. (2.80),

$$\rho(t) = e^{-Ct}\rho(0), \quad (2.81)$$

can be expressed in terms of the right-eigenvectors $|\rho^{(j)}\rangle$, the left-eigenvectors $\langle \rho^{(j)}|$ and the eigenvalues $\lambda^{(j)}$ of C

$$\rho(t) = \sum_j |\rho^{(j)}\rangle \langle \rho^{(j)}|\rho(0)\rangle e^{-\lambda^{(j)}t}. \quad (2.82)$$

¹Superoperators are ordinary operators. They constitute linear maps between operators, which also can be viewed as elements of a vector space.

C is not necessarily hermitian, so the $\lambda^{(j)}$ are usually complex-valued (with non-negative real parts) and the $|\rho^{(j)}\rangle$ do not form an orthonormal basis (however, $\langle\rho^{(i)}|\rho^{(j)}\rangle = \delta_{ij}$ by construction). In order to obtain $\rho_{S11}(t)$, we have to perform the trace over B , $\rho_{S11}(t) = \rho_{SB1111}(t) + \rho_{SB1212}(t)$. (In $\rho_{SBs'b'sb}$ the indices s, s' refer to S , while b, b' refer to B .) We will use the same notation for the components of $\rho^{(j)}$, which is a complex vector. Then we obtain

$$\int_0^\infty dt e^{i\omega t} \rho_{S11}(t) = \sum_j (\rho_{1111}^{(j)} + \rho_{1212}^{(j)}) \frac{\langle\rho^{(j)}|\rho(0)\rangle}{\lambda^{(j)} - i\omega}. \quad (2.83)$$

Taking the real part of this expression gives $K_{zz}^S(\omega)$, see Eq. (2.79).

Numerical results - The following steps have been performed in order to calculate the correlator $K_{zz}^S(\omega)$ of $\hat{\sigma}_z^S(t)$: The entries of the matrix C are obtained from Eq. (2.69). The eigenvalues and eigenvectors of C are calculated numerically and used to get $K_{zz}^S(\omega)$ according to Eqs. (2.83) and (2.79).

The relevant parameters in our model are ϵ_S , Δ_S , Δ , the coupling strength J , and the strength γ of the noise force F . We choose the time scale such that $\Delta \equiv 1$. The results discussed in the following have been calculated for $\Delta_S = 1.2$ (S and B “almost in resonance”).

To begin our discussion, we note some generic features of the results obtained for approaches 1 and 2. Since, in these cases, $K_{zz}^S(\omega)$ is essentially the Fourier transform of a density matrix relaxing according to a master equation, it consists of several Lorentzian peaks. Their number is constrained to be less than the maximum number of transition frequencies of the respective system (6 for $S + B$ in Approach 1, and 1 for S in Approach 2, plus possible zero-frequency “pure” relaxation). In practice, degeneracies between transition frequencies and selection rules reduce that number to 2 (or 5) for Approach 1, and 1 (or 2) for Approach 2, for $\epsilon_S = 0$ (or $\epsilon_S \neq 0$), see discussion in Appendix A.2 and Figs. 2.4, 2.5 and 2.6.

In the limit of weak coupling, $J \rightarrow 0$, all that remains is a broadened peak at the transition frequency $2\Delta_S$ of system S alone. In that limit, the results for all approaches coincide, as expected (see Figs. 2.9 and 2.10). With increasing J , the peaks are broadened and shifted, and additional peaks may appear (in the case of approaches 1,3 and 4).

The most notable difference from the master equation of Approach 2 is the appearance of a second peak at the transition frequency 2Δ of the two-level fluctuator B . At small J , the strength of this peak grows like J^2 , while its width is fixed (depending on γ). In this way, the power spectrum of the bath fluctuations shows up in the short-time behavior of the correlator of the system S . This behavior cannot be captured by the master equation (Approach 2).

Increasing J leads to a frequency shift and a change in the width of the “original” peak at $2\Delta_S$, much like that predicted by the simpler Approach 2. However, in the description of the exact Approach 1, these changes are due to the change in eigenfrequencies and eigenvectors of the combined system $S + B$. At small J , the

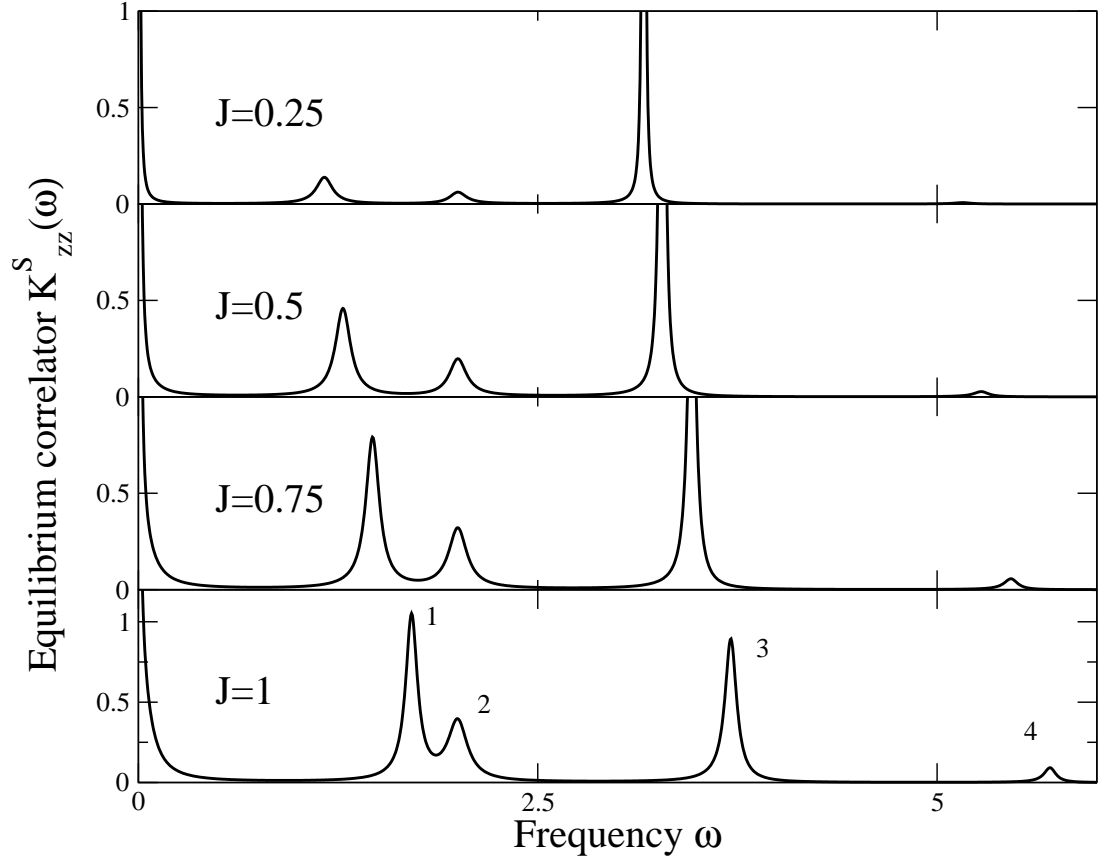


Figure 2.4: The Fourier-transform $K_{zz}^S(\omega)$ of the equilibrium correlator of $\hat{\sigma}_z^S(t)$, for different values of $J = 0.25, 0.5, 0.75$ and 1 from topmost to lowest graph. The values of the other parameters are: $\Delta = 1$, $\Delta_S = 1.2$, $\gamma/(2\pi) = 0.01$ and $\epsilon_S = 1$. The heights of the third dephasing peak are $\sim 19.1, \sim 5.6$ and ~ 1.9 for $J=0.25, 0.5$ and 0.75 , respectively. In the lowest graph the dephasing peaks are numbered from one to four according to the transitions shown in Fig. 2.6.

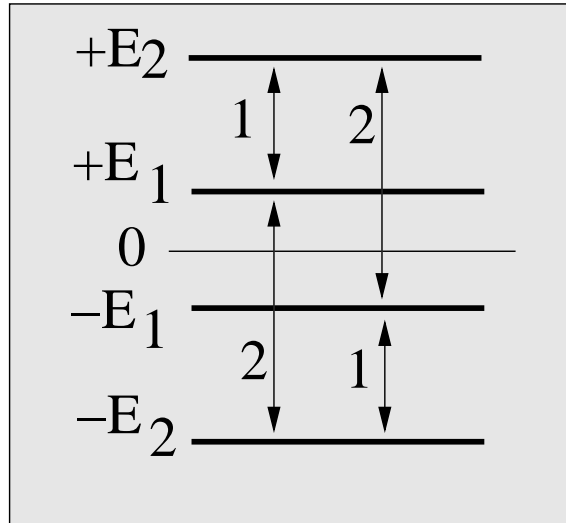


Figure 2.5: Spectrum of the two-spin system $S + B$. In the unbiased case $\epsilon_S = 0$ and low coupling γ , there are two distinct transitions possible, leading to two dephasing peaks of the equilibrium correlator.

results of approaches 1 and 2 can be shown to coincide using perturbation theory. Deviations from Approach 2 appear at higher values of J , where the energy shift of Approach 1 only grows *linearly* with J (see Figs. 2.9 and 2.10, lower graphs). On the contrary, the frequency of the second peak is suppressed to zero. This behavior can easily be found by diagonalizing the Hamiltonian for the combined system $B + S$ in the limit $J \rightarrow \infty$, when one obtains two pairs of degenerate energy levels, separated by $2J$.

Regarding the dependence on the noise strength γ , the same qualitative remarks apply as for Approach 2 (see discussion below, in Sec. 2.10). However, it is interesting to note that there *is* a frequency shift with increasing γ in Approach 1 as well (see Fig. 2.8), in spite of the fact that the additional terms in the nonsecular master equation (2.69) seem to describe a purely relaxational dynamics. This is contrary to the behavior known from the usual form of the master equation, Eq. (2.86), where the energy shifts can be read-off directly from the *imaginary* coefficients in the equation.

2.9 The bath-correlation function

In this section we calculate the equilibrium correlator of $\hat{\sigma}_z^B(t)$, which is needed as input for the master equation describing the relaxation of S alone (Approach 2), the numerical sampling of random processes (Approach 3), and the weak-coupling approximation (Approach 4).

This is done by calculating the relaxation of $\hat{\rho}_B(t)$ under the action of F , starting from the initial condition $\hat{\rho}_B(0) = |\uparrow\rangle_B \langle\uparrow|_B$ and applying the same formulas as

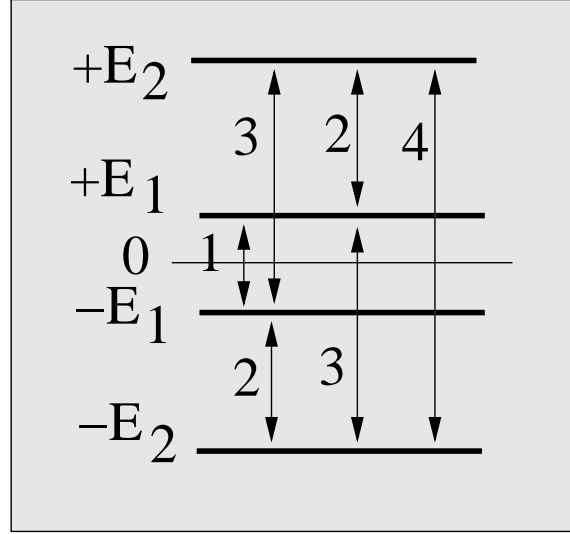


Figure 2.6: Spectrum of the two-spin system $S + B$. In the biased case $\epsilon_S \neq 0$ and low coupling γ , there are four distinct transition possible, leading to four dephasing peaks of the equilibrium correlator plus a relaxation peak at zero frequency.

above (with B instead of S) for the master equation (2.69), adapted to the two-dimensional Hilbert space of B (with a 4×4 matrix C). $\langle \hat{\sigma}_z^B(t) \hat{\sigma}_z^B(0) \rangle$ undergoes damped oscillations.

The Fourier transform of the correlator of $\hat{B} \equiv J \hat{\sigma}_z^B$ defines the “bath spectrum”

$$\begin{aligned} \langle B(t)B(0) \rangle &\equiv \langle \hat{B}(t) \hat{B}(0) \rangle = J^2 \langle \hat{\sigma}_z^B(t) \hat{\sigma}_z^B(0) \rangle, \\ \langle BB \rangle_\omega &\equiv \frac{1}{2\pi} \int_{-\infty}^{+\infty} dt e^{i\omega t} \langle B(t)B(0) \rangle. \end{aligned} \quad (2.84)$$

It is real and symmetric in the limit of infinite temperature considered here, and is therefore equivalent to a classical colored noise force. As explained above, $\langle BB \rangle_\omega$ is found by applying the master equation (2.69) to B alone.

The result for the Fourier transform is given by

$$K_{zz}^B(\omega) = \frac{\langle BB \rangle_\omega}{J^2} = \frac{8\Delta^2\gamma}{\pi} \frac{1}{(\omega^2 - 4\Delta^2)^2 + 4\omega^2\gamma^2}. \quad (2.85)$$

This consists of broad peaks of width γ (for $\gamma^2 < 4\Delta^2$), which is proportional to the strength of the noise force F and may be comparable to the transition frequency 2Δ itself (see Fig. 2.7). Thus, B indeed represents a noisy two-level fluctuator, which acts on S as a *nonlinear* (non-Gaussian) and *non-Markoffian* (colored) bath.

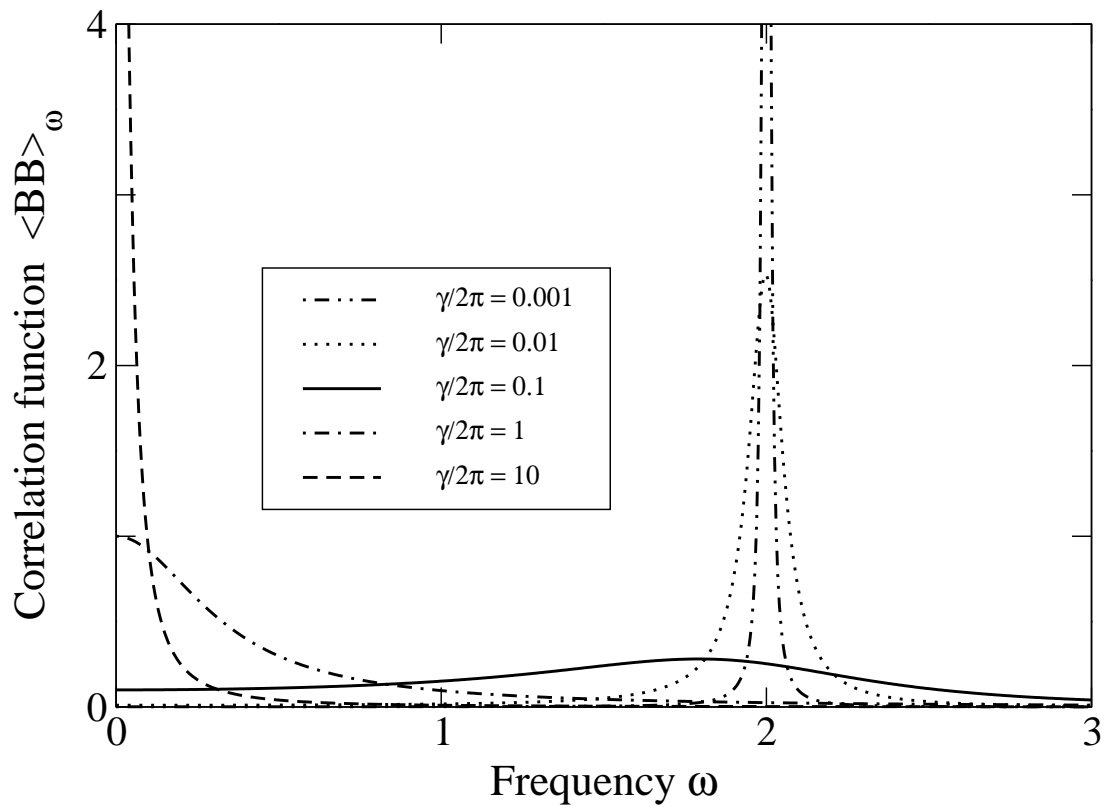


Figure 2.7: The $\langle BB \rangle_\omega$ correlation function for different values of γ and $J = 1, \Delta = 1$.

2.10 The master equation: “Approach 2”

As has been explained above, we will use the master equation description not only for the action of F on the combined system $S + B$ (see Eq. (2.69)), but also for the action of $F + B$ on S alone. This constitutes the approximate “Approach 2”, involving the usual kind of master equation, which is valid only for sufficiently weak coupling J , since it is derived by applying both the Markoff and secular approximation (see [Blum96] and [Gardiner00]). In the unperturbed eigenbasis of system S , it reads

$$\begin{aligned} \frac{d}{dt}\rho_{S kj} &= -(\Gamma_k + \Gamma_j + \tilde{\Gamma}_{kj} + i(\Delta_k - \Delta_j) \\ &+ i(E_k - E_j))\rho_{S kj} + \delta_{kj} \sum_{l \neq k} \rho_{S ll} |A_{kl}|^2 2\pi \langle BB \rangle_{E_l - E_k} . \end{aligned} \quad (2.86)$$

Equation (2.86) describes the relaxation of the reduced density matrix $\hat{\rho}_S$ of system S alone, under the action of the coupling $J\hat{\sigma}_z^S \hat{\sigma}_z^B$ to the bath $B + F$. We have introduced the abbreviation $\hat{A} \equiv \hat{\sigma}_z^S$.

The decay rates are defined by

$$\begin{aligned} \Gamma_k &\equiv \pi \sum_n |A_{kn}|^2 \langle BB \rangle_{E_k - E_n} \\ \tilde{\Gamma}_{kj} &\equiv -2\pi A_{kk} A_{jj} \langle BB \rangle_0 , \end{aligned} \quad (2.87)$$

and the energy shifts are given by

$$\Delta_k \equiv \sum_n |A_{kn}|^2 \int d\omega \frac{\langle BB \rangle_\omega}{E_k - E_n - \omega} . \quad (2.88)$$

Here the indices and energies refer to the unperturbed eigenstates of the original Hamiltonian of S alone: $\mathcal{H}_S \equiv \epsilon_S \hat{\sigma}_z^S + \Delta_S \hat{\sigma}_x^S$. The integral should be understood as a principal value integral.

There is a systematic way to derive the Markoffian master equation, which we will describe in the following. As a starting point, one can use the generalized master equation for the reduced dynamics given in [Fick83, Loss03, DiVincenzo04]. No approximation has been made so far

$$\begin{aligned} \frac{d}{dt}\hat{\rho}_S(t) &= -i\mathcal{L}_S \hat{\rho}_S(t) - i \int_0^t d\tau \Sigma(\tau) \hat{\rho}_S(t - \tau) \\ \Sigma(\tau) &= -i \text{tr}_B \mathcal{L}_{SB} e^{-i\mathcal{Q}\mathcal{L}\tau} \mathcal{L}_{SB} \hat{\rho}_B . \end{aligned} \quad (2.89)$$

The Liouvillian maps are defined by $\mathcal{L}\hat{\rho} = [\mathcal{H}, \hat{\rho}]$, $\hat{\rho}_B = e^{-\beta\mathcal{H}_B} / Z$ is the equilibrium bath density matrix, \mathcal{Q} is the projection operator $\mathcal{Q} = 1 - \hat{\rho}_B \text{tr}_B$. It is further assumed that $\text{tr}_B \mathcal{H}_{SB} \hat{\rho}_B = 0$ and the initial state is given as a product $\hat{\rho}(0) = \hat{\rho}_S(0) \otimes \hat{\rho}_B$. In the case of the weak-coupling approach, one is interested in weak coupling to the

bath. By performing a systematic expansion in powers of the coupling, the lowest order term in this expansion is calculated by replacing $e^{-i\mathcal{L}\tau}$ by $e^{-i\mathcal{L}(\mathcal{L}_S+\mathcal{L}_B)\tau}$. The weak coupling² approximation, or exact Born approximation, leads to the following equation

$$\begin{aligned} \frac{d}{dt}\hat{\rho}_S(t) &= -i[\mathcal{H}_S, \hat{\rho}_S(t)] - \int_0^t d\tau \left[\hat{\sigma}_z^S, e^{-i\mathcal{H}_S\tau} \hat{\sigma}_z^S \hat{\rho}_S(t-\tau) e^{i\mathcal{H}_S\tau} \right] \langle B(\tau)B(0) \rangle \\ &+ \int_0^t d\tau \left[\hat{\sigma}_z^S, e^{-i\mathcal{H}_S\tau} \hat{\rho}_S(t-\tau) \hat{\sigma}_z^S e^{i\mathcal{H}_S\tau} \right] \langle B(0)B(\tau) \rangle. \end{aligned} \quad (2.90)$$

This weak-coupling equation will be studied further in Section 2.13.

As opposed to the weak-coupling equation, the Markoffian master equation includes a second approximation. Note that the weak-coupling equation has a convolution form, it has memory and the behavior of the density matrix at the time t depends on its past. On the other hand, the motion of the system is damped due to the coupling to the environment, which destroys the memory. One can therefore make a second key assumption by substituting $\hat{\rho}_S(t-\tau)$ by $\hat{\rho}_S(t)$. The bath-correlation time τ_B is a measure for the time during which some memory of the interaction is retained. It depends on the bath. The bath-correlation function decays on this time scale. If the bath-correlation time is much smaller than the decay or damping time of the system then the upper integration limit can be extended to infinity with negligible error under the Markoff approximation

$$\begin{aligned} \frac{d}{dt}\hat{\rho}_S(t) &= -i[\mathcal{H}_S, \hat{\rho}_S(t)] - \int_0^\infty d\tau \left[\hat{\sigma}_z^S, e^{-i\mathcal{H}_S\tau} \hat{\sigma}_z^S \hat{\rho}_S(t) e^{i\mathcal{H}_S\tau} \right] \langle B(\tau)B(0) \rangle \\ &+ \int_0^\infty d\tau \left[\hat{\sigma}_z^S, e^{-i\mathcal{H}_S\tau} \hat{\rho}_S(t) \hat{\sigma}_z^S e^{i\mathcal{H}_S\tau} \right] \langle B(0)B(\tau) \rangle. \end{aligned} \quad (2.91)$$

At infinite temperature the equation can be simplified further since the correlation function becomes symmetric in time. Finally, we can write down the equation in the eigenbasis of \mathcal{H}_S and we obtain the Markoffian master equation Eq. (2.86).

Let us now discuss the solution of the master equation, Eq. (2.86). The time-evolution of $\hat{\rho}_S$ is found from Eq. (2.86) using the same approach as in Sec. 2.8, involving the diagonalization of a superoperator C . In the present case, C corresponds to the 4×4 matrix whose entries are read-off from Eq. (2.86). Therefore, the equation corresponding to Eq. (2.83) only contains $\rho_{11}^{(j)}$, instead of the sum inside the brackets.

Numerical results - First the action of F onto B is considered, to obtain the correlation function $\langle BB \rangle_\omega$. This result is given in Eq. (2.85). It is used to set up the master equation describing the action of $F + B$ onto S , Eq. (2.86). Its coefficients define a 4×4 ‘‘C-matrix’’, which is diagonalized. The results are inserted into the appropriately modified Eq. (2.83), in order to obtain $K_{zz}^S(\omega)$.

²What we call the weak-coupling approach is what is denoted as exact Born approximation in [Loss03].

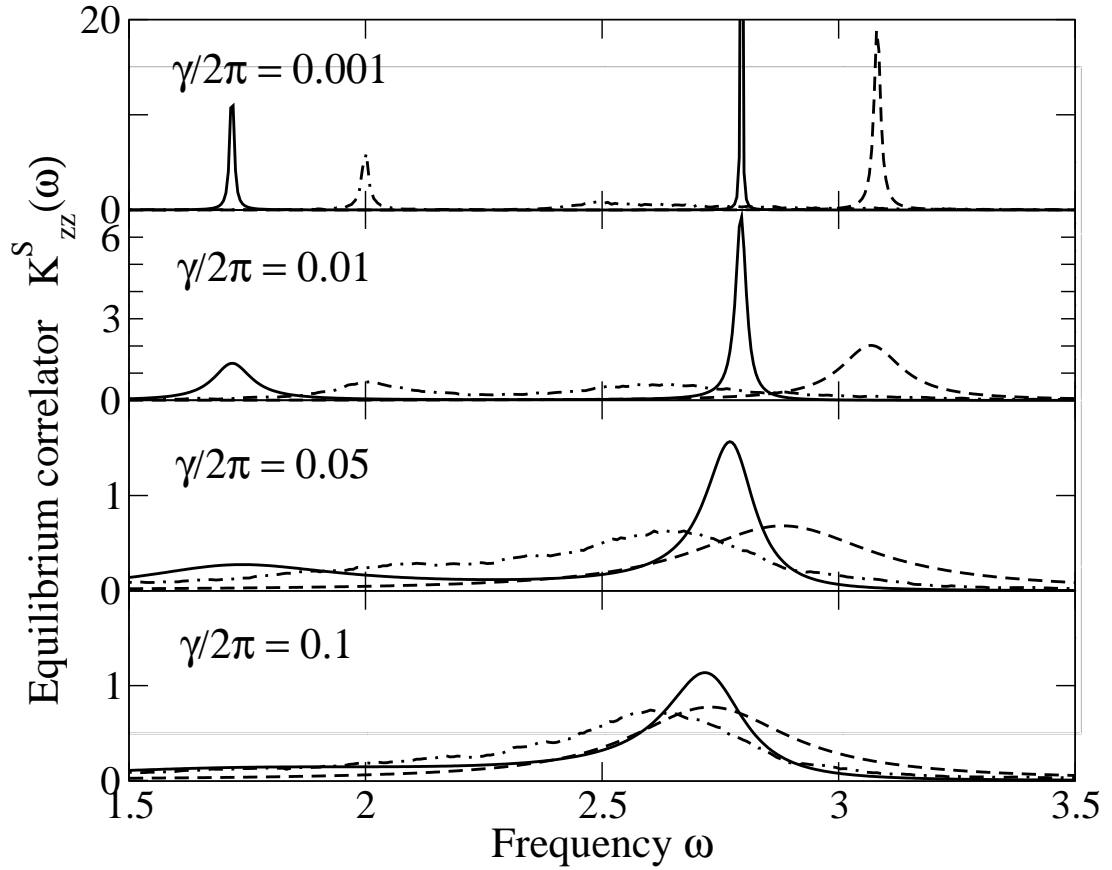


Figure 2.8: The Fourier-transform $K_{zz}^S(\omega)$ of the equilibrium correlator of $\hat{\sigma}_z^S(t)$, for different values of the noise strength $\gamma/(2\pi)=0.001, 0.01, 0.05$ and 0.1 from topmost to lowest graph. The values of the other parameters are: $\Delta = 1$, $\Delta_S = 1.2$, $J = 0.5$ and $\epsilon_S = 0$. Approaches 1 and 4: solid line, Approach 2: dashed line, Approach 3: dash-dotted line.

Naturally, the behavior of Approach 2 is simplest to analyze, since it is the textbook example of a master equation applied to a single two-level system. Since the correlator $\langle BB \rangle_\omega$ is proportional to J^2 , both the shift of the transition frequency and the width of the peak(s) increase like J^2 , for arbitrarily large J . In contrast, the dependence of the peak width and the frequency shift on the noise strength γ is non-monotonic. This dependence is determined by the evolution of $\langle BB \rangle_\omega$ (see Eq. (2.85) and Fig. 2.7) with increasing γ . For very small γ , the two-level fluctuator B performs very weakly damped oscillations at the frequency 2Δ . Unless it is exactly at resonance with the system S , the dissipative effects of B on the dynamics of S will be weak in that regime. The decay rate of S , which is given by the power spectrum of B evaluated at $2\Delta_S$, grows linearly in γ (for $\gamma^2 \ll (\Delta_S^2 - \Delta^2)^2/\Delta_S^2$). The transition frequency of S is shifted upwards or downwards, depending on whether the main weight of the spectrum of B is located below or above Δ_S ($\Delta < \Delta_S$ or $\Delta > \Delta_S$). For increasing γ , B performs more strongly-damped oscillations. In the limit of large γ , the spectrum $\langle BB \rangle_\omega$ is peaked around zero frequency (see Fig. 2.7) such that the decay rate of S *decreases* again (like $1/\gamma$), after having gone through a maximum. The magnitude of the energy shift will also decrease for increasing γ , simply because the contributions of the power spectrum of B lying to either side of $2\Delta_S$ will tend to cancel each other. However, in the limit $\gamma \rightarrow \infty$, the shift always saturates at a positive value which is independent of Δ . These facts can be read off from the analytical result for Approach 2 (written down in the special case of $\epsilon_S = 0$)

$$K_{zz}^S(\omega) = \frac{1}{2\pi} \sum_{s=\pm 1} \frac{\Gamma}{\Gamma^2 + (\omega - s\omega_0)^2}. \quad (2.92)$$

Here, the peak width is given by $\Gamma = 2J^2 \text{Re} \Sigma(2\Delta_S) = 2\pi \langle BB \rangle_{2\Delta_S}$, the shifted transition frequency is $\omega_0 = 2\Delta_S - 2J^2 \text{Im} \Sigma(2\Delta_S)$, and we have defined $\Sigma(\omega) \equiv (2\gamma + i\omega)/(-\omega^2 + 4\Delta^2 + 2i\omega\gamma)$.

The master equation is expected to come close to the true result as long as the conditions of the Markoff and secular approximation are fulfilled. This means the coupling strength J has to be so small that the resulting decay of S proceeds slowly compared with the transition frequency itself (secular approximation) and with the correlation time of the bath (Markoff approximation). The latter is given by $\tau_B = 1/\gamma$ if $\gamma^2 < 4\Delta^2$ and $\tau_B = 1/(\gamma - \sqrt{\gamma^2 - 4\Delta^2})$ if $\gamma^2 > 4\Delta^2$.

2.11 The nonlinear bath replaced by a linear bath: “Approach 3”

In approach 3 we replace the nonlinear bath by a linear one. If the two-level fluctuator B were replaced by a harmonic oscillator [Garg85, Wilhelm03a], this procedure of substituting a linear bath with an appropriate correlation function for the combination of F and B would be exact. Here, it is an approximation whose reliability we want to analyze by comparison with the exact solution. In our case, the fact that

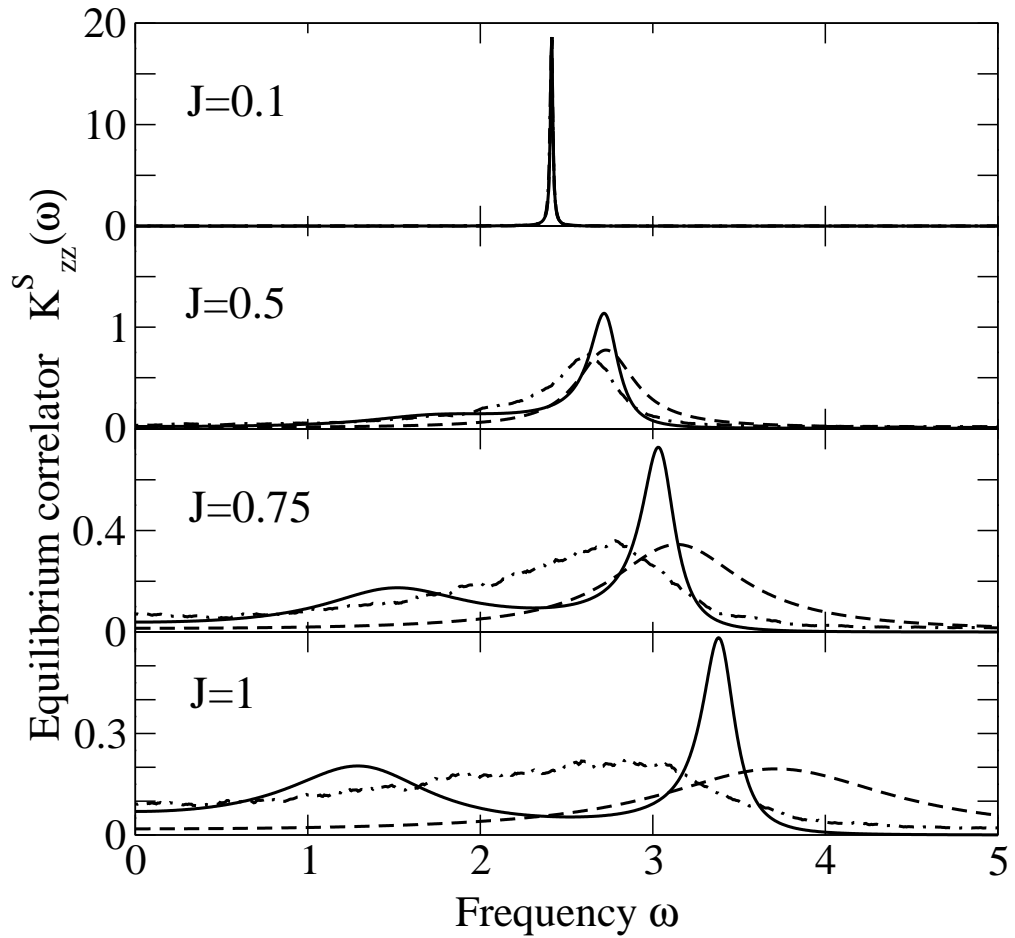


Figure 2.9: The Fourier-transform $K_{zz}^S(\omega)$ of the equilibrium correlator of $\hat{\sigma}_z^S(t)$, for different values of the coupling strength $J = 0.1, 0.5, 0.75$ and 1.0 from topmost to lowest curve. The values of the other parameters are: $\Delta = 1$, $\Delta_S = 1.2$, $\gamma/2\pi = 0.1$ and $\epsilon_S = 0$. Approaches 1 and 4: solid line, Approach 2: dashed line, Approach 3: dash-dotted line.

the power spectrum $\langle BB \rangle_\omega$, given in Eq. (2.85), is real and symmetric means that B can be treated as a classical Gaussian random process. Therefore, we must solve a Langevin equation for the density matrix

$$\frac{d}{dt} \hat{\rho}_S^{(B)}(t) = -i[\mathcal{H}_{\text{stoch}}(t), \hat{\rho}_S^{(B)}(t)], \quad (2.93)$$

with the stochastic time-dependent Hamiltonian

$$\mathcal{H}_{\text{stoch}}(t) = \epsilon_S \hat{\sigma}_z^S + \Delta_S \hat{\sigma}_x^S + B(t) \hat{\sigma}_z^S. \quad (2.94)$$

We calculate (numerically) the time-evolution of $\hat{\rho}_S^{(B)}(t)$ under the action of the stochastic time-dependent Hamiltonian defined in Eq. (2.94), which depends on $B(t)$. The density matrix $\hat{\rho}_S^{(B)}(t)$ must be averaged over a statistical sample of different field configurations $B(t)$. The numerical generation of these random fields $B(t)$ is described in Section 2.12. The description of open quantum systems by a stochastic Schrödinger equation has recently attracted increasing attention [Ankerhold00, Gardiner00, Stockburger02].

Since Approach 3 takes the full bath spectrum $\langle BB \rangle_\omega$ as input, this spectrum may also show up in the result for the system correlator $K_{zz}^S(\omega)$, as is indeed the case. Figure 2.8 demonstrates that this effect is most pronounced for small values of γ , where the bath spectrum has a relatively sharp structure (the noise field $B(\cdot)$ acting on S deviates strongly from white noise). In these cases, the qualitative agreement between Approach 3 and Approach 1 (“exact solution”) is much better than that between Approach 2 (“master equation”) and Approach 1 (see also Fig. 2.12). Nevertheless, there are deviations: In particular, there is no visible shift of the peaks in Approach 3 with increasing J . They become wider and more asymmetric (this applies especially to the peak at frequency $2\Delta_S$). For higher values of γ , the linear bath (Approach 3) shows, in general, less structure than the exact solution, obtained for the actual nonlinear bath.

2.12 Numerical generation of the random field

Let us now describe how we generate the noise force $B(t)$ numerically (see Fig. 2.11). Computer programs can generate Gaussian random numbers with variance equal to one. If one is interested in having the time sample of a noise force $B(t)$ with a certain given correlation between two time points $\langle B(t)B(t') \rangle$, it is best to consider the Fourier transforms B_ω and $\langle BB \rangle_\omega$. If the Gaussian process is given in Fourier space B_ω , the time evolution $B(t)$ of the noise force can be found via FFT (Fast Fourier Transform). This is convenient because for the integration of the differential equations (Eq. (2.93)), we need the noise sample to be defined only at discrete time points. The generated noise force samples should be longer than the integration time of the differential equations. Otherwise the periodicity of the sample generated via a

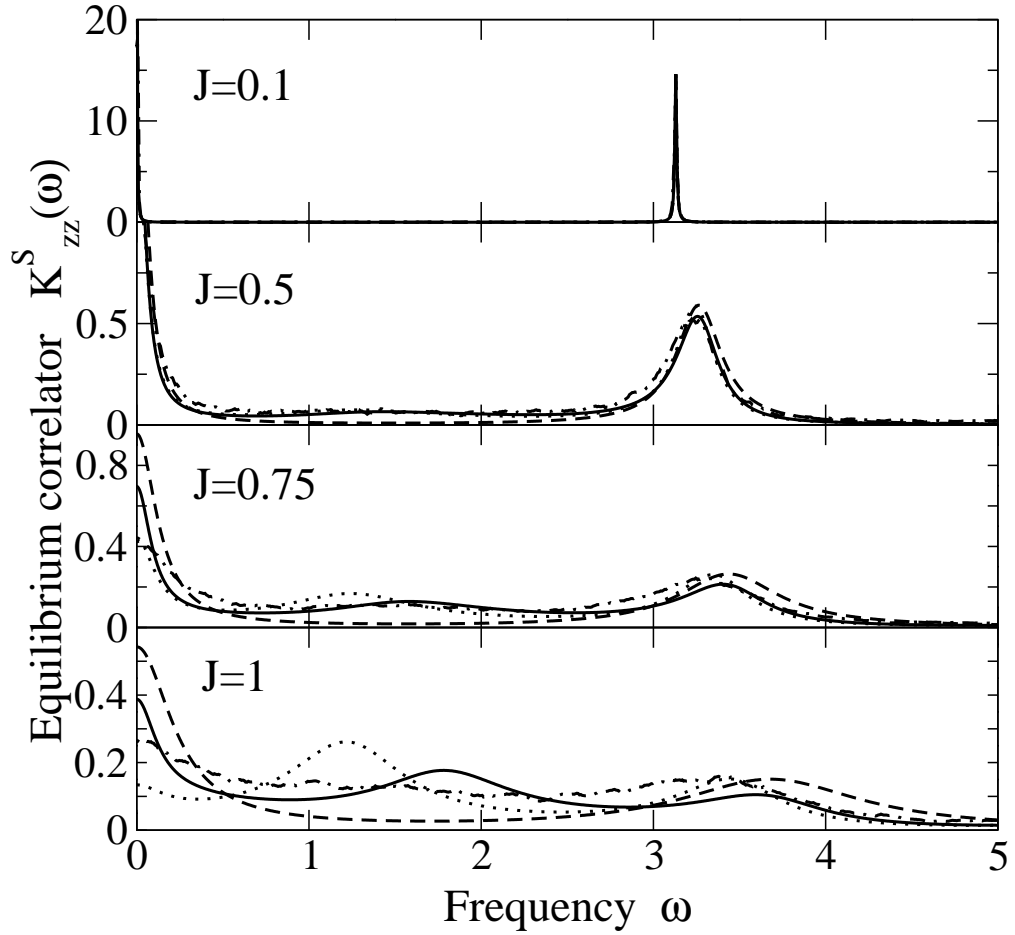


Figure 2.10: The Fourier-transform $K_{zz}^S(\omega)$ of the equilibrium correlator of $\hat{\sigma}_z^S(t)$, for different values of the coupling strength $J = 0.1, 0.5, 0.75$ and 1.0 from topmost to lowest curve. The values of the other parameters are: $\Delta = 1$, $\Delta_S = 1.2$, $\gamma/2\pi = 0.1$ and $\epsilon_S = 1$. Approach 1: solid line, Approach 2: dashed line, Approach 3: dash-dotted line, Approach 4: dotted line.

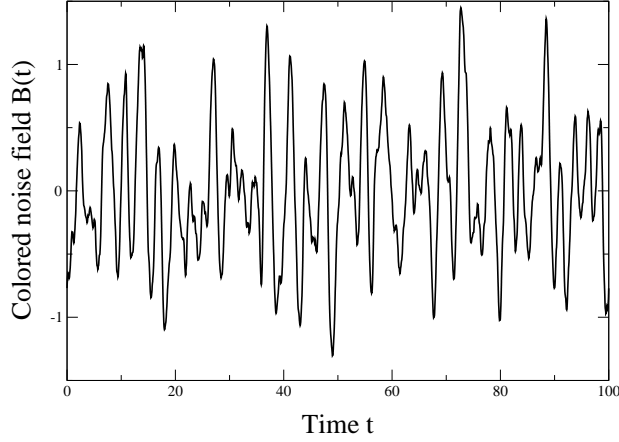


Figure 2.11: Sample of the colored Gaussian noise field $B(t)$. The parameters for the bath correlation function $\langle BB \rangle_\omega$ are $\Delta = 1$, $\gamma/2\pi = 0.1$ and $J = 0.5$.

FFT shows up in the solution of the spin dynamics. The real and imaginary parts of B_ω are independent Gaussian variables given by

$$\text{Re } B_\omega = \left(\frac{\langle BB \rangle_\omega}{\Delta\omega} \right)^{\frac{1}{2}} \times \text{Gaussian random number} \quad (2.95)$$

$$\text{Im } B_\omega = \left(\frac{\langle BB \rangle_\omega}{\Delta\omega} \right)^{\frac{1}{2}} \times \text{Gaussian random number}, \quad (2.96)$$

where $\Delta\omega$ is the frequency step in Fourier space. The samples are produced by generating the Fourier coefficients of B as independent complex Gaussian random variables of appropriate variance, given by the power spectrum $\langle BB \rangle_\omega$. The product with the variance gives the correct variance for each ω in the generated noise fields. $\text{Re } B_\omega$ and $\text{Im } B_\omega$ are only generated for positive frequencies ω because we take into account symmetry conditions to make $B(t)$ real. The field $B(t)$ itself is obtained using a Fast Fourier Transform (FFT). After averaging, we may use

$$\langle \hat{P}(t)\hat{P}(0) \rangle = \frac{1}{2} \langle \rho_{S11}^{(B)}(|t|) \rangle_B \quad (2.97)$$

and Eqs. (2.77) and (2.79) in order to obtain $K_{zz}^S(\omega)$. To this end, the Fourier transform of $\rho_{S11}(|t|)$ is calculated numerically, using a FFT on a time-grid of sufficiently small step size Δt and sufficiently large length. The results displayed in the figures have been obtained using 10^4 samples and a frequency resolution of $\Delta\omega = 2\pi/800$. The curves have been smoothed by averaging over 5 to 20 adjacent frequency bins.

2.13 The weak-coupling approximation: “Approach 4”

Instead of the Markoff approximation one can use a weak-coupling approximation [Gardiner00]. This keeps the full information contained in the correlator $\langle BB \rangle_\omega$, at the price of introducing a kernel for the master equation which has no longer a convolution form. We briefly describe the derivation of the weak-coupling equation in a way alternate to that given in Section 2.10. We use the von Neumann equation in the interaction picture with respect to $\mathcal{H}_0 \equiv \mathcal{H} - \mathcal{V}$. Iterating the von Neumann equation up to second order leads to

$$\begin{aligned} \frac{d}{dt} \hat{\rho}_I(t) &= -i[\mathcal{V}_I(t), \hat{\rho}_I(0)] \\ &\quad - \int_0^t d\tau [\mathcal{V}_I(t), [\mathcal{V}_I(\tau), \hat{\rho}_I(\tau)]] . \end{aligned} \quad (2.98)$$

The density matrix is replaced by an approximate factorized density matrix $\hat{\rho}_I(t) = \hat{\rho}_{SI}(t) \otimes \hat{\rho}_B(0)$, where the bath remains described by a thermal equilibrium distribution. The reduced system dynamics become

$$\begin{aligned} \frac{d}{dt} \hat{\rho}_{SI}(t) &= -i \text{tr}_B [\mathcal{V}_I(t), \hat{\rho}_S(0) \otimes \hat{\rho}_B(0)] \\ &\quad - \int_0^t d\tau \text{tr}_B [\mathcal{V}_I(t), [\mathcal{V}_I(\tau), \hat{\rho}_{SI}(\tau) \otimes \hat{\rho}_B(0)]] , \end{aligned} \quad (2.99)$$

where a trace over the bath, which also includes F , has been taken. Now we introduce the interaction operator \hat{V} , which is given by $\hat{V} = \hat{A} \otimes \hat{B}$. In our case, \hat{B} has zero mean and its correlator is symmetric, see Eq. (2.85). We get

$$\begin{aligned} \frac{d}{dt} \hat{\rho}_{SI}(t) &= \\ &\quad - \int_0^t d\tau [\hat{A}_I(t), [\hat{A}_I(t-\tau), \hat{\rho}_{SI}(t-\tau)]] \langle B(\tau)B(0) \rangle . \end{aligned} \quad (2.100)$$

Going back to the Schrödinger picture and inserting $\hat{A} = \hat{\sigma}_z^S$ then leads to the following weak-coupling equation, which is second order in J

$$\begin{aligned} \frac{d}{dt} \hat{\rho}_S(t) &= -i[\mathcal{H}_S, \hat{\rho}_S(t)] \\ &\quad - \int_0^t d\tau [\hat{\sigma}_z^S, e^{-i\mathcal{H}_S\tau} [\hat{\sigma}_z^S, \hat{\rho}_S(t-\tau)] e^{i\mathcal{H}_S\tau}] \langle B(\tau)B(0) \rangle . \end{aligned} \quad (2.101)$$

This is the same equation as Eq. (2.90) for infinite temperature, i.e., with a symmetric bath-correlation function. This equation is conveniently solved by using the Laplace

transform. The Laplace transform of the equilibrium correlator of the bath B is connected to the Fourier transform in the usual way

$$\begin{aligned} C_{BB}(s) &\equiv \int_0^\infty dt e^{-st} \langle B(t)B(0) \rangle \\ &= \int_{-\infty}^\infty d\omega \frac{\langle BB \rangle_\omega}{s + i\omega} = J^2 \frac{s + 2\gamma}{s^2 + 2\gamma s + 4\Delta^2}. \end{aligned} \quad (2.102)$$

Using the Laplace transform, the system of differential equations becomes a system of linear algebraic equations, which can be solved by matrix inversion. All the results can be obtained analytically. However, here we only present the special case of $\epsilon_S = 0$

$$K_{zz}^S(\omega) = \frac{1}{\pi} \operatorname{Re} \left\{ \frac{s + 4C_{BB}(s)}{s^2 + 4C_{BB}(s) + 4\Delta_S^2} \Big|_{s=-i\omega} \right\}. \quad (2.103)$$

The case $\epsilon_S \neq 0$ is given in Appendix A.3. These analytical results are then evaluated with the appropriate numerical values of the parameters.

In general, we expect the weak-coupling solution to be somewhat worse than the simulation of the linear bath with colored noise correlations (Approach 3), since it is an approximation to the latter case. However, the result for the special case $\epsilon_S = 0$ turns out to coincide with the exact solution (Approach 1). The second peak is present in contrast to the Markoff approximation. The solution for $\epsilon_S = 1$ (or, more generally, $\epsilon_S \neq 0$) is good for small system-bath coupling J . It fails for increasing J , where Approach 3 seems to be the better approximation, provided ϵ_S is not too small (see discussion above).

2.14 Conclusions

We have discussed a model of a nonlinear bath, consisting of a single two-level system subject to a classical white-noise force. Its action on a qubit has been analyzed using four different approaches. Numerical results for various special cases have been obtained and discussed. The regimes where the different approaches work well became clear: The standard Markoff approximation yields good results as long as the coupling strength is so small that the decay is slow compared to the transition frequency and the bath correlation time. However, if the bath spectrum displays sharp structures, their effects on the correlator of the system are only retained in the weak-coupling equation with its memory kernel. As expected, both approaches fail for the regime of large system-bath coupling. In that regime the linear bath may still represent a good approximation to the original nonlinear bath. Again, this applies, in particular, when the bath spectrum has a strongly peaked structure. However, deviations between the linear and the original nonlinear bath are clearly visible. Although we have only discussed a particular type of a nonlinear bath, we expect the statements about the regimes where the different approximations work to be valid for more complicated systems as well.

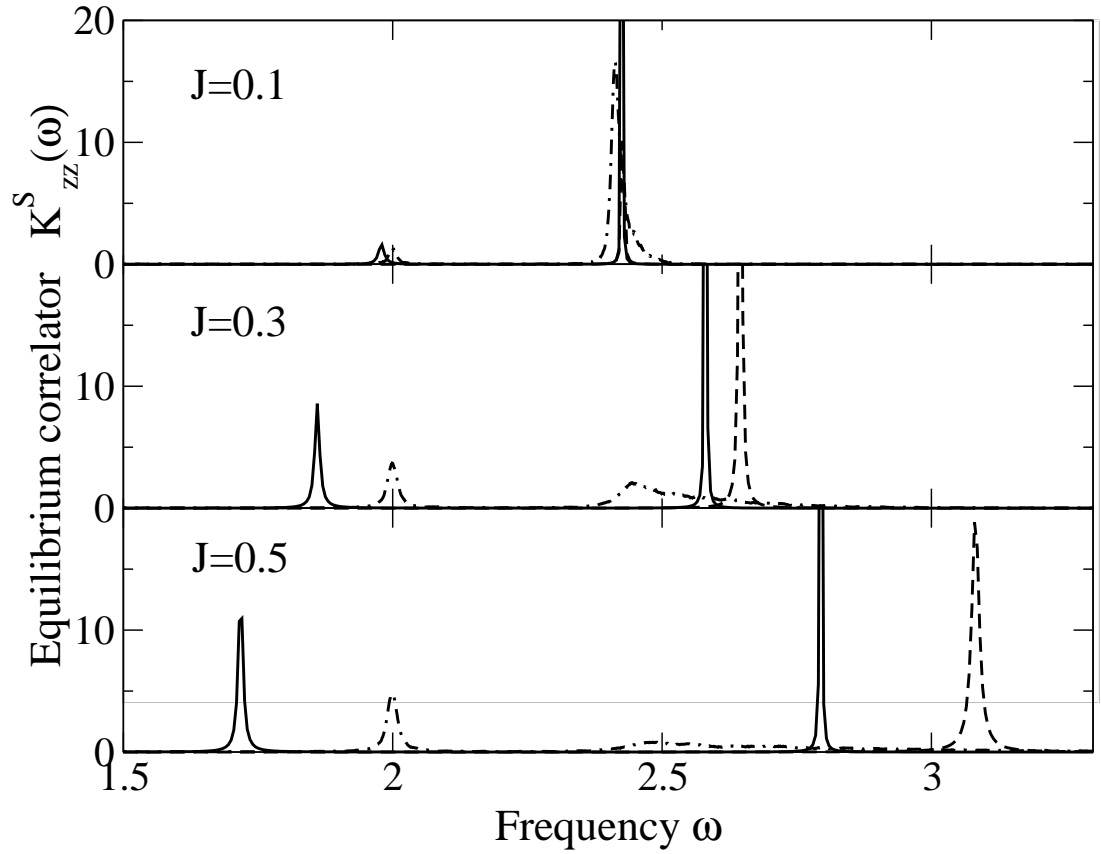


Figure 2.12: The Fourier-transform $K_{zz}^S(\omega)$ of the equilibrium correlator of $\hat{\sigma}_z^S(t)$, for different values of the coupling strength $J = 0.1, 0.3$ and 0.5 from topmost to lowest curve. The values of the other parameters are: $\Delta = 1$, $\Delta_S = 1.2$, $\gamma/2\pi = 0.001$ and $\epsilon_S = 0$. Approaches 1 and 4: solid line, Approach 2: dashed line, Approach 3: dash-dotted line.

From the point of view of computational effort, the stochastic simulation of Approach 3 is clearly the worst, because the differential equations must be integrated numerically many times to obtain the statistical average. The master equation and the weak-coupling approximation require the least effort, in particular because explicit analytical expressions could be found for our model.

Chapter 3

Flow Equation Results for Low Temperatures

In the previous chapter the nonlinear bath was discussed for high temperatures. In this chapter we concentrate on the opposite (low temperature) limit of the same model system. We saw that the investigation of the effects of our nonlinear bath consists of solving dissipative two- and four-state systems. Within the linear bath approximation we had to use a non-Ohmic bath spectral density, corresponding to colored noise in the high-temperature limit. Such systems of one or two spins coupled to linear oscillator baths have been studied in-depth using different methods, such as functional integral approaches [Leggett87, Dube01], master equations [Loss98, Governale01], and numerical calculations within the quasi-adiabatic propagator path integral method [Thorwart02]. In this work we use a different approach: the numerical flow equation renormalization method.

First, we derive flow equations for the more general system consisting of two spins coupled to oscillator baths, i.e., we examine the dissipative four-state system. Flow equations are a nice tool to analyze correlation functions. The numerical integration of the flow equations allows us to study the nonlinear bath model by analyzing the spin-spin correlation functions. The numerical results are obtained at zero temperature. As in Chapter 2, these results are then compared with those obtained from a linear bath with a non-ohmic bath spectral density. The bath-spectral density is chosen in such a way that the linear bath leads to the same results as the original nonlinear bath in the limit of small enough system-bath coupling strength. The bath and system correlation functions are both calculated using flow equations. By carrying out the comparison, we are able to study the effects of the nonlinear bath at zero temperature.

3.1 Introduction

Using the flow-equation method one works in a Hamiltonian framework. The whole procedure is non-perturbative, as it relies on a unitary transformation and has an

energy-scale separation built in. The effective Hamiltonian simplifies due to the fact that the coupling between bath and system disappears and equilibrium functions can be obtained easily. Note that the flow-equation results cannot be obtained using Feynman-diagrammatic techniques. The method is non-perturbative, e.g., neither a Born nor Markoffian approximation are applied, which is what makes it attractive and new. Some drawbacks are that the flow equations for the observables are not closed, and a special ansatz is used. Here we choose a linear ansatz, which works only for low temperatures T smaller than the typical low-energy scale of the system Hamiltonian H_S .

The flow-equation method itself was introduced by Wegner [Wegner94] and by Glasek and Wilson [Wilson93]. The extension to dissipative systems was developed in [Neu96, Kehrein96a, Kehrein96b, Mielke98]. What is new in our work is that we apply the method to a general two-spin (four-state) system coupled linearly to oscillator baths. The flow equations are designed to yield correlation functions for non-ohmic baths as well, which, as we will see below, makes it possible to treat the linear bath approximation to our nonlinear problem on the same footing. In [Kehrein96a, Stauber02a, Kleff03a, Kleff03b], subohmic, superohmic, and a peaked structured environment analogous to the one used in Chapter 4, defined in Eq. (4.31), were studied with flow equations. Similarly, the linear-bath approximation leads to a new peaked structured bath-spectral density, to our knowledge, never studied before. The basic strategy is to calculate first the equilibrium correlator of the two-level system exactly. Then we calculate it within the common linear-bath approximation, where the linear-bath correlation function is chosen to be the same as that of the nonlinear bath.

The rest of this chapter is divided into six sections: First we recall the general framework of the flow equation applied to dissipative systems. It only reflects the major steps in the derivation. After this brief introduction, we quote the flow equations for the general two-spin system coupled to linear oscillator baths. The flow equations for the nonlinear-bath system and its linear approximation are both special cases of these general flow equations. At the end of the chapter, we have collected a discussion of the numerics and a comparison of the results.

3.2 The general framework for a dissipative system

By using the flow equation technique, we would like to approximately diagonalize a model Hamiltonian¹ H containing a linear oscillator bath. In our case the bath is that introduced in Chapter 2 (given in Eq. (2.65)). We diagonalize the Hamiltonian by means of a unitary transformation

$$H(l) = U(l)HU(l)^\dagger. \quad (3.1)$$

¹In this chapter we omit the hats for the operators.

$U(l)$ depends on the flow parameter l . The flow parameter l has the dimension $1/\text{energy}^2$. Therefore, the value of l represents the square of the inverse energy scale, which is decoupled. The unitary transformation can be written in differential form as

$$\frac{dH(l)}{dl} = [\eta(l), H(l)] \quad (3.2)$$

with the anti-Hermitian generator

$$\eta(l) = \frac{dU(l)}{dl} U^{-1}(l), \quad (3.3)$$

where the initial condition is $H(0) = H$. Using $\eta(l)$ in the canonical form $\eta = [H_0, H(l)]$, where $H_0 = \sum_k \omega_k : b_k^\dagger b_k :$ is the linear oscillator bath, leads to the fixed point $H(l \rightarrow \infty) = H_0$. The commutator² $[\eta, H]$ contains coupling terms which are bilinear in the bosonic operators. We neglect these terms by truncating the Hamiltonian after linear bosonic terms. The bilinear terms are included by modifying the generator with an additional bilinear term as follows [Kehrein96b, Stauber02a]

$$\eta = [H_0, H] + \sum_{kq} \eta_{kq} : (b_k + b_k^\dagger)(b_q - b_q^\dagger) : . \quad (3.4)$$

The colons indicate normal ordering, which is defined by $: O := O - \langle O \rangle$ for an operator O . The normal order is defined with respect to the non-interacting Hamiltonian. The coefficients η_{kq} are chosen in such a way that the bilinear terms are not generated. Simply because this can not be done exactly, we neglect terms which have the normal ordered form: system operator times a bilinear bosonic operator.

3.2.1 The model Hamiltonian

The system which couples to the bath is described by a general Hamiltonian H_S , which is not yet specified. It couples linearly to the bosonic degrees of freedom of a linear oscillator bath. This is the only restriction, i.e., one can also treat non-ohmic (especially peaked) bath-spectral densities, which have gained recent interest [Garg85, Wilhelm03a, Thorwart03]. The general Hamiltonian of the system plus environment is given by

$$H = H_S + \sum_k H_k^+ (b_k + b_k^\dagger) + i \sum_k H_k^- (b_k - b_k^\dagger) + \sum_k \omega_k : b_k^\dagger b_k : . \quad (3.5)$$

The operators H_k^+ , H_k^- are the part of the system-bath interaction which acts on the system and b_k and b_k^\dagger are the usual bosonic creation and annihilation operators. We note that in [Kehrein96b], the generator η was chosen such that the Hamiltonian remains form invariant without the term $i \sum_k H_k^- (b_k - b_k^\dagger)$. Our approach is different because we allow the generation of such terms and we take a generator similar to the one used in [Stauber02a] for the dissipative two-state system.

²From now on all the l dependencies are suppressed in the formulas when not necessary.

3.2.2 Flow equations for the Hamiltonian

The continuous unitary transformation, which is applied to the Hamiltonian Eq. (3.5), is defined by a generator η . For the generator we use the following ansatz

$$\eta = i \sum_k A_k (b_k + b_k^\dagger) + \sum_k B_k (b_k - b_k^\dagger) + \sum_{kq} \eta_{kq} : (b_k + b_k^\dagger)(b_q - b_q^\dagger) : . \quad (3.6)$$

Note that the generator is antihermitian, as it should be ($\eta_{kq} = 0$ for $k = q$). A_k and B_k will be specified later by the canonical choice of the generator. As explained before, the last bilinear term in η is introduced to eliminate effective couplings between different bosonic modes with energies ω_k . During the flow, starting with the initial condition $H(0) = H$, the coupling constants become functions of the flow parameter l and evolve in such a way that the final Hamiltonian is H_0 . During the transformation, H_0 does not depend on l , since the flow equations for the energies $\omega_k(l)$ can be shown to be trivial in the thermodynamic limit (when the number of bath modes N goes to infinity [Neu96]). Therefore, the renormalization of the bath modes ω_k vanishes in the thermodynamic limit. Note further that, with this choice of the generator, one can construct the exact solution of the problem in the case of a harmonic oscillator or a free particle coupled to a bosonic bath [Kehrein96b]. The commutator of η with H is found to be

$$\begin{aligned} [\eta, H] = & i \sum_k \omega_k A_k (b_k - b_k^\dagger) + \sum_k \omega_k B_k (b_k + b_k^\dagger) \\ & + i \sum_k [A_k, H_S] (b_k + b_k^\dagger) + \sum_k [B_k, H_S] (b_k - b_k^\dagger) \\ & + i \sum_{kq} \langle [A_k, H_q^+] \rangle : (b_k + b_k^\dagger)(b_q + b_q^\dagger) : + i \sum_k [A_k, H_k^+] (2n_k + 1) \\ & + i \sum_{kq} ([A_k, H_q^+] - \langle [A_k, H_q^+] \rangle) : (b_k + b_k^\dagger)(b_q + b_q^\dagger) : \\ & + \sum_{kq} [B_k, H_q^+] : (b_k - b_k^\dagger)(b_q + b_q^\dagger) : + \sum_k [B_k, H_k^+] + \\ & + 2 \sum_{kq} \eta_{kq} H_q^+ (b_k + b_k^\dagger) \\ & + i \sum_{kq} \langle [B_k, H_q^-] \rangle : (b_k - b_k^\dagger)(b_q - b_q^\dagger) : - i \sum_k [B_k, H_k^-] (2n_k + 1) \\ & + i \sum_{kq} ([B_k, H_q^-] - \langle [B_k, H_q^-] \rangle) : (b_k - b_k^\dagger)(b_q - b_q^\dagger) : \end{aligned}$$

$$\begin{aligned}
& - \sum_{kq} [A_k, H_q^-] : (b_k + b_k^\dagger)(b_q - b_q^\dagger) : + \sum_k [A_k, H_k^-]_+ \quad (3.7) \\
& - 2i \sum_{kq} \eta_{kq} H_k^- (b_q - b_q^\dagger) \\
& + \sum_{kq} \eta_{kq} \omega_k : (b_k - b_k^\dagger)(b_q - b_q^\dagger) : + \sum_{kq} \eta_{kq} \omega_q : (b_k + b_k^\dagger)(b_q + b_q^\dagger) : .
\end{aligned}$$

The expectation value $\langle O \rangle$ is defined by $\langle O \rangle = \text{tr}\{O \exp(-\beta H_S)\} / \text{tr}\{\exp(-\beta H_S)\}$, where the trace is taken over the system alone and not over the bath. For zero temperature, $\langle O \rangle$ is the ground-state expectation value. $n_k = 1/(e^{\beta\omega_k} - 1)$ is the Bose distribution function. We choose η_{kq} such that couplings between different bath modes do not occur. To achieve this, we require the following condition

$$\eta_{kq} \omega_k + \eta_{qk} \omega_q + i \langle [B_k, H_q^-] \rangle + i \langle [B_q, H_k^-] \rangle = 0, \quad (3.8)$$

which eliminates terms of the form $:(b_k - b_k^\dagger)(b_q - b_q^\dagger):$ and also

$$\eta_{kq} \omega_q + \eta_{qk} \omega_k + i \langle [A_k, H_q^+] \rangle + i \langle [A_q, H_k^+] \rangle = 0, \quad (3.9)$$

which eliminates terms of the form $:(b_k + b_k^\dagger)(b_q + b_q^\dagger):$. These two conditions for η_{kq} can be solved

$$\begin{aligned}
\eta_{kq} = \frac{1}{\omega_q^2 - \omega_k^2} \left\{ i\omega_k \langle [B_k, H_q^-] \rangle + i\omega_k \langle [B_q, H_k^-] \rangle \right. \\
\left. - i\omega_q \langle [A_k, H_q^+] \rangle - i\omega_q \langle [A_q, H_k^+] \rangle \right\}. \quad (3.10)
\end{aligned}$$

When the two above conditions are satisfied, only terms which contain couplings of the system to two bosonic modes remain. Following [Kehrein96b, Stauber02a], we neglect these normal-ordered higher-order terms, which are

$$\begin{aligned}
& i \sum_{kq} ([A_k, H_q^+] - \langle [A_k, H_q^+] \rangle) : (b_k + b_k^\dagger)(b_q + b_q^\dagger) : \\
& \sum_{kq} [B_k, H_q^+] : (b_k - b_k^\dagger)(b_q + b_q^\dagger) : \\
& i \sum_{kq} ([B_k, H_q^-] - \langle [B_k, H_q^-] \rangle) : (b_k - b_k^\dagger)(b_q - b_q^\dagger) : \\
& \sum_{kq} [A_k, H_q^-] : (b_k + b_k^\dagger)(b_q - b_q^\dagger) : . \quad (3.11)
\end{aligned}$$

They are of the form of an operator acting on the system Hilbert space multiplied by a bilinear combination of bosonic operators. A rough estimate of these terms and their importance can be obtained if one integrates the corresponding coefficients over the flow parameter l .

3.2.3 Flow equations for the observables

For a subsequent calculation of correlation functions, the observables have to be subjected to the same sequence of infinitesimal transformations as the Hamiltonian.

$$\frac{dO}{dl} = [\eta, O]. \quad (3.12)$$

The flow of the observables cannot be closed and thus a linear ansatz has to be chosen, which is only valid for temperatures smaller than the typical low-energy scale of the system coupling to the linear oscillator bath

$$O = O_S + \sum_k O_k^+(b_k + b_k^\dagger) + i \sum_k O_k^-(b_k - b_k^\dagger). \quad (3.13)$$

We neglect higher normal-ordered terms in the expression for O and obtain the flow equations for the observables

$$\begin{aligned} \frac{dO_S}{dl} &= i \sum_k [A_k, O_k^+](2n_k + 1) - i \sum_k [B_k, O_k^-](2n_k + 1) \\ &+ \sum_k [B_k, O_k^+]_+ + \sum_k [A_k, O_k^-]_+ \end{aligned} \quad (3.14)$$

$$\frac{dO_k^+}{dl} = i[A_k, O_S] + 2 \sum_q \eta_{kq} O_q^+ \quad (3.15)$$

$$\frac{dO_k^-}{dl} = -i[B_k, O_S] - 2 \sum_q \eta_{qk} O_q^-. \quad (3.16)$$

The correlation functions of interested are defined by

$$\langle O(t)O \rangle = \frac{\text{tr}\{e^{-\beta H_0} e^{itH_0} O e^{-itH_0} O\}}{\text{tr}\{1_S \otimes e^{-\beta H_0}\}}. \quad (3.17)$$

For $l \rightarrow \infty$ we deal with the trivial fixed-point Hamiltonian H_0 . Correlation functions can be calculated easily because H_0 is only the bath Hamiltonian without interaction, i.e., H_0 commutes with all the system operators. The correlation function describing the dissipative behavior of the system can, of course, only be obtained if the decoupling procedure works properly and the coefficients to the corresponding operators decay completely for the chosen parameter regime. In our concrete model we confirm the decoupling numerically.

3.3 Flow equations for the dissipative four-state system

Armed with the terminology of the general flow equations, we can now pursue a specialization to the dissipative four-state system. First, the flow equations are obtained

for the most general two-spin system coupling to linear oscillator baths at finite low temperatures. Many other systems can be analyzed with the same flow equations given below. Later, we will focus on our special system, Eq. (3.27), which is a special case of the following Hamiltonian

$$\begin{aligned}
H &= \sum_{\alpha\beta} \Delta^{\alpha\beta} \Sigma_{\alpha\beta} + \sum_k \sum_{\alpha\beta} \lambda_k^{\alpha\beta} \Sigma_{\alpha\beta} (b_k + b_k^\dagger) \\
&+ i \sum_k \sum_{\alpha\beta} \kappa_k^{\alpha\beta} \Sigma_{\alpha\beta} (b_k - b_k^\dagger) + \sum_k \omega_k : b_k^\dagger b_k : .
\end{aligned} \tag{3.18}$$

The $\Sigma_{\alpha\beta}$ are tensor products of the Pauli matrices $\Sigma_{\alpha\beta} = \sigma_\alpha \otimes \sigma_\beta$ and the Greek indices are always summed from zero to three. σ_0 is the unit matrix. The resulting flow equations are listed in Appendix A.4 and constitute the first main result of this chapter. The flow equations are nonlinear ordinary coupled differential equations and they have the same structure as those obtained in [Stauber02a] due to the same truncation procedure. For the operators A_k and B_k showing up in the generator, Eq. (3.6), we find for the canonical choice of η

$$A_k = - \sum_{\alpha\beta} \Sigma_{\alpha\beta} \kappa_k^{\alpha\beta} \omega_k , \tag{3.19}$$

and

$$B_k = - \sum_{\alpha\beta} \Sigma_{\alpha\beta} \lambda_k^{\alpha\beta} \omega_k . \tag{3.20}$$

The result for η_{kq} is listed in Appendix A.5.

Let us now turn to the observable flow. The most general linear ansatz which will be useful in the following analysis is given by

$$\begin{aligned}
O &= \sum_{\alpha\beta} h^{\alpha\beta} \Sigma_{\alpha\beta} + \sum_k \sum_{\alpha\beta} \mu_k^{\alpha\beta} \Sigma_{\alpha\beta} (b_k + b_k^\dagger) \\
&+ i \sum_k \sum_{\alpha\beta} \nu_k^{\alpha\beta} \Sigma_{\alpha\beta} (b_k - b_k^\dagger) .
\end{aligned} \tag{3.21}$$

The observable flow equations Eq. (3.12) are closed according to the same normal ordering scheme as above and are listed in Appendix A.6. By evaluating $\langle O(t)O \rangle = \text{tr}\{e^{-\beta H_0} e^{itH_0} O e^{-itH_0}\} / \text{tr}\{\Sigma_{00} \otimes e^{-\beta H_0}\}$ one can find the correlation functions

$$\begin{aligned}
\langle O(t)O \rangle &= h^{00} h^{00} + h^{0i} h^{0i} + h^{i0} h^{i0} + h^{ij} h^{ij} \\
&+ \sum_k \left[(n_k + 1) e^{-i\omega_k t} c_k + n_k e^{i\omega_k t} c_k \right] ,
\end{aligned} \tag{3.22}$$

where

$$c_k = \mu_k^{00} \mu_k^{00} + \mu_k^{0i} \mu_k^{0i} + \mu_k^{i0} \mu_k^{i0} + \mu_k^{ij} \mu_k^{ij} \tag{3.23}$$

$$\begin{aligned}
&+ \nu_k^{00} \mu_k^{00} + \nu_k^{0i} \mu_k^{0i} + \nu_k^{i0} \mu_k^{i0} + \nu_k^{ij} \mu_k^{ij} \\
&- \mu_k^{00} \nu_k^{00} - \mu_k^{0i} \nu_k^{0i} - \mu_k^{i0} \nu_k^{i0} - \mu_k^{ij} \nu_k^{ij} \\
&- \nu_k^{00} \nu_k^{00} - \nu_k^{0i} \nu_k^{0i} - \nu_k^{i0} \nu_k^{i0} - \nu_k^{ij} \nu_k^{ij} .
\end{aligned} \tag{3.24}$$

The Fourier transform of the correlation function is given by

$$\begin{aligned} \langle OO \rangle_\omega &= (h^{00}h^{00} + h^{0i}h^{0i} + h^{i0}h^{i0} + h^{ij}h^{ij})\delta(\omega) \\ &+ \sum_k \left[(n_k + 1)\delta(\omega - \omega_k)c_k + n_k\delta(\omega + \omega_k)c_k \right], \end{aligned} \quad (3.25)$$

where the Fourier transform is defined by

$$\langle OO \rangle_\omega = \frac{1}{2\pi} \int_{-\infty}^{\infty} dt e^{i\omega t} \langle O(t)O \rangle. \quad (3.26)$$

With these formulas, different correlation functions can be calculated. They can also be used to obtain correlation functions for distinct operators, i.e., $\langle O^{(1)}(t)O^{(2)} \rangle$. The only difference in the result for c_k is that now a sum of products of the form $\mu_k^{(1)0i} \mu_k^{(2)0i}$ occurs and therefore the number of flow equations is increased. Which correlation function one wants to calculate is determined by the initial conditions of the observable flow equations. Further, the zero-temperature results can be obtained by setting $n_k = 0$ in all the equations given above.

3.4 Flow equations for the nonlinear bath

As a model for a nonlinear bath we study the same system as in Chapter 2. The system consists of a two-level system S coupled to a bath, which consists of another two-level system B coupling to a linear oscillator bath F

$$\begin{aligned} H &= \epsilon_S \sigma_z^S + \Delta_S \sigma_x^S + J \sigma_z^S \sigma_z^B + \Delta \sigma_x^B \\ &+ \sigma_z^B \sum_k \lambda_k (b_k + b_k^\dagger) + \sum_k \omega_k : b_k^\dagger b_k : . \end{aligned} \quad (3.27)$$

Here the parameters ϵ_S and Δ_S serve to define any desired two-level system S . This system is coupled to B via σ_z^B , with the coupling strength between S and B being given by J . The λ_k are defined in the following way, see Eq. (2.7)

$$\sum_k \lambda_k^2 \delta(\omega - \omega_k) = \frac{1}{\pi} \alpha \omega \Theta(1 - \omega/\omega_c), \quad (3.28)$$

with the bath cutoff ω_c and the system-bath coupling α . Again, we will analyze the dissipative dynamics of S by studying the decay of the equilibrium correlator $\langle \sigma_z^S(t) \sigma_z^S(0) \rangle$ by calculating its Fourier transform

$$K_{zz}^S(\omega) \equiv \frac{1}{2\pi} \int_{-\infty}^{+\infty} dt e^{i\omega t} \langle \sigma_z^S(t) \sigma_z^S(0) \rangle. \quad (3.29)$$

$K_{zz}^S(\omega)$ is real-valued and the integral over all frequencies yields 1. This sum rule is a sensitive test of the validity of the numerical results. Furthermore, $K_{zz}^S(\omega)$ vanishes on the negative real axis at zero temperature.

Let us now write down the flow equations for the specific case $\epsilon_S = 0$. Only $5N+7$ nontrivial³ equations are left (N is the number of bath modes)

$$\begin{aligned}
\frac{d\Delta^{00}}{dl} &= -2 \sum_k \left(\lambda_k^{31} \lambda_k^{31} + \lambda_k^{03} \lambda_k^{03} + \kappa_k^{21} \kappa_k^{21} + \kappa_k^{02} \kappa_k^{02} \right) \\
\frac{d\Delta^{01}}{dl} &= 4 \sum_k \kappa_k^{02} \lambda_k^{03} \omega_k \\
\frac{d\Delta^{10}}{dl} &= 4 \sum_k \kappa_k^{21} \lambda_k^{31} \omega_k \\
\frac{d\Delta^{22}}{dl} &= -4 \sum_k \kappa_k^{21} \lambda_k^{03} \omega_k \\
\frac{d\Delta^{33}}{dl} &= -4 \sum_k \kappa_k^{02} \lambda_k^{31} \omega_k \\
\frac{d\lambda_k^{03}}{dl} &= -\omega_k^2 \lambda_k^{03} - 2\kappa_k^{02} \Delta^{01} \omega_k + 2\kappa_k^{21} \Delta^{22} \omega_k + 2 \sum_q \eta_{kq} \lambda_q^{03} \\
\frac{d\lambda_k^{31}}{dl} &= -\omega_k^2 \lambda_k^{31} - 2\kappa_k^{21} \Delta^{10} \omega_k + 2\kappa_k^{02} \Delta^{33} \omega_k + 2 \sum_q \eta_{kq} \lambda_q^{31} \\
\frac{d\kappa_k^{02}}{dl} &= -\omega_k^2 \kappa_k^{02} - 2\lambda_k^{03} \Delta^{01} \omega_k + 2\lambda_k^{31} \Delta^{33} \omega_k - 2 \sum_q \eta_{qk} \kappa_q^{02} \\
\frac{d\kappa_k^{21}}{dl} &= -\omega_k^2 \kappa_k^{21} - 2\lambda_k^{31} \Delta^{10} \omega_k + 2\lambda_k^{03} \Delta^{22} \omega_k - 2 \sum_q \eta_{qk} \kappa_q^{21} \\
\frac{d\mu_k^{11}}{dl} &= 2\kappa_k^{02} h^{13} \omega_k + 2\kappa_k^{21} h^{30} \omega_k + 2 \sum_q \eta_{kq} \mu_q^{11} \\
\frac{dh^{13}}{dl} &= -2 \sum_k \kappa_k^{02} \mu_k^{11} \omega_k \\
\frac{dh^{30}}{dl} &= -2 \sum_k \kappa_k^{21} \mu_k^{11} \omega_k.
\end{aligned} \tag{3.30}$$

The first equation for the coefficient Δ^{00} constitutes an energy renormalization. It is not necessary to take this equation into account for the numerical integration of the correlation functions. Note further that the Hamilton flow equations are independent of the observable flow equations. But the converse is not true: the observable flow equations depend on the Hamilton flow equations. Further, if for a certain bath mode k the coupling parameters κ_k^{02} , κ_k^{21} , λ_k^{03} and λ_k^{31} vanish, then all the flow equations

³We call a flow equation trivial whenever the derivative with respect to l is equal to zero.

become trivial. Thus, if a mode is decoupled while integrating the flow equations, a smaller system can be used to integrate further. This fact can be used to achieve fast numerics as we will see below. Comparing this general Hamiltonian with Eq. (3.27) specifies the non-vanishing initial conditions

$$\begin{aligned}
\Delta^{10}(0) &= \Delta_S \\
\Delta^{30}(0) &= \epsilon_S \\
\Delta^{33}(0) &= J \\
\Delta^{01}(0) &= \Delta \\
\lambda_k^{03}(0) &= \lambda_k,
\end{aligned} \tag{3.31}$$

and for the observable-flow equations

$$h^{30}(0) = 1. \tag{3.32}$$

The η_{kq} coefficients are given by ($k \neq q$)

$$\begin{aligned}
\eta_{kq} &= \frac{1}{\omega_q^2 - \omega_k^2} \left\{ 2\omega_k \left[(\lambda_k^{03} \kappa_q^{21} \langle \Sigma_{22} \rangle + \lambda_k^{31} \kappa_q^{02} \langle \Sigma_{33} \rangle - \lambda_k^{03} \kappa_q^{02} \langle \Sigma_{01} \rangle - \lambda_k^{31} \kappa_q^{21} \langle \Sigma_{10} \rangle) \omega_k \right. \right. \\
&+ \left. \left. (\lambda_q^{03} \kappa_k^{21} \langle \Sigma_{22} \rangle + \lambda_q^{31} \kappa_k^{02} \langle \Sigma_{33} \rangle - \lambda_q^{03} \kappa_k^{02} \langle \Sigma_{01} \rangle - \lambda_q^{31} \kappa_k^{21} \langle \Sigma_{10} \rangle) \omega_q \right] \right. \\
&- 2\omega_q \left[(-\kappa_k^{02} \lambda_q^{31} \langle \Sigma_{33} \rangle - \kappa_k^{21} \lambda_q^{03} \langle \Sigma_{22} \rangle + \kappa_k^{02} \lambda_q^{03} \langle \Sigma_{01} \rangle + \kappa_k^{21} \lambda_q^{31} \langle \Sigma_{10} \rangle) \omega_k \right. \\
&+ \left. \left. (-\kappa_q^{02} \lambda_k^{31} \langle \Sigma_{33} \rangle - \kappa_q^{21} \lambda_k^{03} \langle \Sigma_{22} \rangle + \kappa_q^{02} \lambda_k^{03} \langle \Sigma_{01} \rangle + \kappa_q^{21} \lambda_k^{31} \langle \Sigma_{10} \rangle) \omega_q \right] \right\},
\end{aligned} \tag{3.33}$$

where the only non-vanishing expectation values are

$$\begin{aligned}
\langle \Sigma_{00} \rangle &= 1 \\
\langle \Sigma_{01} \rangle &= -\frac{\Delta(\Delta_S^2 + |\Delta||\Delta_S|)}{|\Delta||\Delta_S|\sqrt{J^2 + \Delta^2 + \Delta_S^2} + 2|\Delta||\Delta_S|} \\
\langle \Sigma_{10} \rangle &= -\frac{\Delta_S(\Delta^2 + |\Delta||\Delta_S|)}{|\Delta||\Delta_S|\sqrt{J^2 + \Delta^2 + \Delta_S^2} + 2|\Delta||\Delta_S|}
\end{aligned} \tag{3.34}$$

$$\langle \Sigma_{11} \rangle = \frac{\Delta\Delta_S}{|\Delta||\Delta_S|} \tag{3.35}$$

$$\langle \Sigma_{22} \rangle = \frac{3J\Delta\Delta_S + J|\Delta||\Delta_S| - \Delta\Delta_S\sqrt{J^2 + \Delta^2 + \Delta_S^2} + 2|\Delta||\Delta_S|}{4|\Delta||\Delta_S|\sqrt{J^2 + \Delta^2 + \Delta_S^2} + 2|\Delta||\Delta_S|} + \frac{1}{4}$$

$$\langle \Sigma_{33} \rangle = -\frac{J}{\sqrt{J^2 + \Delta^2 + \Delta_S^2} + 2|\Delta||\Delta_S|}.$$

For our special choice of parameters, h^{13} and h^{30} vanish for $l \rightarrow \infty$. At $T = 0$ the correlation function can then be evaluated according to Eq. (3.25) by setting $O = \sigma_z^S$

and thus analyzing the decay of the equilibrium correlator

$$K_{zz}^S(\omega) = \sum_k (\mu_k^{11}(l \rightarrow \infty))^2 \delta(\omega - \omega_k). \quad (3.36)$$

The flow equations for the biased case $\epsilon_S \neq 0$ are listed in Appendix A.8. The equilibrium correlator then further contains a delta-distribution contribution $\delta(\omega)$.

For a peaked, structured, bath, the equilibrium correlator can also be obtained using different approximate methods to verify the findings, e.g., a Markoff approximation or weak-coupling approximation can be applied to calculate the influence of the linear bath F on the system $S + B$ together, see Appendices A.9 and A.10. The master equation is expected to come close to the true result as long as the conditions of the Markoff and secular approximation are fulfilled. This means the coupling strength J has to be so small that the resulting decay of S proceeds slowly compared with the transition frequency itself (secular approximation) and with the correlation time of the bath (Markoff approximation). The weak-coupling approximation, keeping memory effects, should lead to even better results. The results of these two approximations are shown in Fig. 3.1 in comparison with the flow equation result. The agreement is reasonable within the scope of the applicability of the distinct approximations schemes. In Figs. 3.12 and 3.13 the Markoff approximation is plotted with a dotted line. For $\alpha = 0.025$, deviations become clearly significant.

3.5 The linear-bath approximation

In this section we study an approximation to the nonlinear bath. We do this by replacing the composite bath B and F by a linear oscillator bath acting on the system S . What we obtain is a spin-boson system with a non-ohmic peaked bath spectral density, as we will see below

$$H = \Delta_S \sigma_x^S + \epsilon_S \sigma_z^S + \sigma_z^S \sum_k \lambda_k (b_k + b_k^\dagger) + \sum_k \omega_k : b_k^\dagger b_k : , \quad (3.37)$$

where the bath-spectral density is chosen according to Eq. (2.63), given by the bath correlation function $J(\omega) = \pi \langle BB \rangle_\omega = \pi \sum_k \lambda_k^2 \delta(\omega - \omega_k)$.

We start our discussion by calculating the bath-correlation function, or its Fourier transform as in [Stauber02a]. The Fourier transform of the correlator of $B \equiv J \sigma_z^B$ defines the ‘‘bath spectrum’’ $\langle BB \rangle_\omega$. In the case of zero temperature $\langle BB \rangle_\omega$ vanishes for negative frequencies. The Hamiltonian of the bath alone is given by

$$H_{BF} = \Delta \sigma_x^B + \sigma_z^B \sum_k \lambda_k (b_k + b_k^\dagger) + \sum_k \omega_k : b_k^\dagger b_k : . \quad (3.38)$$

This is the initial Hamiltonian for the flow equations. For the purpose of calculating the bath-correlation function, one has to solve the symmetric spin-boson problem. This cannot be done in a closed analytical way [Weiss00, Grifoni99]. One alternate

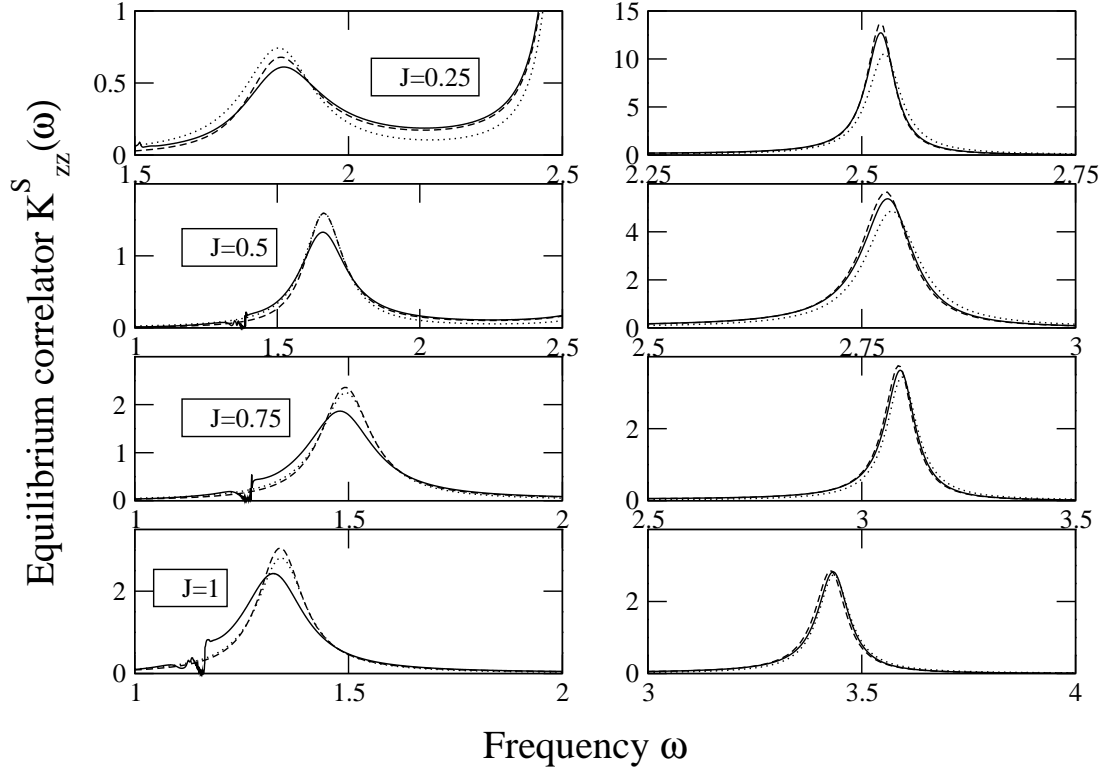


Figure 3.1: The Fourier-transform $K_{zz}^S(\omega)$ of the equilibrium correlator of $\hat{\sigma}_z^S(t)$, for different values of the system-bath coupling $J = 0.25, 0.5, 0.75$ and 1 from topmost to lowest graphs. One graph is split into two parts showing the regions around the peaks. The values of the other parameters are: $\Delta = 1$, $\Delta_S = 1.2$, $\alpha/(2\pi) = 0.01$, $\epsilon_S = 0$, $\omega_C = 5$, $N = 5000$, $l = 500$, except the lowest graphs, where $N = 10000$, $l = 1000$. All graphs show results of the nonlinear bath, where the approximations are applied to obtain the influence for weak-coupling strength α of the linear bath F on the system $S + B$. Flow equations: solid line, weak-coupling approximation: dashed line. Dotted line: Markoff approximation

method involves flow equations, which we apply again. The truncation scheme includes (as before) all coupling terms which are linear in the bosonic modes. The flow equation method is not restricted to any particular bath type, i.e., the bath-spectral density of the linear bath can be chosen freely.

For the Hamiltonian flow there are two nontrivial initial conditions $\Delta^{01}(0) = \Delta$, $\lambda_k^{03}(0) = \lambda_k$, see Fig. 3.2 and the following set of differential equations

$$\begin{aligned}\frac{d\Delta^{01}}{dl} &= -4 \sum_k \omega_k \lambda_k^{03} \kappa_k^{02} \\ \frac{d\lambda_k^{03}}{dl} &= -\omega_k^2 \lambda_k^{03} - 2\Delta^{01} \kappa_k^{02} \omega_k + 2 \sum_q \eta_{kq} \lambda_q^{03} \\ \frac{d\kappa_k^{02}}{dl} &= -\omega_k^2 \kappa_k^{02} - 2\Delta^{01} \lambda_k^{03} \omega_k - 2 \sum_q \eta_{qk} \kappa_q^{02}.\end{aligned}\quad (3.39)$$

The η_{kq} are given by

$$\eta_{kq} = \frac{2(\omega_k^2 + \omega_q^2) \lambda_k^{03} \kappa_q^{02} + 4\omega_k \omega_q \lambda_q^{03} \kappa_k^{02}}{\omega_q^2 - \omega_k^2}.\quad (3.40)$$

The energy is renormalized by a constant

$$\frac{d\Delta^{00}}{dl} = -2 \sum_k \left(\lambda_k^{03} \lambda_k^{03} + \kappa_k^{02} \kappa_k^{02} \right) \omega_k.\quad (3.41)$$

The nontrivial observable flow is given by

$$\begin{aligned}\frac{dh^{03}}{dl} &= -2 \sum_k \omega_k \kappa_k^{02} \mu_k^{01} \\ \frac{d\mu_k^{01}}{dl} &= 2\kappa_k^{02} h^{03} \omega_k + 2 \sum_q \eta_{kq} \mu_q^{01}\end{aligned}\quad (3.42)$$

starting from the initial condition $h^{03}(0) = 1$ and $\mu_k^{01}(0) = 0$. Note that the spin-boson system is a limiting case of the general dissipative four-state system. This fact can be used as a check of the two-spin flow equations.

For the symmetric spin-boson system h^{03} vanishes for $l \rightarrow \infty$. At $T = 0$ the correlation function is given by

$$\langle BB \rangle_\omega = \sum_k (\mu_k^{01}(l \rightarrow \infty))^2 \delta(\omega - \omega_k).\quad (3.43)$$

The results for the bath correlation function $\langle BB \rangle_\omega$ are shown in Fig. 3.3 and Fig. 3.4. $\langle BB \rangle_\omega$ consists of one peak at the frequency $\approx 2\Delta$, for small coupling α . For larger coupling it is shifted towards lower frequencies. Due to the fact the bath

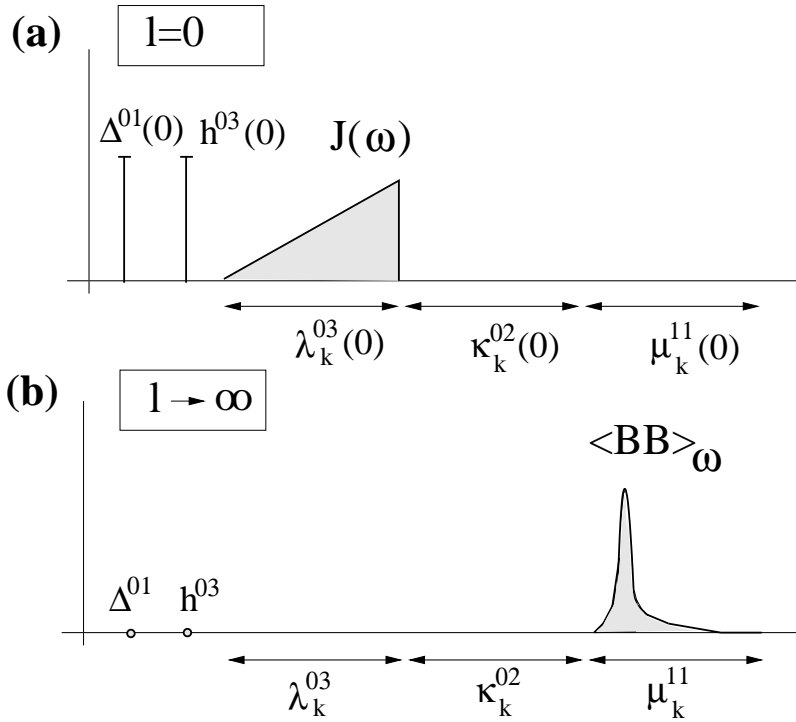


Figure 3.2: Schematic of the flow for $l = 0$ and $l \rightarrow \infty$. Different quantities are plotted in the indicated intervals of the horizontal axis, as a function of frequency (where appropriate). The topmost graph (a) shows the initial conditions for the flow equations starting with an ohmic bath-spectral density, evolving to the final state shown in graph (b), where the bath correlation function $\langle BB \rangle_\omega$ can be found. Note, that κ_k^{02} has finite values during the flow.

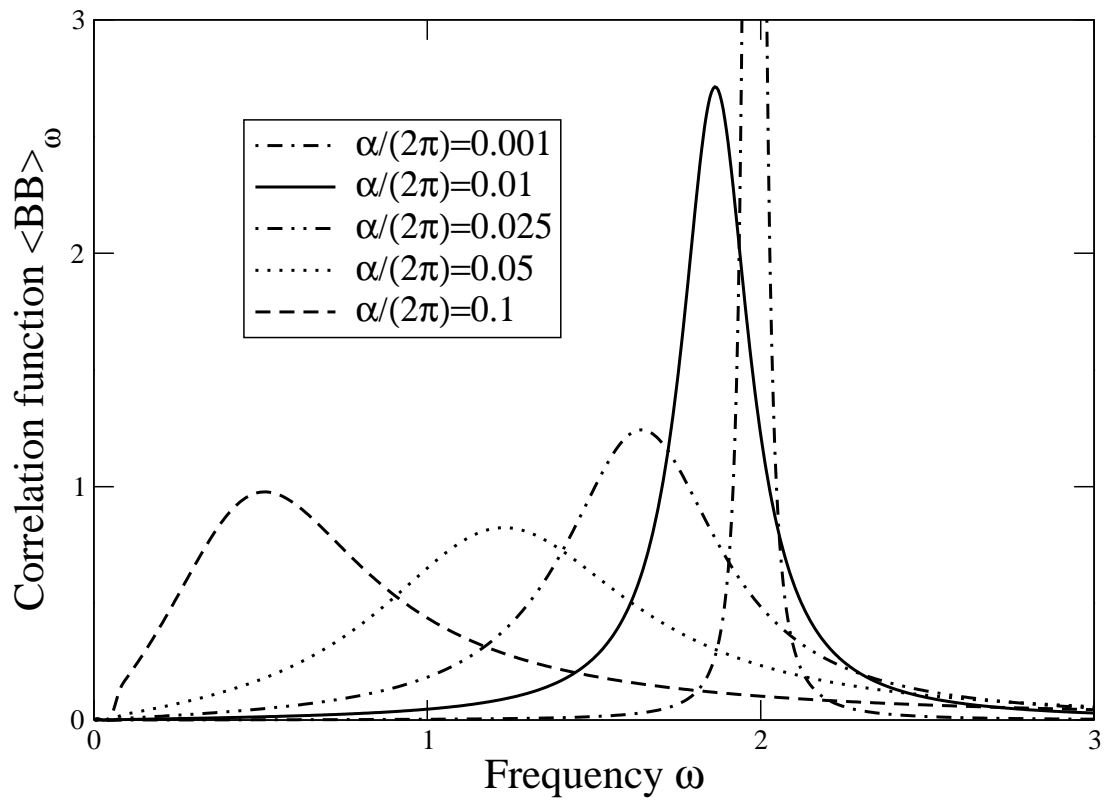


Figure 3.3: The $\langle BB \rangle_\omega$ correlation function for different values of α . The parameters are: $J = 1$, $\Delta = 1$ and $\omega_C = 10$. The height of the $\alpha = 0.001$ peak is ~ 20.7 .

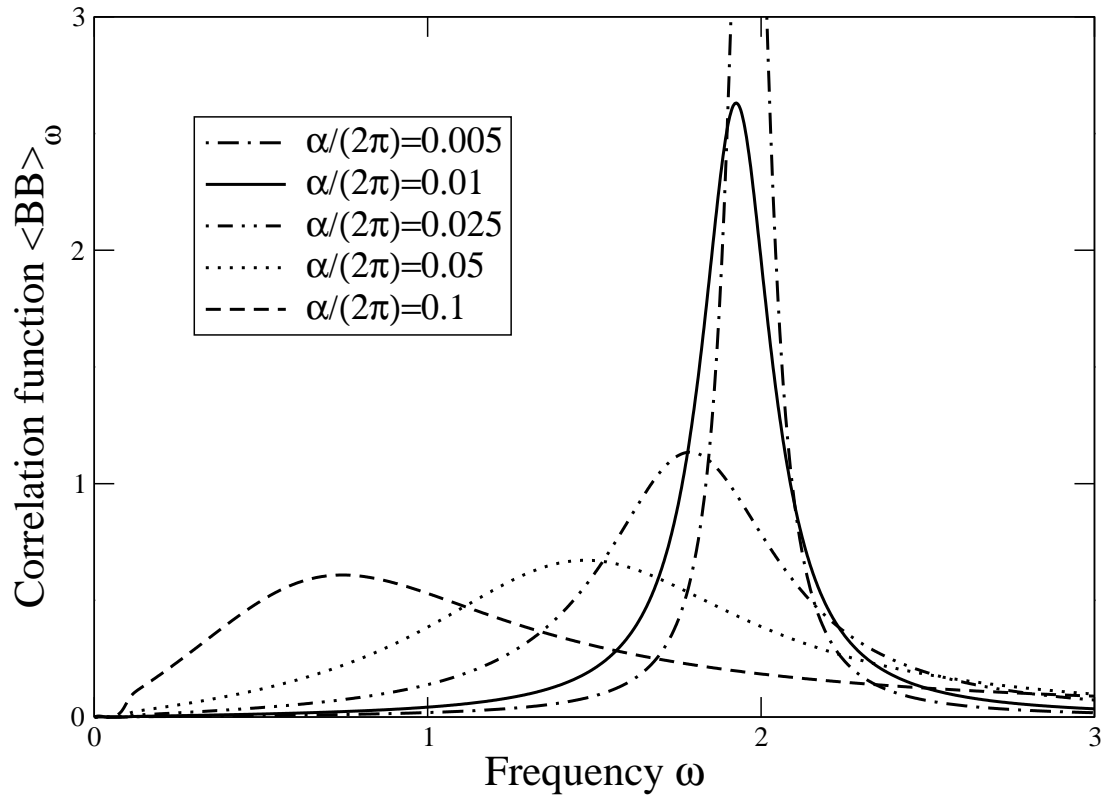


Figure 3.4: The $\langle BB \rangle_\omega$ correlation function for different values of α . The parameters are: $J = 1$, $\Delta = 1$ and $\omega_C = 5$. The height of the $\alpha = 0.005$ peak is ~ 5.2 .

F is an ohmic one, the position of the maximum of $\langle BB \rangle_\omega$ is given approximately by $2\Delta(2\Delta/\omega_c)^{2\alpha/(\pi-2\alpha)}$, which is a result obtained within an adiabatic renormalization scheme [Weiss00]. In our results, the relation is best fulfilled for $\alpha/(2\pi) \lesssim 0.025$. An exact relation, valid at zero temperature, is the Shiba relation given by

$$\lim_{\omega \rightarrow 0^+} \frac{\langle BB \rangle_\omega}{\omega} = \frac{4\alpha}{\pi J^2} \left(\int_0^\infty d\omega \frac{\langle BB \rangle_\omega}{\omega} \right)^2. \quad (3.44)$$

Here, the Shiba relation is shown for an Ohmic bath spectral density. This low-frequency behavior can only be found by solving the asymptotic flow equations [Stauber02a], which is not done in this work (note the deviation from linearity for small $\omega \ll 1$ in Fig. 3.3 and Fig. 3.4). Thus, the bath-spectral density shows a resonance at a characteristic frequency and behaves ohmic at small frequencies. This is why we expect the results to be comparable to the ones obtained in [Kleff03b, Thorwart03], where a bath spectral density of the form given in Eq. (4.31) was used. But we stress that here, in contrast, the linear bath is modified with a second two-state system, compared to an additional oscillator. In the weak-coupling limit, where $\alpha \ll 1$, we find

$$\begin{aligned} \langle BB \rangle_\omega &= \frac{16J^2\Delta^2}{\pi} \Theta(\omega) \Theta(1 - \omega/\omega_c) \\ &\times \frac{\alpha\omega}{[4\Delta^2 - \omega^2 - \frac{2}{\pi}\alpha\omega^2 \log((\omega_c/\omega)^2 - 1)]^2 + [2\alpha\omega^2]^2}. \end{aligned} \quad (3.45)$$

The difference between the above and Eq. (4.31) is apparent in the weak-coupling limit. In Fig. 3.5 we show numerical results for the weak-coupling and Markoff approximation, derived in Appendices A.10 and A.9, for increasing α . For lower coupling strengths ($\alpha \leq 0.01$) we find good agreement between the different approaches. However, for higher coupling, e.g. $\alpha = 0.1$, the flow equations fulfill the Shiba relation to a reasonable extent, where the other two approaches fail, see Fig. 3.5. For larger coupling the sum rule $\int_{-\infty}^{+\infty} \langle BB \rangle_\omega = J^2$ is best fulfilled for the flow equations.

To obtain the final result for the linear bath approximation we use the $\langle BB \rangle_\omega$ correlation function as a bath spectrum $J(\omega) = \pi \langle BB \rangle_\omega$ and solve the flow equations for the spin-boson system with this non-ohmic spectrum. The results are discussed in Section 3.7.

To close this section, we make a short note regarding higher-order correlation functions with respect to the flow equations used here. Higher-order correlation functions are important to understand the behavior of a nonlinear bath. In Chapter 2 we saw that for small-enough system-bath coupling strength, the nonlinear bath is identical to a linear one. In this limit, the two-time bath correlation function played a crucial role. For higher coupling strength, higher-order correlation functions become relevant. The linear bath has the special feature that higher-order correlation functions factorize into two-time correlation functions, since due to the Gaussian nature of the linear bath, the cumulant expansion breaks off at second order. The nonlinear case has generally no such feature, but we will see that the correlation

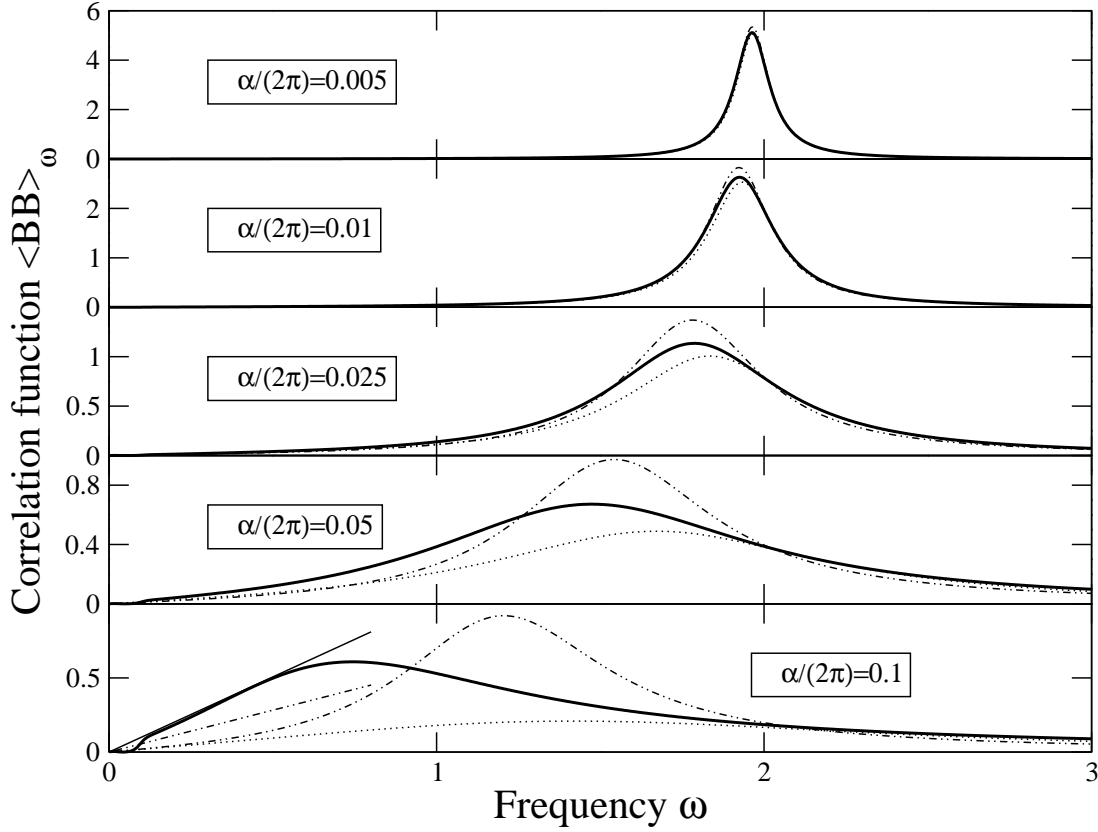


Figure 3.5: The $\langle BB \rangle_\omega$ correlation function for different values of α . The parameters are: $J = 1$, $\Delta = 1$ and $\omega_C = 5$. Solid line: Flow equations, dotted line: Markoff approximation, dashed double dotted line: weak-coupling approximation. In the lowest graph we show, as a check of the Shiba relation, the linear line which has a slope given by the numerical value of the left-hand side of Eq. (3.44). It can be compared with the slope of the corresponding correlation functions at low frequencies.

functions obtained with the flow equations factorize. The reason for this is the choice of a linear ansatz for the observable flow:

$$\sigma_z(l) = h^{03}(l)\sigma_z + \mu_k^{01}(l)\sigma_x(b_k + b_k^\dagger). \quad (3.46)$$

In the limit $l \rightarrow \infty$ we find for the symmetric spin-boson system

$$\sigma_z(l \rightarrow \infty) = \mu_k^{01}(l \rightarrow \infty)\sigma_x(b_k + b_k^\dagger), \quad (3.47)$$

and $H(l \rightarrow \infty) = H_0 = \sum_k \omega_k b_k^\dagger b_k$. So for $l \rightarrow \infty$ the observables behave like linear oscillator variables and all higher-order correlation functions factorize.

3.6 Details of the numerical calculation

The flow equations are coupled ordinary differential equations. The integration method which turns out to be the most appropriate one is the fourth-order Runge

Kutta method with variable step size [Numerical Recipes]. The reason for this is that there are regions where a certain subset of the differential equations does not change much anymore and larger integration steps can be used, see discussion below.

For the bath modes ω_k we have used a linear energy spacing $\delta\omega$ and a sharp cutoff function $f(x) = \Theta(1 - x)$. The results do not depend on these choices. The bath modes ω_k are then given by $\omega_k = (k - 1/2)\delta\omega$ and the coupling constants λ_k are found to be $\lambda_k = (\sqrt{2\alpha/(2\pi)}\sqrt{k - 1/2})\delta\omega$, where $\delta\omega = \omega_c/N$ and N is the number of bath modes used for the numerics. For the two-spin system the number of differential equations is $64N + 32$ in the most general case, $5N + 7$ for the nonlinear bath with $\epsilon_S = 0$, $10N + 14$ for the nonlinear bath with $\epsilon_S \neq 0$ and $3N + 2$ for the symmetric spin boson system. We have used up to $N = 10000$ bath oscillators. For the particular choice $\epsilon_S = 0$, the correlation function at discrete frequencies is given by $K_{zz}^S(\omega_k) = (\mu_k^{11})^2/\delta\omega$. All the $h^{\alpha\beta}$ coefficients vanish for increasing flow $l \rightarrow \infty$, as expected.

We choose the diagonal fixed-point Hamiltonian to be the noninteracting linear oscillator bath, which is scale-independent. Since there is no asymptotic scale present, the flow equations will first decouple the high-energy modes and then the low-energy modes. The same feature is found for the correlation functions, see Fig. 3.6. They are first determined for high energies and the low-energy behavior is calculated last. The frequency regions of interest are centered on the peaks which appear at the shifted transition frequencies of the two-spin system. The spectral function around these resonances is determined by a stable flow away from the asymptotic regime, which must be treated in a different way [Kehrein96b, Stauber02a, Stauber02b]. In practice, the flow equation can only be integrated up to $l^* \approx (\delta\omega)^{-2}$. We find that the integration can be stopped for much lower values; the system is decoupled with a high accuracy for $l > 20$, see again Fig. 3.6.

Let us discuss the consequences for the numerics. The coupling constants of the Hamiltonian, $\lambda_k^{\alpha\beta}$, and $\kappa_k^{\alpha\beta}$ decay while the flow parameter l is varied from zero to infinity. If we take a closer look at the flow equations, we observe that the differential equations for a certain mode k become trivial as soon as the $\lambda_k^{\alpha\beta}$ and $\kappa_k^{\alpha\beta}$ are approximately zero. First the higher modes are decoupled. In the end, there is only a low frequency region left where changes take place, see Fig. 3.6. This is why, in practice, all the differential equations outside of this region can be replaced by trivial ones in the program. This accelerates the calculation significantly.

The correlation function is given as a bilinear form in the $\mu_k^{\alpha\beta}$ and $\nu_k^{\alpha\beta}$. The coefficients $\mu_k^{\alpha\beta}$ and $\nu_k^{\alpha\beta}$ turn out to be zero at certain points. For the special case of the nonlinear bath with $\epsilon_S = 0$, only μ_k^{11} remains, which vanishes (intersects the frequency axis) at different points $\omega < 2$. This feature is contained in the flow equations and was also observed in [Kehrein96b] for the dissipative two-state system. The correlation function, bilinear in μ_k^{11} , therefore has unphysical zero points, which constitute a finite-size effect, only disappearing in the thermodynamic limit.

There are different possibilities to address this problem. In [Kehrein96b] it was observed that for a certain value of the flow parameter, the decoupled two-state

system behaved like a dissipative harmonic oscillator. Further, it was shown that for the dissipative harmonic oscillator there exists a conserved quantity which could be added at a certain value of l in order to complete the correlation function. Another possible way to deal with this problem is to integrate to a large value of l , such that the higher frequencies of the right peak are decoupled, as in Fig. 3.6. Then, to continue the integration in a restricted frequency range with a denser resolution of the bath modes. Finally, only a tiny gap is left which can then be closed by hand.

Furthermore, all the ‘‘Gibbs phenomena’’ like spikes around this singularity, are due to a finite number of bath modes N , i.e., we assume that the phenomena will disappear for increasing N . These spikes, generated via an amplifying effect, are not completely understood. Probably, they occur always if the change in the correlation function happens too abruptly. This suggestion is motivated by the observation that the same feature appears, if the cutoff is chosen too close to the characteristic frequency of the system. There, we find that, due to the intrinsic properties of the differential-equation system, a spike appears at the cutoff frequency. The system always needs a certain frequency range to spread out smoothly.

The sum rules are fulfilled with an accuracy of $\sim 0.5\%$ when not otherwise mentioned.

Two different values were used for the bath cutoff: $\omega_c = 5$ and $\omega_c = 10$. The results depend on the choice of the bath cutoff ω_c . However, the qualitative behavior is independent of the cutoff and remains the same for different large-enough ω_c .

Flow equations give the best results for small coupling α . This does not mean that the approach is perturbative in the usual sense, but the neglected terms in the truncation procedure are smaller in the low-coupling limit.

3.7 Comparison of nonlinear with linear bath

The relevant parameters in our model are ϵ_S , Δ_S , Δ , the coupling strength J , and the coupling strength α to the linear bath F . As in Chapter 2, we choose the time scale such that $\Delta \equiv 1$. Furthermore, the results discussed in the following have been calculated for $\Delta_S = 1.2$, close to 1, to keep the decay strong without being in resonance. The temperature is set to zero ($T = 0$). The two parameters α, J are varied.

To begin our discussion, we note some generic features of the results obtained for the two approaches: linear and nonlinear bath. Since $K_{zz}^S(\omega)$ is essentially the Fourier transform of relaxational dynamics, it consists of several ‘‘Lorentzian like’’ peaks. Their number is constrained to be less than the maximum number of 6 transition frequencies for $S + B$ in the case of the nonlinear-bath system. In practice, degeneracies between transition frequencies and selection rules reduce that number, e.g., to 2 for the unbiased case, see Fig. 3.7. More peaks, than one transition frequency expected for a two level system, are observed in the case of the linear-bath approximation. It turns out that the second peak is induced by the peaked bath spectral density. To summarize, we have found for the unbiased case two peaks for

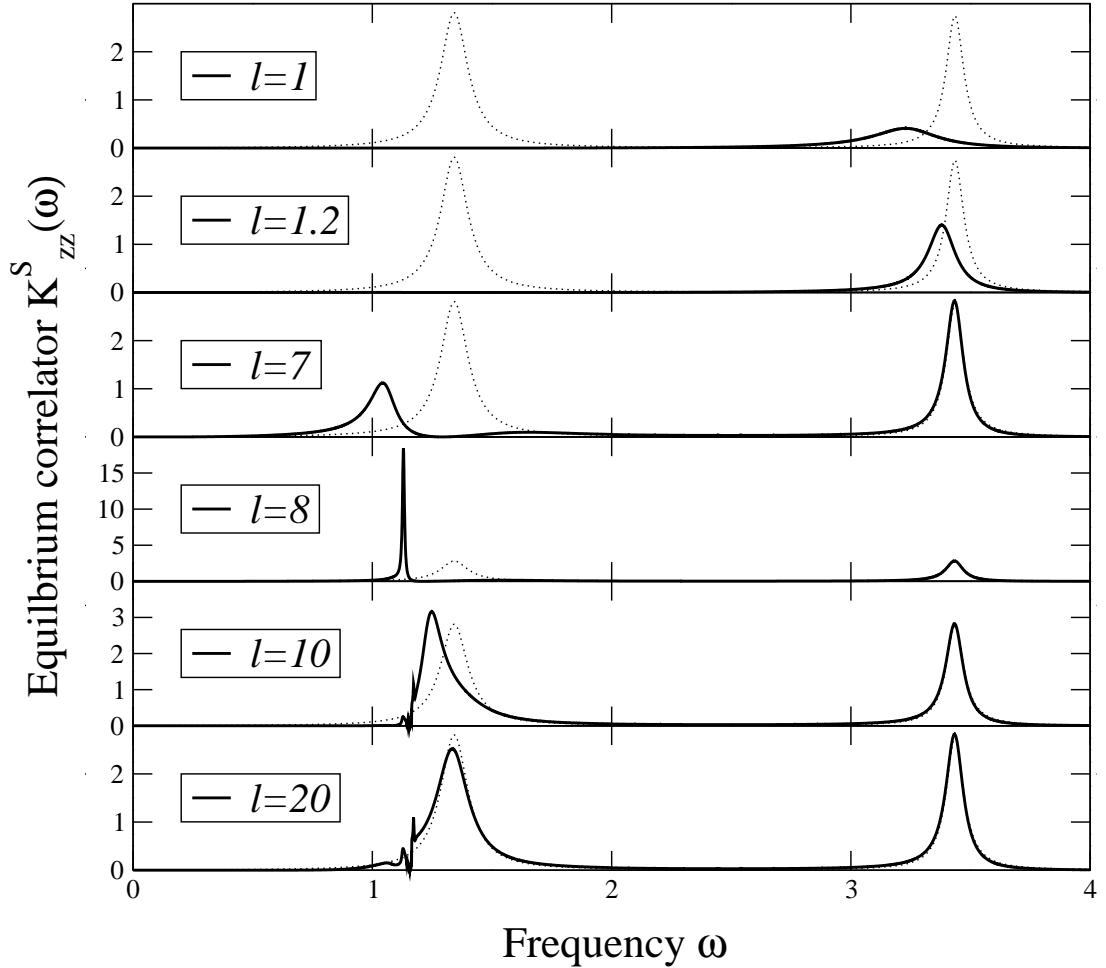


Figure 3.6: Fourier transform of the equilibrium correlator for increasing flow parameter l (solid line), compared with the final result of a Markoff approximation (dotted line). We see that the higher modes are decoupled first, i.e., the peak on the right hand is visible already up for $l = 7$. At $l = 20$ the sum rule is fulfilled with a high accuracy $\approx 0.5\%$. This result is better than the Markoff approximation used to calculate the influence of the linear bath F on the system $S + B$, which should also lead to good results for $\alpha/(2\pi) = 0.01$. The sum rule is naturally not valid at the beginning of the flow. The parameters are: $\Delta = 1$, $\Delta_S = 1.2$, $J = 1$, $\alpha/(2\pi) = 0.01$, $N = 8000$, and $\omega_C = 5$.

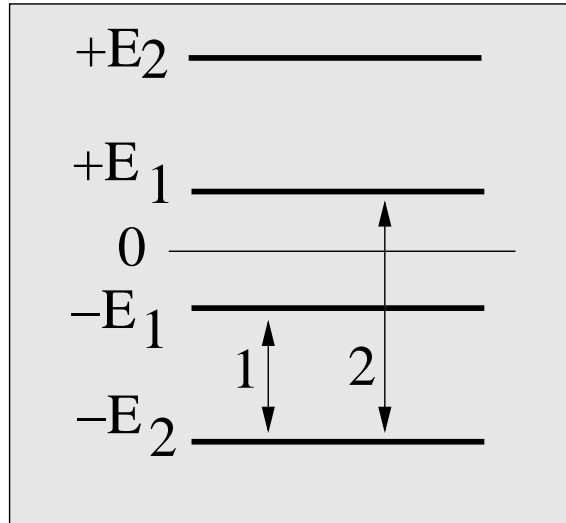


Figure 3.7: Spectrum of the two-spin system $S + B$. In the unbiased case $\epsilon_S = 0$ and for weak coupling α there are two distinct transition possible from the ground state at zero temperature, leading to two dephasing peaks in the equilibrium correlator.

the linear and the nonlinear bath. With the two peaks, one can associate two different decoherence times. Both approaches show a similar behavior for increasing coupling J , where we observe a larger separation between the two peaks. For the unbiased case $\epsilon_S \neq 0$, we expect at least three peaks for weak coupling α , see Fig. 3.8. Additional possible zero-frequency delta-distribution contributions show up for the biased case, due to the definition of the correlation functions. Moreover, in contrast to the high-temperature results, no “pure” relaxation is seen in the biased case.

Let us now focus on the unbiased case, i.e., $\epsilon_S = 0$. In the limit of weak coupling, $J \rightarrow 0$, all that remains is a broadened peak at the transition frequency $2\Delta_S$ of system S alone. In that limit, the results for the two approaches coincide, as expected. See topmost plots of Figs. 3.10–3.13, where the Fourier transform of the equilibrium correlator is shown for increasing system-bath coupling J , while $\alpha/(2\pi) = 0.1, 0.05, 0.025, 0.01$ is kept constant. According to the discussion in Chapter 2, we expect that for small J the nonlinear and the linear bath results fall together, i.e., in this limit a weak-coupling approximation [Gardiner00] or a Markoff approximation [Blum96] are valid and one can therefore not distinguish between linear and nonlinear bath. Furthermore, the bath spectral density was chosen such that the two approaches agree for small enough coupling.

With increasing J , the peaks are broadened and shifted, and additional peaks may appear (see Figs. 3.10 and 3.11). Indeed, the most notable difference from a master equation used for coupling of S and the nonlinear bath is the appearance of a second peak around the transition frequency 2Δ of the two-level fluctuator B . In this way, the power spectrum of the bath fluctuations appears in the short-time behavior of the correlator of the system S . This behavior cannot be captured by a master

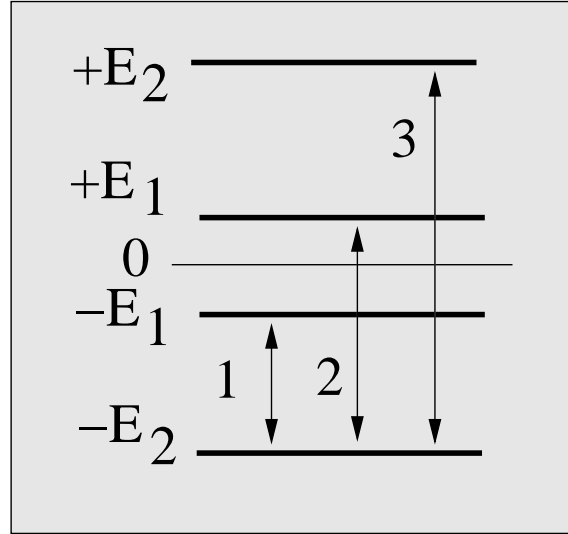


Figure 3.8: Spectrum of the two-spin system $S + B$. In the biased case $\epsilon_S \neq 0$ and for weak coupling α there are three distinct transition possible from the ground state at zero temperature, leading to three dephasing peaks in the equilibrium correlator.

equation, where only one peak is present, see Appendix A.9. Here, for the chosen parameters the linear and nonlinear baths agree very nicely for $J = 0.25$, rather to our surprise, also very well up to $J = 0.5$. For $J > 0.5$ the deviations become significant. Increasing J leads to a frequency shift and a change in the width of the “original” peak at $2\Delta_S$. These changes are due to the change in eigenfrequencies and eigenvectors of the combined system $S + B$. If we keep $J = 1$ constant and compare the results for different increasing α , see Fig. 3.9, the differences between linear and nonlinear bath depend on the ratio J/α . A small $\alpha/(2\pi) = 0.005$ or $\alpha/(2\pi) = 0.01$ corresponds to a structured bath (Figs. 3.3, 3.4) and the results show that the peak shape is similar for nonlinear and linear baths, but the peak position is different. We stress that for higher coupling, $\alpha/(2\pi) = 0.05$, or $\alpha/(2\pi) = 0.1$, the nonlinear bath acquires new structures (other peaks) and the shape of the peak deviates significantly from the linear bath. Thus, the qualitative differences between linear and nonlinear baths are smaller for a structured bath.

Since the linear bath takes the full bath spectrum $\langle BB \rangle_\omega$ as input, this spectrum may also show up in the result for the system correlator $K_{zz}^S(\omega)$, as is indeed the case. The Figures 3.10–3.13 demonstrate that this effect is independent of the α 's considered here, in contrast to the infinite temperature limit, where this effect was most pronounced for small γ , where the bath spectrum has a relatively sharp structure. To emphasize this point, we note that even the asymmetric shape of the bath spectral density $\langle BB \rangle_\omega$ is mapped to the equilibrium correlator, see, e.g., Figs. 3.10 and 3.11 compared with Fig. 3.4. This is an effect of the non-ohmic structure of the bath, which could not be observed for an ohmic linear bath. It can further only be observed when S and B are in resonance, i.e. for low frequencies the bath spectral

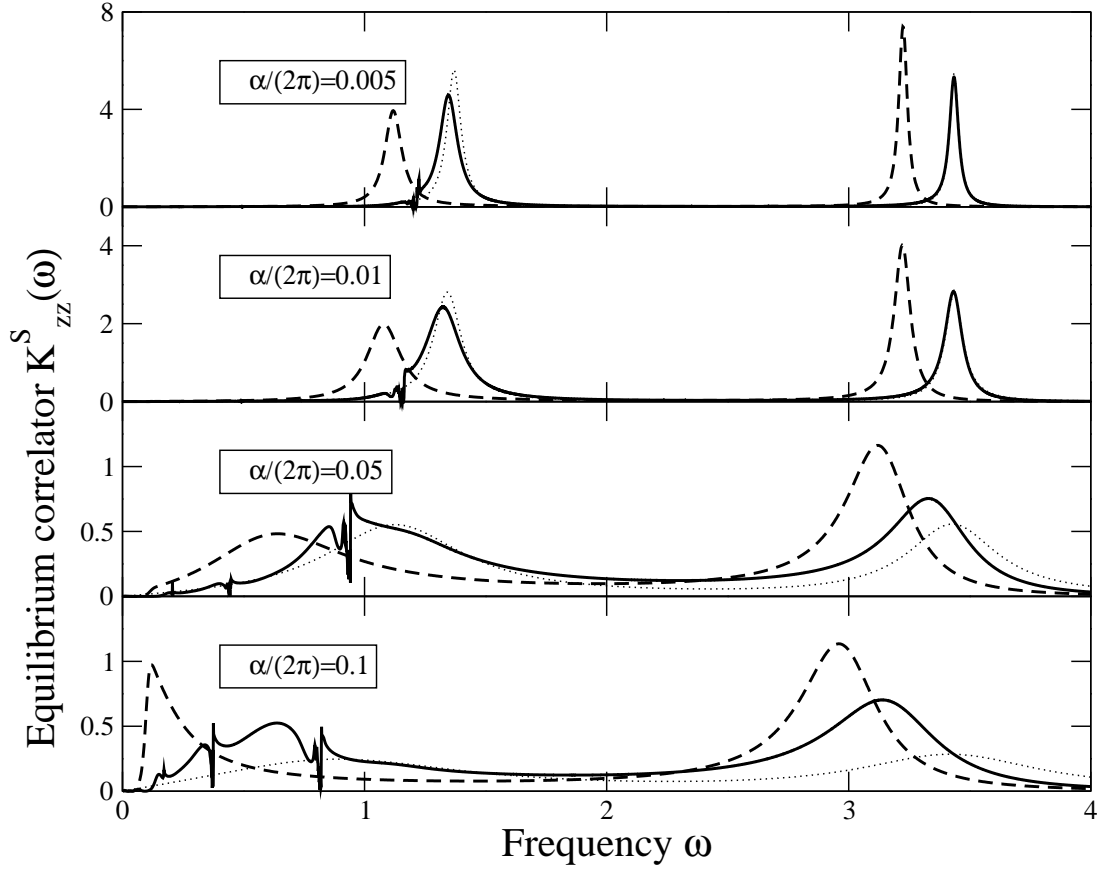


Figure 3.9: The Fourier transform $K_{zz}^S(\omega)$ of the equilibrium correlator of $\hat{\sigma}_z^S(t)$, for different structured nonlinear baths with $\alpha/(2\pi) = 0.005, 0.01, 0.05$ and 0.1 from topmost to lowest graph. The values of the other parameters are: $\Delta = 1$, $\Delta_S = 1.2$, $J = 1$, $\epsilon_S = 0$, $\omega_C = 5$, $N = 5000$, $l = 500$. Nonlinear bath: solid line, linear bath: dashed line. Dotted line: Markoff approximation. In Sec. 3.6 we discuss the singularities appearing in the correlators, e.g., in the lowest graph at frequency $\omega \approx 0.8$.

density behaves ohmically. The second peak, which appears for higher coupling J , is therefore determined by the bath correlation function $\langle BB \rangle_\omega$ with one peak in the vicinity of the system transition frequency and another given by the energy scale $2\Delta_S = 2.4$. For increasing system-bath coupling J , both peaks are shifted away from each other. Within the linear-bath approximation, the peak around $2\Delta_S$ is shifted to higher frequencies to a lesser extent and the second peak around 2Δ is shifted to lower frequencies, more pronounced compared to the nonlinear bath.

The qualitative agreement between the linear and nonlinear bath is especially good up to intermediate coupling strengths, as discussed previously. Nevertheless, there are deviations: In particular, the shifts are different. In contrast to infinite temperature there is a visible shift of the peaks for the linear bath, while changing the parameters J and α . Further, the peaks become wider and more asymmetric, but not as pronounced as the peak around $2\Delta_S$ for infinite temperature. For higher values of α , the linear bath, in general, shows less structure than the actual nonlinear bath, but still the asymmetric shape of the peaks is mimicked to some extent.

Finally, to close this section let us turn to the biased case $\epsilon_S \neq 0$. Fig. 3.14 shows the equilibrium correlator of $\hat{\sigma}_z^S(t)$ for two different values of the bias: $\epsilon_S = 0.5$ and $\epsilon_S = 1$. For comparison, the Markoff approximation is also shown, which should lead to reasonable results for $\alpha/(2\pi) = 0.01$, but the agreement between the two approaches is worse than for the unbiased case. We note that the flow equations do not describe the third peak. What is the reason for this? Flow equations constitute unitary change of basis. Therefore, we expect the same results for each unitarily equivalent Hamiltonian. As soon as approximations are made, things do change, since, depending on the representation of the Hamiltonian, different terms have different significance. Our approximation scheme leads to better results for the unbiased case. This was also seen in [Stauber02a] for the spin-boson problem, where shifts of the bosonic modes were introduced and tuned to an optimal point in order to deal with this problem. We leave such an analysis in the case of the dissipative four-state system for future work.

3.8 Conclusions

The first main result of this chapter is the derivation of the flow equations for the two-spin system coupled to linear baths. With this framework, not only the correlation functions of our nonlinear bath model can be studied, but correlation functions for any four-state system coupled linearly to oscillator baths. An additional key aspect is that there is no restriction for these baths to have an ohmic spectrum.

As an application of these general flow equations, a model of a nonlinear bath was discussed, consisting of a single two-level system subject to a linear oscillator bath. Its action on another two-level system at zero temperature has been analyzed and compared with the results due to a linear oscillator bath substituted for the nonlinear one. Many numerical results for various special cases have been obtained and discussed.

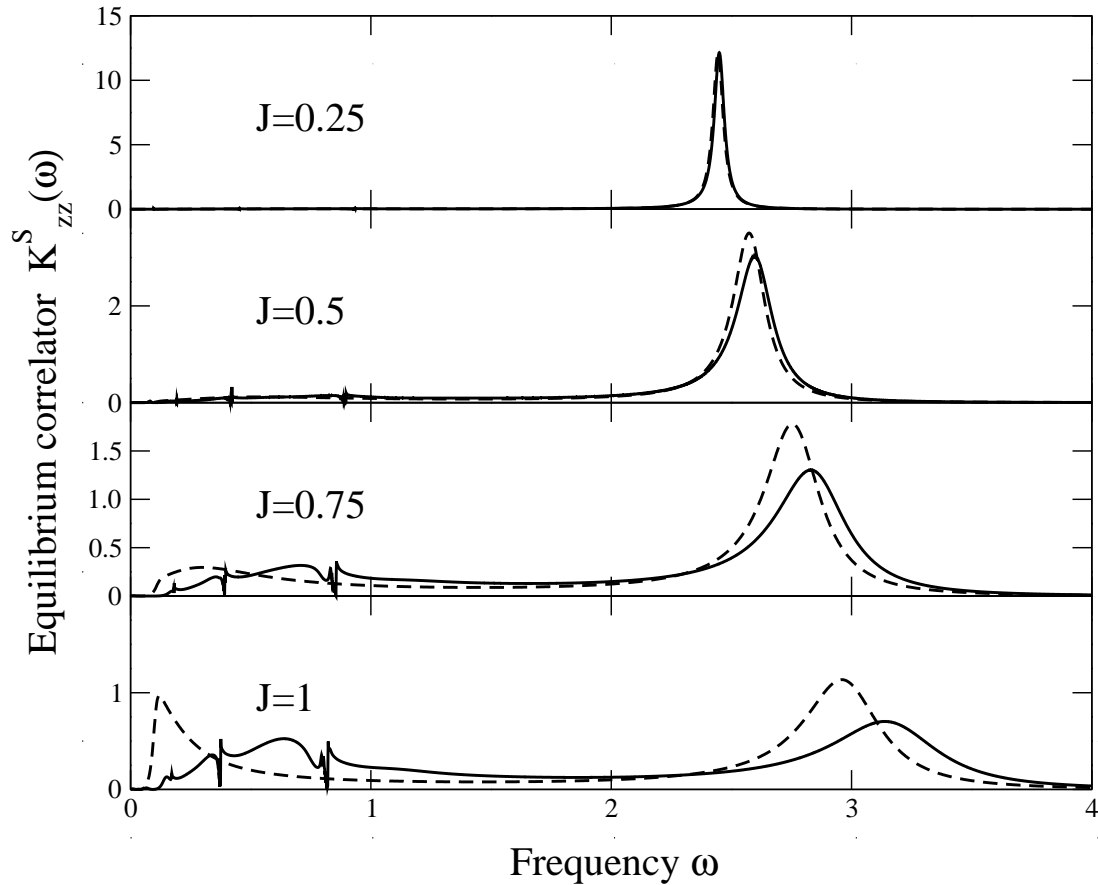


Figure 3.10: The Fourier transform $K_{zz}^S(\omega)$ of the equilibrium correlator of $\hat{\sigma}_z^S(t)$, for different values of the system-bath coupling $J = 0.25, 0.5, 0.75$ and 1 from topmost to lowest graph. The values of the other parameters are: $\Delta = 1$, $\Delta_S = 1.2$, $\alpha/(2\pi) = 0.1$, $\epsilon_S = 0$, $\omega_C = 5$, $N = 5000$, $l = 500$. Nonlinear bath: solid line, linear bath: dashed line.

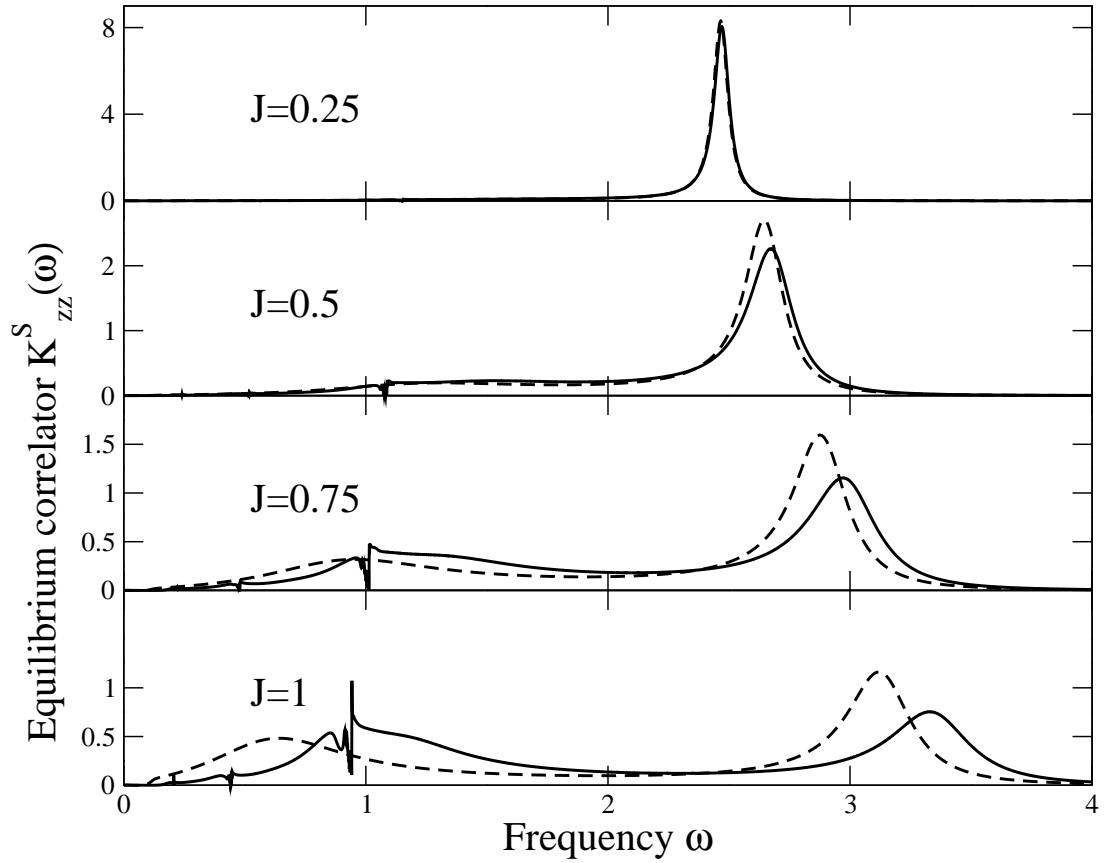


Figure 3.11: The Fourier transform $K_{zz}^S(\omega)$ of the equilibrium correlator of $\hat{\sigma}_z^S(t)$, for different values of the system-bath coupling $J = 0.25, 0.5, 0.75$ and 1 from topmost to lowest graph. The values of the other parameters are: $\Delta = 1$, $\Delta_S = 1.2$, $\alpha/(2\pi) = 0.05$, $\epsilon_S = 0$, $\omega_C = 5$, $N = 5000$, $l = 500$. Nonlinear bath: solid line, linear bath: dashed line.

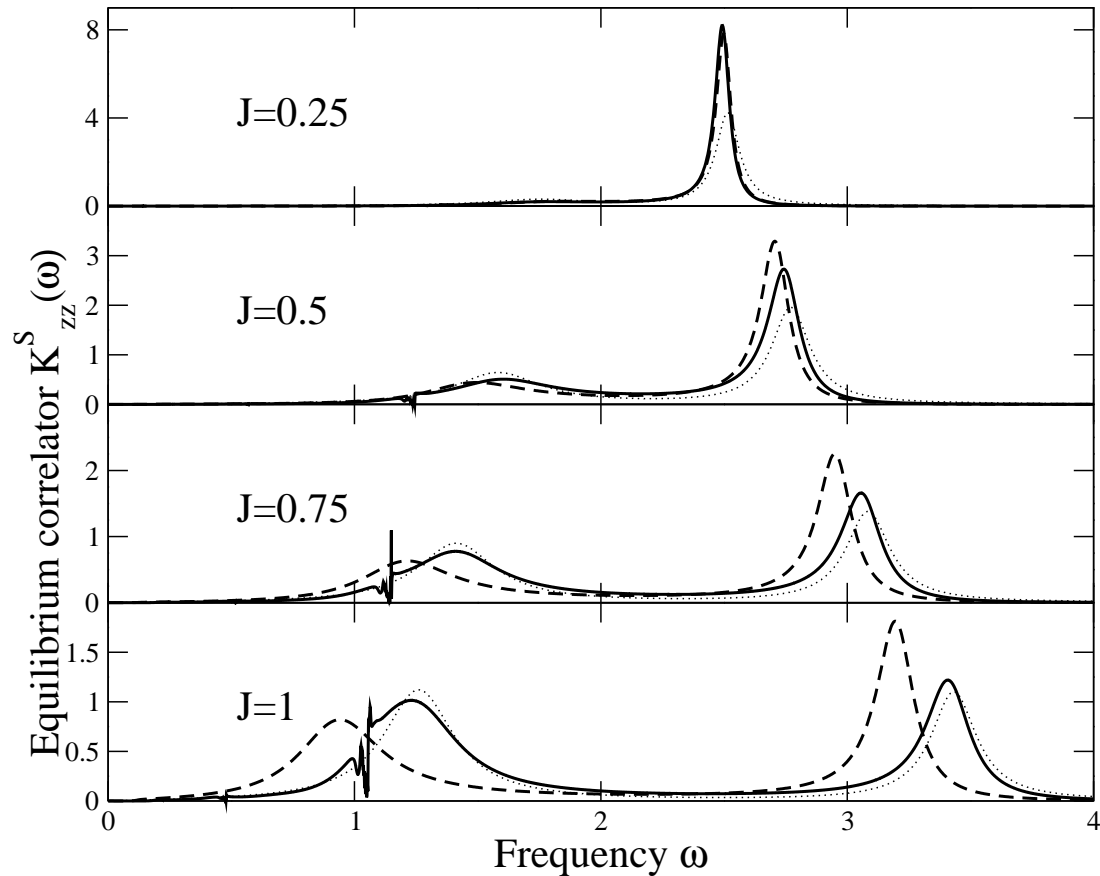


Figure 3.12: The Fourier transform $K_{zz}^S(\omega)$ of the equilibrium correlator of $\hat{\sigma}_z^S(t)$, for different values of the system-bath coupling $J = 0.25, 0.5, 0.75$ and 1 from topmost to lowest graph. The values of the other parameters are: $\Delta = 1$, $\Delta_S = 1.2$, $\alpha/(2\pi) = 0.025$, $\epsilon_S = 0$, $\omega_C = 5$, $N = 5000$, $l = 500$. Nonlinear bath: solid line, linear bath: dashed line, and Markoff approximation used to calculate the influence of the linear bath F on the system $S + B$: dotted line.

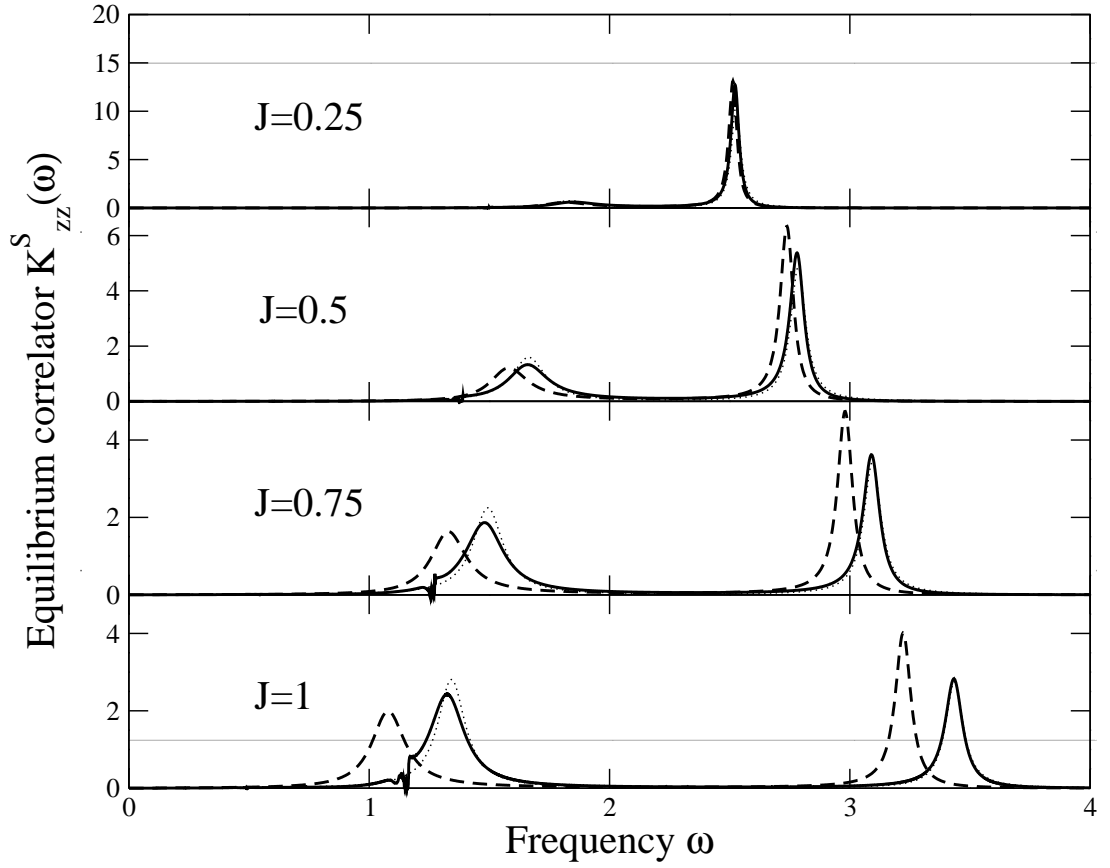


Figure 3.13: The Fourier transform $K_{zz}^S(\omega)$ of the equilibrium correlator of $\hat{\sigma}_z^S(t)$, for different values of the system-bath coupling $J = 0.25, 0.5, 0.75$ and 1 from topmost to lowest graph. The values of the other parameters are: $\Delta = 1$, $\Delta_S = 1.2$, $\alpha/(2\pi) = 0.01$, $\epsilon_S = 0$, $\omega_C = 5$, $N = 5000$, $l = 500$. Nonlinear bath: solid line, linear bath: dashed line, and Markoff approximation used to calculate the influence of the linear bath F on the system $S + B$: dotted line.

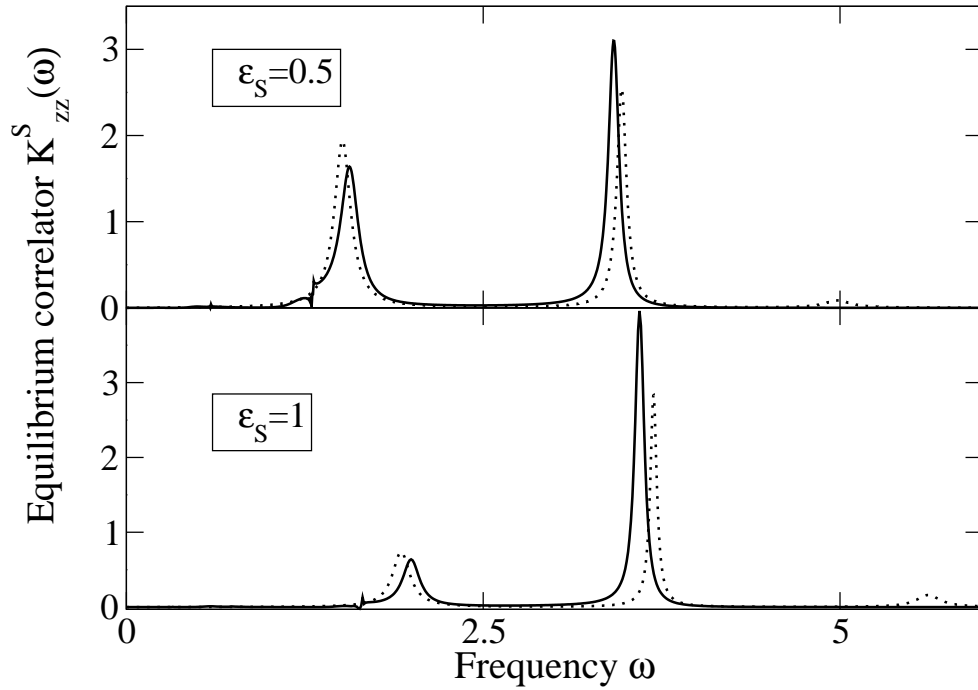


Figure 3.14: The Fourier transform $K_{zz}^S(\omega)$ of the equilibrium correlator of $\hat{\sigma}_z^S(t)$, for two different values of the bias $\epsilon_S = 0.5$ topmost $\epsilon_S = 1$ lowest graph. The values of the other parameters are: $\Delta = 1$, $\Delta_S = 1.2$, $\alpha/(2\pi) = 0.01$, $J=1$, $\omega_C = 10$, $l = 100$. For $\epsilon_S = 0.5$, $N = 2000$ bath modes were used, the height of the delta peak at zero frequency is 0.229 and the sum rule leads to a value 1.048. For $\epsilon_S = 1$, $N = 1000$ bath modes were used, the height of the delta peak at zero frequency is 0.544 and the sum rule leads to a value 1.149. Nonlinear bath: solid line and Markoff approximation used to calculate the influence of the linear bath F on the system $S + B$: dotted line.

For small system-bath coupling the equilibrium correlator contains only one peak which can also be obtained using a Markoff approximation. In contrast the linear bath can also describe the second peak appearing for larger coupling strengths. At least two frequencies are therefore present in the time evolution of the two-state system, and furthermore, the decoherence is strongly increased if the system and bath are in resonance. As expected, the linear-bath approximation fails for the regime of large system-bath coupling. In that regime the linear bath may undoubtedly represent a good approximation to our actual nonlinear bath up to couplings on the order of half of the system energy scale. In the strong coupling regime, on the order of the system energy scale, the agreement of the peak shapes is qualitatively better, when the bath spectrum has a strongly peaked structure. Here, deviations of the linear from the original nonlinear bath became clearly visible. All things considered, we have only discussed the simplest example of a nonlinear bath. We believe that the linear bath approximation might lead to reasonable results in the intermediate-coupling regime, also for other, possibly more sophisticated systems.

As part of the problem, we have to mention the computational effort involved in evaluating the flow equations. For the linear bath approximation one must solve the flow equations twice. Still, one needs less calculation power than for the flow equations for the dissipative four-state system. This can be attributed to the smaller number of necessary differential equations.

Chapter 4

Quantum Dissipative Dynamics of the Magnetic Resonance Force Microscope in the Single-Spin Detection Limit

We study a model of a magnetic resonance force microscope (MRFM) based on the cyclic adiabatic inversion technique as a high-resolution tool to detect single electron spins. We take an open quantum system approach to investigate the quantum dynamics of spin and cantilever in the presence of coupling to an environment. To obtain the reduced dynamics of the combined system of spin and cantilever, we use the Feynman-Vernon influence functional and find results valid at any temperature and at arbitrary system-bath coupling strength. We propose that the MRFM can be used as a quantum measurement device, i.e., the MRFM can be used to detect not only the modulus of the spin, but also its direction.

4.1 Introduction

Magnetic resonance imaging technologies (MRI, NMR, ESR) are widely used to characterize physical, chemical, and biological samples. What makes them so powerful is that they are non-destructive and capable of probing the three-dimensional structure of the sample [Slichter90]. Recently, looking at structures at the molecular or atomic level has become important in a number of scientific disciplines. Magnetic resonance force microscopes (MRFMs) have been developed to bring magnetic resonance imaging technologies to such an ultimate resolution. The MRFM combines conventional magnetic resonance technology with probe microscope technology, e.g., atomic force microscopy, to image individual molecules or atoms [Sidles95]. In an MRFM, a magnetic particle mounted on a cantilever interacts with nuclear or electron spins in the sample via the very weak magnetic dipole force. When modulated at resonance with the cantilever oscillation frequency, even a weak magnetic force induces sufficiently

large vibrations of the cantilever. By probing the resulting vibrational motion of the cantilever, it is possible, in principle, to detect spins with molecular or atomic resolution. The cyclic adiabatic inversion (CAI) technique has been proposed [Sidles95] as a promising method to modulate the magnetic force.

The future of the MRFM depends crucially on the development of proper mechanical micro-resonators, e.g., cantilevers [Bocko96]. Remarkable progress has been made in this direction and the detection of attonewton- or subattonewton-scale forces has already been achieved already [Stowe97, Mamin01]. Recently, a nanomechanical flexural resonator at microwave frequencies has also been realized [Huang03]. The development of the proper technology to detect nanometer-scale mechanical motion is also important. Optical interferometry or electrical parametric transducers are the most common examples [Stowe97, Mamin01]. In recent work, a single-electron transistor capacitively coupled to a nanomechanical resonator has been used to detect the vibrational motion of the resonator even in the quantum regime [Knobel03].

Progress in MRFM and related technologies has also attracted theoretical interest, especially regarding the question of single-spin detection using the MRFM. Mozyrsky *et al.* [Mozyrsky03] have studied the relaxation of a spin, treating the cantilever as a classical noise source. Berman and co-workers [Berman03a, Berman03b] have studied a CAI-based MRFM and treated both the spin and the cantilever as quantum systems that are subject to environmental effects. They addressed two interesting and important issues: First, which component is measured in an MRFM single-spin measurement and second, whether the two spin states (up and down) lead to distinctively different cantilever motions. They solved the time-dependent Schrödinger equation numerically for the spin-plus-cantilever system in the absence of coupling to the environment. In the presence of an environment, they constructed a generalized master equation in the high-temperature limit, and solved it numerically. We note that their master equation is based on the Markov approximation, and is not in Lindblad form [Lindblad76, Diosi93] (the normalization and the positivity of the density matrix are not guaranteed).

In this chapter, we study the measurement of single spins with the MRFM based on the CAI technique. The starting point of our work is closely related to the work by [Berman03a, Berman03b]. In the absence of the coupling to the environment, we solve the time-dependent Schrödinger equation exactly and confirm the numerical results by Berman *et al.* [Berman03a, Berman03b] Taking the influence of the environment into account, we use an open quantum system approach [Breuer02, Weiss00]. To calculate the dynamics of the spin during the measurement process, we take an effective-bath approach, and obtain the exact solution for the reduced density matrix of the spin which is valid at all temperatures (within the CAI-scheme). To find the cantilever dynamics, we solve the Feynman-Vernon influence functional [Feynman63, Grabert88] in order to obtain the reduced density matrix of the spin-plus-cantilever system. The results are valid at any temperature as well as for an arbitrary coupling strength. This analytical approach allows us to interpret the results in a transparent way and to investigate the issue of whether the MRFM can be used as a quantum measurement

device to probe the spin state.

This chapter is organized as follows: In Section 4.2 we introduce the model and discuss our adiabatic Born-Oppenheimer approximation scheme in connection with the CAI-technique. In Section 4.4 we present the exact solution of the time-dependent Schrödinger equation for the spin-plus-cantilever system without coupling to the environment, the results of which will be compared with those in the dissipative case in later sections. In Section 4.5, we assay the quantum dissipative dynamics of the spin alone using an effective-bath approach. The dynamics of the cantilever are discussed in Section 4.6. The physical implications of the solution are analyzed systematically. In Section 4.7 and 4.8 the system is discussed for high and intermediate temperatures using a master equation approach. These results are contained as a special case of the results in Section 4.6, but if one is interested only in this special limit, where a master equation calculation is valid, then the analysis becomes much easier. The possibility to use the MRFM as a quantum measurement device is discussed in Section 4.10. Finally, in Section 4.11 we draw our conclusions.

4.2 Model of the MRFM

The system which we consider is a MRFM setup based on the cyclic adiabatic inversion technique. In this technique the external time-dependent magnetic fields are chosen in such a way (see below) that the frequency of the spin inversion is on resonance with the mechanical motion of the cantilever. This resonance condition amplifies the ultra-weak magnetic force between spin and cantilever so much that the information of the spin state can be transferred to the cantilever motion. As shown in Fig. 4.1, the setup consists of a ferromagnetic particle mounted on the tip of a cantilever, a strong static magnetic field \mathbf{B}_{\parallel} applied in the z -direction, and an rf field $\mathbf{B}_{\perp}(t)$ rotating with frequency ω_{rf} in the x - y plane modulated by $\phi(t)$. The total magnetic field is given by

$$\mathbf{B}(t) = \mathbf{B}_{\perp}(t) + \mathbf{B}_{\parallel} = \begin{bmatrix} B_{\perp} \cos[\omega_{\text{rf}}t - \phi(t)] \\ -B_{\perp} \sin[\omega_{\text{rf}}t - \phi(t)] \\ B_{\parallel} \end{bmatrix}. \quad (4.1)$$

The “sample” consists of a spin interacting with these different magnetic fields. The first one is the non-uniform magnetic field of the ferromagnetic particle, which interacts with the magnetic moment of the spin via the magnetic dipole-dipole interaction. It is assumed that the magnetic moment of the ferromagnetic particle \mathbf{m} points in the z direction. The second magnetic field is the uniform and static field in the positive z direction, which determines the ground state of the spin. Finally, the third field is a rotating radio frequency (rf) field which induces transition between the ground and the excited state of the spin. Let us first define the Hamiltonian of the spin and the cantilever alone without dissipation. This is given by

$$\mathcal{H}(t) = -g\mu_B \mathbf{B}(t) \cdot \hat{\mathbf{S}} - g\mu_B \frac{\partial B_z}{\partial z} \hat{S}_z \hat{z} + \frac{\hat{p}^2}{2m_0} + \frac{m_0 \omega_0^2 \hat{z}^2}{2}, \quad (4.2)$$

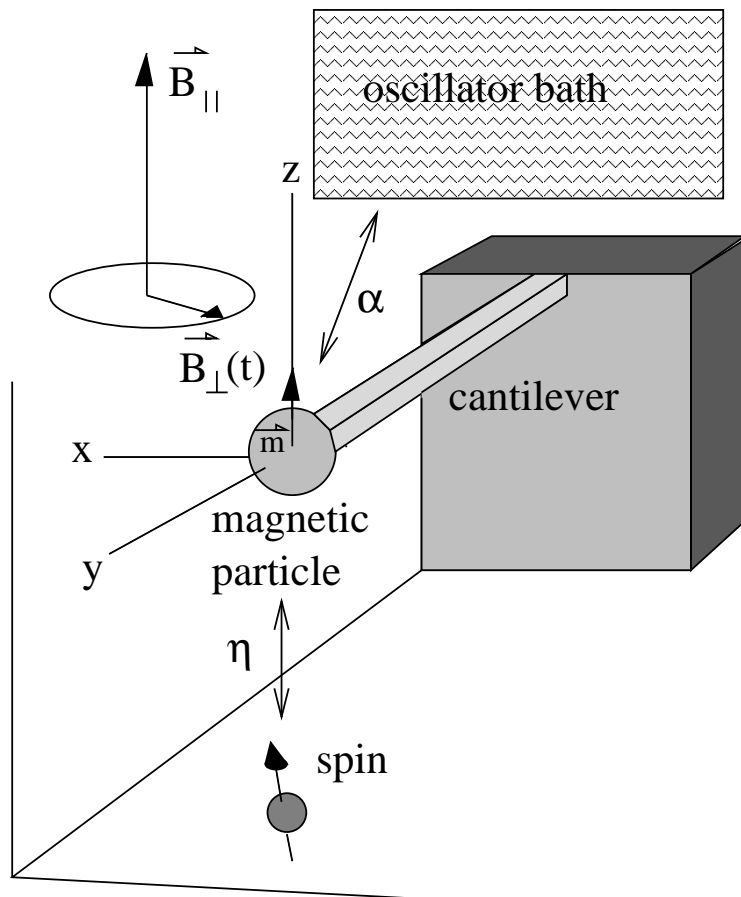


Figure 4.1: MRFM measurement device. A cantilever carrying a magnetic particle is subject to a static magnetic field \mathbf{B}_{\parallel} in the z direction, and a time-dependent field $\mathbf{B}_{\perp}(t)$ rotating with frequency ω_{rf} in the x - y plane. The cantilever is coupled to a sample spin by a magnetic force η .

where \mathbf{S} and \hat{S}_z are the usual spin operators. $\partial B_z/\partial z$ has a constant value independent of z , i.e., the gradient is evaluated at a certain point z_0 . m_0 and ω_0 are the effective mass and the natural frequency of the cantilever. g is the g -factor of the spin and μ_B is the Bohr magneton. Further, \hat{z} is the position operator and \hat{p}_z is the momentum operator of the cantilever. The Hamiltonian describes a spin in a magnetic field $\mathbf{B}(t)$ interacting via a linear coupling to an ideal harmonic oscillator, which is assumed to oscillate only in the z direction. From now on, we use a unit system such that $\hbar = k_B = \omega_0 = \ell_0 = 1$, where $\ell_0 \equiv \sqrt{\hbar/m\omega_0}$ is the harmonic-oscillator length. We define $\epsilon_z \equiv g\mu_B B_{\parallel}$ to be the Larmor frequency and $\epsilon_{\perp} \equiv g\mu_B B_{\perp}$ to be the Rabi frequency. The Hamiltonian can be recast in the following form

$$\mathcal{H}(t) = -\frac{\epsilon_z}{2}\hat{\sigma}_z - \frac{\epsilon_{\perp}}{2} [\hat{\sigma}_{+} e^{i\omega_{\text{rf}}t - i\phi(t)} + H.c.] - \eta \hat{\sigma}_z \hat{z} + \frac{\hat{p}_z^2}{2} + \frac{\hat{z}^2}{2}. \quad (4.3)$$

The $\hat{\sigma}$ operators are Pauli matrices and $\hat{\sigma}_{\pm} = (\hat{\sigma}_x \pm i\hat{\sigma}_y)/2$. The strength of the dipole-dipole force between the ferromagnetic particle and the spin is described by the parameter $\eta = (g\mu_B/2)\partial B_z/\partial z$.

To continue the calculations, it is convenient to move to a frame rotating with the rf field by performing a transformation [Messiah61]

$$\mathcal{H} \rightarrow \mathcal{A}^{\dagger} \mathcal{H} \mathcal{A} - i\mathcal{A}^{\dagger} \dot{\mathcal{A}}, \quad (4.4)$$

with $\mathcal{A} = \exp\left\{\frac{i}{2}[\epsilon_z t - \phi(t)]\hat{\sigma}_z\right\}$. The resulting Hamiltonian reads [Berman03a, Berman03b]

$$\mathcal{H}(t) = -\frac{1}{2}[\epsilon_z - \omega_{\text{rf}} + \dot{\phi}(t)]\hat{\sigma}_z - \frac{1}{2}\epsilon_{\perp}\hat{\sigma}_x - \eta \hat{\sigma}_z \hat{z} + \frac{\hat{p}_z^2}{2} + \frac{\hat{z}^2}{2}. \quad (4.5)$$

As in usual NMR setups, the rotation frequency ω_{rf} fulfils the following condition: $\omega_{\text{rf}} = \epsilon_z$. This means that the average frequency of the applied modulated rf field ω_{rf} equals the Larmor frequency ϵ_z of the spin. Using this condition, we obtain

$$\mathcal{H}(t) = -\frac{1}{2}\dot{\phi}(t)\hat{\sigma}_z - \frac{1}{2}\epsilon_{\perp}\hat{\sigma}_x - \eta \hat{\sigma}_z \hat{z} + \frac{\hat{p}_z^2}{2} + \frac{\hat{z}^2}{2}. \quad (4.6)$$

So far no approximation has been made.

The idea of the CAI-based MRFM is as follows: The frequency modulation $\phi(t)$ of the rf field is assumed to be harmonic and causes adiabatic inversions of the spin, which in turn exert an oscillating force on the cantilever. At resonance, i.e., if the frequency of the rf field is equal to $\omega_0 = 1$, the time derivative of the frequency modulation has the typical form

$$\dot{\phi}(t) = \phi_0 \sin(t - \varphi). \quad (4.7)$$

While the resonance condition is fulfilled the vibration amplitude of the cantilever can be large even for a very small magnetic force strength η .

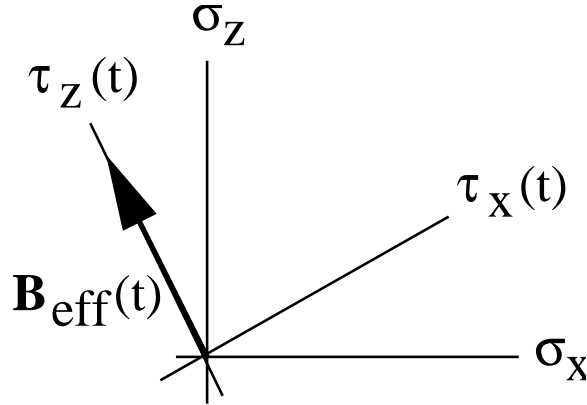


Figure 4.2: Definition of the adiabatic basis.

Equation (4.6) describes a spin which couples to a harmonic oscillator and is itself subject to a time-dependent effective magnetic field $\mathbf{B}_{\text{eff}}(t) = \epsilon_{\perp} \mathbf{e}_x + \dot{\phi}(t) \mathbf{e}_z$ appearing in the rotating frame, where \mathbf{e}_x and \mathbf{e}_z are unit vectors in the rotating system. The Hamiltonian in Eq. (4.6) is not exactly solvable. Here we make a plausible approximation based on the following observations. For typical experimental parameters [Berman03a, Berman03b], \mathbf{B}_{eff} varies slowly compared with the Rabi oscillation frequency: $|\dot{\mathbf{B}}_{\text{eff}}(t)|/|\mathbf{B}_{\text{eff}}(t)| \ll \epsilon(t) \equiv \sqrt{\epsilon_{\perp}^2 + \dot{\phi}^2(t)}$. According to the adiabatic theorem [Avron87, Messiah61], the spin part of the solution should be determined by the adiabatic evolution; i.e., the spin “follows adiabatically” the effective field $\mathbf{B}_{\text{eff}}(t)$. It is therefore convenient to choose the basis states $|\chi_{+}(t)\rangle$ and $|\chi_{-}(t)\rangle$ quantized along the axis parallel to $\mathbf{B}_{\text{eff}}(t)$, see Fig. 4.2 (notice that there is no Berry phase because the solid angle enclosed by $\mathbf{B}_{\text{eff}}(t)$ is zero). In this basis, the Hamiltonian in Eq. (4.6) is recast to

$$\mathcal{H}(t) = -\frac{1}{2}\epsilon(t)\hat{\tau}_z - \eta \frac{\dot{\phi}(t)}{\epsilon(t)} \hat{\tau}_z \hat{z} + \eta \frac{\epsilon_{\perp}}{\epsilon(t)} \hat{\tau}_x \hat{z} + \frac{\hat{p}_z^2}{2} + \frac{\hat{z}^2}{2}. \quad (4.8)$$

$\hat{\tau}_x$ and $\hat{\tau}_z$ are the Pauli matrices with respect to the frame rotating adiabatically with $\mathbf{B}_{\text{eff}}(t)$. We further note that the spin dynamics is much faster than the cantilever motion, $\epsilon(t) \geq \epsilon_{\perp} \gg 1$. The situation is reminiscent of the Born-Oppenheimer approximation [Ashcroft76], where the nuclei interact with the average charge density of the electrons, which move much faster. In our system the nuclei correspond to the harmonic oscillator which is interacting with the averaged motion of the spin. Therefore one can drop the third term in Eq. (4.8). (The deviation of the spin due to this term is also negligibly small since $\eta |\langle \hat{z}(t) \rangle| \ll \epsilon(t)$, see below). Using this approximation we finally obtain the following Hamiltonian, which is the basis of the further considerations in the paper

$$\mathcal{H}(t) = -\frac{1}{2}\epsilon(t)\hat{\tau}_z - \eta f(t)\hat{\tau}_z \hat{z} + \frac{\hat{p}_z^2}{2} + \frac{\hat{z}^2}{2}, \quad (4.9)$$

where $f(t) \equiv \dot{\phi}(t)/\epsilon(t)$. This form is justified in a more rigorous way in the next Section 4.3, also taking into account the influence of the environment (see below).

So far we have described a model for an idealized system of spin and cantilever. In reality they are coupled to various environments, which lead to decoherence as well as damping. In particular, the cantilever is inevitably under the influence of phonons or other vibrational modes which are close in frequency to the single mode in question. The (direct) environmental effects for the spin, e.g., hyperfine interaction, spin-lattice relaxation, etc., are relatively small. Therefore, for simplicity, we assume an Ohmic bath of oscillators [Caldeira83b, Caldeira83a, Caldeira81, Weiss00] directly coupled to the cantilever but not to the spin. Then the total Hamiltonian for the spin and the cantilever plus the oscillator bath is given by

$$\mathcal{H}_{\text{total}}(t) = \mathcal{H}(t) + \sum_k \left[\frac{\hat{p}_k^2}{2m_k} + \frac{m_k \omega_k^2}{2} \left(\hat{x}_k - \frac{c_k}{m_k \omega_k^2} \hat{z} \right)^2 \right]. \quad (4.10)$$

All the relevant features of the Ohmic bath are characterized by the spectral density

$$J(\omega) = \frac{\pi}{2} \sum_k \frac{c_k^2}{m_k \omega_k} \delta(\omega - \omega_k) = \alpha \omega \Theta(1 - \omega/\omega_C), \quad (4.11)$$

where α is a dimensionless parameter characterizing the coupling between the system and the environment and ω_C is the cutoff frequency. The spin dynamics and the probability distribution of the cantilever will not depend on the cutoff.

We describe the system of spin plus cantilever in terms of the reduced density matrix $\hat{\rho}(t) \equiv \text{tr}_B \hat{\rho}_{\text{tot}}(t)$ by tracing out the bath. In the realistic typical experimental situation, the cantilever always remains in contact with the environment. Thus, the cantilever and bath are not in a product state at the beginning of the experiment. For the calculation with the influence functional, we can take this fact into account, assuming that the cantilever and the bath were in a factorized state at a time $t = t_0$. In the limit $t_0 \rightarrow -\infty$ we get then the realistic initial state for the cantilever at the time $t = 0$. If we would start with a factorized state between cantilever and bath, the solution would be very sensitive to the initial condition of the cantilever, see Section 4.5.

Furthermore, it is assumed that the interaction between the spin and the cantilever is turned on at $t = 0$, i.e., $f(t) = 0$ for $t < 0$. The measurement happens at times $t > 0$. The initial state $\hat{\rho}(0)$ of the density matrix is a product state,

$$\hat{\rho}(0) = \hat{\rho}^{(S)}(0) \hat{\rho}^{(C)}(0), \quad (4.12)$$

where $\hat{\rho}^{(S)}$ is the density matrix for the spin only and $\hat{\rho}^{(C)}$ describes the cantilever in thermal equilibrium with the bath. From the CAI scheme and from the associated adiabatic approximation discussed above, it then follows that the density matrix at times $t > 0$ has the form

$$\langle s, z | \hat{\rho}(t) | s', z' \rangle = \rho_{ss'}^{(S)}(0) \rho_{ss'}^{(C)}(z, z', t). \quad (4.13)$$

Namely, the dynamics of the density matrix $\hat{\rho}(t)$ is completely determined by the spin-dependent cantilever part $\rho_{ss'}^{(C)}(z, z', t)$.

Here the spin-dependent cantilever part should not be confused with the density matrix for the cantilever only, which is given by

$$\rho^{(C)}(z, z', t) = \sum_{s=\pm} \langle s, z | \hat{\rho}(t) | s, z' \rangle = \rho_{++}^{(S)}(0) \rho_{++}^{(C)}(z, z', t) + \rho_{--}^{(S)}(0) \rho_{--}^{(C)}(z, z', t). \quad (4.14)$$

Analogously, the density matrix for the spin only at time $t > 0$ is given by

$$\rho_{ss'}^{(S)}(t) = \rho_{ss'}^{(S)}(0) \int_{-\infty}^{\infty} dz \rho_{ss'}^{(C)}(z, z, t). \quad (4.15)$$

There are several ways to prepare the spin in a particular state [Weiss00], and we will assume a general state $\rho_{ss'}^{(S)}(0)$.

4.3 Estimation of the spin-flip rate

The cyclic adiabatic inversion scheme implies two basic assumptions: (i) The variation of the external driving $\dot{\phi}(t)$ is slow enough to allow for an adiabatic approximation [Messiah61], i.e., $|\ddot{\phi}(t)| \ll \epsilon_{\perp}^2$. (ii) The time scales of the spin dynamics and the cantilever dynamics are well separated ($\epsilon_{\perp} \gg 1$) such that the Born-Oppenheimer approximation is justified. Yet, the finite rates of change in the external driving and the cantilever position will induce spin flips. The periodic adiabatic energies $E_{\pm} \approx \pm(\epsilon_{\perp}^2 + \dot{\phi}^2(t))^{1/2}/2$ are shown in Fig. 4.3. When the energy bands come closest to each other the situation resembles the exactly solvable Landau-Zener problem [Avron87, Grifoni98]. Therefore the spin-flip rate can be estimated by the Landau-Zener transition (adiabatic transition) rate. For this purpose, we rewrite Eqs. (4.6) and (4.10) in the form

$$\mathcal{H}_{\text{LZ}}(t) = -\frac{1}{2}F(t)\hat{\sigma}_z - \frac{1}{2}\epsilon_{\perp}\hat{\sigma}_x, \quad (4.16)$$

where $F(t) \equiv \dot{\phi}(t) + 2\eta \langle \hat{z}(t) \rangle$. The back-action of the cantilever has been accounted for by its time-dependent average position, and the contribution from it will be estimated below in a self-consistent way based on the results in Section 4.6. The probability that the spin flips against the effective magnetic field $\mathbf{B}_{\text{eff}}(t)$ during one period (i.e., $2\pi/\omega_0$) is then given by

$$P_{\text{LZ}} \simeq \exp\left(-\frac{\pi\epsilon_{\perp}^2}{\nu}\right), \quad (4.17)$$

where we have taken $\nu \equiv \max |\dot{F}(t)|$ to estimate the worst case.

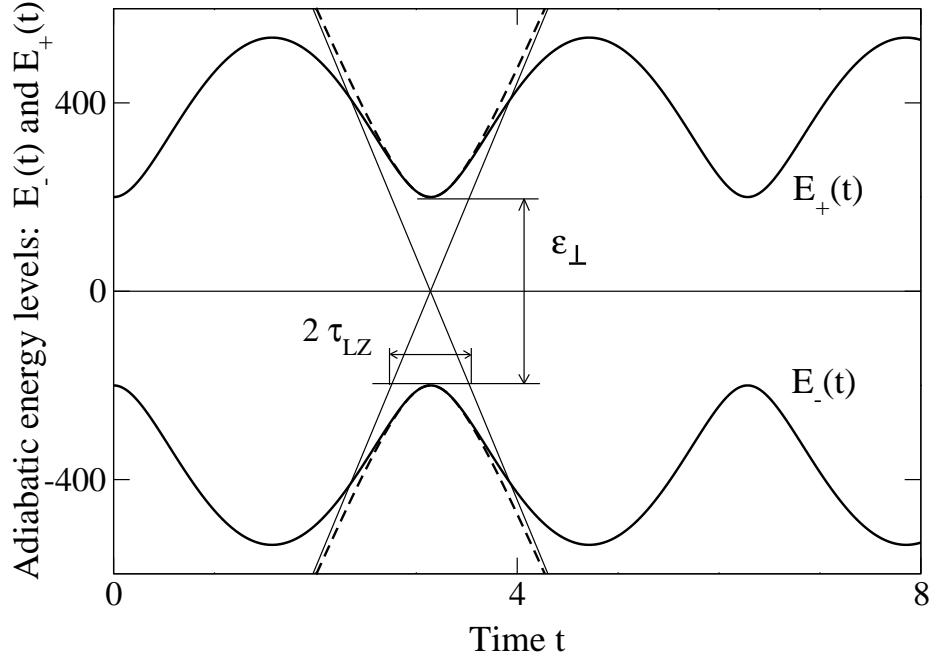


Figure 4.3: The periodic adiabatic energy levels (solid line) approximated by the Landau-Zener adiabatic energy levels $E_{\pm}^{\text{LZ}} \equiv \pm(\epsilon_{\perp}^2 + \nu^2 t^2)^{1/2}/2$ (dashed line) for $\phi_0 = 1000$ and $\epsilon_{\perp} = 400$. The probability that the spin flips against the effective magnetic field $\mathbf{B}_{\text{eff}}(t)$ during one period can therefore be estimated with the Landau-Zener transition probability P_{LZ} depending on the ratio between the time $\tau_{\text{LZ}} \equiv \epsilon_{\perp}/\nu$ spent in the crossover region and the coherent tunneling time $\tau_{\text{coh}} \equiv 2\epsilon_{\perp}^{-1}$.

It follows from Eqs. (4.7) and (4.64) that

$$\nu \leq \max |\ddot{\phi}(t)| + 2\eta \max \left| \frac{d}{dt} \langle \hat{z}(t) \rangle \right| = \phi_0 + 2\frac{\eta^2}{\alpha} f_0. \quad (4.18)$$

Therefore, assuming typical values for the parameters, $\phi_0 \sim 1000$, $\epsilon_{\perp} \sim 400$, $\eta \sim 1$, and $\alpha \sim 0.001$, we have $f_0 \sim 1$ and

$$P_{\text{LZ}} < \exp \left(-\pi \frac{\epsilon_{\perp}^2}{\phi_0 + 2\eta^2 f_0 / \alpha} \right) \sim 10^{-70}. \quad (4.19)$$

Note that the back-action of the cantilever is stronger for larger Q -factors of the cantilever ($Q \simeq 1/\alpha$) since the maximum velocity of the cantilever increases with the Q -factor.

4.4 Coherent solution without bath

Before we analyze the full dissipative Hamiltonian in Eq. (4.10), it will be instructive to consider the problem without a bath, Eq. (4.9). The time-dependent Hamiltonian

in Eq. (4.9) is diagonal and the Schrödinger equation can therefore be solved analytically for arbitrary functions $\epsilon(t)$ and $f(t)$ of t (of course, the variation of $\epsilon(t)$ and $f(t)$ in time should be sufficiently slow that the Hamiltonian Eq. (4.9) is meaningful, i.e., our approximations are applicable).

The result for the time-evolution operator $\mathcal{U}(t_2, t_1) \equiv \hat{T} \exp \left[-i \int_{t_1}^{t_2} dt' \mathcal{H}(t') \right]$ (\hat{T} is the time-ordering operator) is given by

$$\mathcal{U}(t_2, t_1) = \exp \left[ic(t_1, t_2) + \frac{i}{2} \int_{t_1}^{t_2} dt' \epsilon(t') \hat{\tau}_z \right] \mathcal{D}(\hat{\tau}_z \xi(t_2)) \mathcal{U}_0(t_2 - t_1) \mathcal{D}^\dagger(\hat{\tau}_z \xi(t_1)), \quad (4.20)$$

where

$$\xi(t) \equiv i\eta \frac{1}{\sqrt{2}} \int_0^t dt' e^{-i(t-t')} f(t'), \quad (4.21)$$

$$\mathcal{U}_0(t) \equiv \exp(-it\hat{a}^\dagger\hat{a}). \quad (4.22)$$

$\hat{a} = (\hat{z} + i\hat{p}_z)/\sqrt{2}$ is a bosonic annihilation operator for the harmonic oscillator and $\mathcal{D}(\xi)$ is a displacement operator[Gardiner00] defined for a complex number ξ by

$$\mathcal{D}(\xi) = \exp(\xi\hat{a}^\dagger - \xi^*\hat{a}). \quad (4.23)$$

The coefficient $c(t_1, t_2)$ in Eq. (4.20) is a real function of t_1 and t_2 , which doesn't have to be specified further because it drops out of the following calculations.

To illustrate the dynamics generated by the time-evolution operator in Eq. (4.20), we analyze a specific case. Suppose that we start at time $t = 0$ with the cantilever in a coherent state

$$\psi(z, 0) = \frac{1}{\sqrt[4]{\pi}} \exp \left[-\frac{1}{2}z^2 + \sqrt{2}\xi_0 z - (\text{Re } \xi_0)^2 \right] \quad (4.24)$$

and with the spin in a linear superposition with amplitudes c_+ and c_-

$$|\chi(0)\rangle = c_+|\chi_+(0)\rangle + c_-|\chi_-(0)\rangle. \quad (4.25)$$

The total wave function at $t = 0$ is given by

$$|\Psi(z, 0)\rangle = \psi(z, 0) |\chi(0)\rangle, \quad (4.26)$$

and at a later time $t > 0$, by

$$|\Psi(z, t)\rangle = c_+\psi_+(z, t)|\chi_+(t)\rangle + c_-\psi_-(z, t)|\chi_-(t)\rangle. \quad (4.27)$$

The cantilever wave function in Eq. (4.27) for each spin component is given by

$$\psi_\pm(z, t) = \frac{1}{\sqrt[4]{\pi}} \exp \left\{ ic(t, 0) \pm i \int_0^t dt' \epsilon(t') - \frac{1}{2}z^2 + \sqrt{2}\xi'_\pm(t)z - [\text{Re } \xi'_\pm(t)]^2 \right\}, \quad (4.28)$$

where

$$\xi'_{\pm}(t) = \pm\xi(t) + \xi_0 e^{-it}. \quad (4.29)$$

Therefore, the average position of the cantilever is $\langle \hat{z}(t) \rangle_{\pm} = \sqrt{2} \operatorname{Re} \xi'_{\pm}(t)$ for spin $s = \pm$, respectively, whereas the average momentum is given by $\langle \hat{p}_z(t) \rangle_{\pm} = \sqrt{2} \operatorname{Im} \xi'_{\pm}(t)$. Here it is interesting to note (in comparison with the results below) that exactly at resonance [see Eq. (4.7)], $|\xi(t)|$ in Eq. (4.21) [and hence $|\xi'_{\pm}(t)|$ in Eq. (4.29)] contains a term which increases linearly with time t . In other words, the oscillation amplitude of the cantilever becomes indefinitely larger as time passes. This is not surprising since we are driving an *ideal* oscillator at the resonance frequency, and in fact this is what allows the MRFM to detect ultra-small forces. In reality, the cantilever is subject to various environmental effects and the oscillation amplitude is bounded from above (i.e., the Q-factor is finite). This is the case that we will study below.

Before we study the system plus oscillator bath, let us make a short remark about the off-diagonal elements of the reduced spin density matrix. Even though the cantilever is not yet coupled to the oscillator environment, and the system consists only of the spin interacting coherently with the cantilever, the reduced spin dynamics turn out to evolve incoherently, i.e., the off-diagonal elements decay. This can be understood as follows: The off-diagonal elements of the spin density matrix are only nonzero if the oscillator wavepackets corresponding to spin up and down overlap. Without a bath, the separation of the spin-up and the spin-down wavepackets becomes indefinitely larger as discussed before, due to the driving. Although the wavepackets oscillate and overlap for a certain time, the density matrix becomes diagonal, since the overlapping time decreases due to the increasing oscillation amplitude of the cantilever.

4.5 Dynamics of the spin

Now we take the influence of the bath into account. In this section, we analyze the dynamics of the spin. As described above, there are several environmental effects for the spin. In this calculation, we assume that such effects, directly affecting the spin, are small compared to the interaction with the measuring device, i.e., the cantilever coupled to the oscillator bath. Thus, the decoherence time of the spin in the absence of the cantilever is assumed to be much longer than the time we need for the measurement. These different time scales are necessary to provide cyclic inversions of the spin.

A similar situation appears in the well-known Stern-Gerlach experiment, where the environment first collapses the trajectory of the particle which causes collapse of the spin. As in our calculation, other decoherence mechanisms, which act directly on the spin, are neglected.

When we are interested in the dynamics of the spin alone (the dynamics of the cantilever will be discussed in the following section), we can regard the cantilever as a part of the environment. The bath now contains one additional harmonic oscillator.

This is why the bath spectral density must be modified. One expects a non-Ohmic spectral density with a peak around the cantilever frequency. By transforming to normal coordinates one can find the new bath spectral density. Garg *et al.* [Garg85] have shown that the problem is equivalent to a spin coupled linearly to an oscillator bath

$$\mathcal{H}_{\text{tot}}(t) = -\frac{1}{2}\epsilon(t)\hat{\tau}_z - \eta f(t)\hat{\tau}_z \sum_k g_k \left(\hat{b}_k^\dagger + \hat{b}_k \right) + \sum_k \omega_k \hat{b}_k^\dagger \hat{b}_k. \quad (4.30)$$

The distribution of the oscillator frequencies ω_k and the coupling constants g_k are now characterized by a non-Ohmic spectral density

$$J_{\text{eff}}(\omega) \equiv \sum_k g_k^2 \delta(\omega - \omega_k) = \frac{1}{\pi} \frac{\alpha\omega}{(\omega^2 - 1)^2 + (\alpha\omega)^2}. \quad (4.31)$$

To investigate the spin dynamics, we write the reduced density matrix of the spin

$$\hat{\rho}^{(S)}(t) = \text{tr}_B \mathcal{U}_{\text{tot}}(t) \hat{\rho}_{\text{tot}}(0) \mathcal{U}_{\text{tot}}^\dagger(t) \quad (4.32)$$

in terms of the time-evolution operator $\mathcal{U}_{\text{tot}}(t)$ associated with $\mathcal{H}_{\text{tot}}(t)$ in Eq. (4.30). In analogy to Eq. (4.20), the time-evolution operator is given by

$$\mathcal{U}_{\text{tot}}(t) = \exp \left[\frac{i}{2} \int_0^t dt' \epsilon(t') \hat{\tau}_z \right] \prod_k \mathcal{D}(\hat{\tau}_z \xi_k(t)) e^{-i\omega_k t \hat{b}_k^\dagger \hat{b}_k}, \quad (4.33)$$

where

$$\xi_k(t) = i\eta g_k \int_0^t dt' e^{-i(t-t')\omega_k} f(t'), \quad (4.34)$$

and \mathcal{D} is now the displacement operator for the k th mode of the bath, i.e., \hat{a} should be replaced by \hat{b}_k in Eq. (4.23).

For the initial state $\hat{\rho}_{\text{tot}}(0)$, we assume [see Eqs. (4.12)]

$$\hat{\rho}_{\text{tot}}(0) = \hat{\rho}^{(S)}(0) \prod_k \frac{e^{-\beta\omega_k \hat{b}_k^\dagger \hat{b}_k}}{Z_k}. \quad (4.35)$$

For such an initial state the cantilever is in thermal equilibrium with all oscillators of the bath at the time $t = 0$. Another initial condition, where the cantilever is in a coherent state at the beginning of the measurement, is discussed below. In this case, the density matrix for the spin is given by

$$\rho_{ss'}^{(S)}(t) = \rho_{ss'}^{(S)}(0) \exp \left[i \frac{(s - s')}{2} \int_0^t dt' \epsilon(t') \right] \prod_k \langle \mathcal{D}^\dagger(s' \xi_k(t)) \mathcal{D}(s \xi_k(t)) \rangle_k, \quad (4.36)$$

where $\langle \cdots \rangle_k$ is the average with respect to the k th oscillator in the bath.

Equation (4.36) shows that the diagonal elements of the density matrix ($s = s'$) are constant in time

$$\rho_{ss}^{(S)}(t) = \rho_{ss}^{(S)}(0). \quad (4.37)$$

In other words, there is no spin relaxation and the spin dynamics undergoes pure dephasing since there are no transverse fields. This is consistent with the adiabatic approximation we made at the beginning.

On the other hand, the off-diagonal elements ($s \neq s'$) are expected to vanish rapidly with time. This can be seen from [see Eq. (4.36)]

$$\rho_{+-}^{(S)}(t) = \rho_{+-}^{(S)}(0) \exp \left[-\Gamma(t) + i \int_0^t dt' \epsilon(t') \right], \quad (4.38)$$

where

$$\Gamma(t) \equiv 2 \sum_k |\xi_k(t)|^2 \coth \left(\frac{\omega_k}{2T} \right), \quad (4.39)$$

or in terms of the spectral density function

$$\Gamma(t) = 2\eta^2 \int_0^\infty d\omega J_{\text{eff}}(\omega) \coth \left(\frac{\omega}{2T} \right) \left| \int_0^t dt' e^{i\omega t'} f(t') \right|^2. \quad (4.40)$$

Figure 4.4 shows $|\rho_{+-}(t)|$ evaluated using Eqs. (4.38) and (4.40). To compare our results with those of Berman *et al.* [Berman03a, Berman03b], who assumed an initial product state of cantilever and bath, the inset of Fig. 4.4 shows $|\rho_{+-}^{(S)}(t)|$ for a Gaussian initial state of the cantilever. To obtain these results we evaluate the path-integral formulas in Appendix A.11 with $t_0 = 0$ instead of taking the limit $t_0 \rightarrow -\infty$. If we compare the main part of Fig. 4.4 with the inset, the strong dependence on the initial conditions is evident. The additional features shown in the inset are a consequence of the oscillatory relaxation of the cantilever to its thermal equilibrium state if one starts with an initial product state of cantilever and bath. On increasing the coupling α , the oscillatory behavior becomes less visible since the cantilever relaxes immediately to its thermal state.

4.6 Dynamics of the cantilever

In Section 4.4 we described the driven dynamics of the otherwise isolated system of spin and cantilever determined by the Hamiltonian in Eq. (4.9). In this section, we now take into account the influence of the environment starting from the Hamiltonian given in Eq. (4.10). The reduced dynamics are obtained analytically with the Feynman-Vernon influence functional [Feynman63, Grabert88] for arbitrary coupling strength α to the bath and for arbitrary temperature T . The advantage of this method, as compared to [Berman03b], is that no master equation is used and that there is no restriction on the number of basis functions used to numerically integrate the problem.

The reduced dynamics of the cantilever obtained with the influence functional are given by

$$\rho_{ss'}^{(C)}(z_f, z'_f, t) = \int dz_i dz'_i J_{ss'}(z_f, z'_f, t; z_i, z'_i, t_0) \rho_{ss'}^{(C)}(z_i, z'_i, t_0), \quad (4.41)$$

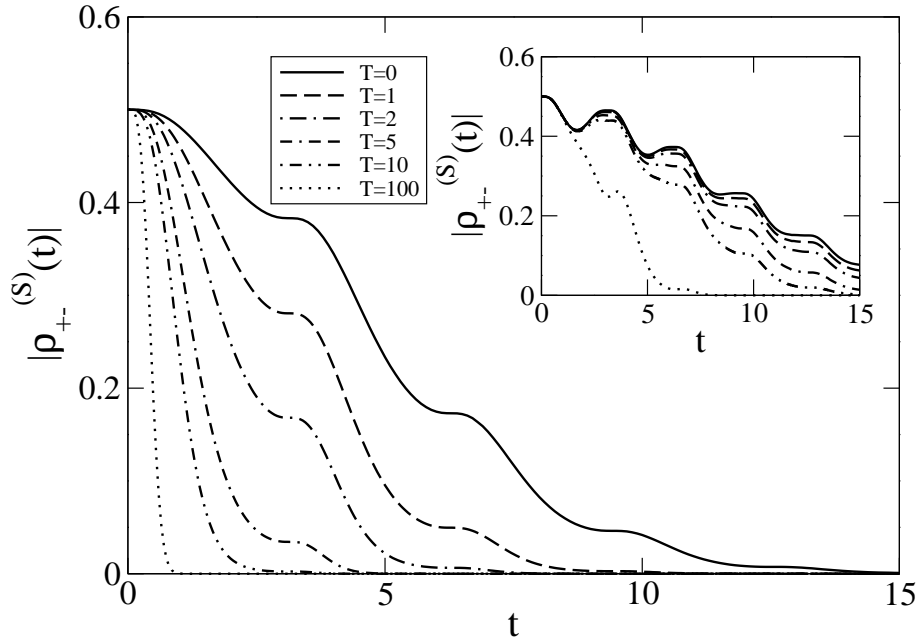


Figure 4.4: Main plot: $|\rho_{+-}(t)|$ for different temperatures $T = 0, 1, 2, 5, 10, 100$, for $\phi_0 = 1000$, $\epsilon_{\perp} = 400$, $\eta = 0.3$, $\alpha = 0.006$, and $\omega_C = 1000$. The initial condition for cantilever and bath is the thermal equilibrium state. Inset: same quantity for an initial product state of cantilever and bath. Initially, the cantilever wave function is a Gaussian with width $\sigma = \sqrt{2}$. In both cases, $\rho_{ss'}^{(S)}(0) = 1/2$ for $s, s' = \pm$.

where

$$J_{ss'}(z_f, z'_f, t; z_i, z'_i, t_0) = \int \mathcal{D}z \mathcal{D}z' \exp(iS_{ss'}[z, z']), \quad (4.42)$$

$s, s' = \pm$, and the action, see Eq. (2.35), is defined by

$$\begin{aligned} S_{ss'}[z, z'] &= S_s^0[z] - S_{s'}^0[z'] - \frac{\alpha}{2} \int_{t_0}^t d\tau [z(\tau) - z'(\tau)][\dot{z}(\tau) + \dot{z}'(\tau)] \\ &+ \frac{i}{2} \int_{t_0}^t d\tau \int_{t_0}^t d\tau' [z(\tau) - z'(\tau)] K_R(\tau - \tau') [z(\tau') - z'(\tau')]. \end{aligned} \quad (4.43)$$

This form of the action is only valid for an Ohmic bath[Caldeira83b]. Furthermore, $K_R(\tau)$ is the real part of the bath correlation function

$$K_R(\tau) \equiv \text{Re} \langle \hat{X}(\tau) \hat{X}(0) \rangle, \quad (4.44)$$

where $\hat{X}(t) = \sum_k c_k \hat{x}_k(t)$. Finally,

$$S_s^0[z] = \int_{t_0}^t d\tau \left[\frac{1}{2} \dot{z}^2(\tau) - \frac{1}{2} z^2(\tau) + \eta s f(\tau) z(\tau) + \frac{1}{2} \epsilon(\tau) s \right] \quad (4.45)$$

is the bare action without oscillator bath.

The action can be simplified further by introducing relative coordinates defined by $R = (z + z')/2$ and $r = z - z'$. The action is then found to be

$$S_{ss'}[R, r] = S_{ss'}^0[R, r] - \alpha \int_{t_0}^t d\tau \dot{R}(\tau) r(\tau) + \frac{i}{2} \int_{t_0}^t d\tau \int_{t_0}^t d\tau' r(\tau) K_R(\tau - \tau') r(\tau'), \quad (4.46)$$

with

$$\begin{aligned} S_{ss'}^0[R, r] &= \int_{t_0}^t d\tau \left\{ \dot{R}(\tau) \dot{r}(\tau) - R(\tau) r(\tau) + \eta f(\tau) R(\tau) (s - s') \right. \\ &\left. + \frac{1}{2} \eta f(\tau) r(\tau) (s + s') + \frac{1}{2} \epsilon(\tau) (s - s') \right\}. \end{aligned} \quad (4.47)$$

In the next step, the action is expanded around the classical path. The classical equations of motion can be found by minimizing this action

$$\frac{\delta S_{ss'}}{\delta r} = 0 \quad (4.48)$$

and

$$\frac{\delta S_{ss'}}{\delta R} = 0. \quad (4.49)$$

The classical equations of motion read

$$\ddot{R}(\tau) + \alpha \dot{R}(\tau) + R(\tau) = F_R(\tau), \quad (4.50)$$

$$\ddot{r}(\tau) - \alpha \dot{r}(\tau) + r(\tau) = F_r(\tau), \quad (4.51)$$

$$F_R(\tau) = \frac{1}{2} \eta f(\tau)(s + s') + i \int_{t_0}^{\tau} d\tau' K_R(\tau - \tau') r(\tau'), \quad (4.52)$$

$$F_r(\tau) = \eta f(\tau)(s - s'), \quad (4.53)$$

with classical solutions $R_{cl}(\tau)$, $r_{cl}(\tau)$, respectively. Note that the solutions are complex [Marquardt02], and the dependence on s, s' of all these quantities has been suppressed. The classical solutions, which are given in Appendix A.11, are linear in the boundary values R_f, r_f, R_i and r_i . Therefore, $S_{ss'}[R_{cl}, r_{cl}]$ is a bilinear form in these variables. We obtain

$$J_{ss'}(R_f, r_f, t; R_i, r_i, t_0) = \frac{1}{\mathcal{N}(t)} \exp\left(i S_{ss'}[R_{cl}, r_{cl}]\right), \quad (4.54)$$

where all contributions from the fluctuations around the classical path are contained in the time-dependent, but spin-independent normalization constant $\mathcal{N}(t)$, which can be obtained from the normalization condition

$$\sum_{s=\pm} \int_{-\infty}^{\infty} dR_f \rho_{ss}(R_f, r_f = 0, t) = 1. \quad (4.55)$$

The Gaussian form of the expressions leads to a final reduced density matrix of Gaussian form if the initial density matrix is Gaussian, which is true for a coherent state. Therefore, we deal with Gaussian wave packets in the dissipative case as well. The explicit formulas are discussed in detail in Appendix A.11, where the solution for the reduced dynamics is obtained starting from a Gaussian wave packet at time t_0 . We then take the limit $t_0 \rightarrow -\infty$ such that the information about the initial state is lost at time $t = 0$.

We will now give analytical expressions of the density matrix for the diagonal and off-diagonal elements with respect to the spin degree of freedom. Let us first discuss the result for $s = s'$

$$\rho_{ss}^{(C)}(R, r, t) = \frac{1}{\sqrt{2\pi}\sigma_R} \exp\left\{-\frac{1}{2\sigma_R^2}[R - x_s(t)]^2 - \frac{1}{2\sigma_r^2}r^2 + ir\dot{x}_s(t)\right\}, \quad (4.56)$$

where the final coordinates have been replaced by $R \equiv R_f$ and $r \equiv r_f$. The widths of the Gaussian peaks are independent of the spin. The width in the R -direction is given by

$$\sigma_R^2 = \int_0^{\infty} d\omega J_{\text{eff}}(\omega) \coth\left(\frac{\omega}{2T}\right). \quad (4.57)$$

σ_R increases with temperature. This is because the cantilever position suffers thermal fluctuations. The width in the r -direction is found to be

$$\frac{1}{\sigma_r^2} = \int_0^{\omega_C} d\omega \omega^2 J_{\text{eff}}(\omega) \coth\left(\frac{\omega}{2T}\right). \quad (4.58)$$

Note that, as is well-known, the momentum width diverges with the cutoff frequency ω_C which was defined after Eq. (4.11). This is why we retained the dependence on the cutoff in this integral. The spin dynamics and the probability distribution of the cantilever will not depend on the cutoff. Unlike σ_R , σ_r decreases with temperature; this is natural since the cantilever approaches a classical oscillator as temperature increases. The temperature behavior of these two integrals can be read-off in the limit of small $\alpha \ll 1$, viz.,

$$\sigma_R^2 \approx \frac{1}{\sigma_r^2} \approx \frac{1}{2} \coth\left(\frac{1}{2T}\right). \quad (4.59)$$

We now investigate the probability density to find the particle at position z at the time t . This is obtained by setting $z = z'$, i.e., $R = z$ and $r = 0$ in Eq. (4.56)

$$\begin{aligned} \rho^{(C)}(z, z, t) &= \rho_{++}^{(S)}(0)\rho_{++}^{(C)}(R = z, r = 0, t) + \rho_{--}^{(S)}(0)\rho_{--}^{(C)}(R = z, r = 0, t) \\ &= \rho_{++}^{(S)}(0) \frac{1}{\sqrt{2\pi}\sigma_R} \exp\left\{-\frac{1}{2\sigma_R^2}[z - x_+(t)]^2\right\} \\ &+ \rho_{--}^{(S)}(0) \frac{1}{\sqrt{2\pi}\sigma_R} \exp\left\{-\frac{1}{2\sigma_R^2}[z - x_-(t)]^2\right\}. \end{aligned} \quad (4.60)$$

We obtain Gaussian wave packets moving according to

$$x_s(t) = \eta_s \int_0^t dt' e^{-\frac{\alpha}{2}(t-t')} \frac{\sin[\omega_R(t-t')]}{\omega_R} f(t'). \quad (4.61)$$

This expression depends on the spin $s = \pm$. The oscillator frequency $\omega_R = \sqrt{1 - (\alpha/2)^2}$ is renormalized due to the coupling to the bath. Furthermore, $x_s(t)$ is the solution of the coordinate of a classical dissipative driven harmonic oscillator with a spin-dependent driving force $\eta_s f(t)$ starting from the initial conditions $x_s(0) = 0$ and $\dot{x}_s(0) = 0$. So the result becomes very clear, because the classical solution is well-known to be an oscillating function, which goes through a transient regime and for $t \gg 1/\alpha$ the amplitude of the oscillation saturates at a finite value. The oscillation is periodic (but not necessarily sinusoidal) in time with unit period ($T_0 = 2\pi/\omega_0$). Consequently, for $t \gg 1/\alpha$ the density matrix will show a generic steady-state behavior independent of the details of the initial preparation of the system.

The density matrix $\rho_{ss}^{(C)}(R, r, t)$ behaves quite differently with respect to the coordinates R and r . As a function of R , $\rho_{ss}^{(C)}(R, r, t)$ is a Gaussian distribution with standard deviation σ_R and average $\langle R(t) \rangle = x_s(t)$. On the other hand, $\dot{x}_s(t)$ is the velocity of a classical oscillator (see above). It shows oscillatory behavior in t and r superimposed on the Gaussian envelope with width σ_r (see Figs. 4.5–4.8). Thus, the off-diagonal elements $\rho_{ss}^{(C)}(z, z', t)$ ($z \neq z'$) exhibit an oscillatory behavior in t . However, this should not be confused with a coherent oscillation, which is not expected in this long-time limit. The oscillation is a consequence of the external driving $f(t)$ (i.e., frequency modulation $\dot{\phi}(t)$). The elements that are diagonal in both s and z $\rho_{ss}^{(C)}(z, z, t)$ do not show such an oscillation.

The behavior of $x_s(t)$ can be illustrated by approximating $f(t)$ by its primary oscillation amplitude

$$f(t) \approx f_0 \sin(t) + (\text{higher harmonics}), \quad (4.62)$$

where

$$f_0 = \frac{4}{\pi} \left(\frac{\epsilon_{\perp}}{\phi_0} \right) [E(-\phi_0^2/\epsilon_{\perp}^2) - K(-\phi_0^2/\epsilon_{\perp}^2)]. \quad (4.63)$$

Here, $K(x)$ and $E(x)$ are the complete elliptic integrals of the first and second kind [Abramowitz72]. One obtains

$$x_s(t) \approx \eta s f_0 \left(-\frac{\cos(t)}{\alpha} + e^{-\frac{\alpha}{2}t} \left[\frac{\cos(\omega_R t)}{\alpha} + \frac{\sin(\omega_R t)}{2\omega_R} \right] \right) + (\text{higher harmonics}). \quad (4.64)$$

This solution shows the main features of the spin-dependent separation $x_s(t)$, namely the transient behavior and the steady-state oscillations: $x_s(t) \approx -\eta s f_0 \cos(t)/\alpha$. It is interesting to notice that the average cantilever motions are exactly in opposite phases (shift by π) for spin up ($s = +1$) and down ($s = -1$). This was also concluded from the numerical simulation presented in [Berman03a, Berman03b]. Thus, the MRFM can be used as a quantum measurement device (as well as to detect the state or presence of the spin), see below. Therefore, if we start initially with the two spin components populated, $\rho_{++}^{(S)}(0), \rho_{--}^{(S)}(0) > 0$, then $\rho^{(C)}(R, r, t) = \rho_{++}^{(S)}(0)\rho_{++}^{(C)}(R, r, t) + \rho_{--}^{(S)}(0)\rho_{--}^{(C)}(R, r, t)$ will show two peaks moving in opposite directions as time goes on, see discussions above and Figs. 4.5–4.8. It should be stressed that to separate the two peaks with sufficient resolution, the widths of the peaks, Eq. (4.57), should not be larger than the maximum separation, $\eta f_0/\alpha$, see Eq. (4.64). Clearly, this criterion restricts the maximum operation temperature of the device. Figures 4.5–4.8 show the typical behavior of the density matrix $\rho^{(C)}(R, r, t)$ of the cantilever if we choose $\rho_{ss'}^{(S)}(0) = 1/2$ (for $s, s' = \pm$) as the initial state. As the coupling to the environment α increases, the distance between the peaks shrinks and they are harder to distinguish (see Figs. 4.5 and 4.6). A similar behavior is observed as the temperature increases with α fixed (see Figs. 4.7 and 4.8).

Now we turn to the off-diagonal elements $s = -s'$

$$\rho_{s,-s}^{(C)}(R, r, t) = \frac{1}{\sqrt{2\pi\sigma_R}} \exp \left\{ -\frac{1}{2\sigma_R^2} [R - i\vartheta_s(t)]^2 - \frac{1}{2\sigma_r^2} r^2 + r\zeta_s(t) - \Gamma(t) + i \int_0^t dt' \epsilon(t') \right\}, \quad (4.65)$$

where

$$\vartheta_s(t) = 2\eta s \int_0^{\infty} d\omega J_{\text{eff}}(\omega) \coth \left(\frac{\omega}{2T} \right) \int_0^t dt' f(t') \cos(\omega(t-t')), \quad (4.66)$$

and

$$\zeta_s(t) = 2\eta s \int_0^{\infty} d\omega \omega J_{\text{eff}}(\omega) \coth \left(\frac{\omega}{2T} \right) \int_0^t dt' f(t') \sin(\omega(t-t')). \quad (4.67)$$

In the r -direction, $\rho_{s,-s}^{(C)}(R, r, t)$ has a Gaussian shape centered at $\zeta_s(t)/\sigma_r^2$ with width σ_r . In the R -direction, it is an oscillatory function imposed on a Gaussian envelope with width σ_R . Overall, the function $\rho_{s,-s}^{(C)}(R, r, t)$ decays with t in the same way as shown in Fig. 4.4, i.e., $\rho_{ss'}^{(C)}(R, r, t)$ for $s \neq s'$ can be observed only in the transient regime. The decay is described by the function $\Gamma(t)$, see Eq. (4.40). Note that a trace over the cantilever dynamics leads us back to the results obtained in a different way in Section 4.5.

4.7 Master equation

In this section a similar calculation as in Section 4.6 is done, again taking the influence of the environment into account. However, instead of the path integral approach, we use now a generalized master equation [Gardiner00, Breuer02]. We obtain a general solution to it, and discuss its physical implications. The results obtained here are the limit of the results from Section 4.6 for small system bath coupling α and intermediate up to high temperatures. Surprisingly, the master equation turns out to be valid for a large temperature range when compared to the exact solution obtained in Section 4.6.

There are several methods widely used in the literature, to derive a generalized master equation. One of the most popular methods is a perturbative expansion in the system-environment coupling of the von Neumann-Liouville equation and subsequent Markov approximation. This method has been used previously [Berman03a, Berman03b], and led to a master equation similar to that considered by Caldeira and Leggett [Caldeira85]. However, this method has certain drawbacks. It is based on the assumption that the temperature is much higher than the bath cutoff frequency ($T \gg \omega_C$) and it is not obvious whether the resulting equation is valid at intermediate temperatures ($T \gtrsim \omega_C$). Furthermore, the master equation for the particular system in question is not in the Lindblad form [Lindblad76]; the normalization and the positivity of the density matrix are not guaranteed. Therefore it is worthwhile to find out to what extent the master equation is valid.

In this paper we follow Diósi [Diosi93] and derive a generalized master equation which can be put in the Lindblad form and is valid in the intermediate-temperature regime as well as in the high-temperature limit. In this method, one uses a high-temperature expansion of the bath correlation function [see Eqs. (4.68) and (4.69) below]. This expansion is different from the usual Markov approximation.

One represents the reduced density matrix $\hat{\rho}$ for the spin plus cantilever system in the real-time path-integral form. The effective action in the path-integral can be evaluated by expanding the bath correlation function to second order [Diosi93] in $1/T$,

$$\text{Re} \langle \hat{X}(t) \hat{X}(0) \rangle = 2\alpha T \tilde{\delta}(t) - \frac{\alpha}{6T} \frac{d^2}{dt^2} \tilde{\delta}(t), \quad (4.68)$$

$$\text{Im} \langle \hat{X}(t) \hat{X}(0) \rangle = \alpha \frac{d}{dt} \tilde{\delta}(t), \quad (4.69)$$

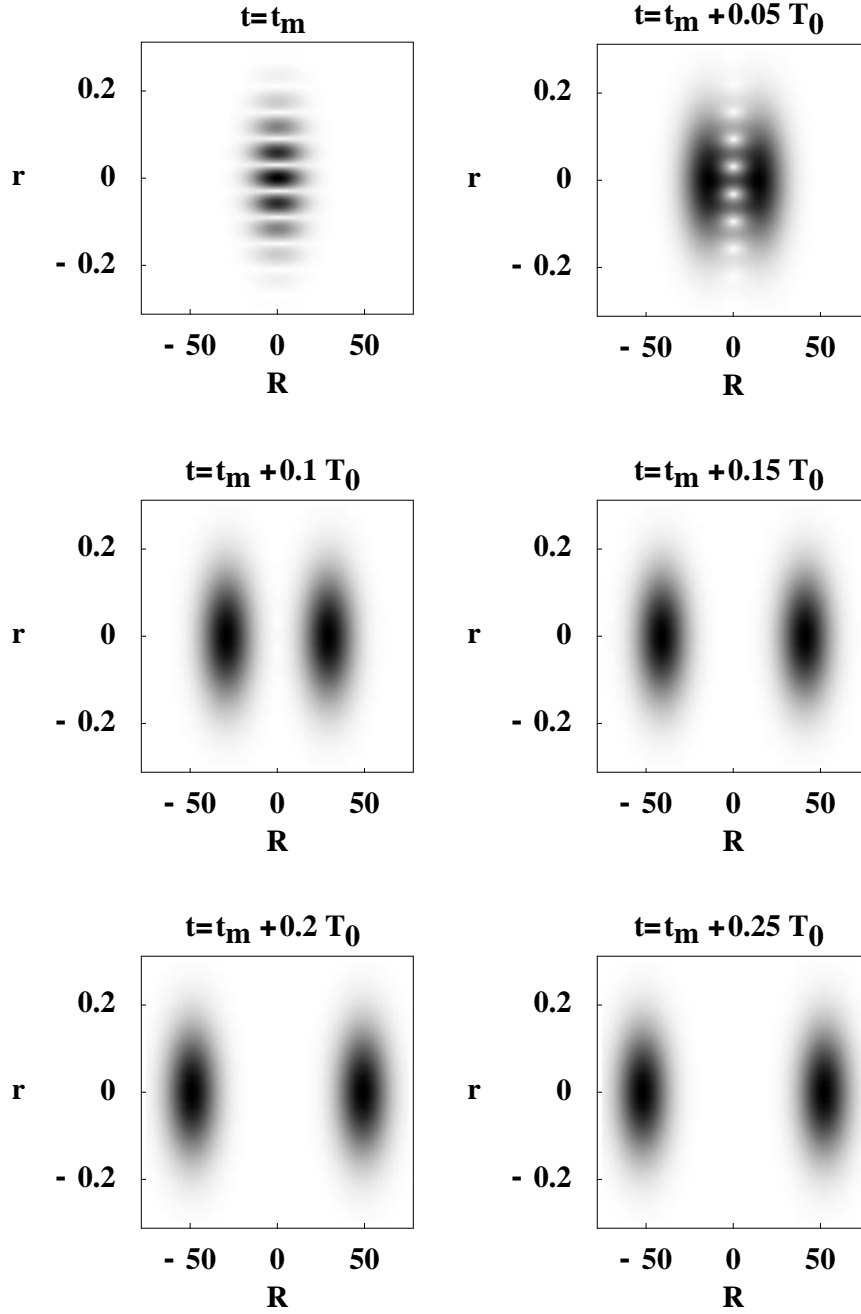


Figure 4.5: $|\rho^{(C)}(R, r, t)|$ for a time series in the steady-state regime starting at time t_m at which the two peaks are not separated, e.g., $t_m = 988$. The units have been chosen such that both the natural frequency ω_0 of the cantilever and its harmonic oscillator length are equal to 1. $T_0 = 2\pi/\omega_0$, $\alpha = 0.006$, $T = 100$; the other parameters are as in the caption of Fig. 4.4. The interference fringes are due to the driving.

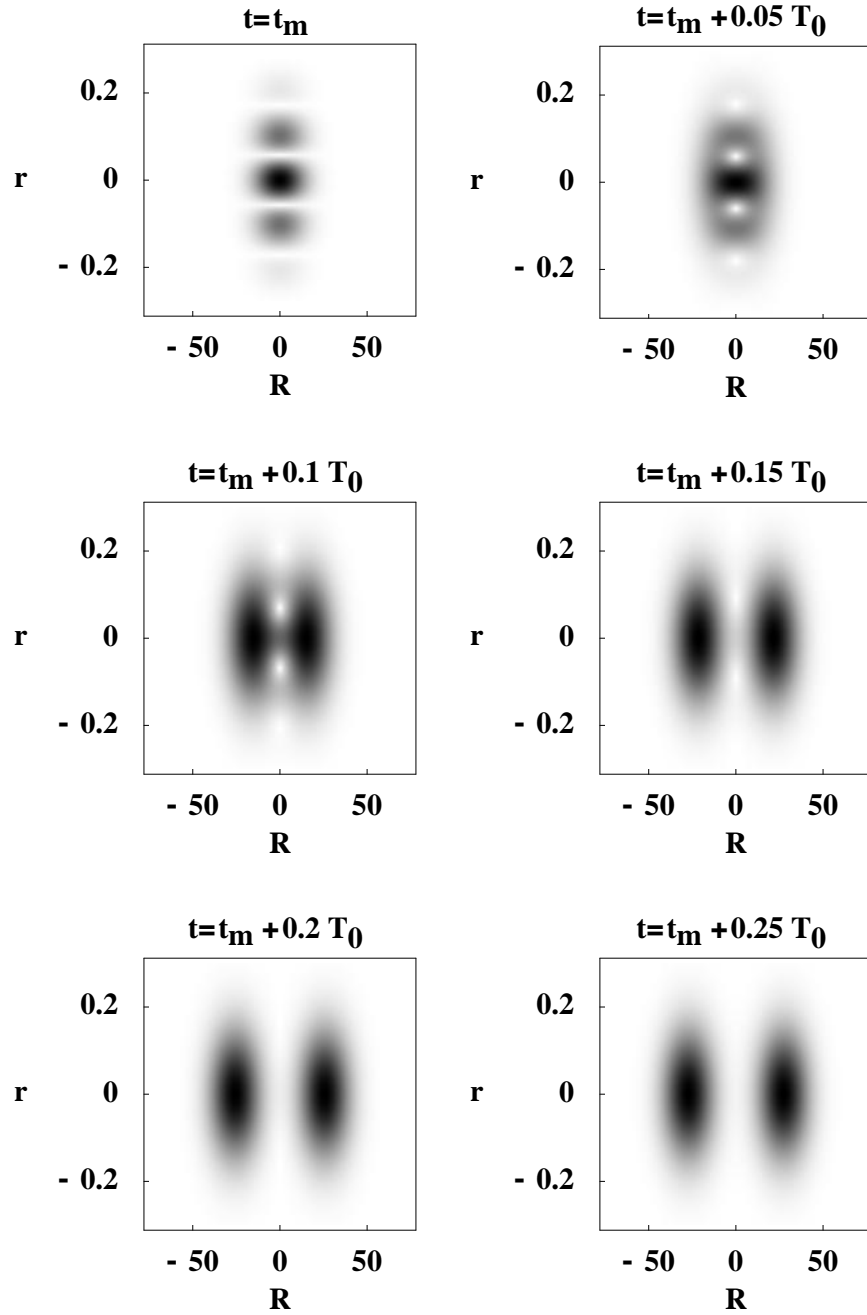


Figure 4.6: $|\rho^{(C)}(R, r, t)|$ for a time series in the steady-state regime for $\alpha = 0.012$ and $T = 100$.

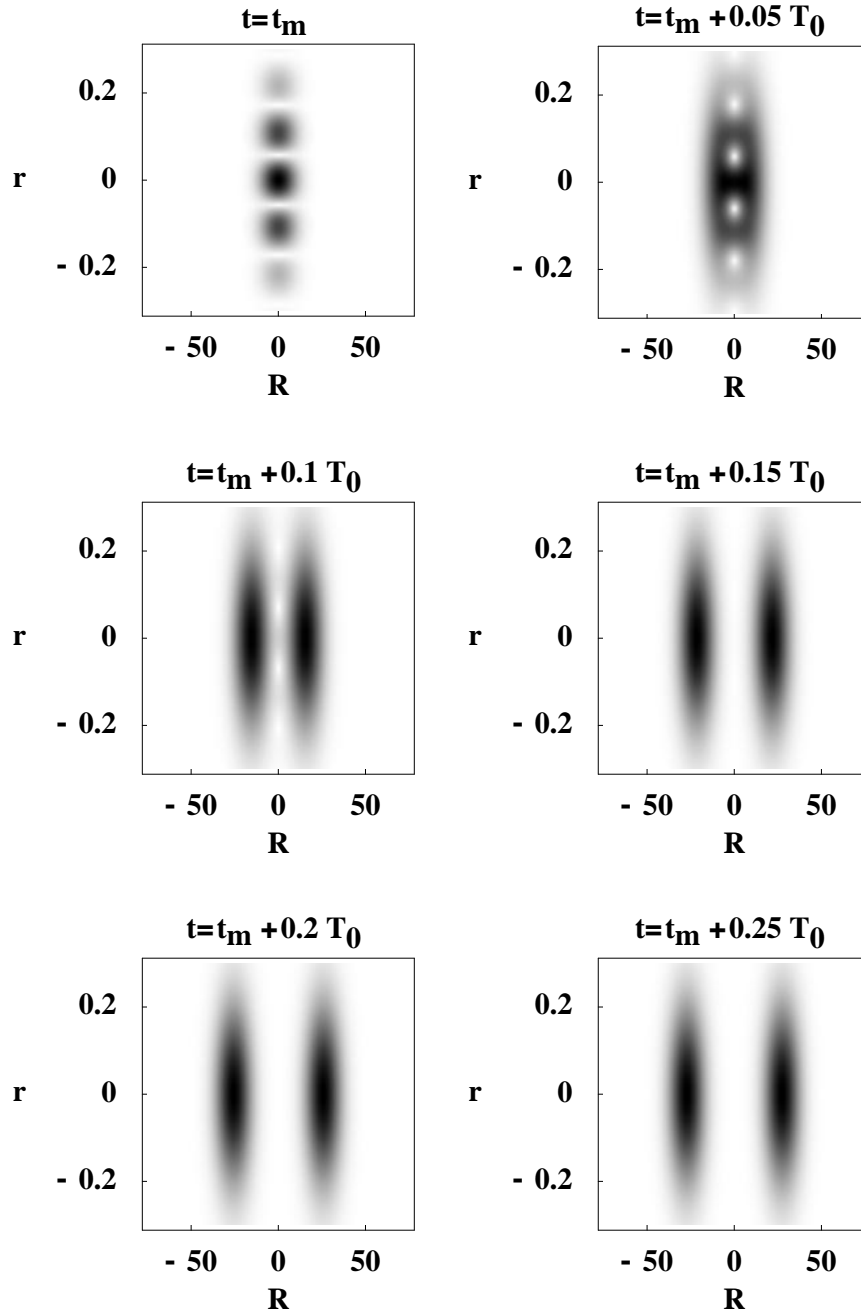


Figure 4.7: $|\rho^{(C)}(R, r, t)|$ for a time series in the steady-state regime for $\alpha = 0.012$ and $T = 50$.

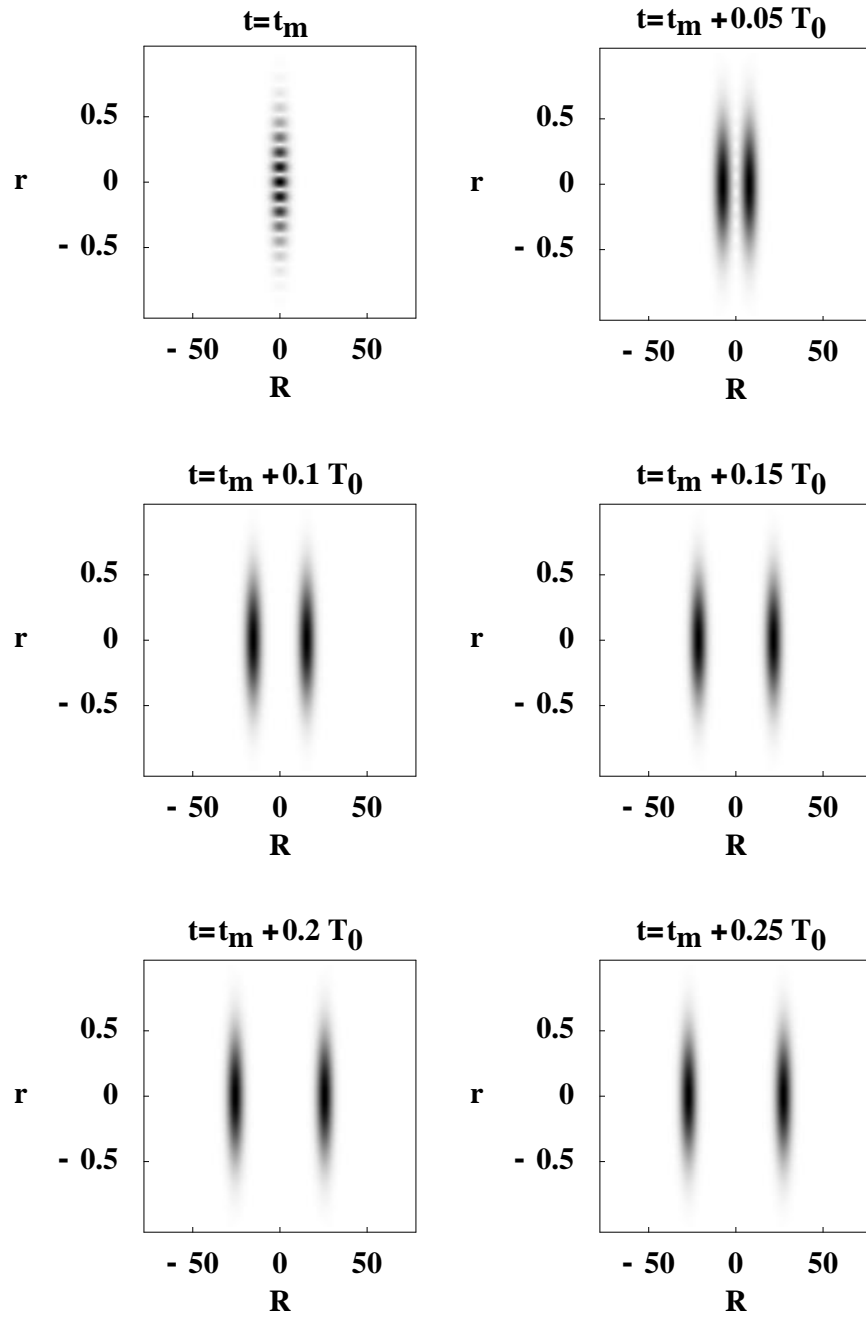


Figure 4.8: $|\rho^{(C)}(R, r, t)|$ for a time series in the steady-state regime for $\alpha = 0.012$ and $T = 10$.

with $\hat{X} \equiv \sum_k c_k \hat{x}_k$. The function $\tilde{\delta}(t) \equiv \sin(\omega_C t)/(\pi t)$ in Eqs. (4.68) and (4.69) will be approximated by a delta distribution $\tilde{\delta}(t) \approx \delta(t)$ and whenever $\tilde{\delta}(0)$ appears, we shall retain its regularized value $\tilde{\delta}(0) = \omega_C/\pi$. The resulting master equation for the reduced density operator $\hat{\rho}$ is given by

$$\begin{aligned} \frac{\partial}{\partial t} \hat{\rho}(t) &= -i[\mathcal{H}(t), \hat{\rho}(t)] - i\frac{\alpha}{2}[\hat{z}, \{\hat{p}, \hat{\rho}(t)\}] \\ &\quad - D_{zz}[\hat{z}, [\hat{z}, \hat{\rho}(t)]] - D_{pp}[\hat{p}, [\hat{p}, \hat{\rho}(t)]] - 2D_{zp}[\hat{z}, [\hat{p}, \hat{\rho}(t)]] , \end{aligned} \quad (4.70)$$

where the Dekker coefficients are defined by

$$D_{zz} = \alpha T, \quad D_{pp} = \frac{\alpha}{12T}, \quad D_{zp} = \frac{\alpha\omega_C}{12\pi T}. \quad (4.71)$$

The master equation in Eq. (4.70) is of exactly the same form as in [Diosi93], with a time-dependent Hamiltonian. As shown in [Diosi93], the master equation (Eq. (4.70)) can be recast in the Lindblad form. Compared with the Caldeira-Leggett high-temperature master equation [Caldeira85] (usual Markov approximation), we see that the term with the prefactor D_{pp} is missing in the usual Markov approximation.

Substituting Eq. (4.13) into Eq. (4.70), one obtains the master equation for the cantilever part

$$\begin{aligned} \frac{\partial}{\partial t} \rho_{ss'}^{(C)}(z, z', t) &= \left[i\frac{1}{2} \left(\frac{\partial^2}{\partial z^2} - \frac{\partial^2}{\partial z'^2} \right) - i\frac{1}{2}(z^2 - z'^2) \right. \\ &\quad + i\frac{1}{2}\epsilon(t)(s - s') + i\eta f(t)(zs - z's') \\ &\quad - \frac{1}{2}\alpha(z - z') \left(\frac{\partial}{\partial z} - \frac{\partial}{\partial z'} \right) + 2D_{zp}(z - z') \left(i\frac{\partial}{\partial z} + i\frac{\partial}{\partial z'} \right) \\ &\quad \left. - D_{zz}(z - z')^2 + D_{pp} \left(\frac{\partial^2}{\partial z^2} + 2\frac{\partial}{\partial z} \frac{\partial}{\partial z'} + \frac{\partial^2}{\partial z'^2} \right) \right] \rho_{ss'}^{(C)}(z, z', t). \end{aligned} \quad (4.72)$$

Equation (4.72) is a linear second-order partial differential equation. It is convenient to make a change of variables from z and z' to the relative and center of mass coordinates $r = z - z'$ and $R = (z + z')/2$, and to perform a Fourier transform with respect to R ,

$$\rho_{ss'}^{(C)}(r, Q, t) \equiv \frac{1}{2\pi} \int_{-\infty}^{\infty} dR e^{iRQ} \rho_{ss'}^{(C)}(r, R, t). \quad (4.73)$$

The equation for $\rho_{ss'}(r, Q, t)$ is given by

$$\begin{aligned} \frac{\partial}{\partial t} \rho_{ss'}^{(C)}(r, Q, t) &= \left[Q \frac{\partial}{\partial r} - r \frac{\partial}{\partial Q} + i\frac{1}{2}\epsilon(t)(s - s') \right. \\ &\quad + \eta f(t) \left[(s - s') \frac{\partial}{\partial Q} + i\frac{s + s'}{2} r \right] \\ &\quad \left. + 2D_{zp}rQ - \alpha r \frac{\partial}{\partial r} - D_{zz}r^2 - D_{pp}Q^2 \right] \rho_{ss'}^{(C)}(r, Q, t). \end{aligned} \quad (4.74)$$

Equation (4.74) is a first-order quasilinear partial differential equation, and can be solved exactly by means of the theory of quasilinear partial differential equations [Smirnov75]. However, since the cantilever is a rather large object, we are mainly interested in the cases where the cantilever evolves from a semiclassical state of the cantilever (either a coherent state or a mixed state with Gaussian distribution), i.e., a Gaussian form of the initial (before interacting with the spin) density matrix for the cantilever. One can further justify such an initial state by noting that in realistic experimental situations, the cantilever always remains in contact with the environment. This initial condition is convenient because any state evolving from a Gaussian state is always Gaussian (see Section 4.6). Alternatively, instead of working with an exact solution, it is natural to use the following Gaussian ansatz

$$\rho_{ss'}^{(C)}(r, Q, t) = \exp \left[-\frac{1}{2}a_{11}r^2 - \frac{1}{2}a_{22}Q^2 - a_{12}rQ + b_1r + b_2Q + c \right], \quad (4.75)$$

where, for brevity, we have suppressed time arguments and spin indices in $a_{11}(t)$, etc. The advantage of the ansatz is that there is no restriction on the number of basis functions used to numerically integrate the master equation [Berman03b]. It should be remembered that for each spin component of the density matrix we have to use an independent ansatz; the coefficients depend, in general, on two spin indices. To determine the coefficients $a_{11}(t)$, etc., we substitute Eq. (4.75) into the master equation Eq. (4.74). It is seen that the coefficients satisfy a set of ordinary coupled inhomogeneous linear differential equations, which in a matrix notation are written as

$$\dot{\mathbf{a}}(t) + A\mathbf{a}(t) = \mathbf{u}, \quad (4.76)$$

$$\dot{\mathbf{b}}(t) + B\mathbf{b}(t) = \mathbf{v}(t), \quad (4.77)$$

and

$$\dot{c}(t) = \left[i\frac{1}{2}\epsilon(t) + \eta f(t)b_2(t) \right] (s - s'). \quad (4.78)$$

The vectors \mathbf{a} and \mathbf{b} are defined by

$$\mathbf{a}(t) = \begin{bmatrix} a_{11}(t) \\ a_{22}(t) \\ a_{12}(t) \end{bmatrix}, \quad \mathbf{b}(t) = \begin{bmatrix} b_1(t) \\ b_2(t) \end{bmatrix}, \quad (4.79)$$

and the matrices A and B by

$$A = \begin{bmatrix} 2\alpha & 0 & 2 \\ 0 & 0 & -2 \\ -1 & 1 & \alpha \end{bmatrix}, \quad B = \begin{bmatrix} \alpha & 1 \\ -1 & 0 \end{bmatrix}. \quad (4.80)$$

The inhomogeneous parts of Eqs. (4.76) and (4.77) are given by the vectors

$$\mathbf{u} = 2 \begin{bmatrix} +D_{zz} \\ +D_{pp} \\ -D_{zp} \end{bmatrix}, \quad (4.81)$$

and

$$\mathbf{v}(t) = \begin{cases} i s \eta f(t) \begin{bmatrix} 1 \\ 0 \end{bmatrix}, & s' = s, \\ -2 s \eta f(t) \begin{bmatrix} a_{12}(t) \\ a_{22}(t) \end{bmatrix}, & s' = -s, \end{cases} \quad (4.82)$$

respectively. The solutions to the ordinary linear different equations (Eqs. (4.76) and (4.77)) can be written formally as

$$\mathbf{a}(t) = e^{-At} [\mathbf{a}(0) - A^{-1} \mathbf{u}] + A^{-1} \mathbf{u}, \quad (4.83)$$

$$\mathbf{b}(t) = e^{-Bt} \mathbf{b}(0) + \int_0^t dt' e^{-B(t-t')} \mathbf{v}(t'), \quad (4.84)$$

where the exponentials e^{-At} and e^{-Bt} can be obtained readily, for instance

$$e^{-Bt} = e^{-\alpha t/2} \left\{ \cos(\omega_R t) + \frac{\sin(\omega_R t)}{\omega_R} \begin{bmatrix} -\alpha/2 & -1 \\ 1 & \alpha/2 \end{bmatrix} \right\}. \quad (4.85)$$

Once $\rho_{ss'}^{(C)}(r, Q, t)$ is known, the density matrix in relative and ‘‘center of mass’’ coordinates r and R can be obtained from an inverse Fourier transform in the coordinate

$$\rho_{ss'}^{(C)}(r, R, t) = \sqrt{\frac{2\pi}{a_{22}}} \exp \left\{ -\frac{1}{2} a_{11} r^2 + b_1 r - \frac{1}{2a_{22}} (R - i a_{12} r + i b_2)^2 + c \right\}. \quad (4.86)$$

The matrix A has three eigenvalues α and $\alpha \pm i2\omega_R$, where $\omega_R \equiv \sqrt{1 - \alpha^2/4}$ is the oscillator frequency renormalized due to the coupling to the bath. The matrix B has eigenvalues $\alpha/2 \pm i\omega_R$. The homogeneous part of the solution for $\mathbf{a}(t)$ therefore decays exponentially over the time $1/\alpha$, and that of \mathbf{b} over time $2/\alpha$. Consequently, for $t \gg 1/\alpha$ the density matrix will show a generic behavior independent of the details of the initial preparation of the system. We now discuss the steady-state behavior in this limit more explicitly. We first summarize a few important general properties of $\mathbf{a}(t)$, $\mathbf{b}(t)$, and $c(t)$. From Eq. (4.83), we see that

$$\mathbf{a}(\infty) = A^{-1} \mathbf{u} = \text{const.} \quad (4.87)$$

Therefore, (i) a_{11} , a_{22} , and a_{12} are all constant in time and real. (Recall also that they are independent of spin). Equation (4.84) exhibits the asymptotic behavior

$$\mathbf{b}(t) \sim \begin{cases} i s \eta U_B(t) \begin{bmatrix} 1 \\ 0 \end{bmatrix}, & s' = s, \\ -2 s \eta U_B(t) \begin{bmatrix} a_{12}(\infty) \\ a_{22}(\infty) \end{bmatrix}, & s' = -s, \end{cases} \quad (4.88)$$

where $U_B(t)$ is a 2×2 matrix defined by

$$U_B(t) \equiv \int_0^t dt' e^{-B(t-t')} f(t'). \quad (4.89)$$

One can show that (for $t \gg 1/\alpha$) $U_B(t)$ is periodic (but not necessarily sinusoidal) in time with unit period ($\tau_0 = 2\pi/\omega_0$ in natural units). It immediately follows that (ii) $b_1(t)$ and $b_2(t)$ are periodic functions of time t with unit period and that (iii) $b_1(t)$ and $b_2(t)$ are purely imaginary for $s = s'$ and real for $s = -s'$. We also note that (iv) $c(t) = c(0) = \text{const.}$ for $s = s'$, see Eq. (4.78).

The properties (i)–(iv) summarized above do not demand an expansion in α and $1/T$, but nevertheless such an expansion is useful for more explicit and clearer presentation of the results. At intermediate and high temperatures ($T \gtrsim \omega_C$) and for sufficiently small α ($\alpha \ll 1$), one has

$$a_{11} = \frac{1}{\alpha} [D_{zz} + D_{pp}] \approx T \left(1 + \frac{1}{12T^2} \right), \quad (4.90)$$

$$\begin{aligned} a_{22} &= \frac{1}{\alpha} [D_{zz} + (1 + \alpha^2)D_{pp} - 2\alpha D_{zp}] \\ &\approx T \left(1 + \frac{1 - 2\alpha\omega_C/\pi}{12T^2} \right), \end{aligned} \quad (4.91)$$

$$a_{12} = -D_{pp} = -\frac{\alpha}{12T} \approx 0. \quad (4.92)$$

One can also obtain

$$U_B(t) = \frac{f_0}{\alpha} \left\{ \sin(t) \begin{bmatrix} 1 & 0 \\ 0 & 1 \end{bmatrix} + \cos(t) \begin{bmatrix} 0 & +1 \\ -1 & 0 \end{bmatrix} + \mathcal{O}(\alpha) + (\text{higher harmonics}) \right\}, \quad (4.93)$$

where f_0 is the primary oscillation amplitude of $f(t)$, see Eq. (4.63). The density matrix in Eq. (4.86) is then reduced to a simple form [see also Eq. (4.92)]

$$\rho_{ss'}^{(C)}(r, R, t) = \sqrt{\frac{2\pi}{a_{22}}} \exp \left\{ -\frac{1}{2}a_{11}r^2 + b_1(t)r - \frac{1}{2a_{22}} [R + ib_2(t)]^2 + c(t) \right\}. \quad (4.94)$$

The widths in the r and R directions are found to be

$$\Delta r \approx \frac{1}{\sqrt{T}} \left(1 - \frac{1}{24T^2} \right) \quad (4.95)$$

and

$$\Delta R \approx \sqrt{T} \left(1 + \frac{1 - 2\alpha\omega_C/\pi}{24T^2} \right), \quad (4.96)$$

respectively. Eq. (4.59) was derived from an expansion of the widths obtained with the path integral for small α . According to the approximation scheme used for the

master equation, Eq. (4.95) and Eq. (4.96) should correspond to the high temperature expansion of σ_r and σ_R in Eq. (4.59). This is clearly true.

For $s = s'$ (diagonal in spin space), $b_1(t)$ is purely imaginary [see (iii) above] and corresponds, as before, to the velocity, whereas

$$\langle R(t) \rangle = -ib_2(t) \approx -s \frac{\eta f_0}{\alpha} \cos(t) \quad (4.97)$$

is the position of a classical driven harmonic oscillator. In the high-temperature weak-coupling limit we find a simple criterion for the separation of the peaks and therefore the possibility of the measurement, namely

$$\eta f_0 / \alpha > \sqrt{T}. \quad (4.98)$$

For $s = -s'$ (off-diagonal in spin space), $b_1(t)$ and $b_2(t)$ are now real. Therefore, $\rho_{ss'}^{(C)}(r, R, t)$ has a Gaussian shape centered at $b_1(t)/a_{11} \approx -(s - s')(\eta f_0 / \alpha) \cos(t)$ being, again, the high temperature limit of Eq. (4.65).

Furthermore, in this case, $c(t)$ is no longer constant in time. Numerical integration of the equation of motion (Eq. (4.78)) shows that it is a monotonically decreasing function of t ($t \gg 1/\alpha$). The function $\rho_{ss'}(r, R, t)$ decays in the same way as shown in Fig. 4.4.

4.8 The correlation function

So far we have discussed the dynamics of the cantilever in terms of the density matrix. In this subsection, we investigate dynamic fluctuations of the cantilever, i.e., we calculate the two-time correlation function for the cantilever z -coordinate

$$\langle \hat{z}(t + \tau) \hat{z}(t) \rangle = \text{tr}_{sys} \{ \text{tr}_B \{ \hat{z}(t + \tau) \hat{z}(t) \hat{\rho}_{sys} \otimes \hat{\rho}_B \} \}, \quad (4.99)$$

where $\hat{\rho}_{sys}$ is the system density matrix (spin and cantilever together) and $\hat{\rho}_B$ is the oscillator bath density matrix. Again, the results in this section are only valid in the high temperature weak coupling limit, i.e., we use the master equation results. We assume to have a nonequilibrium factorized initial density matrix. $\hat{z}(t + \tau)$ and $\hat{z}(t)$ are Heisenberg-picture system operators. We can rewrite the correlation function as

$$\langle \hat{z}(t + \tau) \hat{z}(t) \rangle = \text{tr}_{sys} \{ \hat{z} \text{tr}_B \{ e^{-i\mathcal{H}\tau} \hat{z} \hat{\rho}_{tot}(t) e^{i\mathcal{H}\tau} \} \}. \quad (4.100)$$

For this purpose, we define

$$\mathcal{Z}(t + \tau, t) \equiv \text{tr}_B \{ e^{-i\mathcal{H}\tau} \hat{z} \hat{\rho}_{tot}(t) e^{i\mathcal{H}\tau} \}, \quad (4.101)$$

which, when traced, gives the correlator

$$\langle z(t + \tau) z(t) \rangle = \text{tr}_{sys} \hat{z} \mathcal{Z}(t + \tau, t). \quad (4.102)$$

Then, according to the quantum regression theorem[Gardiner00] $\mathcal{Z}(t + \tau, t)$ satisfies the same master equation (Eq. (4.70)) with respect to τ . Therefore, one can obtain the correlation function by repeating the analysis in the previous subsections. The only difference is the initial condition

$$\mathcal{Z}(t, t) = \hat{z}\hat{\rho}_{\text{sys}}(t). \quad (4.103)$$

Following the lines of the previous subsection gives the correlation function

$$\begin{aligned} \langle \hat{z}(t + \tau)\hat{z}(t) \rangle &= \sum_{s=\pm 1} \rho_{ss}^{(S)}(0) \langle \hat{z}(t + \tau) \rangle_s \langle \hat{z}(t) \rangle_s \\ &+ e^{-\alpha\tau/2} \left[\cos(\omega_R\tau) + \frac{\alpha}{2\omega_R} \sin(\omega_R\tau) \right] a_{22}(t) \\ &- i \frac{e^{-\alpha\tau/2}}{2\omega_R} [1 + 2ia_{12}(t)] \sin(\omega_R\tau), \end{aligned} \quad (4.104)$$

where $\langle \hat{z}(t) \rangle_{\pm}$ are the average values of the position z in the spin state $s = \pm 1$ alone. In Eq. (4.104),

$$\langle \hat{z}(t + \tau)\hat{z}(t) \rangle - \langle \hat{z}(t + \tau) \rangle \langle \hat{z}(t) \rangle \quad (4.105)$$

does not vanish even in the limit $\tau \rightarrow \infty$. This is because of the adiabatic assumption for the spin; the spin never flips. In reality, the spin flips for $\tau \gtrsim \tau_{\text{LZ}}$, where $1/\tau_{\text{LZ}}$ is the Landau-Zener transition rate (adiabatic transition rate), see Section 4.3. Therefore, the expression in Eq. (4.104) is valid only for $\tau \ll \tau_{\text{LZ}}$.

4.9 Classical limit of the cantilever

Classical dynamics takes place in the phase space. The study of the transition from quantum to classical mechanics is facilitated by employing the Wigner transform of the density matrix $\rho^{(C)}(z, z', t)$, which is given by

$$W(z, p) = \frac{1}{2\pi} \int_{-\infty}^{\infty} dy e^{ipy} \rho^{(C)}\left(z - \frac{y}{2}, z + \frac{y}{2}\right). \quad (4.106)$$

For the cantilever motion we obtain

$$\begin{aligned} W(z, p) &= \frac{1}{2\pi} \frac{\sigma_r}{\sigma_R} \left\{ |c_+|^2 \exp \left[-\frac{1}{2\sigma_R^2} (z - x_+(t))^2 - \frac{\sigma_r^2}{2} (p - \dot{x}_+(t))^2 \right] \right. \\ &+ \left. |c_-|^2 \exp \left[-\frac{1}{2\sigma_R^2} (z - x_-(t))^2 - \frac{\sigma_r^2}{2} (p - \dot{x}_-(t))^2 \right] \right\}. \end{aligned} \quad (4.107)$$

The Wigner density turns out to be positive for all the times $t > 0$. Therefore, it can be interpreted as a classical probability distribution. A truly quantum state of the cantilever would have an alternating sign what makes it impossible to regard the

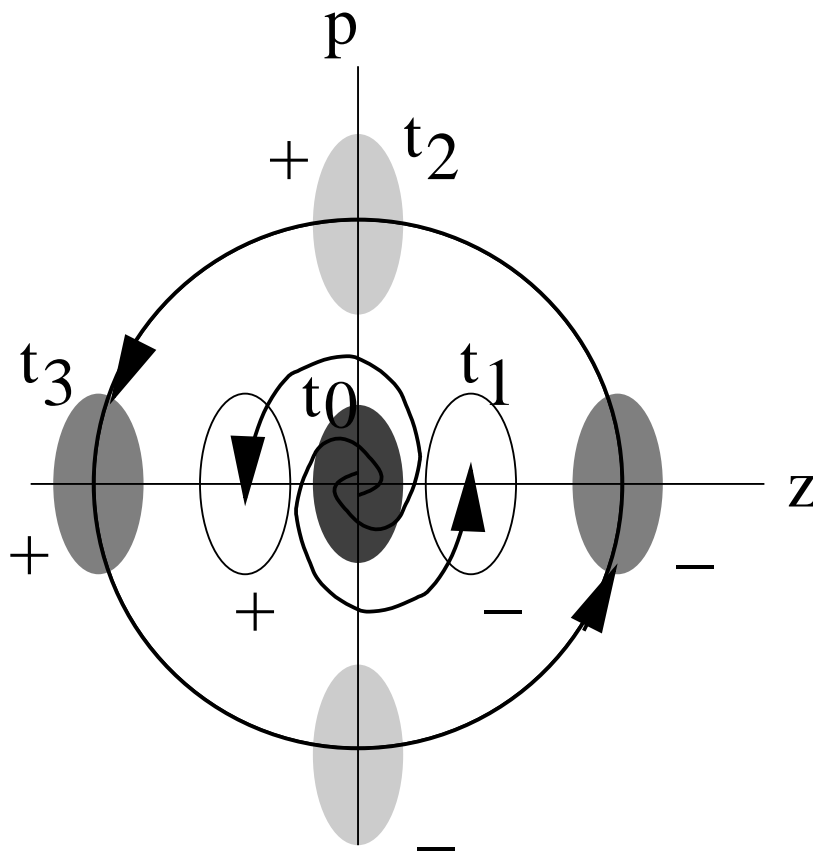


Figure 4.9: Sketch of the motion of the Wigner density starting at the time t_0 with $|c_+|^2 = |c_-|^2 = 1/2$. The Gaussians are separated at the time t_1 and evolve in the steady-state regime at the times t_2 and t_3 . The Gaussians with the plus sign correspond to the spin-up state and the ones with the minus sign to the spin-down state.

function as a probability distribution in phase space. In our case $W(z, p)$ represents a mixture of localized wave packets moving according to the position and momentum of a classical driven harmonic oscillator. In contrast to the spin dynamics, no transition from classical to quantum behavior takes place. Fig. 4.9 shows the motion of the Wigner density. The Gaussians are shown to be well-separated in the steady-state regime for a case in which the measurement would be possible. In the beginning of the experiment, the Gaussians with widths σ_R and $1/\sigma_r$ in the z and p direction, respectively, are located at the point $z = 0, p = 0$ and later, they begin to separate.

4.10 MRFM as a quantum measurement device

In the orthodox theory, the quantum measurement is described as a wave function collapse, which reduces the quantum state (in our case, the spin) in a non-unitary way to one of the two possible eigenstates of the spin z component, the observed quantity, with corresponding state-dependent probabilities. The von Neumann theory of the quantum measurement is one possibility to produce a classical outcome at the end of the measurement. Before we analyze the weak-measurement scheme, let us look at the magnetic resonance force microscope measurement according to the Copenhagen interpretation, where a “sharp” border line is drawn between classical and quantum parts of the measuring device. The quantum part is the spin state

$$|\chi\rangle = c_+|\chi_+\rangle + c_-|\chi_-\rangle \quad (4.108)$$

given at the time point when the projective measurement would happen. In contrast, the cantilever, probing the spin, is assumed to be a classical object described by the following Hamilton function

$$H(t) = \mp\eta f(t)z + \frac{p_z^2}{2} + \frac{z^2}{2}. \quad (4.109)$$

The effect of the spin in the MRFM measurement is assumed to lead to a positive or negative resonant driving force $\mp f(t) = \mp f_0 \sin(t)$ depending on the state of the spin. This leads to two distinct motions of the macroscopically observable classical cantilever, according to the spin state, immediately before the instantaneous projection. Thus, one of the two possible spin values is detected. In a repeated set of measurements, these values occur with probabilities $P_+ = |c_+|^2$ and $P_- = |c_-|^2$.

In a more realistic measurement model, the measurement is done by a device which is also a quantum system, the so-called quantum probe, with a read-out variable which can be probed macroscopically. The classical measurement device then detects the quantum probe instead of probing the quantum object directly. In the quantum theory of measurement, this falls into the category of the indirect quantum measurement scheme [Breuer02]. Our setup exemplifies such an indirect measurement (Fig. 4.10). In our case, the quantum object is the spin, the quantum probe corresponds to the cantilever, and the classical measurement device can be, e.g., a fiber-optic interferometer.

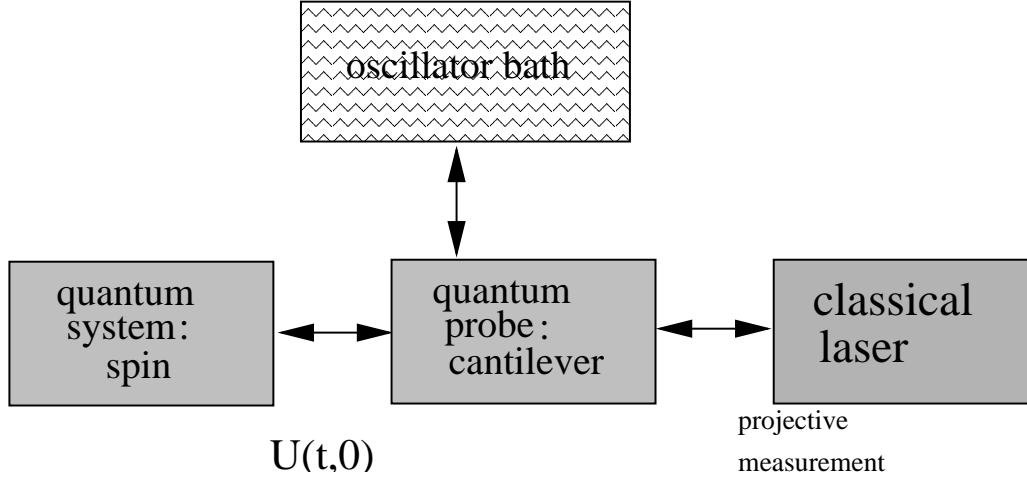


Figure 4.10: Indirect measurement scheme

Let us briefly discuss the different time scales for our weak measurement [Makhlin01]. During the measurement, the spin loses its phase coherence, usually on a short time scale τ_ϕ . Fig. 4.4 shows the decay of the off-diagonal elements of the spin and therefore the typical decoherence times during the measurement. We considered pure dephasing: The off-diagonal elements of the reduced spin density matrix vanish, while the diagonal entries remain unchanged:

$$\rho^{(S)}(0) = \begin{bmatrix} \rho_{++}(0) & \rho_{+-}(0) \\ \rho_{-+}(0) & \rho_{--}(0) \end{bmatrix} \rightarrow \rho^{(S)}(t \gg \tau_\phi) = \begin{bmatrix} \rho_{++}(0) & 0 \\ 0 & \rho_{--}(0) \end{bmatrix}. \quad (4.110)$$

During the decay of the off-diagonal elements, the information about the initial state of the spin is transferred to the quasiclassical, macroscopic state of the cantilever. For an appropriate choice of the parameters and suitable conditions of the environment, the information about the spin state can be read-out after another time scale called the measurement time τ_{meas} . In our measurement, this time corresponds to the moment when the oscillation amplitude has reached a high enough value such that the wavepackets can be distinguished. Note that $\tau_{meas} \geq \tau_\phi$, i.e., the coherence is always destroyed during a measurement.

In the end, there should also be a thermalization of the density matrix of the spin, i.e., the diagonal elements of the spin density matrix go to their stationary or thermal values:

$$\rho^{(S)}(t) \rightarrow \rho^{(S)}(t \gg \tau_{mix}) = \begin{bmatrix} \rho_{++}^{(eq)} & 0 \\ 0 & \rho_{--}^{(eq)} \end{bmatrix}. \quad (4.111)$$

Furthermore, the detector reacts back on the spin and destroys the information contained in the initial state. This time scale is the mixing time τ_{mix} . In our setup this is the time when spin flips occur. In our setup the mixing time is on the order of the Landau-Zener transition time $\tau_{mix} \approx \tau_{LZ}$. The mixing time should be much larger than the measurement time in order to make the measurement possible. The parameters must be chosen such that the occupation probabilities of the spin state do not

change before the information is read out. One finds the criterion $\tau_\phi \leq \tau_{\text{meas}} \ll \tau_{\text{mix}}$. This condition is obviously fulfilled in our case. If the mixing time would be smaller than the measurement time, the measurement would be impossible because the diagonal elements containing the probabilities of the initial spin state would thermalize and the information would be lost.

What is measured with the MRFM setup? Answer: The amplitudes of the spin with reference to the effective magnetic field. At time $t = 0$, the spin has certain amplitudes to be up or down with respect to the effective magnetic field. Because the spin follows the effective magnetic field adiabatically, these amplitudes remain unchanged to a high accuracy. If the spin is up at time $t = 0$, then the the cantilever oscillates with a certain phase. If the spin is down at time $t = 0$, then the the cantilever oscillates exactly with a phase shifted by π compared to the up case. One of the conclusions of the analysis presented here is that the cantilever oscillates with the same amplitude for both initial spin states (up and down). Probing the amplitude of the cantilever vibration can only determine the absolute value of the spin in the direction of $\mathbf{B}_{\text{eff}}(0)$, but not its sign. However, the oscillations for the initial spin-up and spin-down states are completely out of phase (phase difference of π), see Section 4.6. This fact was also noted by Berman *et al.* [Berman03a] in their numerical simulations. Hence, there is the possibility to use the MRFM as a quantum measurement device, i.e., to detect the direction of the spin with the MRFM by probing the (discrete) relative phases of the cantilever oscillations. A conceivable scheme to measure the relative phases of the cantilever oscillations is to use a reference spin which is prepared in a definite known state, for example, by applying a strong magnetic field in a desired direction. The two signals from the reference spin and the spin in an unknown state are superimposed to determine the relative phase of the unknown spin.

4.11 Conclusions

We have studied the CAI-based MRFM as a high-resolution tool to detect single spins. The quantum dynamics of the spin-plus-cantilever system was analyzed in terms of the reduced density matrices, $\hat{\rho}^{(S)}(t)$ (for the spin) and $\hat{\rho}^{(C)}(t)$ (for the cantilever), in the presence of coupling to the environment. Using an effective bath model, we were able to determine the dynamics of the spin during the measurement process. Our results remain valid at all temperatures as long as the adiabatic approximation is satisfied. We have solved the influence functional for the combined system of spin and cantilever to obtain the quantum dissipative dynamics of the cantilever. These results are valid for all temperatures and coupling strengths. Finally, we have proposed that the MRFM can be used as a quantum measurement device, i.e., not only to detect the absolute value of the spin, but also to detect its direction.

Chapter 5

Leakage of Josephson qubits

In several proposals and recent experiments with superconducting qubits [Nakamura99, Cottet02, Chiorescu03] a vector in a restricted two-dimensional Hilbert space is used as a qubit, the basic unit of quantum information. The quantum hardware therefore operates in a two-dimensional subspace of a Hilbert space of high dimensionality. While controlling the system with an external potential, one might excite higher states beyond the two states. This drawback may affect the whole quantum information process. The loss of amplitude into higher states is known as leakage. A mathematical definition and studies of leakage were made in [Fazio99]. There, operations were studied using instantaneous switching, e.g. single qubit operations were implemented by suddenly switching the offset charge to the degeneracy point. Here, we are interested in other pulse forms, especially those used in the Saclay experiment [Vion02], and the consequences of leakage.

5.1 Leakage of Josephson qubits during a NMR-like microwave pulse operation

The system under investigation, the Cooper-pair box, consists of a superconducting island with a small capacitance, separated from a superconducting reservoir by two Josephson tunnel junctions, see Fig. 5.1. Each of these Josephson junctions has a Josephson energy $E_J/2$. The state of the “box” is controlled via a capacitance C_g by an external gate voltage $V_g(t)$. The Hamiltonian of the box is given by [Tinkham]

$$\mathcal{H}(t) = E_C \left(\hat{N} - N_g(t) \right)^2 - E_J \cos(\hat{\phi}), \quad (5.1)$$

where \hat{N} is the number of excess Cooper pairs on the island and $\hat{\phi}$ is the conjugate phase operator and $N_g(t) = C_g V_g(t)/(2e)$. There are two energy scales, the Josephson energy E_J , and the charging energy E_C . Leakage depends on the ratio of these energies defining distinct energy spectrums. The two extreme limits correspond to a “rotor” spectrum for $E_J = 0$, and a “harmonic oscillator” spectrum for $E_C = 0$.

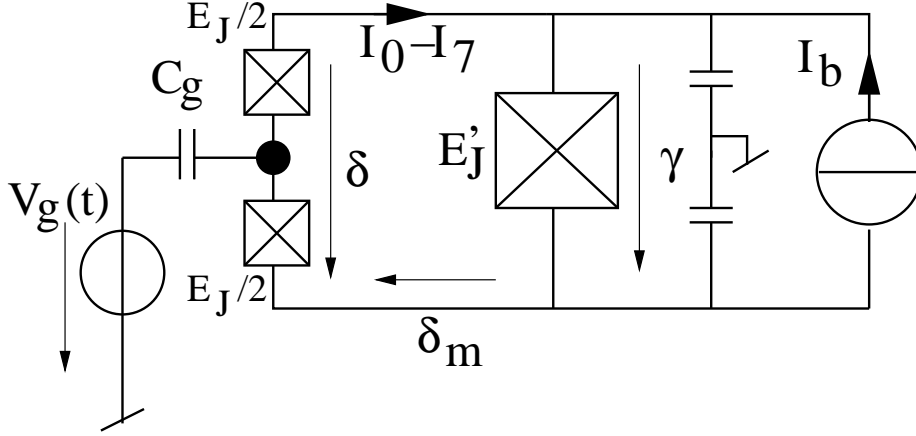


Figure 5.1: The experimental setup used in Saclay. The box consists of a small superconducting island separated by two Josephson junctions from a superconducting reservoir. The phase δ_m is due to an external imposed magnetic flux of magnitude $\phi_0 \delta_m$.

The pulse used in the Saclay experiment at the gate has, in the most ideal case, the following form

$$N_g(t) \equiv \frac{1}{2} + n(t) \equiv \frac{1}{2} + A(t) \cos(\omega t), \quad (5.2)$$

where $A(t)$ is the pulse shape. Leakage is worst for a rectangular pulse, defined by

$$A(t) \equiv A [\Theta(t) - \Theta(t - T)], \quad (5.3)$$

where T is the pulse duration. We consider excitations around the working point $N_g = 1/2$. At this point the qubit is defined by the ground state and the first excited state of the Hamiltonian

$$\mathcal{H}_0 = E_C (\hat{N} - 1/2)^2 - E_J \cos(\hat{\phi}). \quad (5.4)$$

Further, we work in a regime, where $E_C \simeq E_J$ and neither \hat{N} nor $\hat{\phi}$ are good quantum numbers.

The frequency of the oscillating gate voltage matches the transition frequency of the lowest two energy levels, i.e. $\omega = E_1 - E_0$. With such NMR-like pulses any state $|\Psi\rangle = \alpha|0\rangle + \beta|1\rangle$ can be prepared. The population probabilities of the states defining the qubit show Rabi oscillations, see below. In the following we study leakage, the population of higher states, during such an operation using a rectangular pulse shape. The ideal Rabi oscillation result is perturbed.

5.2 The model in a restricted Hilbert space

To study leakage, we restrict the Hilbert space to an eight-dimensional subspace. This choice is motivated two-fold: The first reason is that the numerical analysis shows

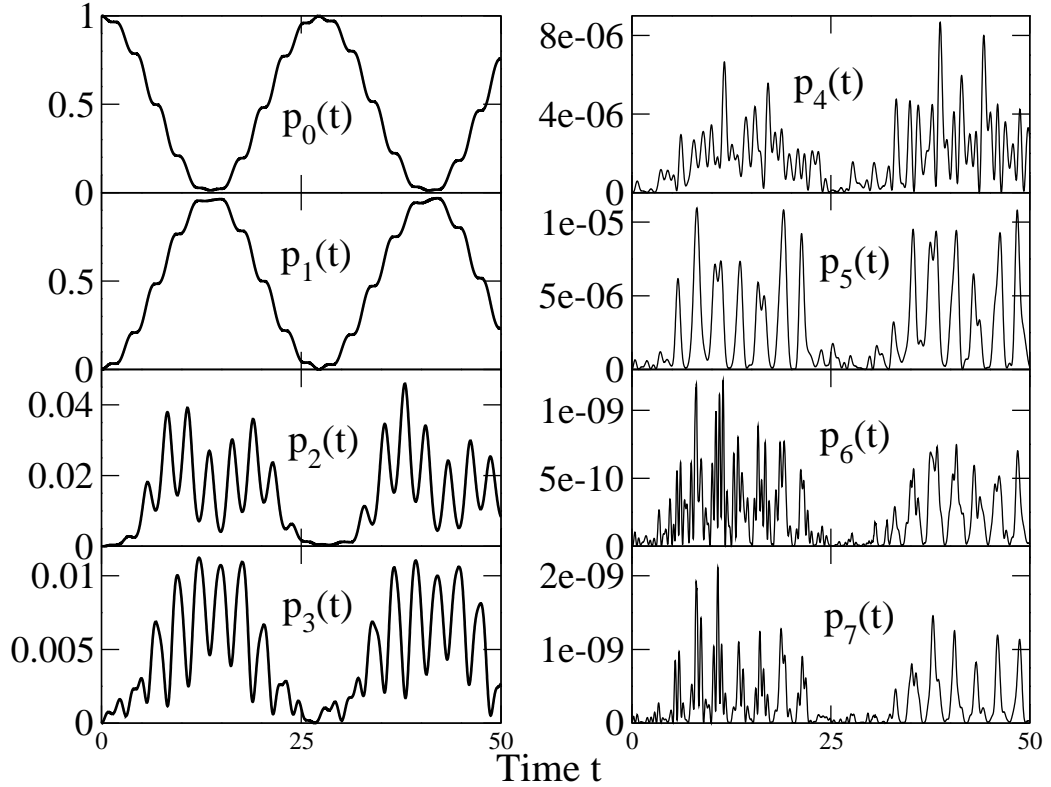


Figure 5.2: Probabilities $p_i(t)$ to be in the eight different states as a function of the time t . The amplitude is chosen to be $A = 0.2$. $p_0(t)$ and $p_1(t)$ in the topmost graphs show Rabi oscillations, which deviate from a perfect sinusoidal behavior due to leakage to the six non-computational states. The non-computational states are populated with maximal probabilities on the order of 4 – 5% respectively.

that the results do not change significantly anymore going beyond six levels and on the other hand the structure of the energy spectrum. For our choice of parameters we are still far away from the harmonic oscillator spectrum. The energy levels turn out to be in pairs together, which are well-separated from each other. The level splitting of each pair gets smaller for increasing energy. We include the next three pairs and include six additional levels to the computational subspace. This leads to reasonable results in the regime $E_C \simeq E_J$. Note that if E_J is chosen much larger than E_C then all the energy levels become equidistant and higher levels should be taken into account, i.e., our approach is not valid anymore.

For the numerical results we choose the time scale such that $E_C \equiv 1$. Let us now list the values of the parameters used in the Saclay experiment. The ratio of the characteristic energies is given by $E_J/E_C = 1.27$. The pulse duration was varied in the range $0.1\mu s$, while a maximal nominal pulse amplitude of $V_g = \max_t(V_g(t)) \approx 122\mu V$ was applied. The observed decoherence time was on the order of $0.5\mu s$. The amplitude $A = C_g V_g / (2e)$ can be calculated from the gate voltage using the value $C_g = 10^{-17} F$ for the gate capacitance. This leads to an amplitude A , which is

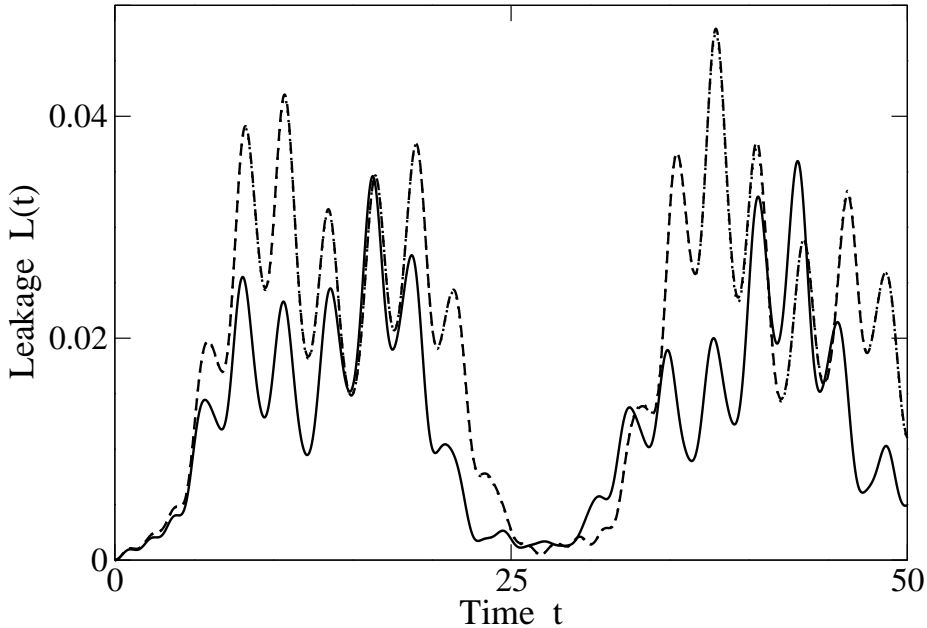


Figure 5.3: Typical leakage as a function of time t using an amplitude $A = 0.2$. Solid line: four levels, dotted line: six levels and dashed line: eight energy levels taken into account. The result for six and eight energy levels does not show any significant difference. Therefore, about six energy levels are enough to study leakage in our parameter regime.

maximally on the order of ~ 0.004 . Therefore it turns out that the leakage for this specific amplitude is negligibly small (compared with all the other perturbing effects like $1/f$ noise) according to the results in Fig. 5.4.

In order to obtain numerical results for leakage the Schrödinger equation can be integrated using the Hamiltonian given in Eq. (5.1) in the restricted Hilbert space spanned by the eight lowest energy levels. All the results are presented with reference to the eigenbasis of the Hamiltonian \mathcal{H}_0 , see Eq. (5.4). The eight eigenstates and eigenvalues are numbered from zero to seven. In Fig. 5.2 we show the probabilities for the population of the eight states as a function of time starting at the time $t = 0$ in the ground state. The amplitude $A = 0.2$ is chosen comparatively high (with respect to the amplitude used in the Saclay experiment) to see a pronounced effect. We find that leakage out of the computational basis

$$L(t) \equiv 1 - (|\langle 0|\psi(t)\rangle|^2 + |\langle 1|\psi(t)\rangle|^2) \quad (5.5)$$

remains smaller than 5%, see Fig. 5.3. The Rabi oscillations $p_0(t)$ and $p_1(t)$ do not have the ideal sinusoidal form. There are higher frequent oscillations with a smaller amplitude added. The frequency of these oscillations corresponds to the transition frequency between the different energy levels, see Section 5.3. The population of the higher levels contains more higher frequent oscillations. Fig. 5.4 shows the maximal leakage out of the computational basis as a function of the amplitude A . The results were obtained by integrating the Schrödinger equation numerically over a time span

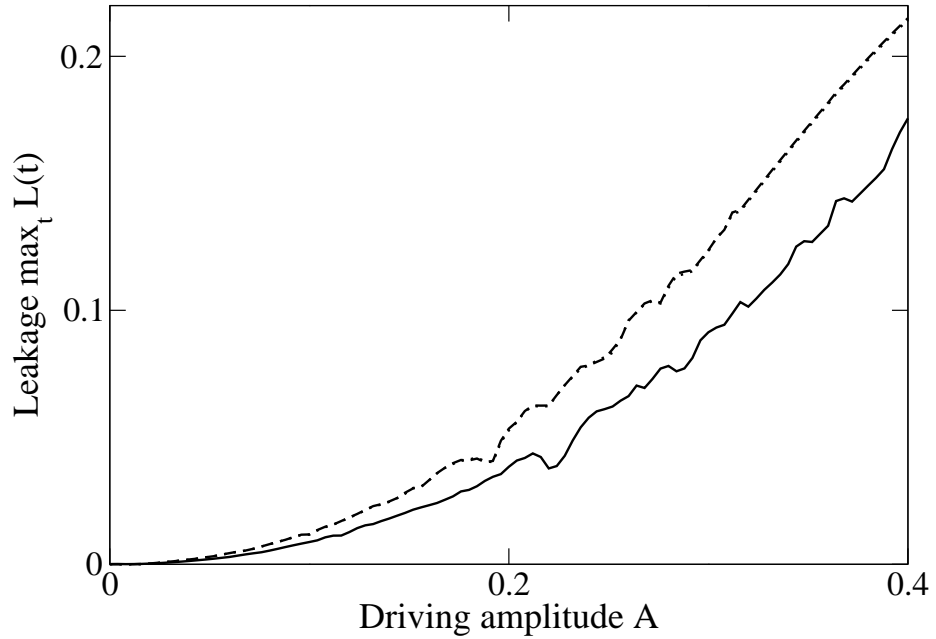


Figure 5.4: Maximal leakage evaluated for times $t \leq 1000$ as a function of the amplitude A of the applied oscillating gate voltage. Solid line: four levels, dotted line: six levels and dashed line: eight energy levels taken into account. The results for six and eight energy levels coincide with high accuracy. For $A \approx 0.4$ a small deviation shows up, i.e., for even higher amplitudes more energy levels would have to be taken into account.

on the order of the experimental observed decoherence time. For the leakage a time evolution, as shown in Fig. 5.3, was found. Then the maximum of the leakage, which is the sum of the maximal probabilities to be in the leakage states $\max_t(\sum_{i=2}^7 p_i)$, was evaluated for different amplitudes A .

5.3 A perturbative approach

For a small driving amplitude A , relevant in the Saclay experiment, one can obtain analytical results using a perturbative approach in order to solve for the time evolution, or the population of the states $|2\rangle$ and $|3\rangle$. Considering these two additional states is enough to get the major contribution to leakage. The Hamiltonian given in Eq. (5.1) can be recast into the form

$$\mathcal{H}(t) = E_C \left(\hat{N} - N_g(t) \right)^2 - \frac{E_J}{2} \sum_N \left(|N+1\rangle\langle N| + |N-1\rangle\langle N| \right), \quad (5.6)$$

where in the charge representation, where \hat{N} is diagonal, the diagonal elements

$$H_{NN} = E_C \left(N - N_g(t) \right)^2 \quad (5.7)$$

and the off-diagonal elements

$$H_{N,N\pm 1} = -\frac{E_J}{2} \quad (5.8)$$

can be read off. For the perturbative approach we use the four lowest energy levels. In the charge basis we find the matrix

$$H(t) = \begin{pmatrix} 2E_C + 3E_C n(t) & -\frac{E_J}{2} & 0 & 0 \\ -\frac{E_J}{2} & E_C n(t) & -\frac{E_J}{2} & 0 \\ 0 & -\frac{E_J}{2} & -E_C n(t) & -\frac{E_J}{2} \\ 0 & 0 & -\frac{E_J}{2} & 2E_C - 3E_C n(t) \end{pmatrix}, \quad (5.9)$$

where for convenience a term $E_C(N_g(t)^2 - n(t))$ times the unity matrix was subtracted, which would modify the global phase of the states and does not affect the result for the probabilities. \mathcal{H}_0 in the considered subspace can be diagonalized analytically. The eigenvalues are found to be

$$\begin{aligned} E_0 &= E_C - E_J/4 - \sqrt{E_C^2 + E_C E_J/2 + 5E_J^2/16} \\ E_1 &= E_C + E_J/4 - \sqrt{E_C^2 - E_C E_J/2 + 5E_J^2/16} \\ E_2 &= E_C - E_J/4 + \sqrt{E_C^2 + E_C E_J/2 + 5E_J^2/16} \\ E_3 &= E_C + E_J/4 + \sqrt{E_C^2 - E_C E_J/2 + 5E_J^2/16} \end{aligned} \quad (5.10)$$

In the following, we work in the eigenbasis of \mathcal{H}_0 . In the eigenbasis the whole Hamiltonian $H(t)$ is given by

$$H(t) = \begin{pmatrix} E_0 & \gamma n(t) & 0 & V_{03}(t) \\ \gamma n(t) & E_1 & V_{12}(t) & 0 \\ 0 & V_{21}(t) & E_2 & V_{23}(t) \\ V_{30}(t) & 0 & V_{32}(t) & E_3 \end{pmatrix}, \quad (5.11)$$

where all the time dependent entries are proportional to $n(t)$ and can be found analytically. The qubit states are denoted by $|0\rangle$ and $|1\rangle$ and the rest of the space is spanned by the leakage basis states $|2\rangle$ and $|3\rangle$.

In the next step, we split the Hamiltonian $H(t)$ in two parts $H_0(t)$ and $\delta V(t)$

$$H_0(t) = \begin{pmatrix} E_0 & \gamma n(t) & 0 & 0 \\ \gamma n(t) & E_1 & 0 & 0 \\ 0 & 0 & E_2 & 0 \\ 0 & 0 & 0 & E_3 \end{pmatrix}, \quad (5.12)$$

$$\delta V(t) = \begin{pmatrix} 0 & 0 & 0 & V_{03}(t) \\ 0 & 0 & V_{12}(t) & 0 \\ 0 & V_{21}(t) & 0 & V_{23}(t) \\ V_{30}(t) & 0 & V_{32}(t) & 0 \end{pmatrix}. \quad (5.13)$$

$\delta V(t)$ can be treated as a time-dependent small perturbation. We find the following equations for the unperturbed system and the perturbation of the state

$$i\partial_t|\Psi_0(t)\rangle = \hat{H}_0(t)|\Psi_0(t)\rangle \quad (5.14)$$

and

$$i\partial_t|\delta\Psi(t)\rangle = \delta\hat{V}(t)|\Psi_0(t)\rangle + \hat{H}_0(t)|\delta\Psi(t)\rangle, \quad (5.15)$$

where $|\Psi(t)\rangle = |\Psi_0(t)\rangle + |\delta\Psi(t)\rangle$. The states $|\Psi_0(t)\rangle$ and $|\delta\Psi(t)\rangle$ can be expressed as

$$|\Psi_0(t)\rangle = \sum_{i=0}^3 a_i(t)|i\rangle \quad (5.16)$$

and

$$|\delta\Psi(t)\rangle = \sum_{i=0}^3 \delta b_i(t)|i\rangle \quad (5.17)$$

The initial conditions are given by the only non-vanishing amplitude of the ground state $a_0(0) = 1$

$$|\Psi_0(0)\rangle = |0\rangle \quad (5.18)$$

and

$$|\delta\Psi_0(0)\rangle = 0. \quad (5.19)$$

We find $a_2(t) = a_3(t) = 0$. The results for the amplitudes to be in state 2 and 3 are further given by

$$\begin{aligned} \delta b_2(t) &= -i \exp(-iE_2t) \int_0^t d\tau \exp(iE_2\tau) V_{21}(\tau) a_1(\tau) \\ \delta b_3(t) &= -i \exp(-iE_3t) \int_0^t d\tau \exp(iE_3\tau) V_{30}(\tau) a_0(\tau). \end{aligned} \quad (5.20)$$

The probabilities to be in states 2 and 3 are given by

$$\begin{aligned} p_2(t) &= \left| \int_0^t d\tau \exp(iE_2\tau) V_{21}(\tau) a_1(\tau) \right|^2 \\ p_3(t) &= \left| \int_0^t d\tau \exp(iE_3\tau) V_{30}(\tau) a_0(\tau) \right|^2. \end{aligned} \quad (5.21)$$

In the next step we determine the amplitudes $a_0(t)$ and $a_1(t)$. The time evolution generated by $H_0(t)$ can be found using the rotating wave approximation, because the whole system is driven at the qubit transition frequency $\omega = E_1 - E_0$. The evolution in the qubit subspace is governed by the Hamiltonian

$$\begin{aligned} \mathbf{P}H(t)\mathbf{P} &= \begin{pmatrix} E_0 & \gamma n(t) \\ \gamma n(t) & E_1 \end{pmatrix} \\ &= \begin{pmatrix} E_0 & \gamma A(t) \cos(\omega t) \\ \gamma A(t) \cos(\omega t) & E_1 \end{pmatrix} \\ &\simeq \begin{pmatrix} E_0 & f(t) \exp(i\omega t) \\ f(t) \exp(-i\omega t) & E_1 \end{pmatrix}, \end{aligned} \quad (5.22)$$

where $\mathbf{P} = |0\rangle\langle 0| + |1\rangle\langle 1|$ is the projector onto the qubit subspace and $f(t) \equiv \frac{\gamma}{2}A(t)$. With the ansatz

$$|\Psi(t)\rangle = c_0(t) \exp(-iE_0t)|0\rangle + c_1(t) \exp(-iE_1t)|1\rangle \quad (5.23)$$

one finds in the case of resonance $\omega = E_1 - E_0$, the following two coupled differential equations for the amplitudes

$$\begin{aligned} i\frac{d}{dt}c_0(t) &= f(t)c_1(t) \\ i\frac{d}{dt}c_1(t) &= f(t)c_0(t). \end{aligned} \quad (5.24)$$

For the initial conditions $c_0(0) = 1$ and $c_1(0) = 0$, the solution is given by

$$\begin{aligned} c_0(t) &= \cos\left(\int_0^t d\tau f(\tau)\right) \\ c_1(t) &= -i \sin\left(\int_0^t d\tau f(\tau)\right). \end{aligned} \quad (5.25)$$

In the end, we find

$$\begin{aligned} a_0(t) &= \cos\left(\frac{\gamma}{2}\int_0^t d\tau A(\tau)\right) \exp(-iE_0t) \\ a_1(t) &= -i \sin\left(\frac{\gamma}{2}\int_0^t d\tau A(\tau)\right) \exp(-iE_1t). \end{aligned} \quad (5.26)$$

The rotating wave approximation holds for $|f| \ll |\omega|$, where $f = \gamma A$ and A is the amplitude of the pulse.

For the rectangular pulse form, the probabilities to be in the states 2 and 3 at time T are given by

$$\begin{aligned} p_2(T) &= V_{21}^2 A^2 \left| \int_0^T dt \exp(i(E_2 - E_1)t) \right. \\ &\quad \times \left. \cos(\omega t) \sin\left(\frac{\gamma}{2}At\right) \right|^2 \\ p_3(T) &= V_{30}^2 A^2 \left| \int_0^T dt \exp(i(E_3 - E_0)t) \right. \\ &\quad \times \left. \cos(\omega t) \cos\left(\frac{\gamma}{2}At\right) \right|^2, \end{aligned} \quad (5.27)$$

where V_{21} and V_{30} are defined by $V_{21}(t) = V_{21}n(t)$ and $V_{30}(t) = V_{30}n(t)$.

To leading order in the small amplitude A , we find for $t < T$

$$\begin{aligned} p_2(t) &\approx A^2 V_{21}^2 \frac{[(E_1 - E_2)^2 \cos^2(\omega t) + \omega^2 \sin^2(\omega t)] \sin^2(\gamma At/2)}{[(E_1 - E_2)^2 - \omega^2]^2} \\ p_3(t) &\approx A^2 V_{30}^2 \frac{1}{[(E_0 - E_3)^2 - \omega^2]^2} \left| (E_3 - E_0) + \exp(-i(E_0 - E_3)t) \right. \\ &\quad \times \left. \cos(\gamma At/2) [(E_0 - E_3) \cos(\omega t) + i\omega \sin(\omega t)] \right|^2. \end{aligned} \quad (5.28)$$

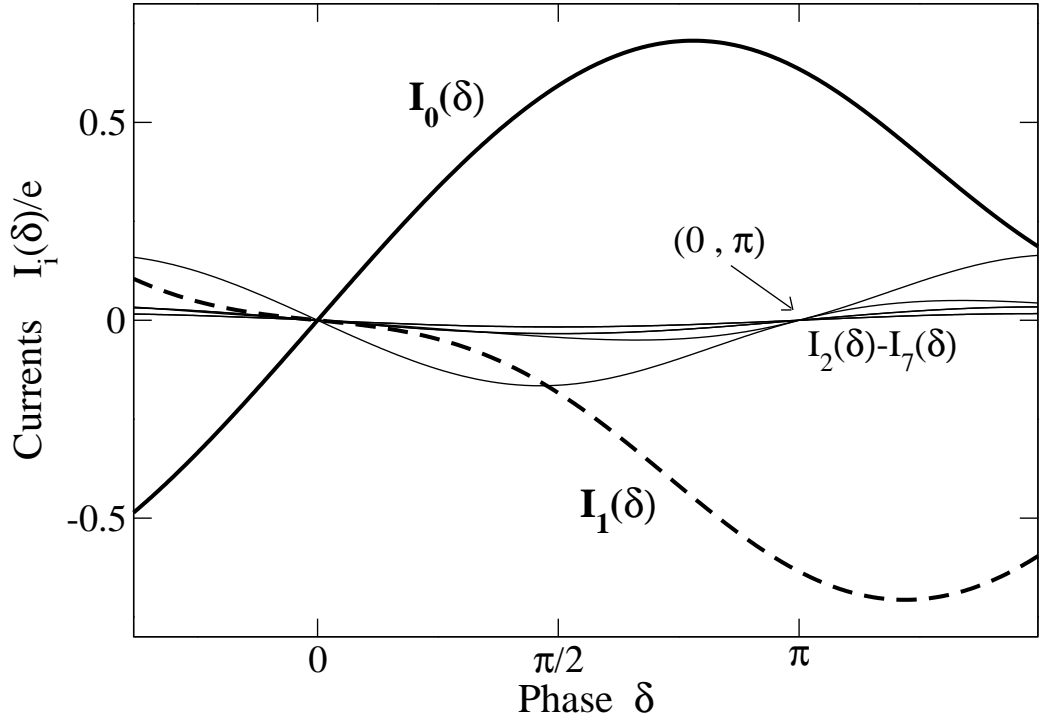


Figure 5.5: The currents in the superconducting loop $I_k(\delta)$ as a function of the phase δ over the box.

The probability $p_2(t)$ contains the two frequencies 2ω and γA appearing in Fig. 5.2.

To close this chapter let us make a short note about the influence of the leakage on the read-out mechanism [Cottet03]. A Josephson junction with a Josephson energy E'_J much larger than that of the box was used to perform the read-out. This read-out junction forms a superconducting loop together with the box, see Fig. 5.1. The loop is biased with a magnetic flux $\phi_0 \delta_m$ (where $\phi_0 = 1/(2e)$). The read-out junction switches to a finite-voltage state if the bias current I_b has the critical value $I_b^{\text{crit}} = E'_J/\phi_0$. To perform the measurement the read-out junction is biased by a current slightly lower than the critical current. The states of the box lead to distinct currents I_k in the superconducting loop. The current through the read-out junction is given by $I_b - I_k(\delta, N_g = 1/2)$. If the current I_k enhances the current through the read-out junction to a value higher than the critical value, a switching of the read-out junction occurs with an increased switching probability P_k . The currents I_0 and I_1 have opposite sign, see Fig. 5.5. This leads to distinct switching probabilities, which makes the measurement possible. The currents I_k , which depend on the state $|k\rangle$ of the box, are shown in Fig. 5.5. The currents are found by evaluating

$$I_k(\delta, N_g = 1/2) = \phi_0^{-1} \frac{\partial}{\partial \delta} E_k(\delta, N_g = 1/2). \quad (5.29)$$

The eigenvalues E_k depend on the phase δ via the Josephson energy $E_J(\delta) = E_J^0 \cos(\delta/2)$. If the system is in the states $|k\rangle$ with probabilities p_k before the measurement, the

switching probability of the read-out junction is given by

$$P_{\text{switch}}(I_P, \tau, N_g = 1/2, \delta_m) = \sum_{k=0}^7 p_k P_k(I_P, \tau, N_g = 1/2, \delta_m). \quad (5.30)$$

I_p is the applied probing current, τ its duration, and δ_m is the phase due to the external magnetic field. Optimal read-out conditions would occur if the parameters τ , δ_m , and I_p , are tuned to values, such that the probability P_1 is one and P_0 vanishes. This cannot be achieved with the setup used in Saclay. According to Fig. 5.5, the magnitudes of the currents I_k are smaller or of the same order as the currents I_0 and I_1 . For certain values of δ they vanish, e.g., $\delta = \pi$. Therefore, we expect that the higher states lead to a switching of the read-out junction with probabilities $P_2 - P_7$ with values between P_0 and P_1 . This fact would disturb the measurement, see Eq. (5.30), if the probabilities $p_2 - p_7$ would be sufficiently large. This is not the case for the parameter regime considered in the Saclay experiment (see above).

5.4 Conclusions

Leakage of a Josephson qubit operated in the regime of the recent Saclay experiment was investigated. The NMR-like microwave pulse operation leads to Rabi oscillations of the qubit. A numerical analysis of the problem including totally eight states was made by calculating the population of the higher states. The magnitude of the leakage during the pulse operation was obtained as a function of the amplitude of the oscillating gate voltage. We find that leakage turns out to be negligibly small for the experimental relevant parameter values.

Chapter 6

Summary and Open Questions

In the first part of this thesis we have devoted considerable attention to the decoherence of a two-state system due to an unconventional nonlinear environment and in the second part, a detailed analysis of a measurement of a spin one-half using a magnetic resonance force microscope was carried out. These investigations concerning the dissipative dynamics of two-state systems are important in the context of recent experiments and theoretical considerations, e.g., in the field of quantum information.

The idea of the Chapters 2 and 3 was to use a specific model for a nonlinear bath to learn about the differences between linear and nonlinear environments for arbitrary system-bath coupling strength. The analyzed nonlinear bath consists of a single two-level system subject to a linear oscillator bath. The effects of its action on a two-state system were examined by calculating spin-spin correlation functions. The high temperature limit was studied. The results stemming from different popular approximation schemes, i.e., Markoff and weak-coupling approximation have been analyzed and discussed in detail and various parameter regimes have been investigated. The Markoff approximation yields good results as long as the coupling strength is small enough, such that the decay is slow compared to the bath correlation time and the transition frequency. However, if the bath spectrum displays sharp structures, their effects on the correlator of the system are only described by the weak-coupling equation with its memory kernel. Both approaches fail for the regime of large system-bath coupling. In contrast, replacing the nonlinear bath approximately by a linear bath may still represent a good approximation to the original nonlinear bath. The bath spectral density for this linear bath is chosen in such a way that it coincides with the nonlinear one at low system-bath coupling. This approach, though valid only in the weak-coupling regime, might fail while increasing the system-bath coupling strength. We discussed its validity in detail.

We find that, as opposed to the Markoff and the weak-coupling approximations the substitution with a linear bath might still be a good approximation for the nonlinear bath also for higher coupling strength, which applies especially for a peaked structured bath with a sharply peaked bath spectral density.

In Chapter 3 the nonlinear bath model was analyzed at zero temperature using

flow equations. The use of this non-perturbative method to treat the dissipative four-state system goes beyond the weak-coupling limit. The analysis was carried out by first obtaining flow equations for the general dissipative four-state system coupling to linear baths with not necessarily Ohmic bath-spectral densities. The basic strategy was to calculate first the equilibrium correlator of the two-level system exactly using flow equations. Then it was calculated within the common linear-bath approximation, where the linear-bath correlation function is chosen to be the same as that of the nonlinear bath. The linear bath approximation involves the solution of the spin-boson problem with flow equations, first with an Ohmic bath-spectral density to obtain the linear-bath correlation function and second with exactly this linear-bath correlation function, which constitutes a new peaked bath-spectral density. In light of the above considerations, we have learned that the phenomenological linear-bath description can lead to results agreeing, to a large extent, with the ones obtained from the nonlinear bath even in the intermediate-coupling regime. As far as peak shapes are concerned, the agreement between the two approaches turned out to be better for a peaked bath spectral density similar to the high temperature case.

Second, in Chapter 4, we discussed an indirect, weak quantum measurement of a single spin by a magnetic resonance force microscope. The goal of various experimental groups is to reach the ultimate goal of single-spin detection, which seems to be possible within present-day technology. The quantum dynamics of the spin-plus-cantilever system were analyzed in terms of the reduced density matrices for the spin and for the cantilever, in the presence of coupling to the environment. Two different ways were used to obtain the dynamics of the density matrix: the path-integral method and a master-equation approach. The path-integral results are valid for all temperatures and coupling strengths, as long as the adiabatic approximation is satisfied. It was shown that the spin is measured in the direction of the effective magnetic field. The cantilever shows two distinct trajectories depending on the spin direction. These two oscillations are completely out of phase, which makes it possible to use the setup as a measurement device, i.e., not only the absolute value of the spin can be detected, but also its direction can be determined.

Chapter 5 contains a discussion of leakage, which turns out to be negligibly small in the Saclay experiment. A number of technical details are given in Appendices A.1–A.12.

To close this chapter let us turn to some open questions. A question showing up in our specific model, discussed in Chapter 2, is the following: Why does the weak-coupling solution for the unbiased case become exact in the high-temperature limit and therefore coincides with the exact approach 1? Thence, a possible extension includes an analysis of the higher-order terms in the weak-coupling equation going beyond the weak-coupling limit. Generally, higher-order correlation functions are important for the analysis of nonlinear environments, since the cumulant expansion does not break off.

In future considerations, one should also derive the asymptotic flow equations and find out if they fit into the universal behavior scheme observed for other similar flow

equations. Asymptotic flow equations can also determine the low frequency behavior of the correlation functions, i.e., one should see if the Shiba relation is also valid for the dissipative four-state system.

Especially for the biased case, one should investigate the effect of shifts of the bosonic modes. The reason to use such an additional unitary transformation is the following one. For each unitarily equivalent Hamiltonian, one obtains the same results. When approximations are made, things might change, because depending on the representation of the Hamiltonian, different terms gain different significance. Thus, one possibility to improve the accuracy of the flow equations is to introduce a shift of the bosonic modes. Additional parameters could be tuned to an optimal point, where the sum rule is fulfilled best.

Another direction for future work could be to try different generators, i.e., a different fixed-point Hamiltonian consisting, for example, of the free bath Hamiltonian and the free four-state system without interaction between them. This might be advantageous. The influence on the zero values in the correlation functions owing to the finite number of bath modes would be especially valuable. Moreover, it could also be expedient to use higher-order truncation schemes for the flow equations.

Furthermore, higher order correlation functions are helpful to learn about further differences of nonlinear and linear environments. Using a linear ansatz for the bosonic operators in the observable flow, the correlation functions factorize, like the correlation functions belonging to a linear environment. This is why higher-order correlation functions could not be investigated up to now. It would be valuable to use higher-order truncation schemes and modify the ansatz for the observable flow in order to calculate higher-order correlation functions.

Yet another interesting nonlinear bath is a nonlinear bath due to nonlinear coupling, which could probably be studied in a convenient way using flow equations.

More insight may be gained by examining the nonlinear bath in the range of temperatures between the two limiting cases covered in this work. This leaves the door open for the use of the quasi-adiabatic propagator path integral method or other numerical methods which might be helpful to learn about intermediate temperatures, specifically in the stronger-coupling regime. Another extension would be the analysis of the transition between the the two limiting cases of the nonlinear bath and the linear bath. In such an analysis one must replace the two-level system B by a spin of larger magnitude in order to observe the transition to the linear bath.

There are several open interesting questions connected to the MRFM: one is the choice of the environment and the discussion of other decohering sources neglected in our work. Hence, direct decohering mechanisms acting on the spin should be included and especially their influence on the measurement should be analyzed further. The dissipative dynamics of an open quantum system are sensitive to the low-frequency behavior of the spectral density of the environment. While the Ohmic model is a plausible model, it will be worthwhile to identify the sources of the environmental fluctuations and construct a physical model of the environment starting from a more microscopic theory of the cantilever.

Appendix A

Appendices

A.1 Spin in a fluctuating field

Here, we discuss the derivation of the results for the spin in a fluctuating magnetic field, presented in Sec. 1.1. The Hamiltonian is given by

$$\mathcal{H}(t) = \epsilon \hat{\sigma}_z + B(t) \hat{\sigma}_z. \quad (\text{A.1})$$

The Gaussian process is characterized by its mean $\langle B(t) \rangle$, assumed to be zero, and the correlation function $\langle B(t)B(t') \rangle$, or its Fourier transform $C(\omega)$

$$c(t-t') \equiv \langle B(t)B(t') \rangle = \int_{-\infty}^{+\infty} d\omega C(\omega) e^{-i(t-t')\omega}. \quad (\text{A.2})$$

We will concentrate on two specific examples, namely white noise

$$C(\omega) = k, \quad (\text{A.3})$$

which stems from an Ohmic bath spectral density at infinite temperature, and colored-noise correlations originating from the linear approximation to the nonlinear bath treated in Chapter 2, also at infinite temperature

$$C(\omega) = \langle BB \rangle_\omega = J^2 \frac{8\Delta^2 \gamma}{\pi} \frac{1}{(\omega^2 - 4\Delta^2)^2 + 4\omega^2 \gamma^2}. \quad (\text{A.4})$$

Let us now discuss the solution for the dynamics. The diagonal elements remain unchanged $\rho_{++}(t) = \rho_{++}(t_0)$ and $\rho_{--}(t) = \rho_{--}(t_0)$, while the off-diagonal elements decay. The solution for the specific sample of a Gaussian random process

$$\rho_{+-}(t) = \exp \left[-2i\epsilon(t-t_0) - 2i \int_{t_0}^t d\tau B(\tau) \right] \rho_{+-}(t_0) \quad (\text{A.5})$$

must be averaged over many different Gaussian noise fields. For a Gaussian field, with arbitrary correlation function $\langle B(s)B(u) \rangle$, the following identity holds

$$\langle \exp(iX) \rangle = \exp \left(-\frac{1}{2} \text{Var}(X) + i \langle X \rangle \right). \quad (\text{A.6})$$

Now we use this identity for our problem. At every point in time, the field $B(\cdot)$ has a Gaussian distribution:

$$\begin{aligned} \left\langle \exp \left(-2i \int_{t_0}^t d\tau B(\tau) \right) \right\rangle &= \exp \left(-\frac{1}{2} \left\langle 4 \int_{t_0}^t ds B(s) \int_{t_0}^t du B(u) \right\rangle \right) \\ &= \exp \left(-2 \int_{t_0}^t ds \int_{t_0}^t du \langle B(s) B(u) \rangle \right). \end{aligned} \quad (\text{A.7})$$

Using Eq. (A.2) and the integral

$$\int_{t_0}^t ds \int_{t_0}^t du e^{-i(s-u)\omega} = \frac{\sin(\frac{\omega}{2}(t-t_0))^2}{(\frac{\omega}{2})^2}, \quad (\text{A.8})$$

we find the result

$$\rho_{+-}(t) = \exp \left[-2i\epsilon(t-t_0) - 2 \int_{-\infty}^{\infty} d\omega C(\omega) \frac{\sin(\frac{\omega}{2}(t-t_0))^2}{(\frac{\omega}{2})^2} \right] \rho_{+-}(t_0). \quad (\text{A.9})$$

For white noise correlations $C(\omega) = k$, the integral

$$\int_{-\infty}^{\infty} d\omega k \frac{\sin(\frac{\omega}{2}(t-t_0))^2}{(\frac{\omega}{2})^2} = 2k\pi|t-t_0| \quad (\text{A.10})$$

has to be solved. For colored noise, the integral

$$I(t-t_0) = \int_{-\infty}^{\infty} d\omega \langle BB \rangle_{\omega} \frac{\sin(\frac{\omega}{2}(t-t_0))^2}{(\frac{\omega}{2})^2} = 2 \int_{-\infty}^{\infty} d\omega \langle BB \rangle_{\omega} \frac{1 - \cos(\omega(t-t_0))}{\omega^2} \quad (\text{A.11})$$

must be calculated. For $\text{Im } \alpha < 0$ (we consider only the case $\gamma^2 < 4\Delta^2$) and $t > 0$ we find

$$\int_{-\infty}^{\infty} dx \frac{1 - \cos(xt)}{x^2(x-\alpha)} = 2\pi i \left[\frac{it}{2\alpha} - \frac{1}{2\alpha^2} + \frac{\exp(-i\alpha t)}{2\alpha^2} \right]. \quad (\text{A.12})$$

If we use the following representation of the correlation function

$$C(x) = \langle BB \rangle_x = \text{Re} \left\{ \frac{J^2 i}{2\pi w} \left(\frac{\gamma + w}{x + i\gamma - iw} + \frac{-\gamma + w}{x + i\gamma + iw} \right) \right\}, \quad (\text{A.13})$$

where $w = i\sqrt{4\Delta^2 - \gamma^2}$, we obtain

$$\begin{aligned} I(t) &= \text{Re} \left\{ \frac{-J^2}{w} \left[(\gamma + w) \left(\frac{t}{w - \gamma} - \frac{\exp((w - \gamma)t) - 1}{w^2 - 2w\gamma + \gamma^2} \right) \right. \right. \\ &\quad \left. \left. + (-\gamma + w) \left(\frac{t}{-w - \gamma} - \frac{\exp((-w - \gamma)t) - 1}{w^2 + 2w\gamma + \gamma^2} \right) \right] \right\}. \end{aligned} \quad (\text{A.14})$$

A.2 Selection rules

Here we would like to determine the possible transitions of the system, discussed in Chapter 2 and 3, leading to different peaks in the Fourier transform of the equilibrium correlator. The Hamiltonian for $S + B$ alone is given by

$$\mathcal{H}_{SB} = \epsilon_S \hat{\sigma}_z^S + \Delta_S \hat{\sigma}_x^S + J \hat{\sigma}_z^S \hat{\sigma}_z^B + \Delta \hat{\sigma}_x^B. \quad (\text{A.15})$$

We define $\mathcal{P} \equiv \hat{\sigma}_x^S \otimes \hat{\sigma}_x^B$ with $\mathcal{P}^2 = \hat{1}$ and $[\mathcal{H}_{SB}, \mathcal{P}] = 0$. This symmetry leads to degeneracies. We obtain two eigenvalue problems

$$\begin{aligned} \mathcal{H}_{SB}|i\rangle &= \lambda_i|i\rangle \\ \mathcal{P}|i\rangle &= \pm|i\rangle, \end{aligned} \quad (\text{A.16})$$

where the eigenvalues λ_i are numbered from lowest to highest. The spectrum contains degeneracies in the transition frequencies. The eigenvalues are

$$\pm \sqrt{J^2 + \Delta^2 + \Delta_S^2 + \epsilon_S^2 \pm 2\sqrt{\Delta^2 \Delta_S^2 + J^2 \epsilon_S^2 + \Delta^2 \epsilon_S^2}}. \quad (\text{A.17})$$

This is why we find generally $-\lambda_1 = \lambda_4$ and $-\lambda_2 = \lambda_3$, see Figs. 2.5 and 2.6. Due to these regularities, we find four distinct frequencies for the biased case $\epsilon_S \neq 0$. No further symmetry is observed, which leads to the same number of dephasing peaks in the Fourier transform of the equilibrium correlator.

For the unbiased case $\epsilon_S = 0$ we find that the following matrix elements vanish $\langle 2|\hat{\sigma}_z^B|3\rangle = 0$ and $\langle 1|\hat{\sigma}_z^B|4\rangle = 0$. This leads to the transitions shown in Fig. 2.5, induced by the operator $\hat{\sigma}_z^B$ coupled to the driving force $F(t)$. For $\hat{\sigma}_z^S$, we find the same selection rules. The equilibrium correlator for $\gamma = 0$

$$\langle \hat{\sigma}_z^S(t) \hat{\sigma}_z^S \rangle = \sum_{ij} p_i |\langle i|\hat{\sigma}_z^S|j\rangle|^2 e^{i(\lambda_i - \lambda_j)t} \quad (\text{A.18})$$

therefore contains two characteristic frequencies $|\lambda_2 - \lambda_1| = |\lambda_4 - \lambda_3|$ and $|\lambda_3 - \lambda_1| = |\lambda_4 - \lambda_2|$, corresponding to two delta function peaks in the Fourier transform, which are broadened for increasing γ .

A.3 Equilibrium correlator for Approach 4

One result of the equilibrium correlator for $\epsilon_S \neq 0$ left out in Sec. 2.13 is listed below:

$$K_{zz}^S(\omega) = \frac{1}{\pi} \text{Re} \left\{ \left(\frac{\Phi(s)}{\Psi(s)} - \frac{1}{s} \right) \Big|_{s=-i\omega} \right\}, \quad (\text{A.19})$$

where

$$\begin{aligned} \Phi(s) &= 2 \left(-16F(s)s\epsilon_S^2\lambda^2 + \lambda \{ (4G(s) + s)\Delta_S^2(s^2 + 4sC_{BB}(s) + 2\Delta_S^2) \right. \\ &\quad \left. + \epsilon_S^2 [s(16F(s)^2 + (4G(s) + s)^2) + 2(4G(s) + 3s)\Delta_S^2] + 4s\epsilon_S^4 \} \right) \end{aligned} \quad (\text{A.20})$$

$$\begin{aligned} \Psi(s) = s \left(-16F(s)s\epsilon_S^2\lambda^2 + \lambda\{(4G(s) + s)\Delta_S^2(s^2 + 4sC_{BB}(s) + 4\Delta_S^2) \right. \\ \left. + \epsilon_S^2[s(16F(s)^2 + (4G(s) + s)^2) + 8(2G(s) + s)\Delta_S^2] + 4s\epsilon_S^4\} \right) \end{aligned} \quad (\text{A.21})$$

$$F(s) = \frac{C_{BB}(s - 2i\lambda) - C_{BB}(s + 2i\lambda)}{2i} \quad (\text{A.22})$$

$$G(s) = \frac{C_{BB}(s - 2i\lambda) + C_{BB}(s + 2i\lambda)}{2}, \quad (\text{A.23})$$

and

$$\lambda = \sqrt{\Delta_S^2 + \epsilon_S^2}. \quad (\text{A.24})$$

A.4 The flow equations for the Hamiltonian

Below we list the result for the dissipative four-state system discussed in Sec. 3.3. A sum over i, j, l and p respectively is suppressed in the formulas.

$$\begin{aligned} \frac{d\Delta^{00}}{dl} &= -2 \sum_k \left(\lambda_k^{00} \lambda_k^{00} + \lambda_k^{ij} \lambda_k^{ij} + \lambda_k^{0j} \lambda_k^{0j} + \lambda_k^{i0} \lambda_k^{i0} \right. \\ &\quad \left. + \kappa_k^{00} \kappa_k^{00} + \kappa_k^{ij} \kappa_k^{ij} + \kappa_k^{0j} \kappa_k^{0j} + \kappa_k^{i0} \kappa_k^{i0} \right) \omega_k \\ \frac{d\Delta^{0n}}{dl} &= 2 \sum_k \left(-2\lambda_k^{i0} \lambda_k^{in} - 2\lambda_k^{00} \lambda_k^{0n} - 2\kappa_k^{i0} \kappa_k^{in} - 2\kappa_k^{00} \kappa_k^{0n} \right. \\ &\quad \left. + [\kappa_k^{0i} \lambda_k^{0l} + \kappa_k^{ji} \lambda_k^{jl} - \lambda_k^{0i} \kappa_k^{0l} - \lambda_k^{ji} \kappa_k^{jl}] \epsilon_{iln} (2n_k + 1) \right) \omega_k \\ \frac{d\Delta^{n0}}{dl} &= 2 \sum_k \left(-2\lambda_k^{0i} \lambda_k^{ni} - 2\lambda_k^{00} \lambda_k^{n0} - 2\kappa_k^{0i} \kappa_k^{ni} - 2\kappa_k^{00} \kappa_k^{n0} \right. \\ &\quad \left. + [\kappa_k^{i0} \lambda_k^{l0} + \kappa_k^{ij} \lambda_k^{lj} - \lambda_k^{i0} \kappa_k^{l0} - \lambda_k^{ij} \kappa_k^{lj}] \epsilon_{iln} (2n_k + 1) \right) \omega_k \\ \frac{d\Delta^{nm}}{dl} &= 2 \sum_k \left(-2\lambda_k^{00} \lambda_k^{nm} - 2\lambda_k^{0m} \lambda_k^{n0} - 2\kappa_k^{00} \kappa_k^{nm} - 2\kappa_k^{0m} \kappa_k^{n0} \right. \\ &\quad + (\lambda_k^{ij} \lambda_k^{pl} + \kappa_k^{ij} \kappa_k^{pl}) \epsilon_{ipn} \epsilon_{jlm} \\ &\quad + [(\kappa_k^{i0} \lambda_k^{lm} + \kappa_k^{im} \lambda_k^{l0} - \lambda_k^{i0} \kappa_k^{lm} - \lambda_k^{im} \kappa_k^{l0}) \epsilon_{iln} \\ &\quad \left. + (\kappa_k^{0i} \lambda_k^{nl} + \kappa_k^{ni} \lambda_k^{0l} - \lambda_k^{0i} \kappa_k^{nl} - \lambda_k^{ni} \kappa_k^{0l}) \epsilon_{ilm} \right] (2n_k + 1) \omega_k \end{aligned}$$

(A.25)

$$\begin{aligned}
\frac{d\lambda_k^{00}}{dl} &= -\omega_k^2 \lambda_k^{00} + 2 \sum_q \eta_{kq} \lambda_q^{00} \\
\frac{d\lambda_k^{0n}}{dl} &= -\omega_k^2 \lambda_k^{0n} + 2(\kappa_k^{0i} \Delta^{0l} + \kappa_k^{ji} \Delta^{jl}) \epsilon_{iln} \omega_k + 2 \sum_q \eta_{kq} \lambda_q^{0n} \\
\frac{d\lambda_k^{n0}}{dl} &= -\omega_k^2 \lambda_k^{n0} + 2(\kappa_k^{i0} \Delta^{l0} + \kappa_k^{ij} \Delta^{lj}) \epsilon_{iln} \omega_k + 2 \sum_q \eta_{kq} \lambda_q^{n0} \\
\frac{d\lambda_k^{nm}}{dl} &= -\omega_k^2 \lambda_k^{nm} + 2 \left((\kappa_k^{0i} \Delta^{nl} + \kappa_k^{ni} \Delta^{0l}) \epsilon_{ilm} + (\kappa_k^{i0} \Delta^{lm} + \kappa_k^{im} \Delta^{l0}) \epsilon_{iln} \right) \omega_k \\
&\quad + 2 \sum_q \eta_{kq} \lambda_q^{nm} \\
\frac{d\kappa_k^{00}}{dl} &= -\omega_k^2 \kappa_k^{00} - 2 \sum_q \eta_{qk} \kappa_q^{00} \\
\frac{d\kappa_k^{0n}}{dl} &= -\omega_k^2 \kappa_k^{0n} - 2(\lambda_k^{0i} \Delta^{0l} + \lambda_k^{ji} \Delta^{jl}) \epsilon_{iln} \omega_k - 2 \sum_q \eta_{qk} \kappa_q^{0n} \\
\frac{d\kappa_k^{n0}}{dl} &= -\omega_k^2 \kappa_k^{n0} - 2(\lambda_k^{i0} \Delta^{l0} + \lambda_k^{ij} \Delta^{lj}) \epsilon_{iln} \omega_k - 2 \sum_q \eta_{qk} \kappa_q^{n0} \\
\frac{d\kappa_k^{nm}}{dl} &= -\omega_k^2 \kappa_k^{nm} - 2 \left((\lambda_k^{0i} \Delta^{nl} + \lambda_k^{ni} \Delta^{0l}) \epsilon_{ilm} + (\lambda_k^{i0} \Delta^{lm} + \lambda_k^{im} \Delta^{l0}) \epsilon_{iln} \right) \omega_k \\
&\quad - 2 \sum_q \eta_{qk} \kappa_q^{nm}
\end{aligned} \tag{A.26}$$

A.5 The generator coefficients

Below we list the coefficients η_{kq} obtained in Sec. 3.3.

$$\begin{aligned}
\eta_{kq} = & \frac{1}{\omega_q^2 - \omega_k^2} \left\{ 2\omega_k \left[(\lambda_k^{0i} \kappa_q^{nl} \epsilon_{ilm} \langle \Sigma_{nm} \rangle + \lambda_k^{i0} \kappa_q^{lm} \epsilon_{iln} \langle \Sigma_{nm} \rangle \right. \right. \\
& + \lambda_k^{nj} \kappa_q^{0l} \epsilon_{jlm} \langle \Sigma_{nm} \rangle + \lambda_k^{im} \kappa_q^{l0} \epsilon_{iln} \langle \Sigma_{nm} \rangle \\
& + \lambda_k^{0i} \kappa_q^{0l} \epsilon_{iln} \langle \Sigma_{0n} \rangle + \lambda_k^{i0} \kappa_q^{l0} \epsilon_{iln} \langle \Sigma_{n0} \rangle \\
& + \lambda_k^{ji} \kappa_q^{jl} \epsilon_{iln} \langle \Sigma_{0n} \rangle + \lambda_k^{ij} \kappa_q^{lj} \epsilon_{iln} \langle \Sigma_{n0} \rangle) \omega_k \\
& + (\lambda_q^{0i} \kappa_k^{nl} \epsilon_{ilm} \langle \Sigma_{nm} \rangle + \lambda_q^{i0} \kappa_k^{lm} \epsilon_{iln} \langle \Sigma_{nm} \rangle \\
& + \lambda_q^{nj} \kappa_k^{0l} \epsilon_{jlm} \langle \Sigma_{nm} \rangle + \lambda_q^{im} \kappa_k^{l0} \epsilon_{iln} \langle \Sigma_{nm} \rangle \\
& + \lambda_q^{0i} \kappa_k^{0l} \epsilon_{iln} \langle \Sigma_{0n} \rangle + \lambda_q^{i0} \kappa_k^{l0} \epsilon_{iln} \langle \Sigma_{n0} \rangle \\
& + \lambda_q^{ji} \kappa_k^{jl} \epsilon_{iln} \langle \Sigma_{0n} \rangle + \lambda_q^{ij} \kappa_k^{lj} \epsilon_{iln} \langle \Sigma_{n0} \rangle) \omega_q \left. \right] \\
& - 2\omega_q \left[(\kappa_k^{0i} \lambda_q^{nl} \epsilon_{ilm} \langle \Sigma_{nm} \rangle + \kappa_k^{i0} \lambda_q^{lm} \epsilon_{iln} \langle \Sigma_{nm} \rangle \right. \\
& + \kappa_k^{nj} \lambda_q^{0l} \epsilon_{jlm} \langle \Sigma_{nm} \rangle + \kappa_k^{im} \lambda_q^{l0} \epsilon_{iln} \langle \Sigma_{nm} \rangle \\
& + \kappa_k^{0i} \lambda_q^{0l} \epsilon_{iln} \langle \Sigma_{0n} \rangle + \kappa_k^{i0} \lambda_q^{l0} \epsilon_{iln} \langle \Sigma_{n0} \rangle \\
& + \kappa_k^{ji} \lambda_q^{jl} \epsilon_{iln} \langle \Sigma_{0n} \rangle + \kappa_k^{ij} \lambda_q^{lj} \epsilon_{iln} \langle \Sigma_{n0} \rangle) \omega_k \\
& + (\kappa_q^{0i} \lambda_k^{nl} \epsilon_{ilm} \langle \Sigma_{nm} \rangle + \kappa_q^{i0} \lambda_k^{lm} \epsilon_{iln} \langle \Sigma_{nm} \rangle \\
& + \kappa_q^{nj} \lambda_k^{0l} \epsilon_{jlm} \langle \Sigma_{nm} \rangle + \kappa_q^{im} \lambda_k^{l0} \epsilon_{iln} \langle \Sigma_{nm} \rangle \\
& + \kappa_q^{0i} \lambda_k^{0l} \epsilon_{iln} \langle \Sigma_{0n} \rangle + \kappa_q^{i0} \lambda_k^{l0} \epsilon_{iln} \langle \Sigma_{n0} \rangle \\
& + \kappa_q^{ji} \lambda_k^{jl} \epsilon_{iln} \langle \Sigma_{0n} \rangle + \kappa_q^{ij} \lambda_k^{lj} \epsilon_{iln} \langle \Sigma_{n0} \rangle) \omega_q \left. \right\} \tag{A.27}
\end{aligned}$$

The expectation values of $\Sigma_{\alpha\beta}$ are defined by

$$\langle \Sigma_{\alpha\beta} \rangle = \frac{\text{tr}\{\Sigma_{\alpha\beta} \exp(-\beta H_S)\}}{\text{tr}\{\exp(-\beta H_S)\}}, \tag{A.28}$$

where H_S is the Hamiltonian of the two-spin system.

A.6 The flow equations for the observables

The flow equations for the observables from Sec. 3.3 are

$$\begin{aligned}
\frac{dh^{00}}{dl} &= -2 \sum_k \left(\lambda_k^{0i} \mu_k^{0i} + \lambda_k^{i0} \mu_k^{i0} + \lambda_k^{00} \mu_k^{00} + \lambda_k^{ij} \mu_k^{ij} \right. \\
&\quad \left. + \kappa_k^{0i} \nu_k^{0i} + \kappa_k^{i0} \nu_k^{i0} + \kappa_k^{00} \nu_k^{00} + \kappa_k^{ij} \nu_k^{ij} \right) \omega_k \\
\frac{dh^{0n}}{dl} &= 2 \sum_k \left(-\lambda_k^{i0} \mu_k^{in} - \lambda_k^{00} \mu_k^{0n} - \lambda_k^{in} \mu_k^{i0} - \lambda_k^{0n} \mu_k^{00} \right. \\
&\quad - \kappa_k^{i0} \nu_k^{in} - \kappa_k^{00} \nu_k^{0n} - \kappa_k^{in} \nu_k^{i0} - \kappa_k^{0n} \nu_k^{00} \\
&\quad \left. + [\kappa_k^{0i} \mu_k^{0l} + \kappa_k^{ji} \mu_k^{jl} - \lambda_k^{0i} \nu_k^{0l} - \lambda_k^{ji} \nu_k^{jl}] \epsilon_{iln} (2n_k + 1) \right) \omega_k \\
\frac{dh^{n0}}{dl} &= 2 \sum_k \left(-\lambda_k^{0i} \mu_k^{ni} - \lambda_k^{00} \mu_k^{n0} - \lambda_k^{ni} \mu_k^{0i} - \lambda_k^{n0} \mu_k^{00} \right. \\
&\quad - \kappa_k^{0i} \nu_k^{ni} - \kappa_k^{00} \nu_k^{n0} - \kappa_k^{ni} \nu_k^{0i} - \kappa_k^{n0} \nu_k^{00} \\
&\quad \left. + [\kappa_k^{i0} \mu_k^{l0} + \kappa_k^{ij} \mu_k^{lj} - \lambda_k^{i0} \nu_k^{l0} - \lambda_k^{ij} \nu_k^{lj}] \epsilon_{ilm} (2n_k + 1) \right) \omega_k \\
\frac{dh^{nm}}{dl} &= 2 \sum_k \left(-\lambda_k^{00} \mu_k^{nm} - \lambda_k^{0m} \mu_k^{n0} - \lambda_k^{n0} \mu_k^{0m} - \lambda_k^{nm} \mu_k^{00} \right. \\
&\quad - \kappa_k^{00} \nu_k^{nm} - \kappa_k^{0m} \nu_k^{n0} - \kappa_k^{n0} \nu_k^{0m} - \kappa_k^{nm} \nu_k^{00} \\
&\quad + (\lambda_k^{ij} \mu_k^{pl} + \kappa_k^{ij} \nu_k^{pl}) \epsilon_{ipn} \epsilon_{jlm} \\
&\quad + [(\kappa_k^{i0} \mu_k^{lm} + \kappa_k^{im} \mu_k^{l0} - \lambda_k^{i0} \nu_k^{lm} - \lambda_k^{im} \nu_k^{l0}) \epsilon_{ilm} \\
&\quad \left. + (\kappa_k^{0i} \mu_k^{nl} + \kappa_k^{ni} \mu_k^{0l} - \lambda_k^{0i} \nu_k^{nl} - \lambda_k^{ni} \nu_k^{0l}) \epsilon_{ilm} \right] (2n_k + 1) \omega_k \\
\frac{d\mu_k^{00}}{dl} &= 2 \sum_q \eta_{kq} \mu_q^{00} \\
\frac{d\mu_k^{0n}}{dl} &= 2(\kappa_k^{0i} h^{0l} + \kappa_k^{ji} h^{jl}) \epsilon_{ilm} \omega_k + 2 \sum_q \eta_{kq} \mu_q^{0n} \\
\frac{d\mu_k^{n0}}{dl} &= 2(\kappa_k^{i0} h^{l0} + \kappa_k^{ij} h^{lj}) \epsilon_{ilm} \omega_k + 2 \sum_q \eta_{kq} \mu_q^{n0} \\
\frac{d\mu_k^{nm}}{dl} &= 2 \left((\kappa_k^{0i} h^{nl} + \kappa_k^{ni} h^{0l}) \epsilon_{ilm} + (\kappa_k^{i0} h^{lm} + \kappa_k^{im} h^{l0}) \epsilon_{ilm} \right) \omega_k + 2 \sum_q \eta_{kq} \mu_q^{nm}
\end{aligned}$$

$$\begin{aligned}
\frac{d\nu_k^{00}}{dl} &= -2 \sum_q \eta_{qk} \nu_q^{00} \\
\frac{d\nu_k^{0n}}{dl} &= -2(\lambda_k^{0i} h^{0l} + \lambda_k^{ji} h^{jl}) \epsilon_{iln} \omega_k - 2 \sum_q \eta_{qk} \nu_q^{0n} \\
\frac{d\nu_k^{n0}}{dl} &= -2(\lambda_k^{i0} h^{l0} + \lambda_k^{ij} h^{lj}) \epsilon_{iln} \omega_k - 2 \sum_q \eta_{qk} \nu_q^{n0} \\
\frac{d\nu_k^{nm}}{dl} &= -2 \left((\lambda_k^{0i} h^{nl} + \lambda_k^{ni} h^{0l}) \epsilon_{ilm} + (\lambda_k^{i0} h^{lm} + \lambda_k^{im} h^{l0}) \epsilon_{iln} \right) \omega_k - 2 \sum_q \eta_{qk} \nu_q^{nm}.
\end{aligned} \tag{A.29}$$

A.7 Formulas for the Pauli matrix tensor products

To derive the flow equations in Sec. 3.3, the following formulas are useful, since one often has to calculate commutators of the Σ_{ij} operators

$$[\Sigma_{ij}, \Sigma_{kl}] = 2i\epsilon_{ikn}\delta_{jl}\Sigma_{n0} + 2i\epsilon_{jln}\delta_{ik}\Sigma_{0n}. \tag{A.30}$$

For the commutator of a superposition of the same operators, we find

$$\begin{aligned}
x_{\alpha\beta} y_{\gamma\delta} [\Sigma_{\alpha\beta}, \Sigma_{\gamma\delta}] &= 2ix_0 y_{nl} \epsilon_{jlm} \Sigma_{nm} + 2ix_{i0} y_{lm} \epsilon_{iln} \Sigma_{nm} \\
&+ 2ix_{nj} y_{0l} \epsilon_{jlm} \Sigma_{nm} + 2ix_{im} y_{l0} \epsilon_{iln} \Sigma_{nm} \\
&+ 2ix_0 y_{0l} \epsilon_{jln} \Sigma_{0n} + 2ix_{i0} y_{l0} \epsilon_{iln} \Sigma_{n0} \\
&+ 2ix_{ij} y_{il} \epsilon_{jln} \Sigma_{0n} + 2ix_{ij} y_{lj} \epsilon_{iln} \Sigma_{n0},
\end{aligned} \tag{A.31}$$

where the $x_{\alpha\beta}$ and $y_{\gamma\delta}$ are arbitrary complex numbers. For the anti-commutator we obtain

$$[\Sigma_{ij}, \Sigma_{kl}]_+ = -2\epsilon_{ikn}\epsilon_{jlm}\Sigma_{nm} + 2\delta_{ik}\delta_{jl} \tag{A.32}$$

and for the anti-commutator of a superposition we find

$$\begin{aligned}
x_{\alpha\beta} y_{\gamma\delta} [\Sigma_{\alpha\beta}, \Sigma_{\gamma\delta}]_+ &= 2x_0 y_{nj} \Sigma_{n0} + 2x_{i0} y_{in} \Sigma_{0n} + 2x_{00} y_{nm} \Sigma_{nm} \\
&+ 2x_{nj} y_{0j} \Sigma_{n0} + 2x_{in} y_{i0} \Sigma_{0n} + 2x_{0m} y_{n0} \Sigma_{nm} \\
&+ 2x_{00} y_{n0} \Sigma_{n0} + 2x_{00} y_{0n} \Sigma_{0n} + 2x_{n0} y_{0m} \Sigma_{nm} \\
&+ 2x_{n0} y_{00} \Sigma_{n0} + 2x_{0n} y_{00} \Sigma_{0n} + 2x_{nm} y_{00} \Sigma_{nm} \\
&+ 2x_0 y_{0j} \Sigma_{00} + 2x_{i0} y_{i0} \Sigma_{00} + 2x_{00} y_{00} \Sigma_{00} \\
&+ 2x_{ij} y_{ij} \Sigma_{00} - 2x_{ij} y_{kl} \epsilon_{ikn} \epsilon_{jlm} \Sigma_{nm}.
\end{aligned} \tag{A.33}$$

A.8 Flow equations for the biased case

Below we note the result for the biased system $\epsilon_S \neq 0$, see Sec. 3.4.

$$\begin{aligned}
\frac{d\Delta^{00}}{dl} &= -2 \sum_k \left(\lambda_k^{11} \lambda_k^{11} + \lambda_k^{31} \lambda_k^{31} + \lambda_k^{03} \lambda_k^{03} + \kappa_k^{21} \kappa_k^{21} + \kappa_k^{02} \kappa_k^{02} \right) \omega_k \\
\frac{d\Delta^{01}}{dl} &= 4 \sum_k \kappa_k^{02} \lambda_k^{03} \omega_k \\
\frac{d\Delta^{10}}{dl} &= 4 \sum_k \kappa_k^{21} \lambda_k^{31} \omega_k \\
\frac{d\Delta^{13}}{dl} &= -4 \sum_k \kappa_k^{02} \lambda_k^{11} \omega_k \\
\frac{d\Delta^{30}}{dl} &= -4 \sum_k \kappa_k^{21} \lambda_k^{11} \omega_k \\
\frac{d\Delta^{22}}{dl} &= -4 \sum_k \kappa_k^{21} \lambda_k^{03} \omega_k \\
\frac{d\Delta^{33}}{dl} &= -4 \sum_k \kappa_k^{02} \lambda_k^{31} \omega_k \\
\frac{d\lambda_k^{03}}{dl} &= -\omega_k^2 \lambda_k^{03} - 2\kappa_k^{02} \Delta^{01} \omega_k + 2\kappa_k^{21} \Delta^{22} \omega_k + 2 \sum_q \eta_{kq} \lambda_q^{03} \\
\frac{d\lambda_k^{11}}{dl} &= -\omega_k^2 \lambda_k^{11} + 2\kappa_k^{02} \Delta^{13} \omega_k + 2\kappa_k^{21} \Delta^{30} \omega_k + 2 \sum_q \eta_{kq} \lambda_q^{11} \\
\frac{d\lambda_k^{31}}{dl} &= -\omega_k^2 \lambda_k^{31} + 2\kappa_k^{02} \Delta^{33} \omega_k - 2\kappa_k^{21} \Delta^{10} \omega_k + 2 \sum_q \eta_{kq} \lambda_q^{31} \\
\frac{d\kappa_k^{02}}{dl} &= -\omega_k^2 \kappa_k^{02} - 2\lambda_k^{03} \Delta^{01} \omega_k + 2\lambda_k^{31} \Delta^{33} \omega_k + 2\lambda_k^{11} \Delta^{13} \omega_k - 2 \sum_q \eta_{qk} \kappa_q^{02} \\
\frac{d\kappa_k^{21}}{dl} &= -\omega_k^2 \kappa_k^{21} + 2\lambda_k^{03} \Delta^{22} \omega_k - 2\lambda_k^{31} \Delta^{10} \omega_k + 2\lambda_k^{11} \Delta^{30} \omega_k - 2 \sum_q \eta_{qk} \kappa_q^{21}
\end{aligned} \tag{A.34}$$

The flow equations for the observables are

$$\begin{aligned}
\frac{dh^{00}}{dl} &= -2 \sum_k \left(\lambda_k^{03} \mu_k^{03} + \lambda_k^{11} \mu_k^{11} + \lambda_k^{31} \mu_k^{31} + \kappa_k^{02} \nu_k^{02} + \kappa_k^{21} \nu_k^{21} \right) \omega_k \\
\frac{dh^{01}}{dl} &= 2 \sum_k \left(\kappa_k^{02} \mu_k^{03} + \lambda_k^{03} \nu_k^{02} \right) \omega_k \\
\frac{dh^{10}}{dl} &= 2 \sum_k \left(\kappa_k^{21} \mu_k^{31} + \lambda_k^{31} \nu_k^{21} \right) \omega_k \\
\frac{dh^{13}}{dl} &= -2 \sum_k \left(\kappa_k^{02} \mu_k^{11} + \lambda_k^{11} \nu_k^{02} \right) \omega_k \\
\frac{dh^{30}}{dl} &= -2 \sum_k \left(\kappa_k^{21} \mu_k^{11} + \lambda_k^{11} \nu_k^{21} \right) \omega_k \\
\frac{dh^{22}}{dl} &= -2 \sum_k \left(\kappa_k^{21} \mu_k^{03} + \lambda_k^{03} \nu_k^{21} \right) \omega_k \\
\frac{dh^{33}}{dl} &= -2 \sum_k \left(\kappa_k^{02} \mu_k^{31} + \lambda_k^{31} \nu_k^{02} \right) \omega_k \\
\frac{d\mu_k^{03}}{dl} &= -2\kappa_k^{02} h^{01} \omega_k + 2\kappa_k^{21} h^{22} \omega_k + 2 \sum_q \eta_{kq} \mu_q^{03} \\
\frac{d\mu_k^{11}}{dl} &= 2\kappa_k^{02} h^{13} \omega_k + 2\kappa_k^{21} h^{30} \omega_k + 2 \sum_q \eta_{kq} \mu_q^{11} \\
\frac{d\mu_k^{31}}{dl} &= 2\kappa_k^{02} h^{33} \omega_k - 2\kappa_k^{21} h^{10} \omega_k + 2 \sum_q \eta_{kq} \mu_q^{31} \\
\frac{d\nu_k^{02}}{dl} &= -2\lambda_k^{03} h^{01} \omega_k + 2\lambda_k^{31} h^{33} \omega_k + 2\lambda_k^{11} h^{13} \omega_k - 2 \sum_q \eta_{qk} \nu_q^{02} \\
\frac{d\nu_k^{21}}{dl} &= 2\lambda_k^{03} h^{22} \omega_k - 2\lambda_k^{31} h^{10} \omega_k + 2\lambda_k^{11} h^{30} \omega_k - 2 \sum_q \eta_{qk} \nu_q^{21}.
\end{aligned} \tag{A.35}$$

The η_{kq} coefficients are

$$\begin{aligned}
\eta_{kq} = & \frac{1}{\omega_q^2 - \omega_k^2} \left\{ 2\omega_k \left[(\lambda_k^{03} \kappa_q^{21} \langle \Sigma_{22} \rangle + \lambda_k^{31} \kappa_q^{02} \langle \Sigma_{33} \rangle + \lambda_k^{11} \kappa_q^{02} \langle \Sigma_{13} \rangle - \lambda_k^{03} \kappa_q^{02} \langle \Sigma_{01} \rangle \right. \right. \\
& + \lambda_k^{11} \kappa_q^{21} \langle \Sigma_{30} \rangle - \lambda_k^{31} \kappa_q^{21} \langle \Sigma_{10} \rangle) \omega_k + (\lambda_q^{03} \kappa_k^{21} \langle \Sigma_{22} \rangle + \lambda_q^{11} \kappa_k^{02} \langle \Sigma_{13} \rangle \\
& + \lambda_q^{31} \kappa_k^{02} \langle \Sigma_{33} \rangle - \lambda_q^{03} \kappa_k^{02} \langle \Sigma_{01} \rangle + \lambda_q^{11} \kappa_k^{21} \langle \Sigma_{30} \rangle - \lambda_q^{31} \kappa_k^{21} \langle \Sigma_{10} \rangle) \omega_q \left. \right] \\
& - 2\omega_q \left[(-\kappa_k^{02} \lambda_q^{31} \langle \Sigma_{33} \rangle - \kappa_k^{02} \lambda_q^{11} \langle \Sigma_{13} \rangle - \kappa_k^{21} \lambda_q^{03} \langle \Sigma_{22} \rangle + \kappa_k^{02} \lambda_q^{03} \langle \Sigma_{01} \rangle \right. \\
& - \kappa_k^{21} \lambda_q^{11} \langle \Sigma_{30} \rangle + \kappa_k^{21} \lambda_q^{31} \langle \Sigma_{10} \rangle) \omega_k + (-\kappa_q^{02} \lambda_k^{11} \langle \Sigma_{13} \rangle - \kappa_q^{02} \lambda_k^{31} \langle \Sigma_{33} \rangle \\
& \left. - \kappa_q^{21} \lambda_k^{03} \langle \Sigma_{22} \rangle + \kappa_q^{02} \lambda_k^{03} \langle \Sigma_{01} \rangle - \kappa_q^{21} \lambda_k^{11} \langle \Sigma_{30} \rangle + \kappa_q^{21} \lambda_k^{31} \langle \Sigma_{10} \rangle) \omega_q \right] \left. \right\}. \tag{A.36}
\end{aligned}$$

The non-vanishing expectation values are found to be

$$\begin{aligned}
\langle \Sigma_{00} \rangle &= 1 \\
\langle \Sigma_{31} \rangle &= \frac{\Delta \epsilon_S}{w_1} \\
\langle \Sigma_{13} \rangle &= -\frac{J \Delta_S \epsilon_S}{w_1 w_2} \\
\langle \Sigma_{33} \rangle &= -J \frac{\epsilon_S^2 + w_1}{w_1 w_2} \\
\langle \Sigma_{22} \rangle &= \frac{3J \Delta \Delta_S + \epsilon_S (J^2 + \Delta^2 + J \epsilon_S) + (J + \epsilon_S) w_1 + (-\Delta \Delta_S + J \epsilon_S) w_2 + w_1 w_2}{4w_1 w_2} \\
\langle \Sigma_{11} \rangle &= \frac{\Delta \Delta_S}{w_1} \\
\langle \Sigma_{10} \rangle &= -\Delta_S \frac{\Delta^2 + w_1}{w_1 w_2} \\
\langle \Sigma_{01} \rangle &= -\Delta \frac{\Delta_S^2 + \epsilon_S^2 + w_1}{w_1 w_2} \\
\langle \Sigma_{03} \rangle &= \frac{J \epsilon_S}{w_1} \\
\langle \Sigma_{30} \rangle &= -\epsilon_S \frac{J^2 + \Delta^2 + w_1}{w_1 w_2}, \tag{A.37}
\end{aligned}$$

where

$$w_1 \equiv \sqrt{\Delta^2 \Delta_S^2 + (J^2 + \Delta^2) \epsilon_S^2} \tag{A.38}$$

$$w_2 \equiv \sqrt{J^2 + \Delta^2 + \Delta_S^2 + \epsilon_S^2 + 2w_1}. \tag{A.39}$$

A.9 The master-equation solution for the nonlinear bath

In Secs. 3.4,3.5 a master-equation solution was compared with the flow-equation results. Here, we present its derivation. The special case of small-enough α corresponding to a peaked, structured, bath spectral density, can be treated using a Markoffian master equation to calculate the influence of the linear bath F on the system $S + B$. This does not restrict the choice of the system-bath coupling J . It leads to the following equation with respect to the eigenbasis of $H_s|n\rangle = E_n|n\rangle$, see, e.g., [Blum96]

$$\frac{d}{dt}\rho_{m'm}(t) = \sum_{n'n} [-i(E_{m'} - E_m)\delta_{mn}\delta_{m'n'} + R_{m'mn'n}] \rho_{n'n}(t), \quad (\text{A.40})$$

where

$$R_{m'mn'n} = - \sum_k \delta_{mn} \Gamma_{m'kkn'}^+ + \Gamma_{nmm'n'}^+ + \Gamma_{nmm'n'}^- - \sum_k \delta_{n'm'} \Gamma_{nkkm}^-. \quad (\text{A.41})$$

We assume here that $R_{m'mn'n} = 0$ if $E_{m'} - E_m - E_{n'} + E_n \neq 0$, which constitutes the secular approximation, i.e., the coarse-grained time evolution occurs over longer time scales than the system time evolution. Furthermore,

$$\Gamma_{mkl n}^+ = Q_{mk} Q_{ln} N(E_l - E_n) \quad (\text{A.42})$$

$$\Gamma_{mkl n}^- = Q_{mk} Q_{ln} L(E_m - E_k), \quad (\text{A.43})$$

where $\hat{Q} \equiv \hat{\sigma}_z^B$, $Q_{mk} = \langle m | \hat{Q} | k \rangle$ and

$$L(x) = \int_0^\infty ds \exp(-ixs) \langle \hat{X} \hat{X}(s) \rangle \quad (\text{A.44})$$

$$N(x) \equiv L(-x)^*. \quad (\text{A.45})$$

For the Ohmic bath spectral density with a sharp cutoff, we find

$$L(x) = \alpha x \Theta(x) \Theta(1 - x/\omega_C) + \frac{i}{\pi} \alpha [\omega_C + x \log(\omega_C - x) - x \log(|x|)]. \quad (\text{A.46})$$

The time evolution of the density matrix for a certain initial condition $\rho(0)$ can be found by integrating

$$\frac{d}{dt}\rho(t) = e^{Ct}\rho(t). \quad (\text{A.47})$$

C is, as in Chapter 2, again a 16×16 matrix. The correlation function is obtained using linear response theory and the Kubo formula [Enz92]

$$\delta \langle \hat{A}(t) \rangle = \text{tr} \left\{ \delta \hat{\rho}(t) \hat{A} \right\}, \quad (\text{A.48})$$

with the initial condition $\delta\hat{\rho}(0) = -i[\hat{V}, \hat{\rho}_{eq}]\Delta t$, where $\hat{\rho}_{eq} = e^{-\beta\hat{H}_S}/\text{tr}\{e^{-\beta\hat{H}_S}\}$,

$$\delta\langle\hat{A}(t)\rangle = -i\text{tr}\left\{\hat{\rho}_{eq}[\hat{A}(t), \hat{V}]\right\}\Delta t = -i\langle[\hat{A}(t), \hat{V}]\rangle_{eq}\Delta t. \quad (\text{A.49})$$

In our application, we have $\hat{A} \equiv \hat{\sigma}_z^S$ and $\hat{V} \equiv \hat{\sigma}_z^S$. The Fourier transform of the equilibrium correlator $K_{zz}^S(\omega)$ can be calculated using the fluctuation-dissipation theorem [Schwabl97, Rickayzen80] at $T = 0$

$$K_{zz}^S(\omega) = \frac{1}{1 - e^{-\omega/T}} \frac{1}{2\pi} \int_{-\infty}^{+\infty} e^{+i\omega t} \langle[\hat{\sigma}_z^S(t), \hat{\sigma}_z^S]\rangle, \quad (\text{A.50})$$

where

$$\lim_{T \rightarrow 0} \frac{1}{1 - e^{-\omega/T}} = \Theta(\omega). \quad (\text{A.51})$$

At $T = 0$ the equilibrium correlator $K_{zz}^S(\omega)$ vanishes on the negative ω -axis. Using that $\langle[\hat{\sigma}_z^S(t), \hat{\sigma}_z^S]\rangle$ is an anti-symmetric function we find

$$K_{zz}^S(\omega) = \Theta(\omega) \frac{i}{\pi} \int_0^{\infty} dt \sin(\omega t) \langle[\hat{\sigma}_z^S(t), \hat{\sigma}_z^S]\rangle_{eq} = \Theta(\omega) \frac{i}{\pi} \int_0^{\infty} dt \sin(\omega t) \frac{\text{tr}\{\delta\hat{\rho}(t)\hat{\sigma}_z^S\}}{-i\Delta t}. \quad (\text{A.52})$$

The time integral can be evaluated using the diagonalized matrix C in the time evolution of the density matrix

$$\begin{aligned} \int_0^{\infty} dt \sin(\omega t) \delta\rho(t) &= \int_0^{\infty} dt \sin(\omega t) e^{Ct} \delta\rho(0) \\ &= \int_0^{\infty} dt \sin(\omega t) b e^{\text{diag}(\lambda_i)t} b^{-1} \delta\rho(0) = b e^{\text{diag}(\omega/(\lambda_i^2 + \omega^2))t} b^{-1} \delta\rho(0) \end{aligned} \quad (\text{A.53})$$

provided $\text{Re } \lambda_i < 0$. b is the transformation which diagonalizes the matrix C given with respect to the eigenbasis of H_S . Therefore, the initial condition $\delta\hat{\rho}(0)$ must be evaluated in the same basis. The result for the vector $b e^{\text{diag}(\omega/(\lambda_i^2 + \omega^2))t} b^{-1} \delta\rho(0)$ with 16 entries is rewritten as a 4×4 matrix M and used in the formula for the equilibrium correlator Eq. (A.52)

$$K_{zz}^S(\omega) = \Theta(\omega) \frac{i}{\pi} \text{tr}\{M[\sigma_z^S, \rho_{eq}]\}, \quad (\text{A.54})$$

which can be evaluated numerically.

The same master equation can also be used to calculate an approximation for the bath correlation function. The result can be obtained using the same calculation as above. We note only the results for the unbiased case.

$$\langle BB \rangle_{\omega} = \frac{J^2}{\pi} \Theta(\omega) \left[\frac{-a}{(\omega + b)^2 + a^2} + \frac{a}{(\omega - b)^2 + a^2} \right], \quad (\text{A.55})$$

where

$$a \equiv -\text{Re}\{N(-2\Delta) + L(-2\Delta)\} = -2\Delta\alpha \quad (\text{A.56})$$

and

$$\begin{aligned} b &\equiv -2\Delta - \text{Im} \{N(-2\Delta) + L(-2\Delta)\} \\ &= \frac{2\Delta\alpha}{\pi} [\log(\omega_C + 2\Delta) + \log(\omega_C - 2\Delta) - 2\log(2|\Delta|)] . \end{aligned} \quad (\text{A.57})$$

A.10 The weak-coupling solution of the nonlinear bath

We use the weak-coupling approximation to solve the model of the nonlinear bath and compare it with the flow-equation results in Secs. 3.4, 3.5. We use the weak-coupling approximation [Gardiner00] between system $S + B$ together and system F . This approximation does not affect the coupling between S and B . The advantage of the weak-coupling approximation is that the discussion can be extended to finite temperatures. The only restriction is that the coupling strength α to the linear bath must be small enough to keep the approximation valid. The regime of such small coupling strengths corresponds to a nonlinear bath with peaked structure, i.e., we expect the $\langle BB \rangle_\omega$ to have sharp peaks around the frequency 2Δ .

First, we recall the weak-coupling equation also used in Chapter 2

$$\begin{aligned} \dot{\hat{\rho}}(t) &= -i[\mathcal{H}_{SB}, \hat{\rho}(t)] - \int_0^t d\tau [\hat{\sigma}_z^B, e^{-i\mathcal{H}_{SB}\tau} \hat{\sigma}_z^B \hat{\rho}(t-\tau) e^{i\mathcal{H}_{SB}\tau}] \langle \hat{X}(\tau) \hat{X}(0) \rangle \\ &\quad + \int_0^t d\tau [\hat{\sigma}_z^B, e^{-i\mathcal{H}_{SB}\tau} \hat{\rho}(t-\tau) \hat{\sigma}_z^B e^{i\mathcal{H}_{SB}\tau}] \langle \hat{X}(0) \hat{X}(\tau) \rangle . \end{aligned} \quad (\text{A.58})$$

To obtain the correlation function $\langle BB \rangle_\omega$, we replace \mathcal{H}_{SB} by \mathcal{H}_B . If we look at the weak-coupling equation for infinite temperature, which means we set $\langle \hat{X}(t) \hat{X}(0) \rangle = \gamma\delta(t)$, we find again the exact master equation used in Chapter 2 for ‘‘Approach 1’’. Thus, the weak-coupling approximation becomes exact in this limit.

The Laplace transforms of the Ohmic linear bath correlation function with sharp cutoff is found to be

$$K'(s) = \frac{\alpha}{2\pi} s \log \left(1 - \frac{\omega_C^2}{s^2} \right) \quad (\text{A.59})$$

$$K''(s) = -\frac{\alpha}{\pi} \left[\omega_C - s \arctan \left(\frac{\omega_C}{s} \right) \right] , \quad (\text{A.60})$$

where the Laplace transform [Doetsch67, Leuthold94] is defined by

$$\mathcal{L}f(t) \equiv F(s) \equiv \int_0^\infty dt e^{-st} f(t) . \quad (\text{A.61})$$

The weak-coupling equation is most conveniently solved in the eigenbasis of \hat{H}_{SB} and it contains convolutions, which become products in Laplace space.

$$A(s)R(s) = \rho(0) , \quad (\text{A.62})$$

where $A(s)$ is a 16×16 matrix and $R(s)$ is a vector with 16 entries containing the Laplace transforms of the 16 elements of the density matrix. What is left to obtain the Laplace transform of the density matrix is the inversion of the matrix $A(s)$. Knowing the time evolution of the density matrix is enough to find the equilibrium correlator in the weak-coupling limit. This is done as follows.

$$\langle \hat{\sigma}_z^S(t + \tau) \hat{\sigma}_z^S(t) \rangle = \text{tr}_{SB} \{ \text{tr}_F \{ \hat{\sigma}_z^S(t + \tau) \hat{\sigma}_z^S(t) \hat{\rho}_{SB} \otimes \hat{\rho}_F \} \}, \quad (\text{A.63})$$

where $\hat{\rho}_{SB}$ is the two-spin density matrix $S + B$ and $\hat{\rho}_F$ is the oscillator bath density matrix of system F . $\hat{\sigma}_z^S(t)$ is a Heisenberg-picture system operator. We can rewrite the correlation function as

$$\langle \hat{\sigma}_z^S(t + \tau) \hat{\sigma}_z^S(t) \rangle = \text{tr}_{SB} \{ \hat{\sigma}_z^S \text{tr}_F \{ e^{-i\mathcal{H}\tau} \hat{\sigma}_z^S \hat{\rho}_{\text{tot}}(t) e^{i\mathcal{H}\tau} \} \}. \quad (\text{A.64})$$

For this purpose, we define

$$\mathcal{Z}(t + \tau, t) \equiv \text{tr}_F \{ e^{-i\mathcal{H}\tau} \hat{\sigma}_z^S \hat{\rho}_{\text{tot}}(t) e^{i\mathcal{H}\tau} \}, \quad (\text{A.65})$$

which when traced, gives the correlator

$$\langle \hat{\sigma}_z^S(t + \tau) \hat{\sigma}_z^S(t) \rangle = \text{tr}_{SB} \hat{\sigma}_z^S \mathcal{Z}(t + \tau, t). \quad (\text{A.66})$$

$\mathcal{Z}(t + \tau, t)$ satisfies the same weak-coupling equation (Eq. (A.58)) with respect to τ , starting from the initial condition

$$\mathcal{Z}(t, t) = \hat{\sigma}_z^S \hat{\rho}_{SB}(t). \quad (\text{A.67})$$

The whole procedure is exemplified by showing the derivation of the $\langle BB \rangle_\omega$ -correlation function at zero temperature. We consider system B and F alone. The weak-coupling equation for the density matrix of system B is found to be

$$\begin{aligned} \dot{\rho}_{11}(t) &= i\Delta\rho_{12}(t) - i\Delta\rho_{21}(t) \\ \dot{\rho}_{12}(t) &= i\Delta\rho_{11}(t) - i\Delta\rho_{22}(t) - 4 \int_0^t d\tau f(\tau) \rho_{12}(t - \tau) + 4 \int_0^t d\tau g(\tau) \rho_{21}(t - \tau) \\ &\quad + 2 \int_0^t d\tau h(\tau) (\rho_{11}(t - \tau) + \rho_{22}(t - \tau)) \\ \dot{\rho}_{21}(t) &= -i\Delta\rho_{11}(t) + i\Delta\rho_{22}(t) + 4 \int_0^t d\tau g(\tau) \rho_{12}(t - \tau) - 4 \int_0^t d\tau f(\tau) \rho_{21}(t - \tau) \\ &\quad + 2 \int_0^t d\tau h(\tau) (\rho_{11}(t - \tau) + \rho_{22}(t - \tau)) \\ \dot{\rho}_{22}(t) &= -i\Delta\rho_{12}(t) + i\Delta\rho_{21}(t), \end{aligned} \quad (\text{A.68})$$

where we have defined

$$\begin{aligned} f(\tau) &\equiv K'(\tau) \cos(\Delta\tau)^2 \\ g(\tau) &\equiv K'(\tau) \sin(\Delta\tau)^2 \\ h(\tau) &\equiv K''(\tau) \sin(2\Delta\tau). \end{aligned} \quad (\text{A.69})$$

We find

$$A(s)R(s) = \rho(0), \quad (\text{A.70})$$

where now $A(s)$ is the 4×4 matrix

$$A(s) \equiv \begin{pmatrix} s & -i\Delta & i\Delta & 0 \\ -i\Delta - 2H(s) & s + 4F(s) & -4G(s) & i\Delta - 2H(s) \\ i\Delta - 2H(s) & -4G(s) & s + 4F(s) & -i\Delta - 2H(s) \\ 0 & i\Delta & -i\Delta & s \end{pmatrix} \quad (\text{A.71})$$

and $R(s)$ is the vector containing the Laplace transforms of the density matrix

$$R(s) \equiv \begin{pmatrix} R_{11}(s) \\ R_{12}(s) \\ R_{21}(s) \\ R_{22}(s) \end{pmatrix}. \quad (\text{A.72})$$

The matrix $A(s)$ can be inverted and we find the Laplace transform of the solution for the density matrix for weak-coupling

$$R(s) = A^{-1}(s)\rho(0). \quad (\text{A.73})$$

The inverse matrix $B \equiv A^{-1}(s)$ is given by

$$\begin{aligned} B_{11}(s) &= \frac{s(4K'(s) + s) + 2\Delta^2}{s(s(4K'(s) + s) + 4\Delta^2)} \\ B_{12}(s) &= \frac{i\Delta}{s(4K'(s) + s) + 4\Delta^2} \\ B_{13}(s) &= -\frac{i\Delta}{s(4K'(s) + s) + 4\Delta^2} \\ B_{14}(s) &= \frac{2\Delta^2}{s(s(4K'(s) + s) + 4\Delta^2)} \\ B_{21}(s) &= \frac{2H(s)}{s(4M(s) + s)} + \frac{i\Delta}{s(4K'(s) + s) + 4\Delta^2} \\ B_{22}(s) &= \frac{1}{2} \left(\frac{1}{4M(s) + s} + \frac{s}{s(4K'(s) + s) + 4\Delta^2} \right) \\ B_{23}(s) &= \frac{2(2G(s)s + \Delta^2)}{(4M(s) + s)(s(4K'(s) + s) + 4\Delta^2)} \\ B_{24}(s) &= \frac{2H(s)}{s(4M(s) + s)} - \frac{i\Delta}{s(4K'(s) + s) + 4\Delta^2} \end{aligned}$$

$$\begin{aligned}
B_{31}(s) &= \frac{2H(s)}{s(4M(s) + s)} - \frac{i\Delta}{s(4K'(s) + s) + 4\Delta^2} \\
B_{32}(s) &= \frac{2(2G(s)s + \Delta^2)}{(4M(s) + s)(s(4K'(s) + s) + 4\Delta^2)} \\
B_{33}(s) &= \frac{1}{2} \left(\frac{1}{4M(s) + s} + \frac{s}{s(4K'(s) + s) + 4\Delta^2} \right) \\
B_{34}(s) &= \frac{2H(s)}{s(4M(s) + s)} + \frac{i\Delta}{s(4K'(s) + s) + 4\Delta^2} \\
B_{41}(s) &= \frac{2\Delta^2}{s(s(4K'(s) + s) + 4\Delta^2)} \\
B_{42}(s) &= -\frac{i\Delta}{s(4K'(s) + s) + 4\Delta^2} \\
B_{43}(s) &= \frac{i\Delta}{s(4K'(s) + s) + 4\Delta^2} \\
B_{44}(s) &= \frac{s(4K'(s) + s) + 2\Delta^2}{s(s(4K'(s) + s) + 4\Delta^2)},
\end{aligned} \tag{A.74}$$

where we have used that

$$\begin{aligned}
K'(s) &= F(s) + G(s) \\
M(s) &\equiv F(s) - G(s) = \mathcal{L}\{K'(t) \cos(2\Delta t)\} = \\
&= \frac{\alpha}{4\pi} \left[4\Delta \arctan\left(\frac{\omega_C - 2\Delta}{s}\right) + 8\Delta \arctan\left(\frac{2\Delta}{s}\right) - 4\Delta \arctan\left(\frac{\omega_C + 2\Delta}{s}\right) \right. \\
&\quad + s \log\left(\frac{\omega_C^2 + s^2 - 4\omega_C\Delta + 4\Delta^2}{s^2}\right) + s \log\left(\frac{\omega_C^2 + s^2 + 4\omega_C\Delta + 4\Delta^2}{s^2}\right) \\
&\quad \left. - s \log\left(1 + \frac{4\Delta^2}{s^2}\right) \right] \\
G(s) &= \mathcal{L}\{K'(t) \sin(\Delta t)^2\} = \frac{1}{2}K'(s) - \frac{1}{2}M(s) \\
H(s) &= \mathcal{L}\{K''(t) \sin(2\Delta t)\} = \\
&= -\frac{\alpha}{4\pi} \left[4\Delta \arctan\left(\frac{\omega_C - 2\Delta}{s}\right) + 4\Delta \arctan\left(\frac{\omega_C - 2\Delta}{s}\right) \right. \\
&\quad \left. + s \log\left(\frac{s^2 + (\omega_C - 2\Delta)^2}{s^2}\right) - s \log\left(\frac{s^2 + (\omega_C + 2\Delta)^2}{s^2}\right) \right].
\end{aligned} \tag{A.75}$$

We need the equilibrium density matrix in order to calculate the two-time correlation function of the $\hat{\sigma}_z^B$ -operator. Knowing the Laplace transform the equilibrium density matrix can be found easily using the following theorem

$$\lim_{t \rightarrow \infty} u(t) = \lim_{s \rightarrow 0} sU(s). \tag{A.76}$$

We can start from any initial condition and will end in the equilibrium state after an

infinitely long time. Therefore, for any initial condition we find

$$\hat{\rho}_B^{eq} = \frac{1}{2} \begin{pmatrix} 1 & -1 \\ -1 & 1 \end{pmatrix}, \quad (\text{A.77})$$

which is equal to $\hat{\rho}_B^{eq} = e^{-\beta\Delta\hat{\sigma}_z^B}/Z$. The result is reasonable because in the weak-coupling limit the density matrix always remains a tensor product and there is no other physically reasonable state to relax to at a given temperature.

We obtain first the following correlation function

$$S_z(t) = \frac{1}{2} \langle \{\hat{\sigma}_z(t), \hat{\sigma}_z\} \rangle - \langle \hat{\sigma}_z \rangle_{eq}^2, \quad (\text{A.78})$$

which is a symmetric function in time and further, for our system we have $\langle \hat{\sigma}_z \rangle_{eq} = 0$. The Fourier transform $\tilde{S}_z(\omega)$ is also a symmetric function in ω and is connected to the bath correlation function for $\omega > 0$ as follows

$$\langle BB \rangle_\omega = 2J^2\Theta(\omega)\tilde{S}_z(\omega). \quad (\text{A.79})$$

The formula contains a factor of J^2 due to the definition of $\langle BB \rangle_\omega$. $\langle BB \rangle_\omega$ vanishes on the negative axis $\omega < 0$, which can be seen from the fluctuation-dissipation theorem

$$\frac{1}{2\pi} \int_{-\infty}^{\infty} d\omega e^{i\omega t} \langle [B(t), B(0)] \rangle = (1 - e^{-\beta\omega}) \langle BB \rangle_\omega. \quad (\text{A.80})$$

From the the time evolution of the density matrix we can deduce the Laplace transform

$$S_z(s) = \frac{4K'(s) + s}{s(4K'(s) + s) + 4\Delta^2} \quad (\text{A.81})$$

and the Fourier transform

$$\tilde{S}_z(\omega) = \frac{1}{\pi} \text{Re} \{ S_z(s)|_{s=-i\omega+0^+} \} \quad (\text{A.82})$$

$$\tilde{S}_z(\omega) = \frac{1}{\pi} \frac{16\Delta^2 R(\omega)}{[4\Delta^2 - \omega^2 + 4\omega I(\omega)]^2 + [4\omega R(\omega)]^2}, \quad (\text{A.83})$$

where

$$R(\omega) \equiv \text{Re} K'(s = -i\omega + 0^+) = \frac{\alpha}{2} \omega \Theta(1 - \omega/\omega_C) \quad (\text{A.84})$$

$$I(\omega) \equiv \text{Im} K'(s = -i\omega + 0^+) = -\frac{\alpha}{2\pi} \omega \log(|1 - \omega_C^2/\omega^2|). \quad (\text{A.85})$$

The high temperature limit Eq. (2.85) is obtained by setting $K'(s) = \gamma/2$ and $K''(s) = 0$. In this limit, the bath correlation function is given by $\langle BB \rangle_\omega = \tilde{S}_z(\omega)$.

In the next step the Shiba relation is checked. This relation is an exact general result, valid at zero temperature, and is given by

$$\lim_{\omega \rightarrow 0} \frac{\tilde{S}_z(\omega)}{|\omega|} = \frac{2}{\pi} \alpha (\pi \bar{\chi}_z)^2 \quad (\text{A.86})$$

for an Ohmic bath-spectral density. In order to check the validity of the relation in the Born limit, we calculate

$$\chi_z(t) = i\Theta(t) \langle [\hat{\sigma}_z(t), \hat{\sigma}_z] \rangle \quad (\text{A.87})$$

or its Fourier transform $\tilde{\chi}_z(\omega)$ in order to obtain the static susceptibility

$$\bar{\chi}_z = \tilde{\chi}_z(\omega = 0). \quad (\text{A.88})$$

The Fourier transform

$$\tilde{\chi}_z(\omega) = \frac{1}{2\pi} \chi_z(s) \Big|_{s=-i\omega+0^+} \quad (\text{A.89})$$

is again calculated via the Laplace transform, given by

$$\chi_z(s) = \frac{4\Delta}{s(4K'(s) + s) + 4\Delta^2}. \quad (\text{A.90})$$

For the left side of the Shiba relation, we find

$$\lim_{\omega \rightarrow 0} \frac{\tilde{S}_z(\omega)}{|\omega|} = \frac{\alpha}{2\pi} \frac{1}{\Delta^2}. \quad (\text{A.91})$$

and for the static susceptibility, we obtain

$$\bar{\chi}_z = \frac{1}{2\pi} \frac{1}{\Delta}. \quad (\text{A.92})$$

Therefore, the Shiba relation is fulfilled in the Born limit for weak coupling α .

A.11 Path-integral formulas

In this appendix we will fill in some of the details left out of Section 4.6. It is convenient to define $\gamma \equiv \alpha/2$ as the friction constant. The classical solutions to Eqs. (4.50,4.51) are given by

$$\begin{aligned} r_d(\tau) = & \frac{1}{\sin(\omega_R(t-t_0))} \left\{ r_i \sin(\omega_R(t-\tau)) e^{\gamma(\tau-t_0)} \right. \\ & \left. + [r_f - r_p(t)] \sin(\omega_R(\tau-t_0)) e^{\gamma(\tau-t)} \right\} + r_p(\tau), \end{aligned} \quad (\text{A.93})$$

$$\begin{aligned} R_{cl}(\tau) = & \frac{1}{\sin(\omega_R(t-t_0))} \left\{ R_i \sin(\omega_R(t-\tau)) e^{-\gamma(\tau-t_0)} \right. \\ & \left. + [R_f - R_p(t)] \sin(\omega_R(\tau-t_0)) e^{-\gamma(\tau-t)} \right\} + R_p(\tau), \end{aligned} \quad (\text{A.94})$$

where

$$r_p(\tau) = \int_{t_0}^{\tau} d\tau' G_r(\tau - \tau') F_r(\tau'), \quad (\text{A.95})$$

$$R_p(\tau) = \int_{t_0}^{\tau} d\tau' G_R(\tau - \tau') F_R(\tau'), \quad (\text{A.96})$$

and the Green's functions are defined by

$$G_R(\tau) = \Theta(\tau) e^{-\gamma\tau} \frac{\sin(\omega_R \tau)}{\omega_R}, \quad (\text{A.97})$$

$$G_r(\tau) = \Theta(\tau) e^{\gamma\tau} \frac{\sin(\omega_R \tau)}{\omega_R}. \quad (\text{A.98})$$

The influence functional for $s' = s$ is found to be

$$\begin{aligned} J_{ss}(R_f, r_f, t; R_i, r_i, t_0) = & \quad (\text{A.99}) \\ & \frac{|N(t)|}{2\pi} \exp \left(i[K_f(t)R_f r_f + K_i(t)R_i r_i - L(t)R_i r_f - N(t)R_f r_i \right. \\ & \left. + a_i(t)r_i + a_f(t)r_f] - A(t)r_f^2 - B(t)r_f r_i - C(t)r_i^2 \right), \end{aligned}$$

where the functions appearing in the influence functional are all real and defined by

$$K_f(t) = \omega_R \cot(\omega_R(t - t_0)) - \gamma, \quad (\text{A.100})$$

$$K_i(t) = \omega_R \cot(\omega_R(t - t_0)) + \gamma, \quad (\text{A.101})$$

$$L(t) = \frac{\omega_R e^{-\gamma(t-t_0)}}{\sin(\omega_R(t - t_0))}, \quad (\text{A.102})$$

$$N(t) = \frac{\omega_R e^{\gamma(t-t_0)}}{\sin(\omega_R(t - t_0))}, \quad (\text{A.103})$$

$$\begin{aligned} A(t) = & \frac{1}{2} \frac{e^{-2\gamma t}}{\sin^2(\omega_R(t - t_0))} \\ & \times \int_{t_0}^t d\tau \int_{t_0}^t d\tau' \sin(\omega_R(\tau - t_0)) K_R(\tau - \tau') \sin(\omega_R(\tau' - t_0)) e^{\gamma(\tau + \tau')}, \end{aligned} \quad (\text{A.104})$$

$$\begin{aligned} B(t) = & \frac{e^{-\gamma(t+t_0)}}{\sin^2(\omega_R(t - t_0))} \\ & \times \int_{t_0}^t d\tau \int_{t_0}^t d\tau' \sin(\omega_R(t - \tau)) K_R(\tau - \tau') \sin(\omega_R(\tau' - t_0)) e^{\gamma(\tau + \tau')}, \end{aligned} \quad (\text{A.105})$$

$$C(t) = \frac{1}{2} \frac{e^{-2\gamma t_0}}{\sin^2(\omega_R(t-t_0))} \quad (\text{A.106})$$

$$\times \int_{t_0}^t d\tau \int_{t_0}^{\tau} d\tau' \sin(\omega_R(t-\tau)) K_R(\tau-\tau') \sin(\omega_R(t-\tau')) e^{\gamma(\tau+\tau')},$$

$$a_f(t) = \dot{x}(t) - K_f(t)x(t), \quad (\text{A.107})$$

$$a_i(t) = N(t)x(t), \quad (\text{A.108})$$

$$x(\tau) = \eta s \int_{t_0}^{\tau} d\tau' G_R(\tau-\tau') f(\tau'), \quad (\text{A.109})$$

$$\dot{x}(\tau) = \eta s \int_{t_0}^{\tau} d\tau' \partial_{\tau} G_R(\tau-\tau') f(\tau'). \quad (\text{A.110})$$

In all of these expressions, the dependence on t_0 has been suppressed.

Let us now discuss the solution for the density matrix. At time $t = t_0$ we start in a product state of the cantilever and bath. The cantilever density matrix is assumed to be a Gaussian wave packet with width σ at $t = t_0$,

$$\rho_{ss'}^{(C)}(z, z', t_0) = \frac{1}{\sqrt{2\pi}\sigma} \exp\left(-\frac{1}{4\sigma^2}(z^2 + z'^2)\right). \quad (\text{A.111})$$

One could start from a more general initial state, but we will later take the limit $t_0 \rightarrow -\infty$, such that all the information regarding the initial state is lost completely at time $t = 0$. The experiment starts at time $t = 0$ by switching-on the magnetic field. At this time the cantilever has interacted with the bath for a very long time and is in equilibrium with the bath, i.e., it is no longer in a product state.

The general solution for the diagonal elements of $\rho_{ss'}^{(C)}$, starting from this initial condition, is

$$\begin{aligned} \rho_{ss}^{(C)}(R_f, r_f, t) = & \frac{|N(t)|}{\sqrt{2\pi}} \frac{2\sigma}{\sqrt{D(t)}} \exp \left\{ \left[r_f^2 \left(-A(t) + [2B^2(t) - 8A(t)C(t) \right. \right. \right. \\ & \left. \left. - \frac{L^2(t)}{2} \right] \sigma^2 - 4 \left(A(t)K_i^2(t) + L(t)[B(t)K_i(t) + C(t)L(t)] \right) \sigma^4 \right) \\ & + ir_f \left(a_f(t) - 4[a_i(t)B(t) - 2a_f(t)C(t)] \sigma^2 + 4K_i(t)[a_f(t)K_i(t) + a_i(t)L(t)] \sigma^4 \right) \\ & + iR_f r_f \left(K_f(t) + 4[2C(t)K_f(t) + B(t)N(t)] \sigma^2 \right. \\ & \left. + 4K_i(t)[K_f(t)K_i(t) - L(t)N(t)] \sigma^4 \right) - 2[a_i(t) - N(t)R_f]^2 \sigma^2 \Big/ D(t) \Big\}, \quad (\text{A.112}) \end{aligned}$$

where

$$D(t) = 1 + 8C(t)\sigma^2 + K_i^2(t)\sigma^4. \quad (\text{A.113})$$

In the limit $t_0 \rightarrow -\infty$ we obtain the final result presented in Eq. (4.56).

The influence functional for $s' = -s$ is found to be given by

$$\begin{aligned}
J_{s,-s}(R_f, r_f, t; R_i, r_i, t_0) = & \quad (A.114) \\
& \frac{|N(t)|}{2\pi} \exp \left(i[K_f(t)R_f r_f + K_i(t)R_i r_i - L(t)R_i r_f - N(t)R_f r_i \right. \\
& \left. + A_f(t)R_f + A_i(t)R_i + \int_{t_0}^t d\tau \epsilon(\tau) \right] \\
& \times \exp \left(-A(t)r_f^2 - B(t)r_f r_i - C(t)r_i^2 + b_i(t)r_i + b_f(t)r_f + b(t) \right),
\end{aligned}$$

where

$$A_f(t) = \dot{y}(t) - K_i(t)y(t), \quad (A.115)$$

$$A_i(t) = L(t)y(t), \quad (A.116)$$

$$b_f(t) = 2A(t)y(t) - \int_{t_0}^t d\tau \int_{t_0}^t d\tau' y(\tau') K_R(\tau - \tau') \frac{\sin(\omega_R(\tau - t_0)) e^{-\gamma(t-\tau)}}{\sin(\omega_R(t - t_0))}, \quad (A.117)$$

$$b_i(t) = B(t)y(t) - \int_{t_0}^t d\tau \int_{t_0}^t d\tau' y(\tau') K_R(\tau - \tau') \frac{\sin(\omega_R(t - \tau)) e^{\gamma(\tau-t_0)}}{\sin(\omega_R(t - t_0))}, \quad (A.118)$$

$$\begin{aligned}
b(t) = -A(t)y^2(t) & + y(t) \int_{t_0}^t d\tau \int_{t_0}^t d\tau' y(\tau') K_R(\tau - \tau') \frac{\sin(\omega_R(\tau - t_0)) e^{-\gamma(t-\tau)}}{\sin(\omega_R(t - t_0))} \\
& - \frac{1}{2} \int_{t_0}^t d\tau \int_{t_0}^t d\tau' y(\tau) K_R(\tau - \tau') y(\tau'), \quad (A.119)
\end{aligned}$$

$$y(\tau) = 2\eta s \int_{t_0}^{\tau} d\tau' G_r(\tau - \tau') f(\tau'), \quad (A.120)$$

$$\dot{y}(\tau) = 2\eta s \int_{t_0}^{\tau} d\tau' \partial_{\tau} G_r(\tau - \tau') f(\tau'). \quad (A.121)$$

This leads to the following general expression for the off-diagonal elements of $\rho_{ss'}^{(C)}$:

$$\begin{aligned}
\rho_{s,-s}^{(C)}(R_f, r_f, t) = & \frac{|N(t)|}{\sqrt{2\pi}} \frac{2\sigma}{\sqrt{D(t)}} \exp \left\{ \left[r_f^2 \left(-A(t) + [2B^2(t) - 8A(t)C(t)] \right. \right. \right. \\
& \left. \left. - \frac{L^2(t)}{2} \right] \sigma^2 - 4 \left(A(t)K_i^2(t) + L(t)[B(t)K_i(t) + C(t)L(t)] \right) \sigma^4 \right) \\
& + r_f \left(b_f(t) + [-4B(t)b_i(t) + 8b_f(t)C(t) + A_i(t)L(t)] \sigma^2 \right. \\
& \left. + 4[A_i(t)B(t)K_i(t) + b_f(t)K_i^2(t) + 2A_i(t)C(t)L(t) + b_i(t)K_i(t)L(t)] \sigma^4 \right) \\
& + iR_f r_f \left(K_f(t) + 4[2C(t)K_f(t) + B(t)N(t)] \sigma^2 \right. \\
& \left. + 4K_i(t)[K_f(t)K_i(t) - L(t)N(t)] \sigma^4 \right) \\
& + iR_f \left(A_f(t) + 8A_f(t)C(t)\sigma^2 + 4K_i(t)[A_f(t)K_i(t) + A_i(t)N(t)] \sigma^4 \right) \\
& \left. + 2[b_i(t) - iN(t)R_f]^2 \sigma^2 - \frac{A_i^2(t)}{2} \sigma^2 - 4A_i(t)[A_i(t)C(t) + b_i(t)K_i(t)] \sigma^4 \right] / D(t) \\
& + i \int_{t_0}^t d\tau \epsilon(\tau) + b(t) \left. \right\}. \tag{A.122}
\end{aligned}$$

The reduced dynamics of the spin alone are found by tracing out the cantilever coordinates. The result is

$$\begin{aligned}
\rho_{s,-s}^{(S)}(t) = & \rho_{s,-s}^{(S)}(0) \exp \left(-A_f^2(t) \frac{C(t)}{N^2(t)} + \frac{A_f(t)b_i(t)}{N(t)} + b(t) - \frac{A_f^2(t)}{8\sigma^2 N^2(t)} \right. \\
& \left. - \frac{\sigma^2}{2N^2(t)} [A_f(t)K_i(t) + A_i(t)N(t)]^2 + i \int_{t_0}^t d\tau \epsilon(\tau) \right). \tag{A.123}
\end{aligned}$$

In the limit $t_0 \rightarrow -\infty$, one finds

$$\rho_{s,-s}^{(S)}(t) = \rho_{s,-s}^{(S)}(0) \exp \left(-\Gamma(t) + i \int_{t_0}^t d\tau \epsilon(\tau) \right). \tag{A.124}$$

and the decay rate $\Gamma(t)$, see Eq. (4.40), can be obtained after a straightforward but tedious calculation. In the same limit, we obtain the result for the density matrix presented in Eq. (4.65). In this limit the dependence on the initial conditions is lost.

A.12 Relaxation of a non-thermal initial state

If we want to study the dependence on the initial conditions, we have to set $t_0 = 0$.

There are three contributions: One proportional to σ^2 , another proportional to $1/\sigma^2$, and one independent of σ (σ is the width of the wave packet at $t = 0$).

The $1/\sigma^2$ -term is found to be

$$\begin{aligned}
& -\frac{A_f^2(t)}{8\sigma^2 N^2(t)} \\
& = \frac{e^{-2\gamma t}}{\sigma^2} \left\{ -\frac{\sin(\omega_R t)^2}{8\omega_R^2} \dot{y}^2(t) \right. \\
& + \left[\frac{\sin(\omega_R t) \cos(\omega_R t)}{4\omega_R} + \frac{\gamma \sin(\omega_R t)^2}{4\omega_R^2} \right] \dot{y}(t) y(t) \\
& \left. + \left[-\frac{\cos(\omega_R t)^2}{8} - \frac{\gamma \sin(\omega_R t) \cos(\omega_R t)}{4\omega_R} - \frac{\gamma^2 \sin(\omega_R t)^2}{8\omega_R^2} \right] y^2(t) \right\}
\end{aligned} \tag{A.125}$$

and the σ^2 -term is

$$\begin{aligned}
& -\frac{\sigma^2}{2N^2(t)} [A_f(t)K_i(t) + A_i(t)N(t)]^2 = \frac{\sigma^2 e^{-2\gamma t}}{\omega_R^2} \left\{ -\frac{1}{2} [\omega_R \cos(\omega_R t) + \gamma \sin(\omega_R t)]^2 \dot{y}^2(t) \right. \\
& + [\omega_R \cos(\omega_R t) + \gamma \sin(\omega_R t)] [2\omega_R \gamma \cos(\omega_R t) + (\gamma^2 - \omega_R^2) \sin(\omega_R t)] \dot{y}(t) y(t) \\
& \left. - \frac{1}{2} [2\omega_R \gamma \cos(\omega_R t) + (\gamma^2 - \omega_R^2) \sin(\omega_R t)]^2 y^2(t) \right\}.
\end{aligned} \tag{A.126}$$

The σ -independent term is

$$\begin{aligned}
& -A_f^2(t) \frac{C(t)}{N^2(t)} + \frac{A_f(t)b_i(t)}{N(t)} + b(t) = -\Gamma(t) \\
& + (2\eta)^2 \left[\frac{\gamma}{\omega_R} F_s(t) \int_0^\infty d\omega J_{\text{eff}}(\omega) \coth\left(\frac{\omega}{2T}\right) \int_0^t dt' f(t') \cos(\omega t') \right. \\
& + F_c(t) \int_0^\infty d\omega J_{\text{eff}}(\omega) \coth\left(\frac{\omega}{2T}\right) \int_0^t dt' f(t') \cos(\omega t') \\
& - \frac{1}{2} \sigma_R^2 F_c^2(t) - \frac{\gamma}{\omega_R} \sigma_R^2 F_s(t) F_c(t) \\
& - \frac{1}{2} \frac{\gamma^2}{\omega_R^2} \sigma_R^2 F_s^2(t) - \frac{1}{2\omega_R^2 \sigma_r^2} F_s^2(t) \\
& \left. + \frac{1}{\omega_R} F_s(t) \int_0^\infty d\omega J_{\text{eff}}(\omega) \coth\left(\frac{\omega}{2T}\right) \int_0^t dt' f(t') \sin(\omega t') \right],
\end{aligned} \tag{A.127}$$

where

$$F_s(t) = \int_0^t dt' \sin(\omega_R t') e^{-\gamma t'} f(t') \tag{A.128}$$

and

$$F_c(t) = \int_0^t dt' \cos(\omega_R t') e^{-\gamma t'} f(t'). \tag{A.129}$$

Bibliography

- [Abramowitz72] M. Abramowitz and I. A. Stegun, *Handbook of Mathematical Functions with Formulas, Graphs, and Mathematical Tables* (John Wiley & Sons, New York, 1972).
- [Ankerhold00] J. Ankerhold and P. Pechukas, *Europhys. Lett.* **52**, 264 (2000).
- [Ashcroft76] N. W. Ashcroft and N. D. Mermin, *Solid State Physics* (Holt Rinehart and Winston, New York, 1976).
- [Avron87] J. E. Avron, R. Seiler, and L. G. Yaffe, *Commun. Math. Phys.* **110**, 33 (1987).
- [Berman03a] G. P. Berman, F. Borgonovi, G. Chapline, S. A. Gurvitz, P. C. Hammel, D. V. Pelekhov, A. Suter, and V. I. Tsifrinovich, *J. Appl. Phys.* **36**, 4417 (2003).
- [Berman03b] G. P. Berman, F. Borgonovi, H. S. Gaon, S. A. Gurvitz, and V. I. Tsifrinovich, *Phys. Rev. B* **67**, 094425 (2003).
- [Blum96] K. Blum, *Density Matrix Theory and Applications* (Plenum Press, New York, 1996).
- [Bocko96] M. F. Bocko and R. Onofrio, *Rev. Mod. Phys.* **68**, 755 (1996).
- [Breuer02] H.-P. Breuer and F. Petruccione, *The Theory of Open Quantum Systems* (Oxford University Press, New York, 2002).
- [Caldeira81] A. O. Caldeira and A. J. Leggett, *Phys. Rev. Lett.* **46**, 211 (1981).
- [Caldeira83a] A. O. Caldeira and A. J. Leggett, *Ann. Phys.* **149**, 374 (1983).
- [Caldeira83b] A. O. Caldeira and A. J. Leggett, *Physica A* **121**, 587 (1983).
- [Caldeira83c] A. O. Caldeira and A. J. Leggett, *Ann. Phys. (N.Y.)* **140**, 374 (1983).
- [Caldeira85] A. O. Caldeira and A. J. Leggett, *Phys. Rev. A* **31**, 1059 (1985).
- [Caldeira93] A. O. Caldeira, A. H. Castro Neto, and T. Oliveira de Carvalho, *Phys. Rev. B* **48**, 18 (1993).

- [Choi00] M.-S. Choi, R. Fazio, J. Siewert, and C. Bruder, *Europhys. Lett.* **53**, 251 (2001).
- [Chiorescu03] I. Chiorescu, Y. Nakamura, J. P. M. Harmans, J. E. Mooij, *Science* **299**, 1869 (2003).
- [Coish04] W. A. Coish and D. Loss, cond-mat/0405676
- [Cottet02] A. Cottet, D. Vion, A. Aassime, P. Joyez, D. Esteve, and M. H. Devoret, *Physica C* **367** 197 (2002).
- [Cottet03] A. Cottet, PhD thesis, Université Paris VI, (2002); www-drecam.cea.fr/drecam/spec/Pres/Quantro/
- [Diosi93] L. Diósi, *Physica A* **199**, 517 (1993).
- [DiVincenzo04] D. P. DiVincenzo and D. Loss, cond-mat/0405525.
- [Doetsch67] G. Doetsch, *Anleitung zum Praktischen Gebrauch der Laplace-Transformation und der z-Transformation* (Oldenbourg, München, 1967).
- [Dube01] M. Dube and P.C.E. Stamp, *Chem. Phys.* **268**, 257 (2001).
- [Enz92] C. P. Enz, *A Course on Many-Body Theory Applied to Solid-State Physics* (World Scientific, Singapore, 1992).
- [Fazio99] R. Fazio, G.M. Palma, and J. Siewert, *Phys. Rev. Lett.* **83**, 538 (1999).
- [Feynman63] R.P. Feynman and F.L. Vernon, *Ann. Phys.* **24**, 118 (1963).
- [Fick83] E. Fick and G. Sauermaun, *Quantenstatistik dynamischer Prozesse* (Verlag Harri Deutsch, Thun, Frankfurt/ M., 1983).
- [Gardiner00] C. W. Gardiner and P. Zoller, *Quantum Noise* (Springer-Verlag, Berlin, 2000).
- [Garg85] A. Garg, J. N. Onuchic, and V. Ambegaokar, *J. Chem. Phys.* **83**, 3391 (1985).
- [Gassmann02] H. Gassmann, F. Marquardt, and C. Bruder, *Phys. Rev. E* **66**, 041111 (2002).
- [Gassmann04] H. Gassmann, M.-S. Choi, H. Yi, and C. Bruder, *Phys. Rev. B* **69**, 115419 (2004).
- [Governale01] M. Governale, M. Grifoni, and G. Schön, *Chem. Phys.* **268**, 273 (2001).

- [Grabert88] H. Grabert, P. Schramm, and G.-L. Ingold, Phys. Rep. **168**, 115 (1988).
- [Grifoni98] M. Grifoni and P. Hänggi, Phys. Rep. **304**, 229 (1998).
- [Grifoni99] M. Grifoni, E. Paladino, and U. Weiss, Eur. Phys. J. B **10**, 719 (1999).
- [Huang03] X. M. H. Huang, C. A. Zorman, M. Mehregany, and M. L. Roukes, Nature (London) **421**, 496 (2003).
- [Kampen92] N. P. van Kampen, *Stochastic Processes in Physics and Chemistry* (North-Holland, New York, 1992).
- [Kehrein96a] S. K. Kehrein and A. Mielke, Phys. Lett. A **219**, 313 (1996).
- [Kehrein96b] S. K. Kehrein and A. Mielke, Ann. Physik (Leipzig) **6**, 90 (1997).
- [Kehrein96c] S. K. Kehrein and A. Mielke, J. of Stat. Phys. **90**, 889 (1998).
- [Khaetskii02] A. V. Khaetskii, D. Loss, and L. Glazman, Phys. Rev. Lett. **88**, 186802 (2002).
- [Kleff03a] S. Kleff, S. Kehrein, and J. von Delft, Physica E **18**, 343 (2003).
- [Kleff03b] S. Kleff, S. Kehrein, and J. von Delft, cond-mat/0304177.
- [Knobel03] R. G. Knobel and A. N. Cleland, Nature (London) **424**, 291 (2003).
- [Leggett87] A. J. Leggett, S. Chakravarty, A. T. Dorsey, M. P. A. Fisher, A. Garg, and W. Zwerger, Rev. Mod. Phys. **59**, 1 (1987).
- [Lesovik02] G. B. Lesovik, A. V. Lebedev, and A. O. Imambekov, JETP Lett. **75**, 474 (2002).
- [Leuthold94] P. Leuthold, *Signale und Systeme IV* (Amiv Verlag, Zürich, 1994).
- [Lindblad76] G. Lindblad, Commun. Math. Phys. **48**, 119 (1976).
- [Loss98] D. Loss and D. P. DiVincenzo, Phys. Rev. A **57**, 120 (1998).
- [Loss03] D. Loss and D. P. DiVincenzo, cond-mat/0304118.
- [Makhlin01] Y. Makhlin, G. Schön, and A. Shnirman, Rev. Mod. Phys. **73**, 357 (2001).
- [Makhlin03a] Y. Makhlin and A. Shnirman, Phys. Rev. Lett. **92**, 178301 (2004).
- [Makhlin03b] Y. Makhlin and A. Shnirman, JETP Lett. **78**, 497 (2003).

- [Mamin01] H. J. Mamin and D. Rugar, *Appl. Phys. Lett.* **79**, 3358 (2001).
- [Marquardt01a] F. Marquardt and C. Bruder, *Phys. Rev. B* **63**, 054514 (2001).
- [Marquardt02] F. Marquardt, cond-mat/0207692.
- [Marquardt03] F. Marquardt, *Models of dephasing at low temperatures* (Shaker Verlag, Aachen, 2003).
- [Messiah61] A. Messiah, *Quantum Mechanics, Vol II* (North-Holland Publishing Co., Amsterdam, 1961).
- [Mielke98] A. Mielke, *Eur. Phys. J. B* **5**, 605 (1998).
- [Mozyrsky03] D. Mozyrsky, I. Martin, D. Pelekhov, and P. C. Hammel, *Appl. Phys. Lett.* **82**, 1278 (2003).
- [Nakamura99] Y. Nakamura, Yu. A. Pashkin, and J. S. Tsai, *Nature* **398**, 786 (1999).
- [Neu96] S. K. Kehrein, A. Mielke, and P. Neu, *Z. Phys. B* **99**, 269 (1996).
- [Nielsen00] M. A. Nielsen and I. L. Chuang, *Quantum Computation and Quantum Communication* (Cambridge University Press, Cambridge, 2000).
- [Numerical Recipes] W. H. Press et al., *Numerical Recipes in C* (Cambridge University Press, 1992)
- [Paladino02] E. Paladino, L. Faoro, G. Falci, and R. Fazio, *Phys. Rev. Lett.* **88**, 228304 (2002).
- [Rickayzen80] G. Rickayzen, *Green's Functions and Condensed Matter* (Academic Press, London, 1980).
- [Risken89] H. Risken, *The Fokker-Planck Equation* (Springer, Heidelberg, 1989).
- [Schwabl97] F. Schwabl, *Quantenmechanik für Fortgeschrittene* (Springer, Berlin, 1997).
- [Shnirman02] A. Shnirman, Y. Makhlin, and G. Schön, *Physica Scripta* **T102**, 147-154 (2002).
- [Sidles95] J. A. Sidles, J. L. Garbini, K. J. Bruland, D. Rugar, O. Züger, S. Hoen, and C. S. Yannoni, *Rev. Mod. Phys.* **67**, 249 (1995).
- [Slichter90] C. P. Slichter, *Principles of Magnetic Resonance* (Springer, Berlin, 1990).

- [Smirnov75] W. I. Smirnov, *Lehrgang der höheren Mathematik*, Band 5 (VEB Deutscher Verlag der Wissenschaften, Berlin, 1975).
- [Stamp00] N. Prokof'ev and P. Stamp, Rep. Prog. Phys. **63**, 669 (2000).
- [Stauber02a] T. Stauber and A. Mielke, Phys. Lett. A **305**, 275-280 (2002).
- [Stauber02b] T. Stauber, Phys. Rev. B **68**, 125102 (2003).
- [Stockburger02] J. T. Stockburger and H. Grabert, Phys. Rev. Lett. **88**, 170407 (2002).
- [Stowe97] T. D. Stowe, K. Yasumura, T. W. Kenny, D. Botkin, K. Wago, and D. Rugar, J. Appl. Phys. **71**, 288 (1997).
- [Thorwart00] M. Thorwart, L. Hartmann, I. Goychuk, and P. Hänggi, J. mod. Opt. **47**, 2905 (2000).
- [Thorwart02] M. Thorwart and P. Hänggi, Phys. Rev. A **65**, 012309 (2002).
- [Thorwart03] M. Thorwart, E. Paladino, and M. Grifoni, Chem. Phys. **296**, 333-344 (2004).
- [Tinkham] M. Tinkham, *Introduction to Superconductivity* (McGraw-Hill, Inc., New York, 1996).
- [Vion02] D. Vion, A. Aassime, A. Cottet, P. Joyez, H. Pothier, C. Urbina, D. Esteve, and M. H. Devoret, Science **296** 886 (2002).
- [Wegner94] F. J. Wegner, Ann. Phys. **3**, 77 (1994).
- [Weiss00] U. Weiss, *Quantum Dissipative Systems* (World Scientific, Singapore, 2000).
- [Wilhelm03a] F. K. Wilhelm, Phys. Rev. B **68**, 1338 (2003).
- [Wilhelm03b] F.K. Wilhelm, S. Kleff, and J. von Delft, Chem. Phys. **296**, 345 (2004).
- [Wilson93] S. D. Glazek and K. G. Wilson, Phys. Rev. D **48**, 5863 (1993); Phys. Rev. D **49**, 4214 (1994).
- [Zurek81] W. H. Zurek, Phys. Rev. D **24**, 1516 (1981).

Danksagung

Ich möchte mich bedanken bei Christoph Bruder für die Betreuung und Unterstützung während meiner Doktorarbeit. Danken möchte ich weiter allen Leuten unserer Gruppe, die auf irgendeine Weise zum Gelingen dieser Arbeit beigetragen haben, speziell Florian Marquardt für die Zusammenarbeit und die vielen Diskussionen, Florian Meier der mir in Rat und Tat beigestanden ist, Bill Coish, Christian Schroll und Oliver Gywat für das kritische Durchlesen des Manuskripts und schlussendlich Mahn-Soo Choi für die Einladung nach Korea, wo ein Teil der Arbeit ausgeführt wurde.

Lebenslauf

von Hanno Gassmann

- 17.9.1973 Geburt in Zürich, als zweiter Sohn von H. Gassmann und B. Gassmann (geb. Boss), zwei Brüder
- 1980-86 Besuch der Primarschule in Rüti (ZH)
- 1986-89 Besuch der Sekundarschule in Rüti (ZH)
- 1989-93 Besuch der Kantonsschule in Wetzikon (ZH), Abschluss mit der Matur
- 1993-94 Militärdienst bei der Gebirgsinfanterie in Graubünden
Beginn des Elektrotechnikstudiums an der ETH Zürich
- 1994-96 Elektrotechnikstudium mit 2. Vordiplom abgeschlossen
- 1996-2000 Fortsetzung des Studiums an der ETH in Physik, davon 4 Monate Diplomarbeit "Excitonic Ferromagnetism" unter Prof. T. M. Rice
- 2000-2004 Dissertation am Institut für Physik der Universität Basel unter Prof. C. Bruder, seit Okt. 2000

An der Ausbildung beteiligte Dozenten: (ETH Zürich:) Profs.

R. Bacher, V. Baladi, H. Baltes, E. H. Berninger, J. Bilgram, C. Blatter, J. W. Blatter, H. Brauchli, M. Bronstein, H. Eberle, R. Eichler, P. Embrechts, K. Ensslin, G. Felder, K. Frey, J. Fröhlich, H. Geiges, G. M. Graf, F. Grogg, P. Günter, J. Hugel, W. Hunziker, H. Jäckel, U. Keller, K. F. Kneubühl, H. Knörrer, J. P. Kunsch, J. Lang, U. Lang, P. Leuchtman, P. Leuthold, J. Marti, E. Meister, H. Melchior, H. R. Ott, B. Plattner, T. M. Rice, T. Rösigen, C. Schmid, H. C. Siegmann, R. Sperb, H. Stemmler, D. Stoffer, M. Struwe, L. Thiele, E. Trubowitz, J. Waldvogel, J. Weiler (Basel:) C. Bruder, D. Loss, C. Schönenberger, P. Talkner.